



Durham E-Theses

A study of electron avalanches in electric fields

Moulding, D. G.

How to cite:

Moulding, D. G. (1967) *A study of electron avalanches in electric fields*, Durham theses, Durham University. Available at Durham E-Theses Online: <http://etheses.dur.ac.uk/8855/>

Use policy

The full-text may be used and/or reproduced, and given to third parties in any format or medium, without prior permission or charge, for personal research or study, educational, or not-for-profit purposes provided that:

- a full bibliographic reference is made to the original source
- a [link](#) is made to the metadata record in Durham E-Theses
- the full-text is not changed in any way

The full-text must not be sold in any format or medium without the formal permission of the copyright holders.

Please consult the [full Durham E-Theses policy](#) for further details.

A STUDY OF ELECTRON AVALANCHES
IN ELECTRIC FIELDS

by

D. G. MOULDING, B. Sc.

Being an account of the work carried out
in the University of Durham during the
period October, 1963 to December, 1966.

March, 1967.



ACKNOWLEDGEMENTS

The author wishes to thank sincerely Dr. W.A. Prowse, his research supervisor, for his interest and patient criticism during the course of this work. He is also deeply indebted to Dr. J.M. Breare for his constant support and for his considerable practical assistance.

He would also like to extend his thanks to Drs. J.H. Vincent, S. Goswami and Mr. R. Kirkwood for many illuminating discussions, not always relevant to Gas Discharges, but always of great interest.

He is also indebted to Professor G.D. Rochester for providing laboratory facilities and to the staff of the Physics Department: to Mrs. E.J. Templeton for her assistance with the computer program: to Mrs. P. Wilson who patiently undertook the typing: and finally to the Science Research Council for their provision of a maintenance grant.

D.G. Moulding.
March 1967.

PREFACE

This thesis describes experiments which have been performed in Durham to study the behaviour of electron swarms drifting under the influence of a uni-directional electric field. The electron swarms were admitted into a plane parallel electrode gap, (~ 7 cm), through small holes in the cathode. These swarms were in general of $3 \cdot 10^{-7}$ sec duration, and contained initially about 10^6 electrons. Most of the measurements were made in hydrogen at a gas pressure of about 60 mm Hg, although some work has been done in nitrogen.

The value of the reduced field E/p_0 , (~ 23 v cm $^{-1}$ mm $^{-1}$), in the drift section was sufficient for exciting and ionizing electron-molecule collisions to occur, but was always below that required for the gap breakdown. The motion of the swarm was followed by observation of the radiation emitted by excited gas molecules, and these light signals were detected at the side of the electrode gap with a photomultiplier. However, it was so arranged that only the radiation emitted from a thin slice of the avalanche path was collected by the photomultiplier, so that a comparison of the light intensities emitted from the path at various distances from the cathode, enabled several discharge parameters to be determined; e.g. the ionization coefficient, the electron drift velocity, and the diffusion coefficient.

It was found that when the number of starting electrons in a swarm was maintained below 10^6 , the rates of ionization,

for both primary and secondary electrons moving in the gap, were constant and in agreement with those found by other workers. However, when the initial electron density was increased, it was found that the rate of multiplication by collision ionization was reduced in the primary swarms. This effect has been attributed to local distortions of the applied field, which tend to reduce the ionization coefficient as seen by electrons moving in the swarm. Confirmation of this argument has been obtained from a computer simulation of the development of a primary avalanche under the experimental conditions.

The measurements of the electron drift velocity tended to be higher than would be expected at this value of E/p_0 . This result is however in agreement with other workers at the same gas pressure, and is attributed to a diffusive motion of the electrons within the swarm which is superimposed upon the drift motion.

CONTENTS

	Page
ACKNOWLEDGEMENTS	
PREFACE	
Chapter 1	INTRODUCTION 1
1.1	Ionization growth in uniform electric fields 2
1.2	Secondary processes 6
1.3	Generation mechanism 6
1.3.1	Influence of space charges 8
1.4	Streamer mechanism 13
Chapter 2	THE PRESENT EXPERIMENT 17
2.1	Choice of the working gas and operating conditions 18
2.2	Methods of observation 19
2.3	The nature of the light emission from a hydrogen discharge 24
2.4	Gas breakdown in u.h.f. fields 26
Chapter 3	THE APPARATUS 27
3.1	The discharge vessel 27
3.2	The vacuum system 29
3.3	The production of pure hydrogen 31
3.4	The photomultiplier 32
3.5	The oscilloscope and film measurements 34
3.6	The electrodes 35
3.6.1	Test electrodes 35

3.6.2	The present electrodes	36
3.6.3	Electrode supports	37
3.7	The high voltage supply	37
Chapter 4	THE ELECTRON SOURCE	42
4.1	Previous work	42
4.2	The present source	43
4.3	Measurements on the emission of the source	45
4.3.1	Effect of hole size	46
4.3.2	Effect of gas pressure	48
4.3.3	Effect of a wide range of applied field strengths	48
4.4	Source emission at low values of E/p ($E/p < 3 \text{ v cm}^{-1} \text{ mm}^{-1}$)	51
4.5	Source emission at higher values of E/p , ($E/p \sim 23 \text{ v cm}^{-1} \text{ mm}^{-1}$)	51
4.6	Comments	54
Chapter 5	THE EXPERIMENTAL MEASUREMENTS	56
5.1	Experimental procedure	56
5.2	The path swept out by a primary electron swarm drifting across the electrode gap	58
5.3	Measurements of the ionization coefficient	60
5.3.1	Comments	64
5.4	Measurements of the electron drift velocities	65
5.5	Drift and diffusion	67
5.5.1	Basic diffusion relations and particle distribution under diffusion	67
5.5.2	The velocity of the primary electron swarms	69

5.6	Measurements of the electron diffusion coefficient	74
5.6.1	Axial diffusion of the electron swarms	74
5.6.2	Radial diffusion	78
5.7	Electron distribution within a primary swarm	80
5.8	Comments	80
Chapter 6	A THEORETICAL STUDY OF THE DEVELOPMENT OF THE PRIMARY ELECTRON SWARMS	82
6.1	General description of the program	82
6.2	Local field distortions	85
6.3	Parameters used in the program	87
6.4	The initial charge distribution	89
6.4.1	The initial axial distribution of electrons	89
6.4.2	The production of positive ions	90
6.5	Development of the avalanche	92
6.6	Field dependence of the ionization and excitation coefficients	93
6.7	Order of computation	95
Chapter 7	A DISCUSSION OF THE MEASUREMENTS OF THE IONIZATION COEFFICIENT	101
7.1	Electron attachment	101
7.1.2	Experimental factors	106
7.2	Initial conditions	107
7.3	A comparison of the measured and computed growth curves	109
7.4	Comments	118

Chapter 8	SUGGESTIONS FOR FUTURE WORK	122
Appendix 1	The computer program	125
Appendix 2	Gas breakdown in u.h.f. electric fields	131
References		134

CHAPTER ONE

INTRODUCTION

The electrical breakdown of a gas is the term used to describe the transition in the gas from an insulating to a highly conducting state. A characteristic of the breakdown is that the voltage applied between electrodes in the gas, drops by a process producing a high conductivity between cathode and anode. The transition occurs in a very short time period, during which it is not possible to maintain the electrostatic energy of the gap capacitance; consequently, a breakdown of the gap voltage occurs. One of the problems of Gas Discharge physics has been to account for this breakdown in terms of fundamental gas processes.

The basic process involved in d.c. discharges is the electron avalanche; that is the ionization processes started by one or more electrons. Two known mechanisms⁽¹⁾ which account for the breakdown of a gas stressed by a unidirectional electric field are:

i) a relatively slow mechanism, which requires a large number of avalanche generations to produce breakdown (Generation or Townsend mechanism).

ii) a rapid mechanism, in which breakdown results directly



from a primary electron avalanche (Streamer mechanism or Kanalaufbau).

This thesis is concerned with the development of primary electron avalanches in a plane parallel electrode gap prior to the gap breakdown, and subject to space charge distorted electric fields.

The method of observation of the avalanches, initially used by Corrigan and Von Engel⁽²⁾ to measure excitation coefficients, is known generally as the optical method. Electrons moving under the influence of an electric field besides producing new electrons by ionizing collisions, also excite radiation. The emitted photons are detected by a photomultiplier and indicate the temporal growth of the electron avalanche.

1.1 Ionization growth in uniform electric fields

The conduction of electricity in gases may be studied by expressing the electrical properties of the discharge in terms of atomic data such as charge, mass, mean free path, etc. Electrons moving through a gas suffer many collisions with gas molecules, and as a result acquire a certain distribution of energies. The majority of these collisions are of the elastic type, however in hydrogen for example, the onsets of various inelastic processes are fairly evenly distributed over the whole electron energy range. This even distribution means that in

hydrogen and other molecular gases, a Maxwellian distribution may, to a first approximation, be used to describe the energy distribution of the electrons. (In rare gases a Druyvesteyn distribution is probably more suitable). It follows therefore that under the conditions of the present experiment, the majority of electrons will have energies less than that required for ionization, and only a small fraction in the tail of the distribution, will be very energetic. In hydrogen the sequence of exciting processes by which electrons are brought into equilibrium with the electric field are: rotational excitation, vibrational excitation, excitation of valency electrons to a wide range of energy levels, some of which lead finally to dissociation of the molecule, while others decay by quantum emission; and energy losses by ionization. The relative energy losses by these processes obtained by Corrigan and Von Engel⁽²⁾, are shown in the following table, (approximate values). Here E is the electric field strength, and p the hydrogen gas pressure.

E/p	Elastic	Rot.	Vib.	Diss.	Excit.	Ioniz.
40	1.25%	-	5.0%	62.5%	25.0%	6.25%

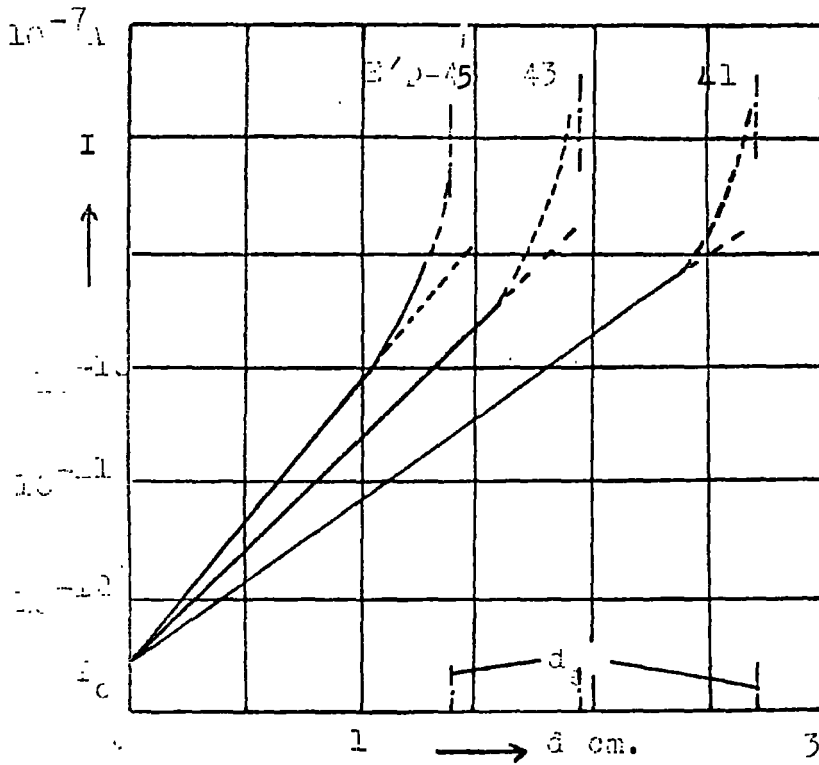
Energy losses caused by rotational excitation play an insignificant part in swarm experiments in hydrogen where the mean electron temperature is several electron volts. The measured cross-sections for vibrational excitations are also quite small⁽¹⁹⁾, and the

calculated energy losses for electrons varying in energy from 1-10 eV is only a small percentage. However the measured cross-section^s for dissociation losses are such that in hydrogen it is apparent that a large percentage of the energy gained by the electrons from the electric field, is lost finally in the dissociation of the molecules.

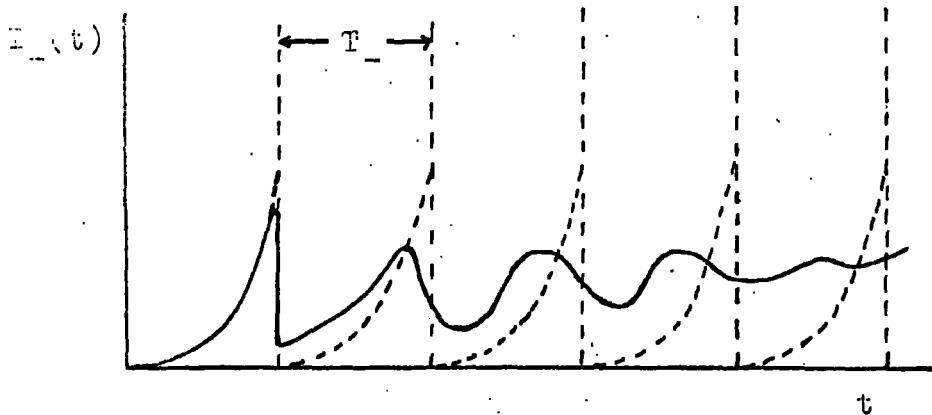
In an electron-molecule collision sufficient energy may be transferred in the collision for a valency electron to be ejected from the molecule. This electron together with the original one, may ionize other molecules in the same way, thus starting a chain of ionizing collisions, known as the electron avalanche. If a plane-parallel electrode gap is considered, with a voltage V applied between the electrodes producing a uniform field $E(=V/d)$ at all points in the gap. Then, if the electrode separation is d cm, and provided the gas pressure p and the parameter E/p are kept constant, the total steady-state current flowing in the gap initiated by a small photo-electric current I_0 at the cathode, is given by the Townsend equation

$$I = \frac{I_0 e^{\alpha d}}{(1 - (\frac{W}{\alpha})(e^{\alpha d} - 1))} \quad (1.1)$$

Under these conditions α and $(\frac{W}{\alpha})$ are constants, known as the Townsend primary and generalized secondary coefficients. This equation has been verified experimentally with these low cathode currents over a wide range of gap separations, and for a very



Fig(1.1) Multiplication ratio I/I_0 as a function of the electrode separation.



Fig(1.2) Electron current at $\mu=1$ as a function of time released by a flash of primary electrons ($\mu \gg 1$)

large range of the parameter pd . (In air, from $pd \sim 1$ to $pd \sim 1,000$ mm Hg cm, by Dutton, Llewellyn Jones, and Palmer⁽³⁾). Fig. (1.1) shows a series of graphs for nitrogen showing the increase in current I as a function of the electrode separation for different reduced fields E/p .

Inspection of this equation shows that the current becomes indeterminate when the denominator approaches zero. In a practical case, the magnitude of the current is controlled by the series resistance of the power supply, and the degree to which d can approach d_s , the sparking distance, is controlled by the constancy of this supply, and by the presence of field distortions caused by space charges in the gap. These become appreciable for large values of the current I . The condition for breakdown in the gap is

$$\left(\frac{E}{E_0}\right) (e^{\alpha d} - 1) = 1 \quad (1.2)$$

That is the condition at which the original discharge goes over into a self-sustaining discharge which may be maintained without the irradiation of the cathode. The sparking distance d_s is defined as the value of d which satisfies this condition.

This expression has been found to be a very good approximation for the breakdown criterion in gases, even though in practise the assumption of a uniform field during the later stages of current growth cannot be correct. The general conclusion which has been drawn, is that in many cases the value of the

applied field at which space charge distortion becomes appreciable is very close to the actual breakdown voltage.

1.2 Secondary processes

A physical interpretation of α may be obtained by regarding αdx as the average number of ionizing collisions in a distance dx in the field direction. while $(\frac{\delta}{\alpha})$ represents several distinct processes, the most important of these under laboratory conditions are:

i) secondary emission from the cathode caused by the impact of positive ions;

ii) photo-electric emission from the cathode by the incidence of photons produced in the body of the gas.

The operation of these processes may be represented by coefficients, the sum of the coefficients being approximately equal to the generalized coefficient $(\frac{\omega}{\alpha})$

$$\left(\frac{\omega}{\alpha}\right) = \gamma + \left(\frac{\delta}{\alpha}\right) \quad (1.3)$$

where γ is the mean number of secondary electrons produced by the impact of positive ions on the cathode, and $(\frac{\delta}{\alpha})$ is defined as the mean number of electrons ejected by a photon incident on the cathode, per ionizing collision in the gas. It has been found that both α and $(\frac{\omega}{\alpha})$ are functions of (E/p) .

1.3 Generation mechanism

The preceding sections have described gas processes which account for steady state, ionization currents flowing through an

a) $n = 0.1$

b) $n = 1$

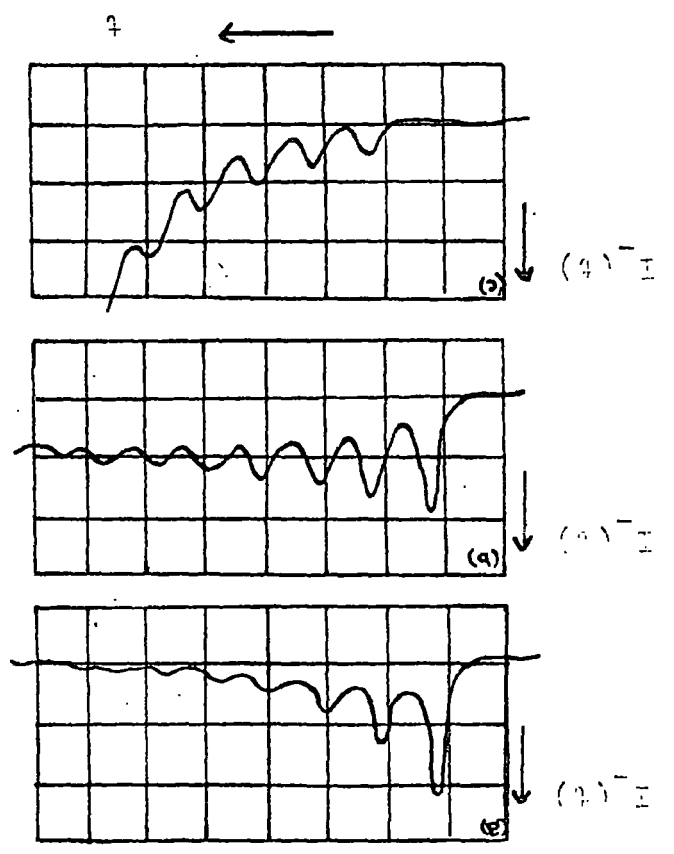
c) $n = 0.62$

• $\lambda = 0.33$ cm. $f = 1.46$ cm.

$(n \sim 10^4)$ in $\lambda + 0.1 \lambda$.

FIGURE 1. Theoretical curves of electron beam

with frequency of electron beam



electrode gap stressed by electric fields below that required for the breakdown of the gap. This section sets out to describe the development of ionization in time, when a sufficiently high voltage is applied to the gap.

Consider a plane parallel gap in which a primary avalanche is released from the cathode by a brief flash of ultra-violet light. If the amplification of the avalanche is sufficiently high, the number of photons emitted and also the number of positive ions formed will be sufficient to release secondary electrons from the cathode. These secondary electrons, the mean number of which is

$$\mu = \left(\frac{\xi}{\alpha}\right)(e^{\alpha d} - 1)$$

or

$$\mu = \gamma(e^{\alpha d} - 1) \quad \text{per avalanche,} \quad (1.4)$$

will then produce new avalanches in the next generation. If the primary avalanche begins with n_0 electrons, all emitted at the same moment, then the secondary avalanche will begin with μn_0 electrons.

Using the optical method it is possible to observe the oscillatory nature of the electron component of the current in the discharge. If the secondary electrons are produced mainly by photoelectric emission at the cathode, as is usually the case, then the interval between avalanches T_g is nearly equal to the electron transit time (d/v_-) . However if the secondary emission is by the impact of positive ions, then the generation time is the order of the positive ion transit time (d/v_+) . The interval

T_g differs by a factor $10^2 - 10^3$ for the two processes.

The dotted curve in Fig. (1.2) indicates the electron current if the whole of the radiation from the avalanche is emitted as the electrons enter the anode. However this is an idealized case, and in general, the light is radiated during the whole transit time of the avalanche electrons. Consequently, the oscillations tend to fade away with time, and the time separation of the secondary avalanches decreases. The figure shows the case when $\mu = 1$, i.e. the case of a self-sustaining current.

Fig. (1.3) shows oscillograms of the electron current in a mixture of nitrogen and methane, for different values of μ .

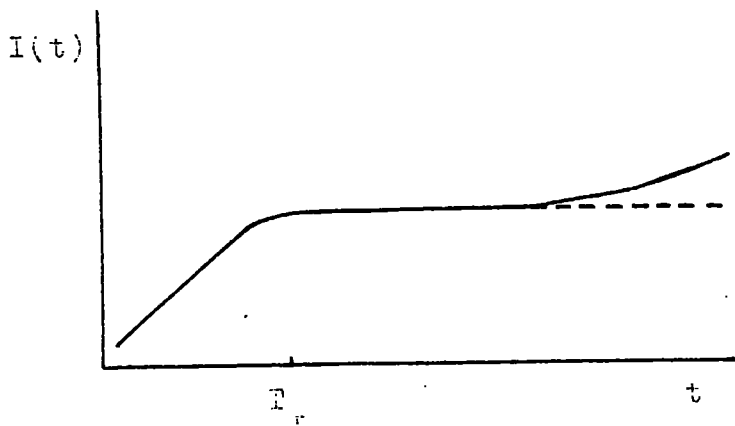
The log I-d curves shown in Fig. (1.1) therefore represent the initial build-up of current in a discharge gap, which is made up of successive generations of avalanches. The discharge in this case is initiated by a few starting electrons, and the upcurving observed in these graphs is caused by secondary action at the cathode. This was confirmed by calculations performed by Crowe, Bragg and Thomas⁽⁴⁾, who showed that for all but the largest currents recorded, the current density in the gap was below that which could cause appreciable space charge distortion of the applied field.

1.3.1 Influence of space charges

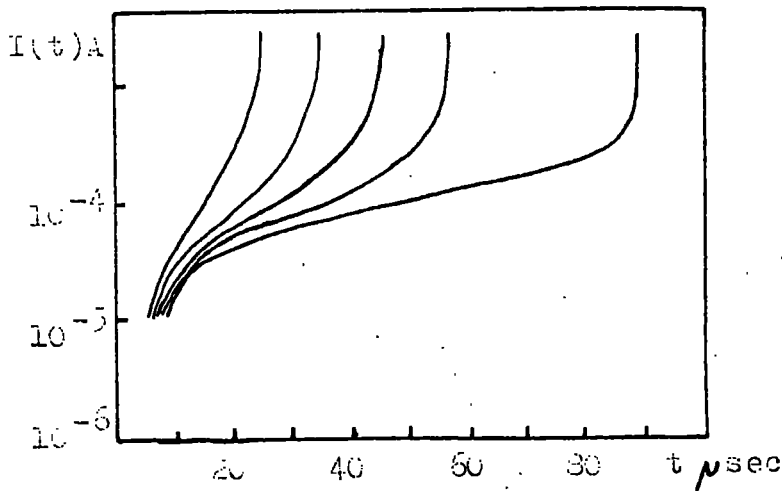
It is apparent that the growth of ionization currents in a gap beyond a point at which the electron density exceeds

10^8 electrons/cc, must to some extent be dependent upon local field distortions produced by space charges. This dependence upon the number density of electrons has not been considered in the Townsend relation. Measurements of the current growth in this region are however extremely difficult to perform, as space charge effects will not become significant until the gap voltage is within $\frac{1}{2}\%$ of that required for the gap breakdown. The majority of experiments performed to measure these currents have therefore used oscillographic techniques, in which a high voltage pulse is applied to the electrode gap. This voltage is usually considerably above the breakdown voltage, and the technique is of the "single shot" type and it has the advantage that very-high stability voltage supplies are not required. The discharge current is measured by either the electrical or optical methods. Only the electron component of the discharge is observed if the optical technique is employed; however, if the current induced in the anode circuit is measured, the total current caused by the drift of electrons and positive ions can be measured. The dotted line in Fig. (1.4) shows the predicted total current measured by the electrical method, and produced by a flash of electrons at the cathode ($n_0 \gg 1$). The current should remain constant for $t > T_+^*$ upto $t = \infty$, since every avalanche pulse produces the same number of electrons ($n_0 \mu = n$) which started the preceding pulse, i.e. electrons lost from the gap

T_+^* - positive ion gap transit-time.



Fig(1.4) Growth of a discharge current started by a flash of electrons with space charge influence.

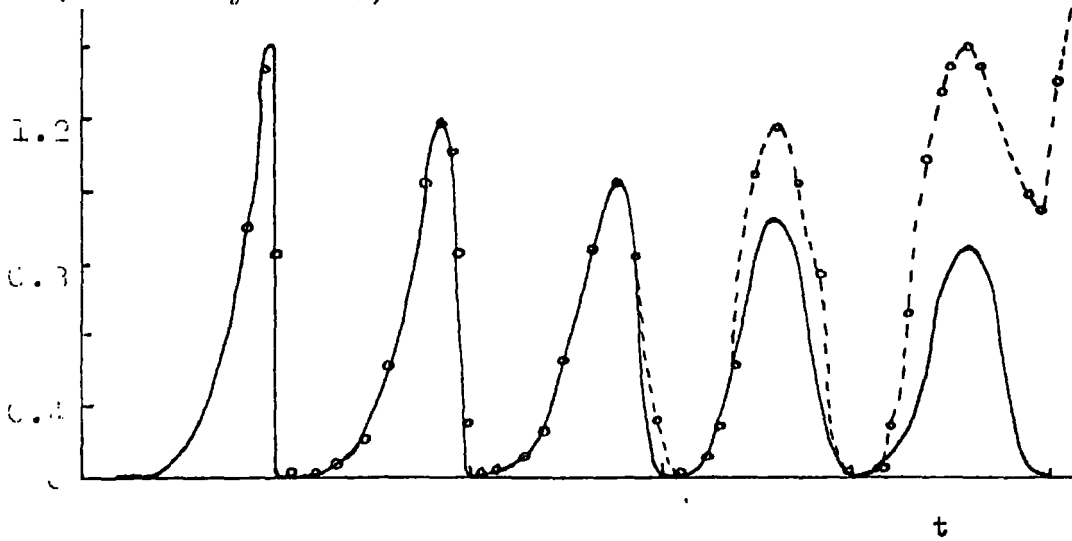


Fig(1.5) Growth of a discharge current in air (Bandel).

$p=724$ mm Hg, $d=1$ cm, $i_0=50$ electrons/ μsec .

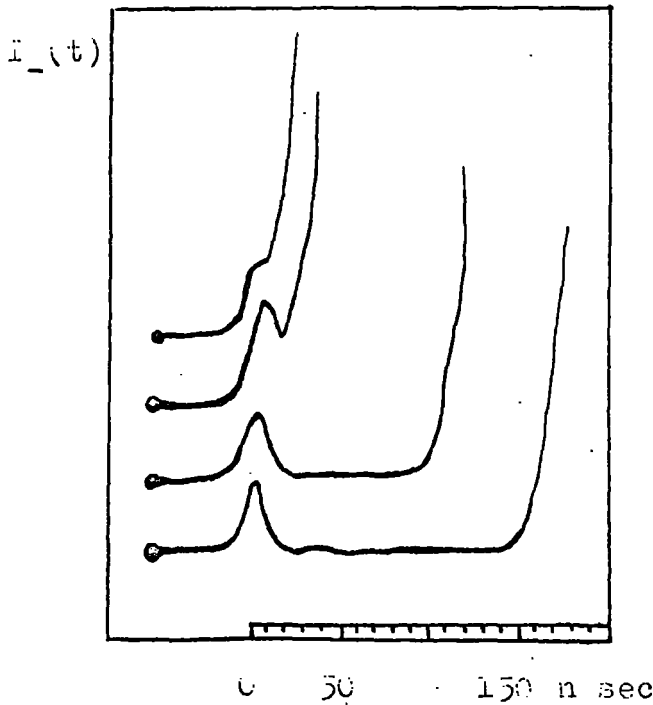
are replaced by secondary electrons at the cathode, thus maintaining a constant number of electrons in the gap at one time. However, experiments performed by Kluckow⁽⁵⁾ and others, produce results which lie on the full curve in Fig. (1.4). The current begins to rise after some hundred nano-seconds to high values which lead to breakdown. Measurements by the same method, when $\mu \gg 1$, have been made by Bandel⁽⁶⁾, Menes⁽⁷⁾, and others. Typical results are shown in Fig. (1.5). The current rises towards a limiting value during the earlier stages of the discharge, but later it is seen that an over-exponential growth occurs. Calculations performed by Bandel show conclusively that the up-curving of the oscillograms is caused by the influence of space charge fields. These fields are produced by the accumulation of positive ions in the electrode gap which eventually enhance the applied electric field, and lead to breakdown. The influence of space charge becomes more apparent as the number of positive ions produced per generation increases. This number is determined by the quantity $n_0 e^{\alpha d}$, and space charge effects have been observed at $t < T_+$ using single avalanches developed from a single electron ($n_0 = 1$). Alternatively, a high number of avalanches per generation may be used ($n_0 > 1$), with lower values of amplification (medium values of αd). experiments using the latter method have been performed by Schlumbohm⁽⁸⁾, who measured the current growth in CO_2 started by an α -particle. The influence of space charge

I (arbitrary units)



Fig(1.6) Series of photoaccelerators in CO_2 started by an α -particle.

$\mu \sim 1$; $E/p = 50.2$, — without space charge, \circ observed.



Fig(1.7) Current oscillograms of static breakdown, optical method.

$E/p = 64.4$, $pd = 230$ mm cm, $T_{\text{f}} = 90$ n sec.

is detected in the fourth generation (dotted line), while the full line represents the calculated current growth without space charge influence Fig. (1.6).

An account of the influence of small space charges on collision ionization has been given by Steenbeck and Von Engel⁽⁹⁾. An electrode gap was considered in which positive ions had accumulated as a result of the passage of several electron avalanches. The applied field E_0 was subsequently increased between the positive ions and the cathode, and decreased in the region of the gap between the anode and the ions. If the change in the applied field was Δ , then the potential across the gap changed from V to $V + \Delta V$ where

$$\Delta V = \int_0^d \Delta dx .$$

α/p is function of E/p , taken to have the form

$$\alpha/p = A e^{-\frac{Bp}{E}}$$

At a distance x from the cathode

$$\begin{aligned} \alpha_x/p &= A e^{-\frac{Bp}{E+\Delta}} \\ &= A e^{-\frac{Bp}{E} \left(\frac{1}{1+\Delta/E} \right)} \\ &= A e^{-\frac{Bp}{E} \left(1 - \frac{\Delta}{E} + \frac{\Delta^2}{E^2} \right)} \\ &= \alpha_0/p \left(1 + \frac{Bp}{E} + \frac{Bp}{E^4} \left(\frac{Bp}{2} - E \right) \Delta^2 \right) \end{aligned}$$

where $\alpha_0 = \alpha_x$ for $\Delta = 0$.

The change in the total number of ion pairs produced in the gap caused by a small space charge is

$$\int_0^d \alpha_x dx - \alpha_0 d = \alpha_0 \frac{Bp}{E^2} \Delta V + \frac{Bp}{E^4} \left(\frac{Bp}{2} - E \right) \int_0^d \Delta^2 dx.$$

The integral on the right in the above expression is always positive; hence the last term is positive when $E/p < B/2$ and vice-versa. If V is a constant, i.e. if $\Delta V = 0$, the equation shows that for $E/p < B/2$ the total ionization in a space charge distorted field is larger than would be the case in a uniform field. The condition $E/p = B/2$ corresponds to the point of inflexion on the curve $\alpha/p = f(E/p)$. It is concluded therefore that the effect of space charge is to increase the total ionization in the region of the (α/p) curve below the point of inflexion. Also, that the ionization in an electrode gap is reduced if (α/p) is above the point of inflexion on the $\alpha/p = f(E/p)$ curve.

It has also been shown from the last relation that a value of ΔV may be obtained for which the ionization is the same, whether or not space charge effects are considered.

$$\text{If } \int_0^d \alpha_x dx - \alpha d = 0$$

$$\text{then } \Delta V = \frac{B - Bp/2}{E^2} \int_0^d (\Delta E)^2 dx$$

If $\Delta E \propto$ charge density (ρ), and $\rho \propto j$, the current density, then

$$V = V_0 \pm cj^2$$

depending on whether $E_0 > Bp/2$ or $E_0 < Bp/2$. Thus if the field is such that (α/p) is below the point of inflexion, the voltage V_0 decreases with increasing number density; a result which agrees with experiment^{(10),(11),(12)}.

It has been concluded therefore, that in a plane discharge, the current develops to high values as a result of space charge influence, and that space charge is not merely a phenomenon accompanying the current growth.

1.4 Streamer mechanism

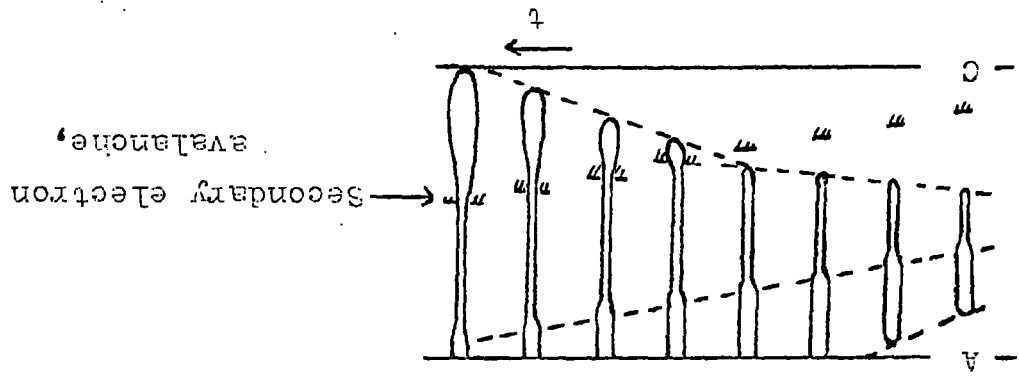
From the preceding sections it is apparent that the formative breakdown time of a plane parallel gap should be the order of several electron transit times. However, measurements of the formative time t_f as a function of gap overvoltage show that the formative time is reduced as the overvoltage is increased. When large overvoltages are employed, the formative times can be less than an electron transit time, and this has been taken as an indication that the generation mechanism is inadequate to explain the gap breakdown⁽¹³⁾. Further evidence to support this view was obtained from cloud chamber photographs of the development of high-number-density electron avalanches⁽¹⁴⁾. A sequence of photographs were obtained, showing how an avalanche developed in the normal manner until a certain critical carrier density was reached. Then, in a period of some tens of nano-seconds, the formation of an anode-directed streamer is shown, followed

immediately by a cathode-directed streamer. During this time the avalanche head moved only a few mm in the discharge gap, and further, no successors from the cathode of the gap were observed. After a further short interval, spark breakdown of the gap occurred in the streamer channel. Because of the nature of the technique, these photographs could not have been of the first stage of the discharge, but in fact refer to the later development of the spark.

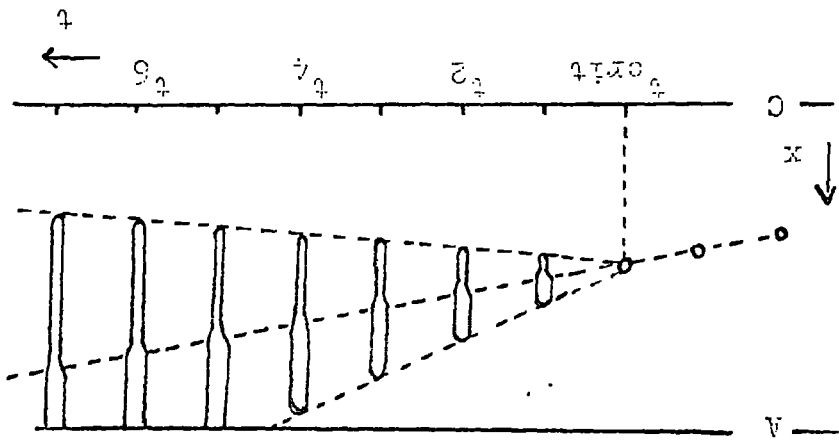
However, more detailed studies of the phenomena have been made using the optical method and high speed oscilloscopes. Fig. (1.7) shows four typical oscillograms produced by primary avalanches moving in a 0.8 cm electrode gap⁽¹⁵⁾. The amplitude of the pulses increases as the voltage U_0 applied to the electrode gap is increased, and in each case the final upturn of the trace leads to breakdown of the gap. The avalanches remain single avalanches, and no secondary emission from the cathode was recorded. A breakdown mechanism was therefore formulated in which breakdown resulted directly from the development of the primary avalanche by photoionization.

A recent paper published by wagner⁽¹⁶⁾ has shown more clearly this transition of a slow moving, primary avalanche to a different process of development which is characterised by its faster rate of propagation. The method of observation of these avalanche-streamer transitions was by means of an image-intensifier,

FIG(1.9) Intensification of the cathode directed streamer.



FIG(1.3) Development of both anode and cathode directed streamers.



streak-shutter technique. A significant point here is that in contrast to the cloud chamber method of observation, the development of the avalanche is followed from quite low values of the electron number density, through a critical number density, to the development of the anode and cathode directed streamers. The sensitivity of the apparatus is therefore sufficient to enable the streak photographs to be identified with the first stages of the discharge current. The development of the anode and cathode directed streamers are shown schematically in Fig. (1.8). The paper also indicates how the intensification and acceleration of the cathode directed streamers takes place, Fig. (1.9). This abrupt intensification shown in wagner's photographs is attributed to the streamer encountering a second generation of avalanches generated at the cathode by the photo-electric effect.

However, another interpretation of this phenomenon has been put forward by Ward⁽¹⁷⁾ in a recent paper on mid-gap breakdown. Here the development of high density avalanches has been simulated on an electronic computer, using basic data from experiments performed by Tholl⁽¹⁸⁾ (working in the same laboratory as wagner). Tholl's measurements however, made using the optical method, are not as detailed as those made by wagner. The calculations of the mid-gap breakdown are made using a one-dimensional Townsend model, when space charge effects are taken into consideration.

These calculations indicate that the rates of propagation of the streamers may be accounted for using the Townsend model, and that gas-photoionization is not required to produce the breakdown. The cathode streamers produced in the gap are in fact associated with secondary electron avalanches from the cathode. These conclusions however, do not appear to be substantiated by Wagner's results, which show that the initiation of the cathode streamer is not dependent on the presence of secondary electrons, and also that the streamer would reach the cathode surface even in the absence of any secondary emission. Whether or not the particular ionization process postulated, i.e. gas photoionization, is able to produce sufficient ionization is not proved, and the mathematical analysis of the phenomena is not yet far advanced.

CHAPTER 2

THE PRESENT EXPERIMENT

In the preceding chapter two breakdown mechanisms have been described in which space charge fields have significant effects upon the later growth of discharge currents. Although several theoretical models have been put forward (e.g. by Ward, Llewellyn Jones, Lucas), no experiments have been performed in which the spatio-temporal development of high-number density avalanches is studied under static voltage conditions. This is so chiefly because of the extreme rapidity with which the discharge current grows during the final stages before the gap breakdown, rendering step-by-step measurements difficult to perform. One method of overcoming this difficulty has been to use a 'single-shot' technique in which a high-voltage pulse is applied to the gap (the pulse amplitude exceeding the gap breakdown voltage), however this method has the disadvantage that the electron velocities, multiplication rates, etc., are much removed from those occurring under static voltage conditions when the ionization currents are small. Therefore, as a first step towards the study of space charges in gas breakdown, and in particular on the development of primary electron avalanches, a limited discharge is studied. That is, the applied voltage

to the gap, and the electrode separation, are maintained below that required for breakdown. Further, as the current densities in the discharge are relatively small, the rates of change of the parameters of interest are slow enough to be measured with the conventional instruments.

If the effects of space charges upon the development of a primary avalanche under static voltage conditions is to be studied experimentally, an important condition which must be realized is that the number of electrons within the diffusion radius of the avalanche must exceed a certain critical number n_c . Above this number the particle density is such that the resulting distortions of the applied field significantly change the rate of ionization. To meet this condition with the limited amplification available in the electrode gap, primary electron avalanches are initiated by a large number of locally concentrated electrons ($n_0 \geq 10^6$).

2.1 Choice of the working gas and operating conditions

Most of the experimental readings have been made in hydrogen for the following reasons. In general theoretical calculations of the properties of atomic and molecular states are complex, and tend to be limited to simple structures. Consequently, some considerable work has been done in hydrogen and many properties of the hydrogen molecule are well understood. Further these properties may be used to infer those of other more-complicated molecules by allowing for the perturbations which occur.

The energy levels and the decay processes in molecular hydrogen will be described in a later section, however the half-life of the excited state relevant to the experiment is extremely short, so that radiative emission from excited molecules occurs before the molecule has moved appreciably from the point of the original exciting collision. This is an important consideration if accurate spatial resolution of an avalanche is to be attained. In addition, complications introduced by the presence of metastable states do not arise in molecular hydrogen. In the text therefore, references to the working gas refer to molecular hydrogen except where otherwise stated.

A plane parallel electrode gap was used in the experiment with an electrode separation of up to 7 cms. This spacing was chosen so that adequate time resolution could be attained, and also that the amplification of an electron avalanche during the transit of the gap was sufficient to increase the particle number density from a figure at which space charge fields were negligible, to one at which they were appreciable.

The reasons determining the operating voltage and the working gas pressure will be discussed in Chapter 4, but a typical value for the gas pressure in the system was 60 mm Hg, with a reduced field $E/p = 23.5 \text{ volts cm}^{-1} \text{ mm}^{-1}$ at 0°C .

2.2 Methods of observation

Many experiments have been performed to study the nature of

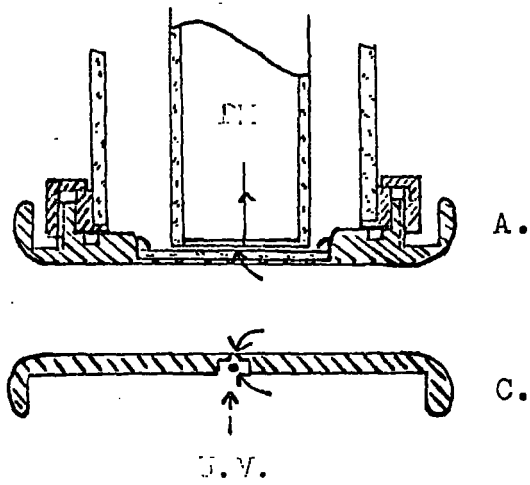
the motion of electrons through gases. This section sets out to survey briefly some of the methods used, and to indicate why the optical method was chosen for this investigation.

The majority of recent experiments have been based on the fact that charges moving in an electrode gap induce electrical signals in the electrodes. In general, the voltage developed across a resistor connected in the anode supply lead is displayed on a fast oscilloscope. If the electrons are contained within a thin layer initiated at the cathode, then it is assumed that the amplitude of the voltage pulse observed reaches a maximum when this electron layer enters the anode. However the method is subject to two principal limitations: firstly it can be argued that there exists a considerable uncertainty as to the exact position of the electrons in the gap, and consequently average values are obtained for the drift velocity, ionization coefficient, etc. Also inaccuracies arise when the dimensions of the swarm become comparable with the electrode separation, and when there is appreciable diffusive motion. This poor spatial resolution of the electrons in the gap means that the method is not well suited to detect local changes in the ionization coefficient. Secondly, to obtain appreciable induced-voltage signals an electrode gap is required with a small capacitance. This condition is difficult to meet and yet retain a uniform-field drift section.

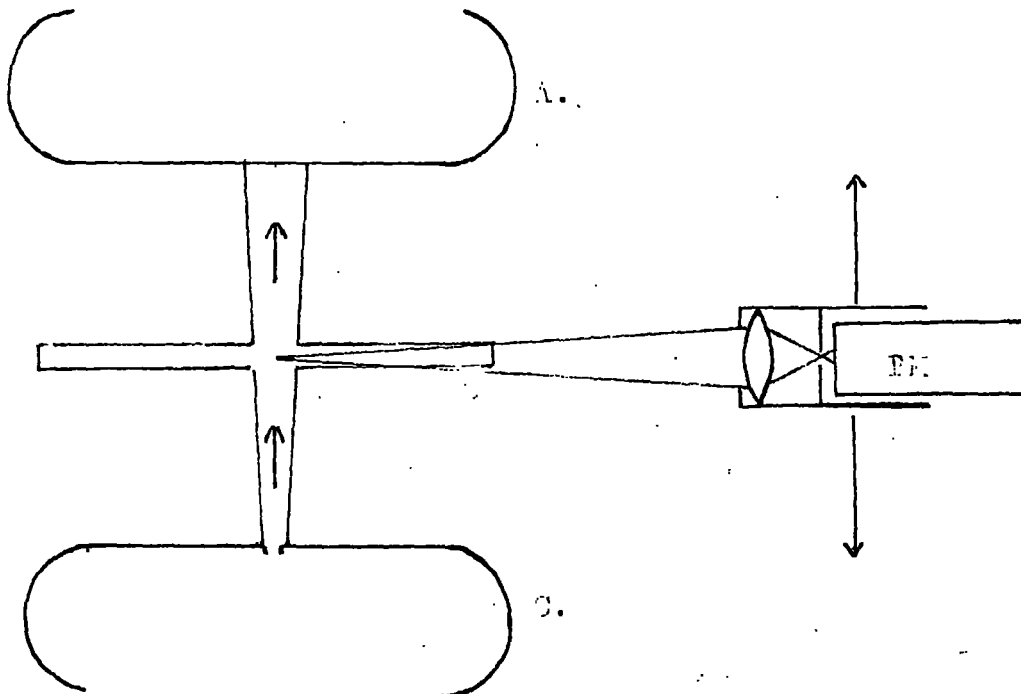
Other possible methods by which various parameters may be measured at a series of points across the gap include microwave

absorption, and the placing of probes at intervals between the electrodes. However both these methods have the disadvantage that the method of measurement will probably interfere with the phenomenon under observation.

In the optical method, the light emission produced by inelastic electron collisions is used to detect the avalanches. This emission is detected with a photomultiplier and refers only to the drifting electrons; the motion of positive ions is not detected using this method. However the method of observation is by means of a phenomenon caused by the motion of the electrons, and the observations themselves do not cause perturbations of this motion. A real limitation on the method is the range of the reduced field E/p over which observations may be carried out, i.e. E/p must be sufficiently large for exciting electron-molecule collisions to occur. In the present experiment it was found that insufficient light was collected from the passage of a single avalanche to produce smooth oscillograms. The pulses displayed on the oscilloscope were very ragged and subject to statistical fluctuations. However, because the transit of a single avalanche did not lead to gap breakdown, a complete picture of the electron distribution within an avalanche could be built up by collecting the radiation from several-hundred consecutive avalanches, i.e. identical single avalanches were initiated at the cathode at two to three millisecond intervals. The period between avalanches was then



Fig(2.1) Gibbert's experimental arrangement.



Fig(2.2) Present experimental arrangement.

sufficient for all the particles produced during the passage of the preceding avalanche to be swept from the gap by either the electric field or by diffusion.

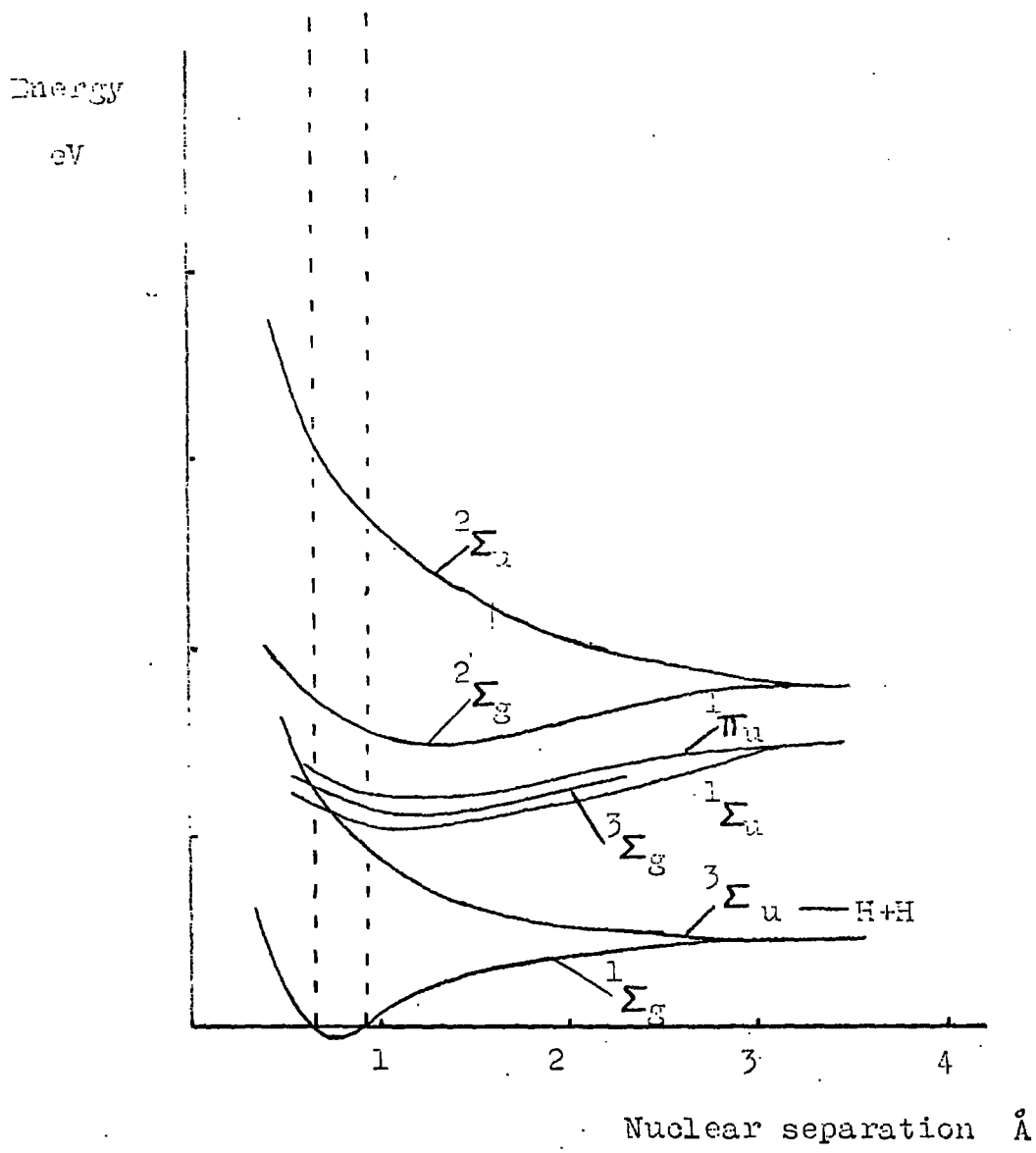
Experiments using the optical method to detect the motion of drifting electrons have been carried out by Dibbern^(18'), and his experimental arrangement is shown in Fig. (2.1). The object of this experiment was to study the motion of electron swarms moving in a plane-parallel gap through a mixture of nitrogen and methane. However his arrangement had no particular advantage over the electrical method in that no discrimination between photons originating from different parts of the discharge was possible, as the line of sight of the photomultiplier was in the direction of the electron motion. This disadvantage was overcome in an experiment by Breare^(20,21) to measure the drift velocities of low density electron swarms, and also in the present experiment. -

A photomultiplier was used to view the discharge from the side of the electrode gap (Fig. (2.2)), and it was so arranged that only radiation from a thin slice of the avalanche path was detected. In this diagram the path taken by the primary electron swarms is shown, and only photons emitted from the thin section of the path were collected at the photo-cathode. A detailed description of the lens and slit arrangements giving this spatial resolution is left to section 3.4. By altering the position of

the photomultiplier it was possible not only to measure the drift velocities of the front and centre parts of the swarm, but also the electron distribution within it and the amplification of the swarm as it moved across the electrode gap. The procedure used to determine these parameters will be found in sections 5.2 and 5.3.

The method is well suited to detect small changes in the electron ionization coefficient, a quantity which is sensitive to small changes in the electric field strength; caused for example, by space charge distortion. This sensitivity can readily be accounted for: a lumped excitation coefficient \mathcal{E}/p , analogous to the reduced ionization coefficient α/p , has been defined and measured by Corrigan and Von Engel⁽²⁾. \mathcal{E}/p is the total number of emitted quanta per electron, per cm of path in the field direction, per mm Hg. The quantity has been measured in hydrogen for $E/p = 15$ to $E/p = 100$ v/cm/Hg by Corrigan and Von Engel and by Legler⁽²²⁾. \mathcal{E}/p is a function of E/p , and the relation is very similar to that between α/p and E/p . If it is assumed that the number of photons (dp), created by an electron swarm moving a distance dx , is proportional to the number of drifting electrons (n_e), then

$$dp = \mathcal{E} n_e dx \quad (2.1)$$



Fig(2.3) Potential energy curves for the electronic states of molecular hydrogen.

An electron swarm moving through a decreased field region, will emit fewer quanta per cm of path. Thus the change in light intensity emitted from such a swarm, will be greater than would be the case if the coefficient ϵ was not field dependent. The small changes in electron number in a swarm produced by local field distortions are difficult to measure directly; however corresponding changes in the photon emission from the swarm are larger and more readily detected. The effect is analogous to that of a reflected light beam from a plane mirror in that a rotation of the mirror through an angle θ , produces a change of 2θ in the angle of reflection of the reflected beam.

2.3 The nature of the light emission from a hydrogen discharge.

Fig. (2.3) shows the electronic energy levels of the hydrogen molecule. Electrons of higher energy are able to produce excitation to the singlet states 'B' and 'C', which may decay directly to the groundstate by quantum emission, giving rise to the well known Lyman and Werner bands. It has been shown that the Werner bands are by far the more prominent of the two, and that the wavelength of the radiation lies in the spectral region 1,000 - 1,200 \AA .

From a consideration of the experiments of Ramien⁽¹⁹⁾ and of Jones and Whiddington⁽²⁴⁾, it is possible to show that the cross-section for excitation to the triplet state 'b' is larger than that to the singlet state 'C' for electrons whose energies are

just above threshold. However a transition from this state to the groundstate by quantum emission is a 'forbidden transition', and the decay process is therefore by quantum emission to the triplet state 'a', followed by the dissociation of the hydrogen molecule, as the state 'a' is a repulsive one. The dissociation energy of H_2 is 4.4 eV and the excess energy is carried away by the two atoms. The spectra corresponding to this transition is a continuum extending from $2,000\overset{\circ}{\text{A}}$ into the visible region.

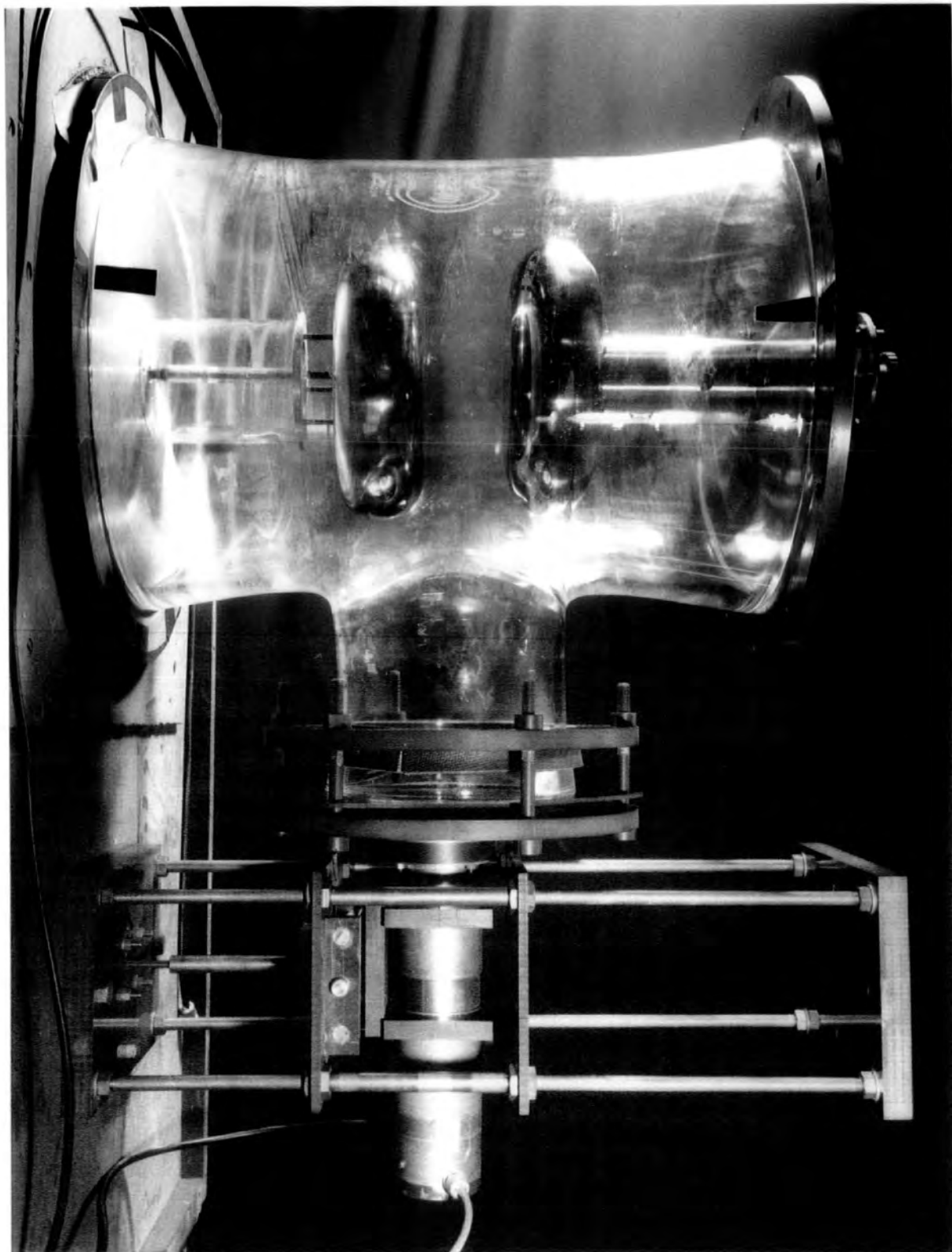
In the experiment it was found that sufficient light was emitted in the visible region at pressures of 60 mm Hg to produce smooth oscillograms without the use of sodium salicylate light converters. It is worthwhile to note here that some controversy exists between English and German workers in this field over the wavelengths of the light emitted. In particular Legler⁽²²⁾ in his experiment states that he was unable to detect any visible radiation at all from a discharge in hydrogen. While in an experiment reported by Corrigan and Von Engel⁽²⁾ to measure excitation coefficients, it is stated that some 20% of the total radiation emitted from their discharge was in the visible region, (also Nygaard⁽²⁶⁾). The discharge in the present experiment was viewed through a Pyrex window which will not transmit radiation of wavelength below $3,000\overset{\circ}{\text{A}}$, and in addition sufficient visible light was emitted for photographs of the discharge to be taken using normal panchromatic film.

It is concluded therefore that the radiation continuum emitted from a discharge in molecular hydrogen extends from $2,000\overset{\circ}{\text{A}}$ into the visible region, the radiation being similar to the emission from a spectral hydrogen lamp, made to give the ultra-violet continuum.

A wave mechanical treatment by Coolidge and James⁽²⁵⁾ has shown that the theoretical mean life of the continuum is 1.1×10^{-3} second. This life time is between one to two orders of magnitude less than the electron-gap transit time; a condition which must be realised if good spatial resolution of the discharge is to be obtained.

2.4 Gas breakdown in uhf fields

The work on the development of electron avalanches in dc fields was carried out in the period Jan 1965 - Dec. 1966. However the work of the laboratory as a whole is concerned with pre-breakdown ionization currents in general, and during the period Oct. 1963 - Dec. 1964 the author with R. Kirkwood, made measurements of ionization currents produced in uhf fields. An account of this work is given in a separate appendix.



CHAPTER 3

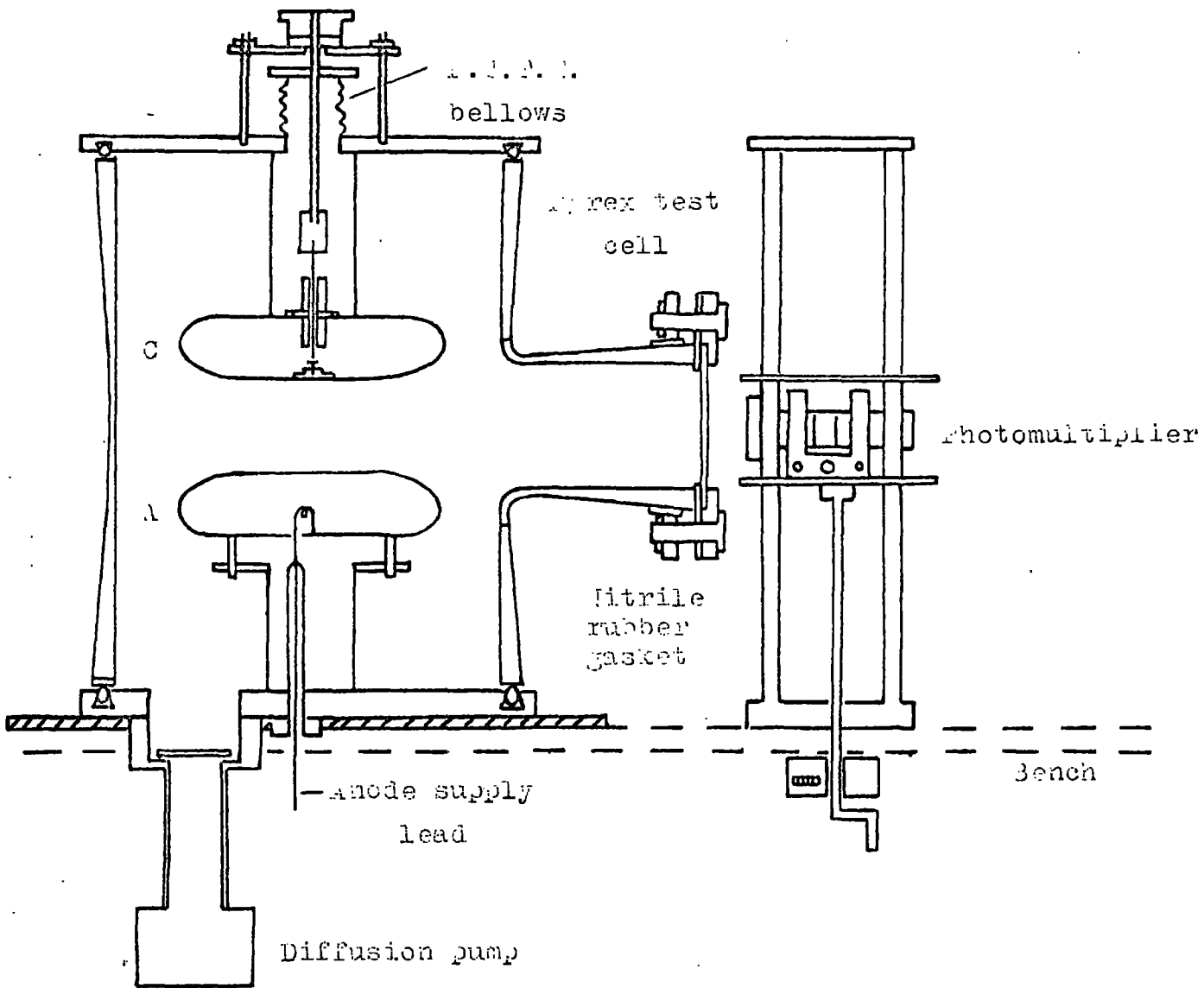
THE APPARATUS

The main features of the experimental system are mentioned here, and are described in detail in the following sections. An electrode gap was constructed to provide a drift section through which primary and secondary electron swarms moved in a uniform electric field. Because the ratio of the primary ionization coefficient to the gas pressure changes rapidly with E/p in the region considered ($E/p \sim 20$) it was necessary that this applied field should be uniform, and great care was taken to ensure that this condition was fulfilled. Also, because of the sensitivity of the ionization coefficient to impurities at this value of E/p , the system was designed to have high vacuum properties. A thermionic electron source was constructed which was capable of injecting variable density electron swarms into the drift section, but which did not cause appreciable distortion of the applied field in this section.

The exact design for the present apparatus was drawn up after a period of experimentation with a smaller system in which many electrode and source configurations were tested, and their shortcomings determined.

3.1 The discharge vessel

The pyrex discharge vessel was a standard unequal tee-piece made by the Quick Fit Visible Flow Company. A laboratory bench



Fig(3.1) The discharge vessel.

was used to support the vessel, while the vacuum system and power supplies, etc., were constructed to fit under the bench top. The vessel stood on a circular base plate of $\frac{3}{4}$ " thick, bright steel, separated from the bench by a sheet of asbestos. A vacuum seal was effected using a Viton O-ring fitted into a dove-tailed groove cut in the base plate. The upper end plate was of $\frac{1}{2}$ " thick, bright steel, and a vacuum seal was effected in a similar manner. Initially it was planned to clamp down both end plates using back flanges, however the combined weight of the cell and the electrode assemblies proved sufficient for the backing pump to create a partial vacuum in the cell. The dove-tailed grooves ensure^d positive retention of the O-rings, and made a very effective leak-free seal without the use of vacuum grease.

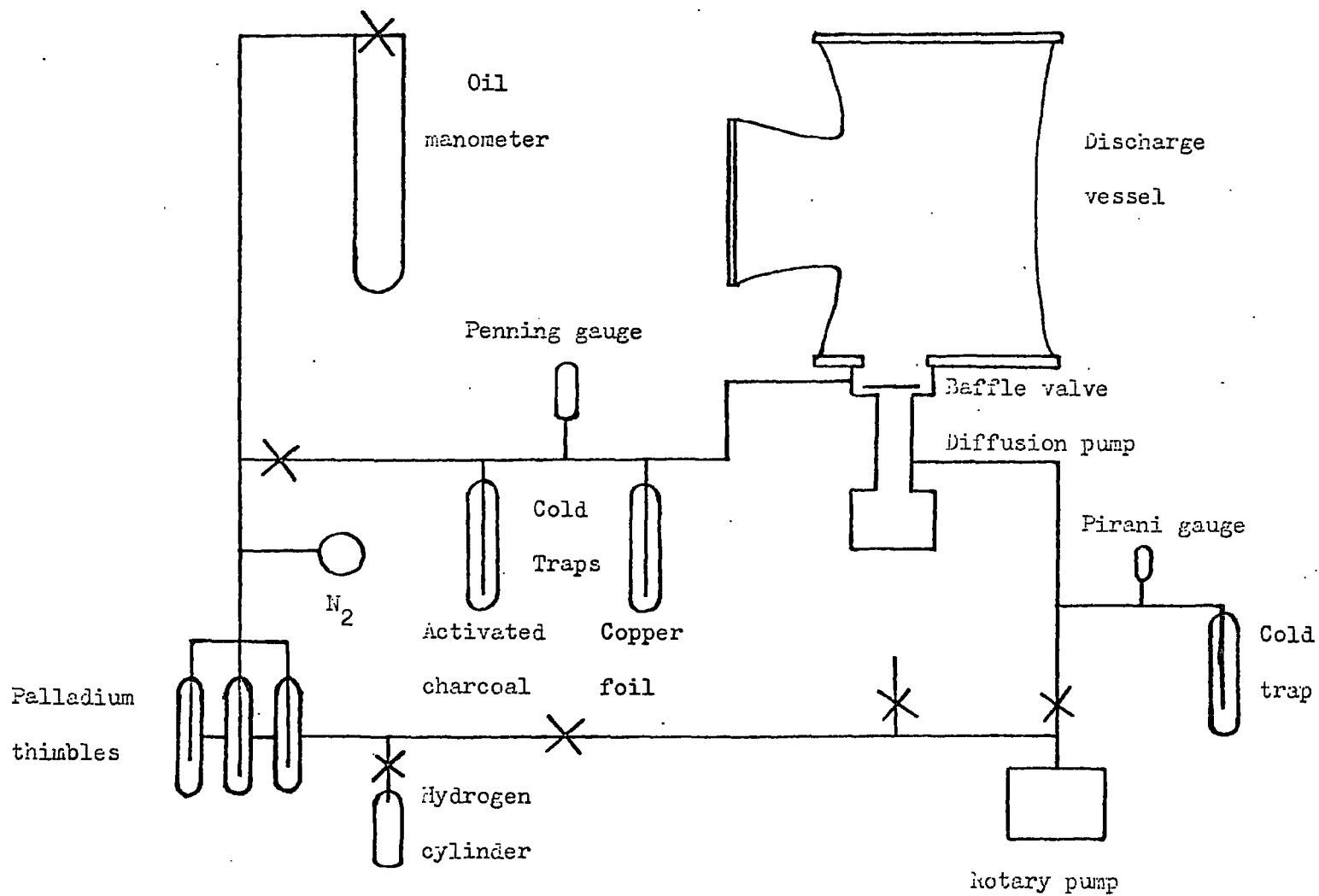
The observation port was sealed with a $7\frac{1}{4}$ " diameter, polished glass disc. This disc was held in position with a clamp plate and backing flange turned out of non-conducting tufoel. Between the disc and the fine ground open end of the cell was a nitrile rubber gasket. The high voltage supply lead to the anode led through a hole in the bench top and into the cell through a re-entrant glass-to-metal seal. A Viton O-ring was located in a groove in the metal flange connected to this seal, and this flange was clamped to the base plate. The high voltage lead lay along a line parallel to and about 2 cm from the central electrode axis. The use of a re-entrant seal ensured that there was no sparking between the lead and the base plate, Figs. (3.1 and 3.8).

with the exception of the area around the observation port, the cell and the electrode assemblies were baked under vacuum for a week at 160°C with electric heating tape. The observation port was baked at 100°C, the upper temperature limit for nitrile rubber. The cell temperature and glass temperatures of other parts of the system were monitored with copper-constantan thermo-couples attached to the glass surface under the heating tape.

3.2 The vacuum system

The discharge vessel was evacuated using two pumps; an Edwards two-stage rotary pump, which could be run with an air ballast, and an Edwards 203B three stage diffusion pump. The pumping fluid used was Edwards 705 silicone oil.

After consideration of the pumping speed of the diffusion pump, (50 litres/second), and the volume of the vessel, approximately 30 litres, it was decided that the diffusion pump should be clamped to the under side of the base plate. The pump passed through a hole cut in the top of the laboratory bench, thus avoiding the use of a long length of low conductance glass tubing. The only obstruction between the pump and the vessel was a baffle valve, which limited backstreaming of the pumping fluid and which was also used to seal the vessel from the pumps. Vacuum seals were effected with Viton O-rings and the original nitrile rubber seals on the valve drive shaft were replaced by Viton ones to allow baking to 160°C.



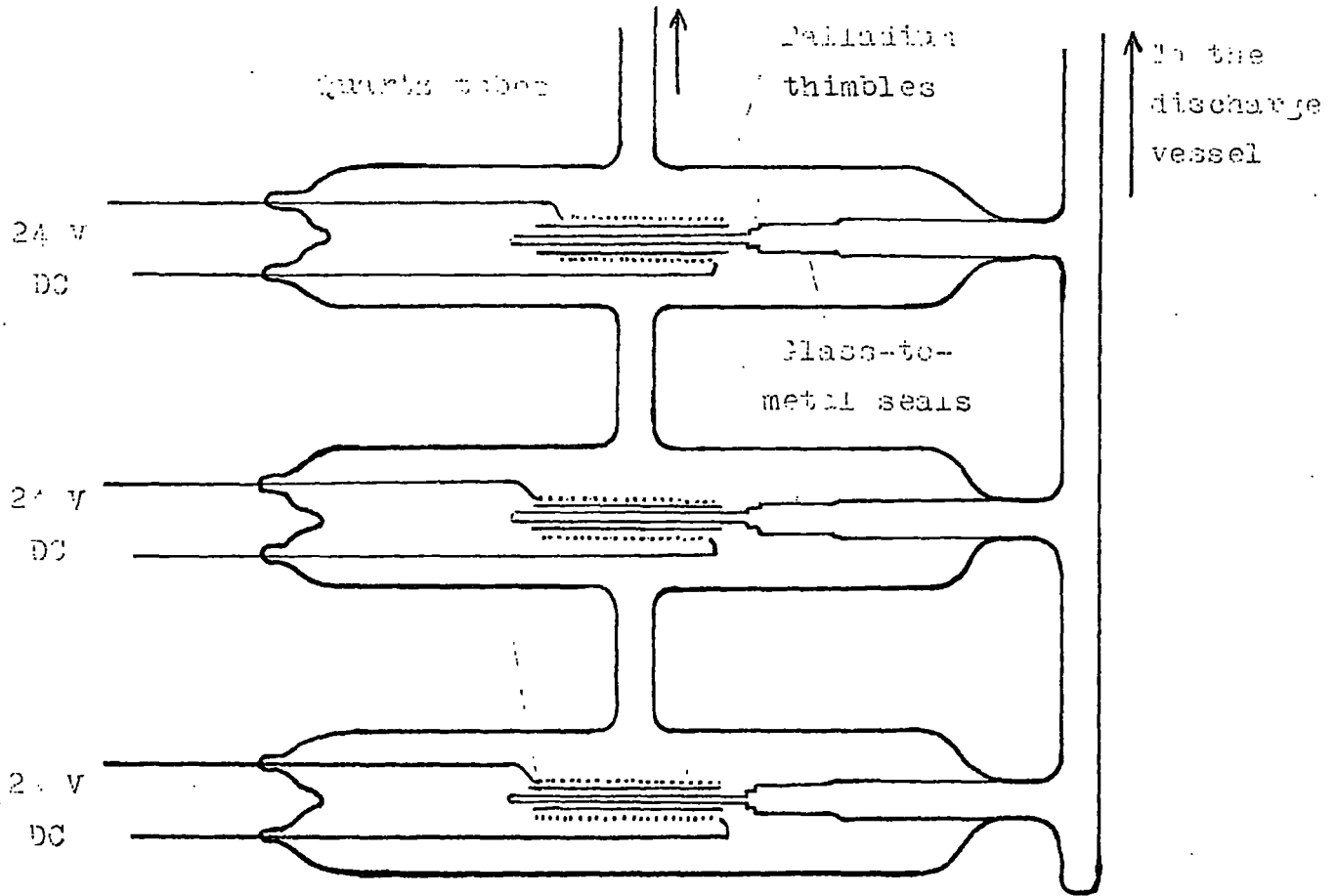
Fig(3.2) The vacuum system.

The vacuum system is shown in Fig. (3.2). A side arm led off the diffusion pump just above the baffle valve to a Penning gauge, two nitrogen vapour traps, the palladium thimbles, nitrogen bottles, and the manometer. This side arm was supported from a metal rod running the length of the bench. No part of the glassware was clamped directly to the bench, but rather through a metal rod framework which ensured a degree of flexibility. Thus any sudden jolts given to the bench were not transmitted to the glassware. The glass taps were greased with Silicone High Vacuum Grease, and the side arm and taps with the exception of the manometer were baked at 160°C.

Pressure measurements in the system were made in the following manner. Gas pressures upto 70 mm Hg were measured using a U tube manometer containing Edwards 704 silicone oil. Because of the low relative density of the oil, (1.07) it was estimated that gas pressures of the order of 60 mm Hg could be measured to within 0.5%. Pressures in the range 10^{-6} - 10^{-3} mm Hg were measured with an Edwards Penning gauge, and in the range 10^{-5} - 10^{-1} mm Hg with a Pirani gauge located between the diffusion pump and the backing pump.

The system included three liquid nitrogen vapour traps; one between the diffusion and backing pumps; one containing a rolled length of corrugated copper sheet in the side arm from the vessel; and another containing activated charcoal leading off

To the hydrogen
cylinder



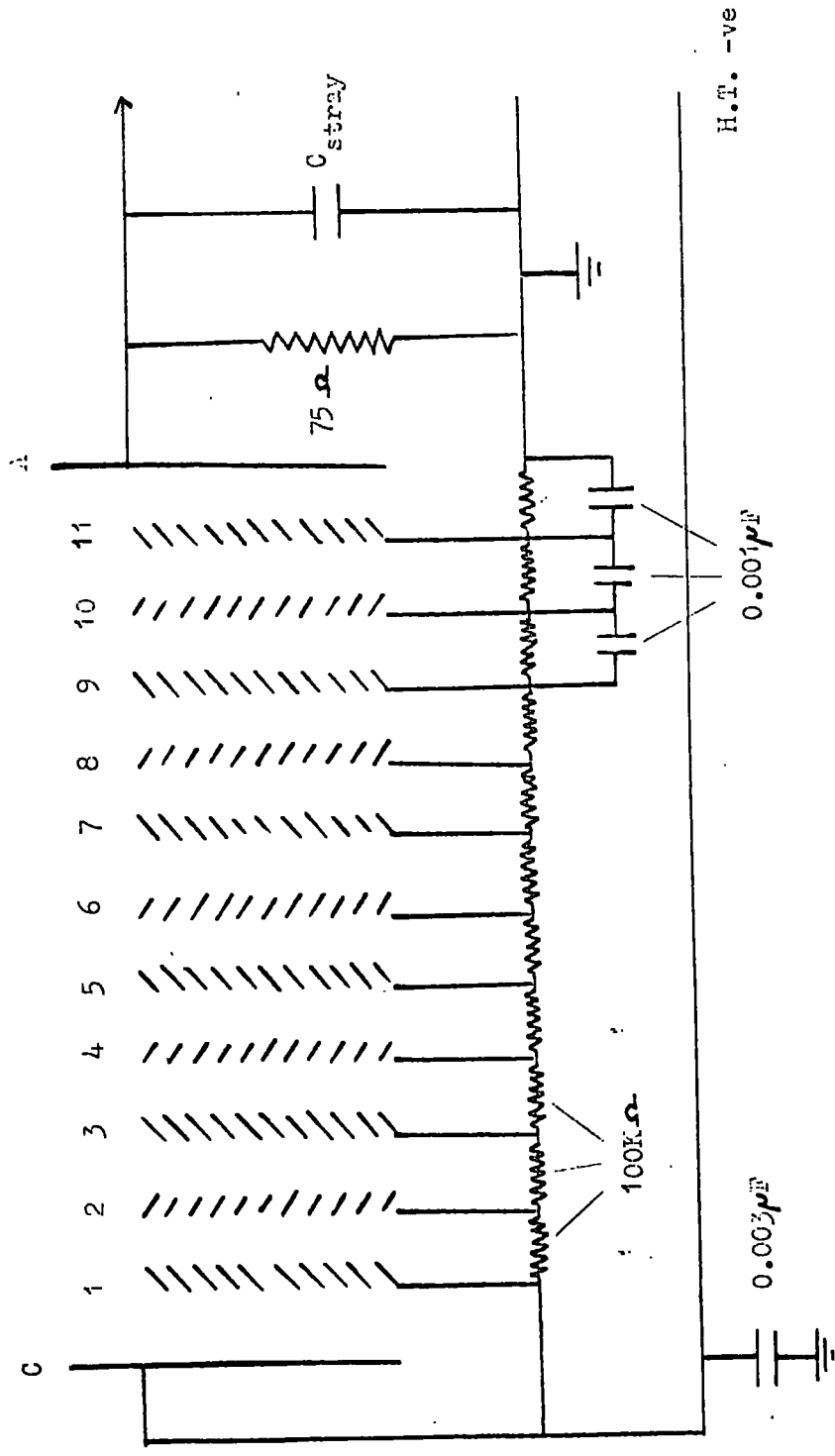
Fig(3.3) The palladium thimbles.

this side arm. The copper sheet tends to adsorb organic molecules which strike it, thus reducing the amount of non-pumpable vapours in the system. Activated charcoal also readily adsorbs vapours when it is cooled below room temperature. Unfortunately, it also adsorbed large quantities of the working gas, even when cooled to solid carbon dioxide temperatures. In addition slight temperature changes produced a marked variation in the gas pressure in the system, and so the use of this trap during an experimental run was discontinued.

The ultimate vacuum obtained in the system after outgassing was better than 10^{-6} mm Hg. A set of measurements took about four hours to carry out, and during a similar period with the pumps closed off, the pressure in the system rose to 10^{-4} mm Hg.

3.3 The production of pure hydrogen

Pure hydrogen was admitted to the system through three heated palladium thimbles, each 5 cm long with an outside diameter of 1.5 mm. Fig. (3.3). A length of quartz tubing was fitted over each thimble and lengths of resistance wire were coiled around these. Sufficient current was passed through these wires to heat the quartz to a dull red heat. When the pressure of hydrogen around the thimbles was maintained at atmospheric pressure the system took about an hour to fill to a pressure of about 60 mm Hg. Further purification of the hydrogen in the system was not attempted.



Fig(3.4) Dynode circuit : 6097B type 6097B.

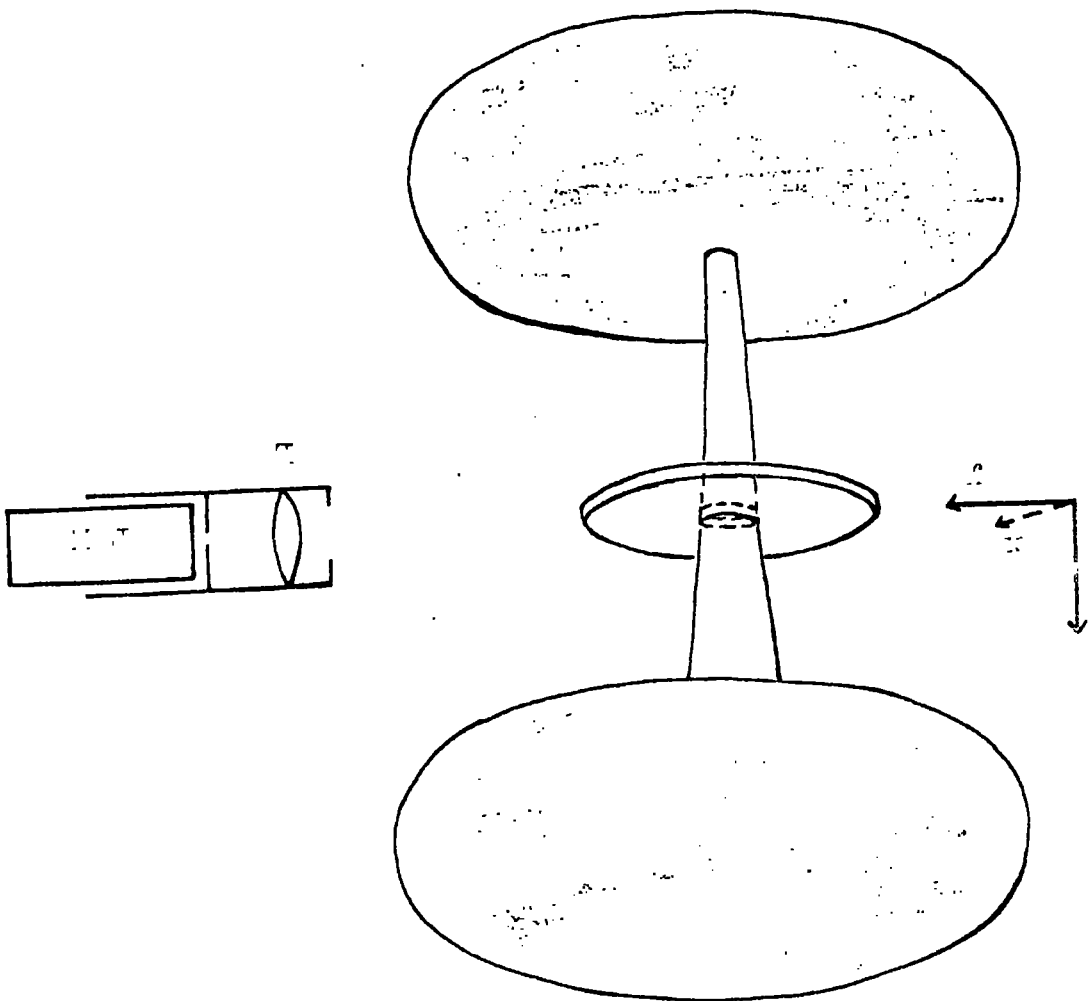
The system could also be filled from flasks of spectroscopically pure nitrogen supplied by the British Oxygen Company.

3.4 The photomultiplier

The photomultiplier was an E.M.I. type 6097B with a Venetian-blind-type dynode arrangement. The photo-cathode material was an antimony-caesium compound which showed a maximum sensitivity at a wavelength of about $4,300\overset{\circ}{\text{A}}$. Sufficient photomultiplier gain was obtained by operating with an overall voltage of 1500 volts; the dynode circuit is shown in Fig. (3.4). The useful cathode area was reduced to about 1 cm^2 in the centre of the photo-cathode to reduce the time spread of a pulse of electrons arriving at the anode. Under these operating conditions the manufacturers state that the time spread of anode pulses is less than $2 \cdot 10^{-8}$ second. The time constant of the anode circuit was calculated to be $2 \cdot 10^{-9}$ second; less than the time spread of the pulses.

In order that the electric field between the electrodes might remain uniform, Bruce⁽²⁷⁾ showed that earthed conductors must not be positioned within four gap spacings of the electrodes. The outer casing of the photomultiplier was in fact some 14 cms from the edges of the electrodes. This is twice the corresponding distance in the smaller test system, (see section 3.6.1), and led to a reduction by a factor four of the light intensity collected. Further reduction of the collected light intensity to meet Bruce's condition was not acceptable, and a compromise

FIG(3.5) Diagram to indicate the field of view of the photomultiplier; the distance between the lens and the central electrode axis was 22.7 cm.



was made.

An alternative solution would have been to use a large diameter, short-focal-length lens fixed inside the vessel, and to traverse the photomultiplier. This method however has the serious disadvantage that light from either end of the electrode gap would follow different paths through the lens to the photomultiplier. An accurate picture of the ionization in the gap could only be built up if the transmission coefficient of the lens for different incident angles was constant, or unless a difficult calibration was made. Also a slanting view of the avalanche would be obtained. In view of these drawbacks, and other practical difficulties in mounting the lens, this method was not employed.

Fig. (3.5) shows the photomultiplier and the arrangement used for focussing the light from the discharge onto the photocathode. Light was collected from a 6 mm thick disc lying in a plane perpendicular to the central electrode axis, (z-axis). It would have been preferable to measure the light signals emitted from a narrower section in the gas, however a 6 mm wide slice was necessary to obtain appreciable signals from the photomultiplier. The slit dimensions were such that the field of view and the depth of focus of the lens extended over more than the flat sections of the electrodes along the other two axes, (x and y). At the gas pressures used, (~ 60 mm Hg), diffusive motion of the electrons within a swarm caused the dimensions of the swarm

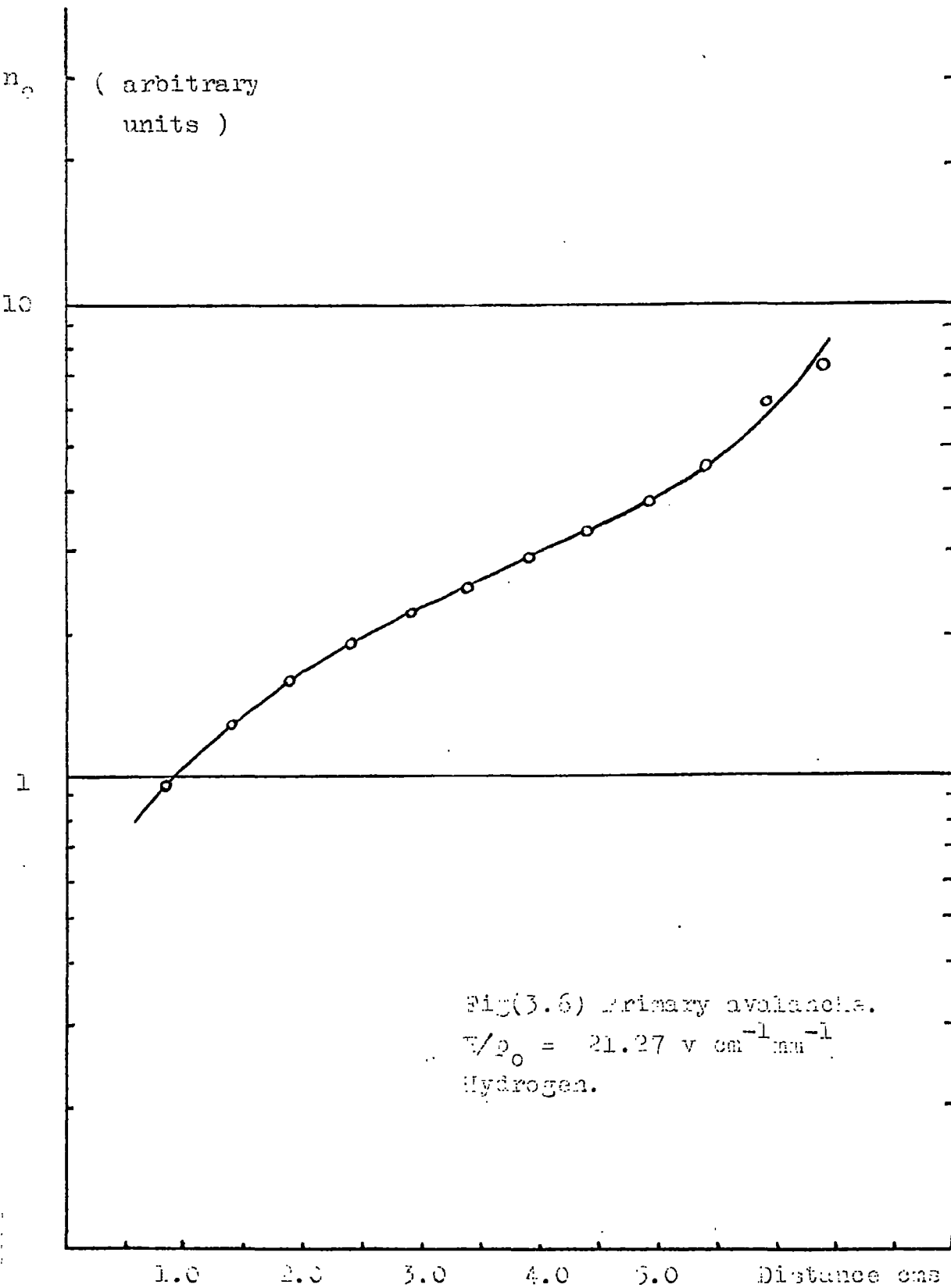
to increase as the swarm drifted from cathode to anode. It was therefore necessary to ensure that in the measurements of the electron number, that electrons did not diffuse radially out of the field of view of the photomultiplier. In general, electrons in the primary swarms were contained within a tube of 1-2 cms radius, and were thus well in focus.

The photomultiplier was clamped into a cradle which could be traversed along the z-axis and which had a 10 cm travel horizontally along the x-axis. The cell and the photomultiplier mounting were covered by a large light-tight box which fitted onto the bench. This box had a matt black finish inside, while the controls for moving the photomultiplier and for counting the number of drive shaft revolutions were mounted under the bench.

3.5 The oscilloscope and film measurements

The signals from the photomultiplier were led directly into a Tektronix type 551 dual beam oscilloscope. This oscilloscope had a maximum sweep speed of 0.02 $\mu\text{sec}/\text{cm}$, and was used in conjunction with an L type pre-amplifier plug-in unit. The rise time of the combined unit was 0.012 μsec , and the oscilloscope sweep was triggered externally from the electron source.

An Exa I 35 mm camera with an f 2.8 lens was adapted to fit the oscilloscope. Ilford HP3 film was used to record the traces, and this was processed in PQ Universal developer at 13°C. This low developer temperature was found to produce a greater degree



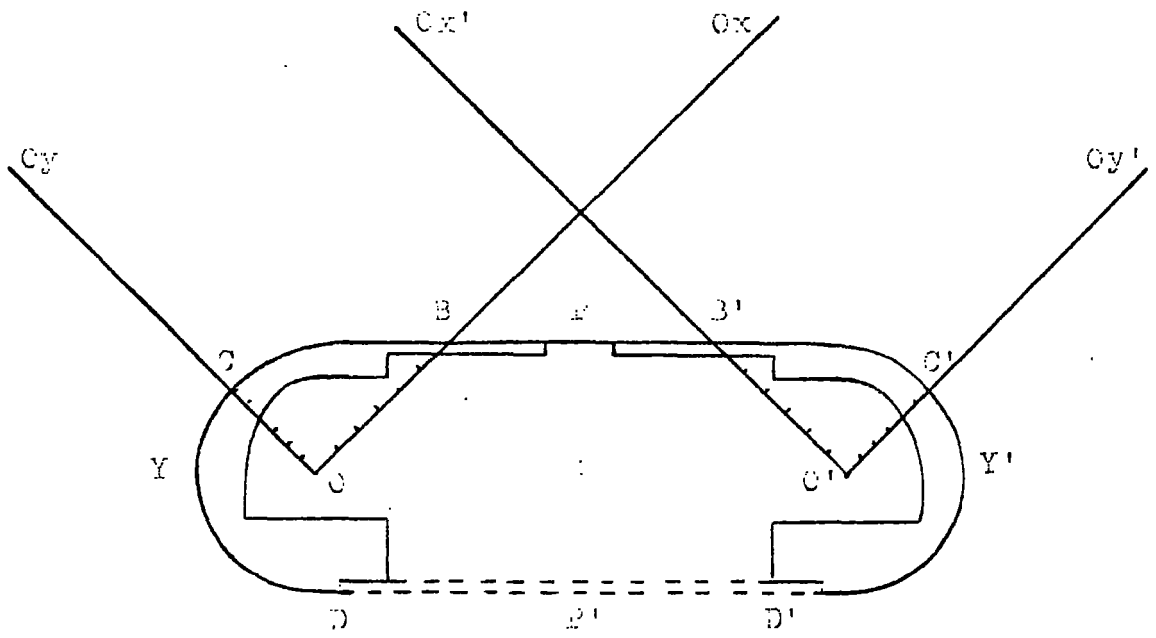
degree of contrast in the film. Using an enlarger, the films were projected onto graph paper and the shape of the signal traced out. Time delay and amplitude measurements could then be read directly, while the area under the pulse was measured using an Albrit planimeter.

3.6 The electrodes

3.6.1 Test electrodes

Exploratory experiments were carried out using the small test system to measure the amplification of low number density electron swarms drifting across an electrode gap. The steel electrodes used formed a 6 cm gap, and had an overall diameter of 9 cm. The edges of these electrodes were curved, but as the electrode depth was only 1 cm, the curvature at the edges was rather abrupt.

Fig. (3.6) is a semi-logarithmic plot showing the increase in the number of electrons contained in a section of a swarm as it moves across the electrode gap. It is seen that the amplification is not a linear function of distance, but that the slope of the graph (equal to the ionization coefficient α), becomes higher near the electrodes. At first this effect was thought to be caused by the reflection of light from the curved edges of the electrodes, into the photomultiplier. However, when the measurements were repeated, this time with the electrode surfaces blackened to prevent reflections, identical plots were obtained. The upcurving exhibited in the plot therefore, was



BB'	YY'	PP'	DD'
2.77"	3.00"	2.59"	5.54"

Fig(3.7) The electrode profile.

Thickness of the cathode surface at P - 0.004"

not caused by reflected light from the anode entering the photomultiplier.

The ionization coefficient α is particularly sensitive to changes in the reduced field E/p , for values of $E/p \sim 20$. It was concluded therefore, that the observed increase in α near the electrodes was produced by enhanced electric fields; and that the electrodes were not producing a uniform field in the gap, but one which was distorted in the vicinity of the electrodes

3.6.2 The present electrodes

The bright steel electrodes used in the present experiment were machined to a Bruce-Stevenson profile. Bruce⁽²⁷⁾ has performed a comprehensive series of experiments to investigate the uniformity of the electric fields produced by these electrodes. The electrodes were made to dimensions for use at a maximum gap spacing of 7.04 cms although it is concluded from Bruce's results that no appreciable distortion can be detected until a spacing of 8.2 cms is reached. Bruce states that the contour of the electrodes was designed graphically after consideration of data obtained from sphere gap measurements at small gap lengths. The contour is in three parts each merging tangentially into the next, namely:

a) a flat surface BB' of diameter not less than the maximum gap spacing at which the electrodes will be used.

b) a portion BC of gradually increasing curvature to minimise

FIG. 3. (1) Inside supports.

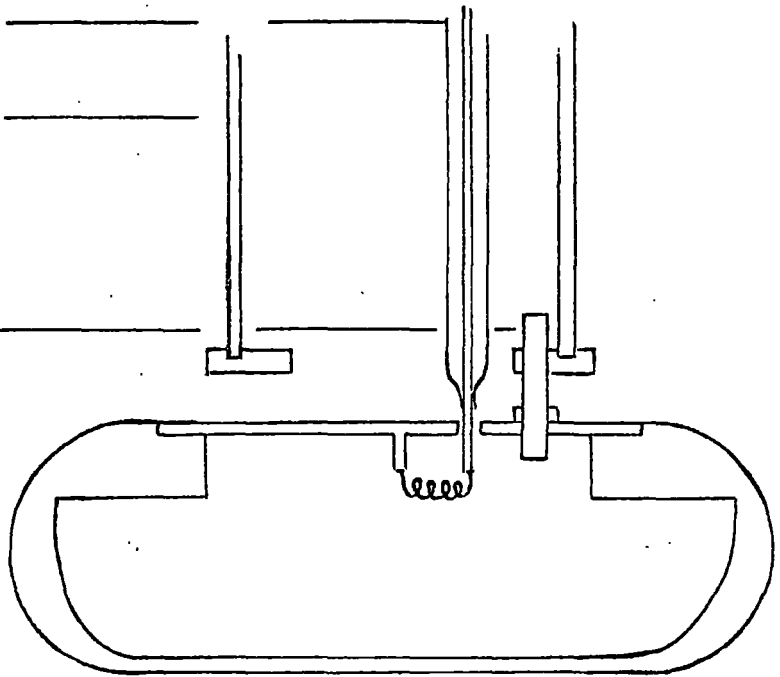
inside of Pyrex tube.

inside support lead

Pyrex tube

steel rod

for electrode



edge effects, the initial radius of curvature at B being not less than ten times the minimum gap spacing.

c) a circular portion CD to complete the edge.

The electrode surface is formed by the revolution of the curve PBCD about the vertical axis through P, (Fig. 3.7).

The electrodes were machined to a rough approximation of the contour and then polished until a template cut to the contour PBCD fitted well. Great care was taken to merge the electrode flat into the curve BC.

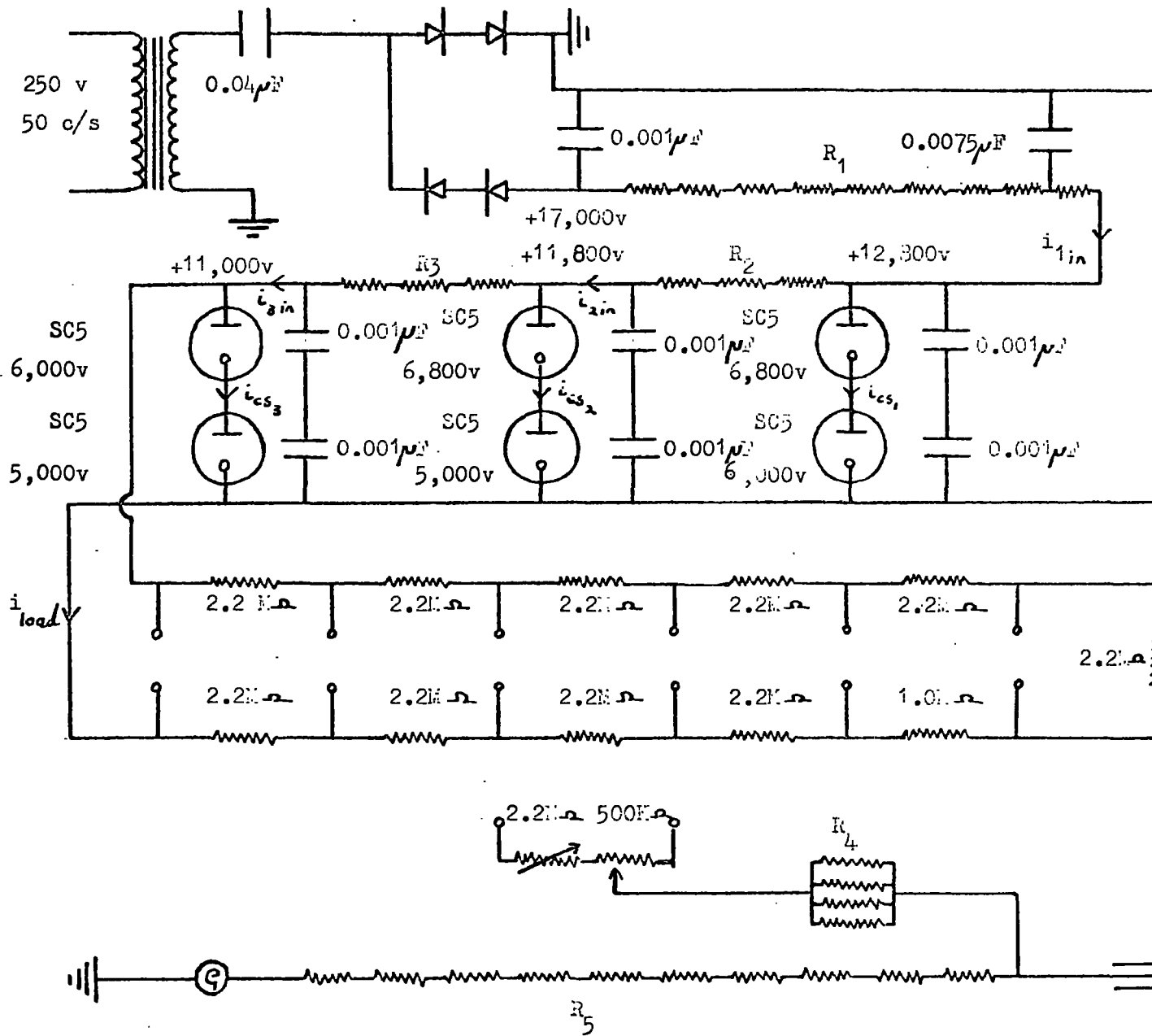
3.6.3 Electrode supports

The anode, the lower electrode in the cell was supported on the base plate by a glass tube insulator. Provision was made to level the electrode surface, by means of three threaded rods, Fig. (3.8). Several sets of rods were made of varying lengths, so that the electrode separation was variable from 4-8 cms.

The cathode was suspended from the upper end plate by a stainless steel cylinder, and the electrode surface lay in a plane parallel to the end plate. These end plates and the cathode were all maintained at earth potential.

3.7 The high voltage supply

It is known that space charges modify the development of an electron avalanche only in the last stages of growth before the electrode gap breaks down. To study these effects while avoiding breakdown it is necessary to maintain an anode voltage



Fig(3.9) The high voltage supply.

just below the sparking potential. A stabilized high voltage source is therefore required which has no appreciable ripple superimposed on the dc level, and which does not drift appreciably during the time required for an experimental run. A supply meeting these requirements was designed and the circuit is shown in Fig. (3.9). The output from the mains-supplied transformer was rectified, doubled, and then smoothed using a condenser bank. This dc voltage was then stabilized against mains fluctuations by three stages of corona stabilizers. Tests showed that a 7% mains fluctuation produced a 0.07% variation in output voltage. This degree of stability was achieved by ensuring that the corona stabilizers operated at the correct current ratings. The choice of the size and stability of the resistors R_1 , R_2 and R_3 was therefore very important. They consisted of chains of 1W Oxide resistors, which operated at the given current ratings gave a stability of better than 2%. Calculated values of the currents flowing in the supply are shown in Table (1), together with the variations produced by a $\pm 7\%$ fluctuation in the mains supply. It is noted that a variation of this order was never approached during the experiments. The supply was continuously variable from 1 - 11kV and the maximum output current was 50 μ A. Voltage measurements were made using a Scalamp galvanometer and a chain of 1% cracked carbon resistors and both the current sensitivity of the galvanometer and the resistance of the chain were determined in the laboratory.

R_1 - 9 x 333K Ω , 1W Oxide resistors in series: - 2.97M Ω .

R_2 - 3 x 333K Ω , 1W Oxide resistors in series: - 0.98M Ω .

R_3 - 3 x 333K Ω , 1W Oxide resistors in series: - 1.04M Ω .

R_4 - 4 x 100M Ω , 1% cracked carbon resistors in parallel: - 25M Ω .

R_5 - 10 x 100M Ω , 1% cracked carbon resistors in series: - 10⁹ Ω .

The resistors comprising R_1 , R_2 , and R_3 , were operated so as to give a dissipation of 0.68W per resistor; giving a drift stability of better than 2%.

The max. and min. values shown in the table below are the calculated current variations produced by a mains fluctuation of $\pm 7\%$. The currents are given in μA .

		Mean	Max.	Min.		Mean	Max.	Min.
$R_1 =$ 2.96M	i_{cs_1}	400	710	121	i_{in_1}	1420	1820	1050
$R_2 =$ 0.98M	i_{cs_2}	250	333	152	i_{in_2}	1020	1110	929
$R_3 =$ 1.04M	i_{cs_3}	250	257	243	i_{in_3}	770	777	763

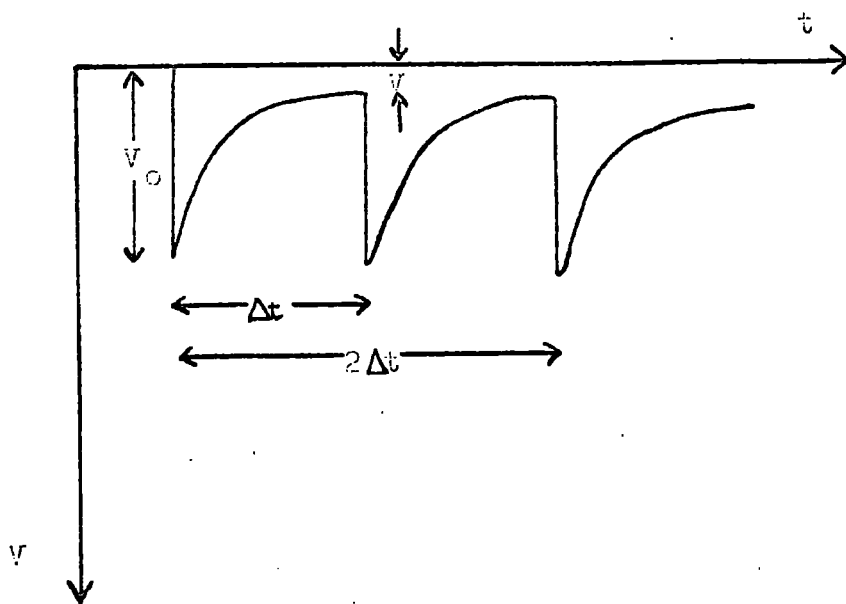
$$i_{load} = 520\mu A.$$

Table (1).

It was necessary to introduce a high value resistor into the anode lead to prevent overloading of the supply when the gap broke down. This also served to limit the gas current, high values of which could produce gas impurities and burning of the electrodes. However the introduction of this resistor meant that the movement of charge in the electrode gap would produce an induced potential difference across the resistor. As has been pointed out this forms the basis of one method of studying electron motion in electrode gaps. It is therefore necessary to show that in the present experiment the reduction of the applied field so caused is not a significant factor in determining the development of the avalanche. In the present experiments the maximum number of charged particles moving in the gap during an electron transit time was of the order 10^8 . The gap capacitance and associated stray capacitance was of the order 30 pF, so the reduction in the applied anode voltage was

$$\begin{aligned}
 V &= n.e / C \\
 &= \frac{10^8 \times 1.6 \times 10^{-19}}{30 \times 10^{-12}} \text{ volts} \\
 &= 0.53 \text{ volts, } (\Delta E = 0.53/d \text{ volt/cm.})
 \end{aligned}$$

The time constant of the anode circuit RC was 0.75m sec, while the maximum source repetition rate was 1,000 swarms/sec., i.e. a period of 1m sec. The repetition rate was kept below this value to ensure that the positive ions created in the passage of an



Fig(3.11) Fluctuation in anode voltage.

electron avalanche had time to drift out of the electrode gap before the appearance of the next avalanche.

It is now necessary to show that the sum of the reductions in anode voltage by individual avalanches is that of a converging series of terms. In Fig. (3.11) V_0 is the reduction in anode voltage after one avalanche has crossed the gap; V is the reduction at a time t . The transit time of an avalanche was approximately 10^{-6} second, compared with the source period Δt of 10^{-3} second. After a time Δt ,

$$V = V_0 e^{-\Delta t/RC}$$

and after the second avalanche has crossed the gap

$$V = V_0 (1 + e^{-\Delta t/RC}).$$

The corresponding voltage reductions after a time $2\Delta t$ are

$$V = (V_0(1 + e^{-\Delta t/RC})) e^{-\Delta t/RC}$$

and

$$V = V_0 + (V_0(1 + e^{-\Delta t/RC}))e^{-\Delta t/RC}$$

and after a time $3\Delta t$

$$V = (V_0 + (V_0(1 + e^{-\Delta t/RC}))e^{-\Delta t/RC})e^{-\Delta t/RC}$$

$$V = V_0 + (V_0 + (V_0(1 + e^{-\Delta t/RC}))e^{-\Delta t/RC})e^{-\Delta t/RC}.$$

The sum to infinity of this series is the sum of a geometric series of constant multiple $e^{-\Delta t/RC}$;

$$\text{sum} = \frac{V_0 \cdot e^{-\Delta t/RC}}{1 - e^{-\Delta t/RC}}$$

$$\text{sum} = 0.20 \text{ volts,}$$

a change in E/p of $0.003 \text{ V cm}^{-1} \text{ mm}^{-1}$.

It may therefore be concluded that the overall effect of successive avalanches is a very small reduction of the anode voltage, and that the reduction caused by a single avalanche is not a significant factor.

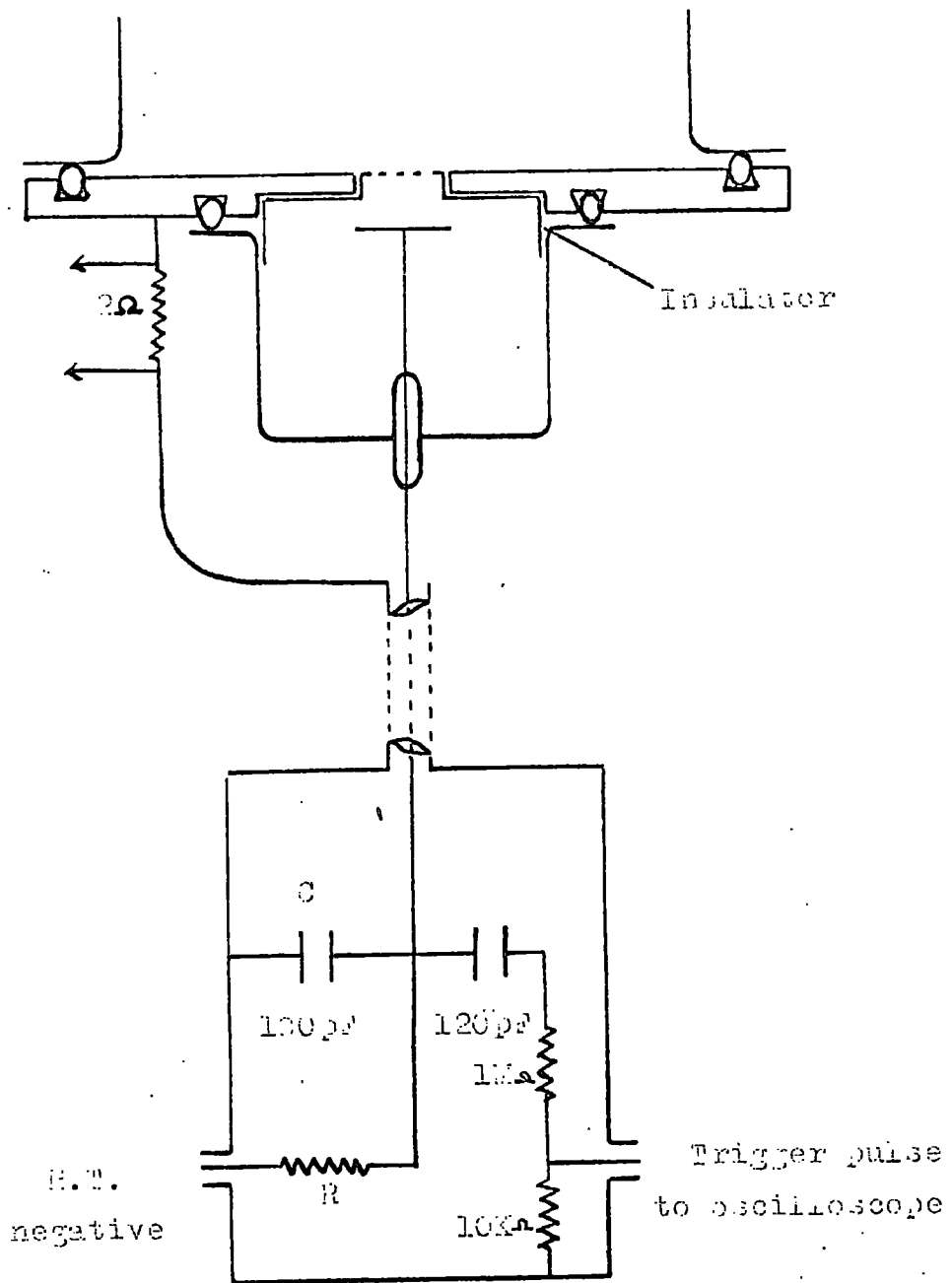
CHAPTER 4

THE ELECTRON SOURCE

It was required for the purposes of the present experiment that the electron source should be capable of injecting variable density electron swarms into the electrode gap with a repetition rate of upto 1,000 swarms per second. In addition the electrons, $\sim 5 \times 10^6$ per swarm, had to be contained in a swarm whose dimensions were small compared with the gap dimensions. It was also necessary to ensure that the electric fields associated with the source did not distort the uniform field applied in the drift section. The gas pressure in the system was such that the electron mean free path was very small, so that electrons moving even a short distance suffered a large number of collisions with gas molecules. Thus once the electron swarms had moved into the drift region they came into equilibrium with the field very quickly.

4.1 Previous work

Breare has shown the impracticability of electron gating methods at pressures exceeding 20 mm Hg, and has introduced a new method for the injection of electrons. The primary reason for the unsuitability of gating methods at higher gas pressures is the increased number of collisions which the electrons make in transit between the electrode grids. With the result that there is a tendency for the electrons which are in equilibrium with the



Fig(4.1) Details of the electron source used by Breare.

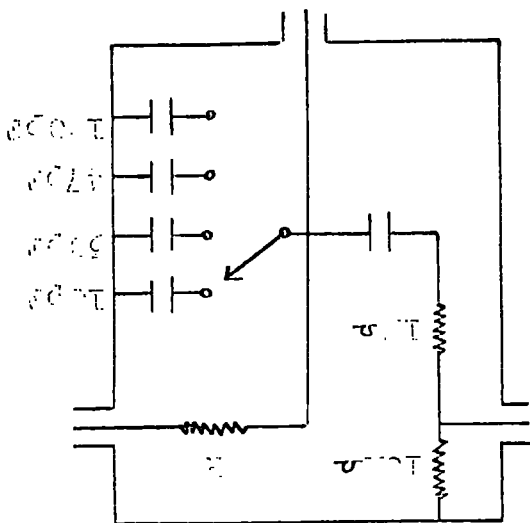
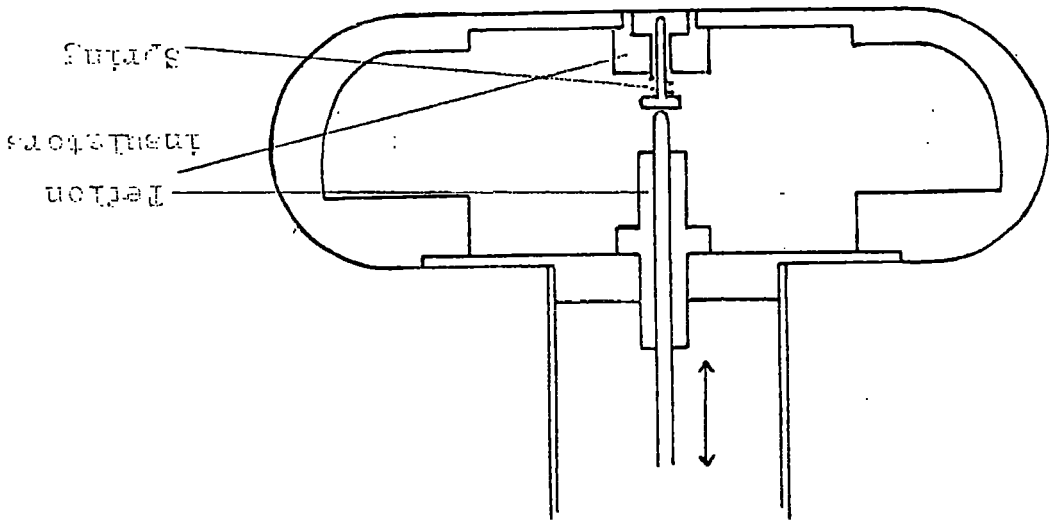
field, to drift along the field lines into the cathode surface rather than through the holes.

In his high pressure experiments, Breare found that a form of relaxation oscillator gave sufficient electron emission, Fig. (4.1). A condenser C was connected across a plane-parallel gap of separation about 5 mm, comprising a 1 cm nickel disc, and an anode, which was the cathode of the drift section. The voltage and charge on the condenser were built up slowly via the leak R, until breakdown occurred across the gap. At pressures above 20 mm Hg formative breakdown times are very small, and the condenser almost completely discharged is less than 5×10^{-7} second. The voltage developed across a 2Ω resistor, placed between the earthed side of the capacitor and the cathode, indicated the current in the source. Currents of several amperes flowed during the discharge, a small fraction of which passed into the drift area through small pin holes in the cathode. Variation of the discharge repetition rate was effected by altering the voltage applied to the leak resistor R. The oscilloscope time base was triggered from a small pulse produced from the rapid discharge of C; this also acted as a time-zero marker.

4.2 The present source

The principle of operation of the source was the same as that used in Breare's experiments; however, it was possible to inject swarms into the drift space with an increased number density. The following sections describe the measurements and

Figure 2. Details of the present electron source.



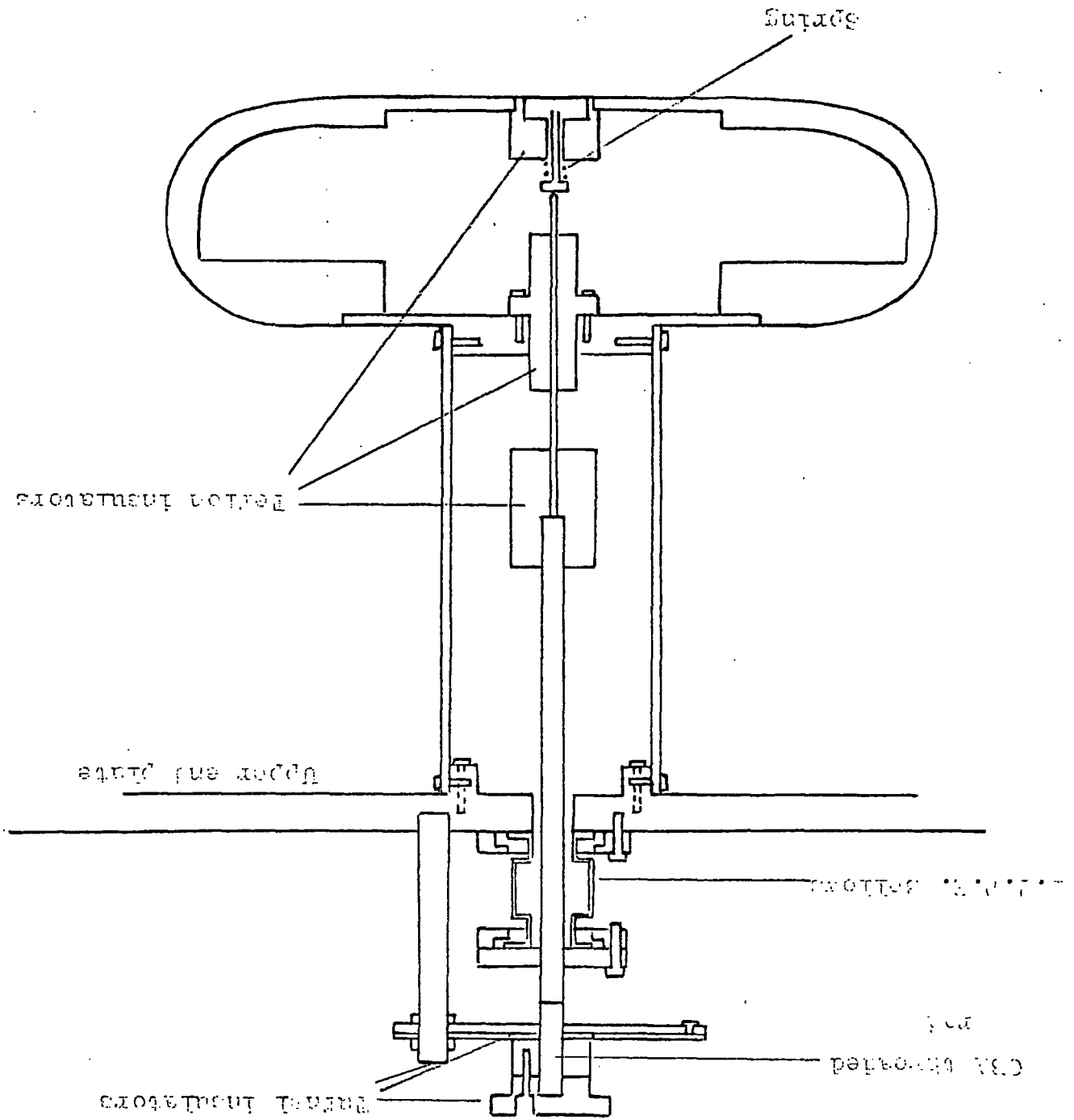
changes made in the development of the source.

Figs. (4.2 and 4.3) show the source used in the present experiment. A discharge was struck between the rounded, polished end of a silver steel rod and the centre of the cathode in which four holes were drilled. The diameter of the holes was 0.01 cm (4 thou'), and the thickness of the cathode surface at this point was also 0.01 cm, (4 thou'). A gap of this type gave a very stable swarm repetition rate, and also ensured that the discharge actually occurred behind the holes in the cathode. To achieve a constant repetition rate it is essential that the metal in, and close to, the gap is clean, and free from impurities; if it is not, large fluctuations in the discharge frequency occur. It was in fact necessary to repolish the wire with emery cloth between experimental runs to maintain this stability, and it is noted that tungsten rod is preferable in this respect to silver steel.

The use of ring-insulators to limit the area on the under-side of the cathode to which the discharge might strike, was abandoned because of the instability which they caused. It was suspected that this instability in the repetition rate was caused by sputtering of the metal from the point onto the insulator, resulting in tracking across the surface.

It was found possible to vary the number of electrons per swarm, without varying the swarm dimensions, by changing the point-plane separation. Provision was made to do this using a P.T.F.E. flexible bellows Fig. (4.3), enabling the gap separation

FIG. 4. (3) The cathode assembly.



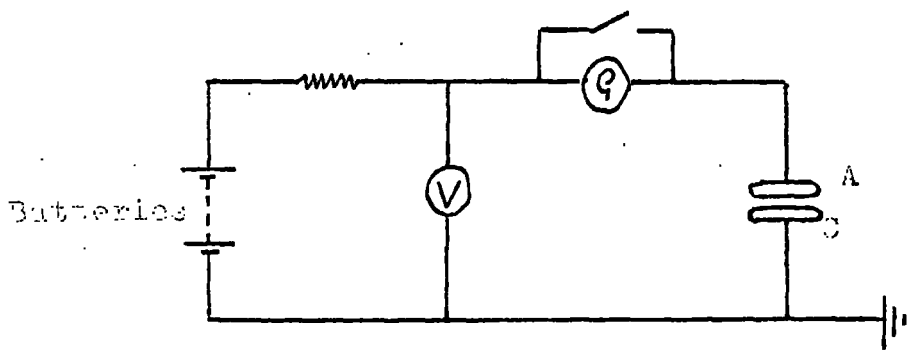
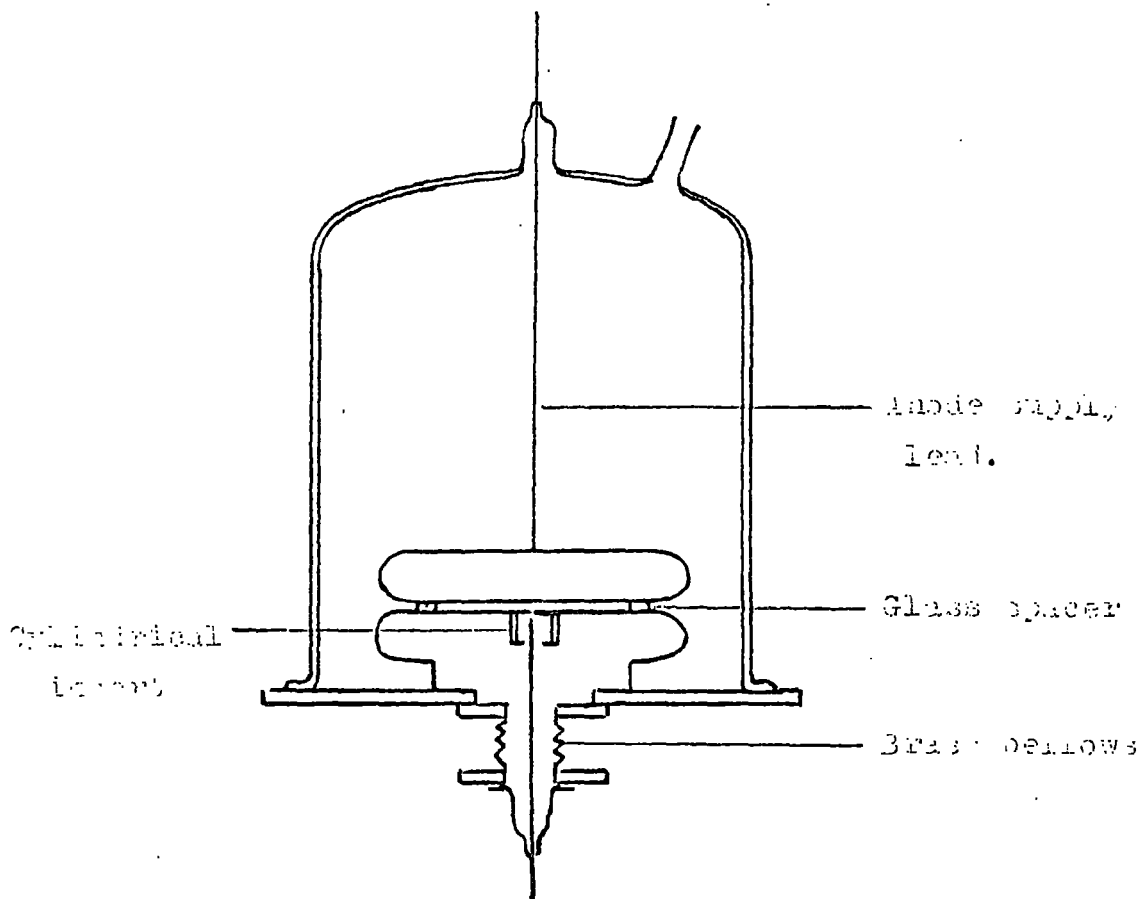
to be varied in units of 0.0025 cm (1 thou'). It was found that the number of electrons per swarm passing into the drift section increased as the point-plane separation was reduced.

The number of electrons per swarm could also be varied by discharging different condensers through the gap. Unfortunately capacitances of greater than 10pF had finite inductances and the time taken to discharge these condensers increased, thus increasing the physical dimensions of the swarm without any significant increase in the number density.

4.3 Measurements on the emission of the source

Measurements of the emission of various source configurations were made using the small test apparatus mentioned earlier, and shown in Fig. (4.4). The object of these experiments was primarily to determine the number of electrons per swarm entering the drift section through holes in the cathode as a function of the applied field strength E in the plane-parallel gap, the state of the source (wire-plate spacing, wire voltage, hole size, gas pressure, etc.) being kept constant. In subsequent experiments these listed parameters were changed one at a time to determine conditions under which satisfactory emission occurred; i.e. the emission of sufficiently high-number density swarms.

To this end a plane-parallel gap spacing of about 1 mm was used, Fig. (4.4). So that during their transit of this gap, no appreciable multiplication of the swarm electrons occurred by collision ionization. In addition this spacing allowed the



Fig(4.3) Test cell and associated circuit used to measure the surface emission.

$n \times 10^7$
electrons
per swarm

(13, 4.5)

0.145 cm

0.120 cm

0.063 cm

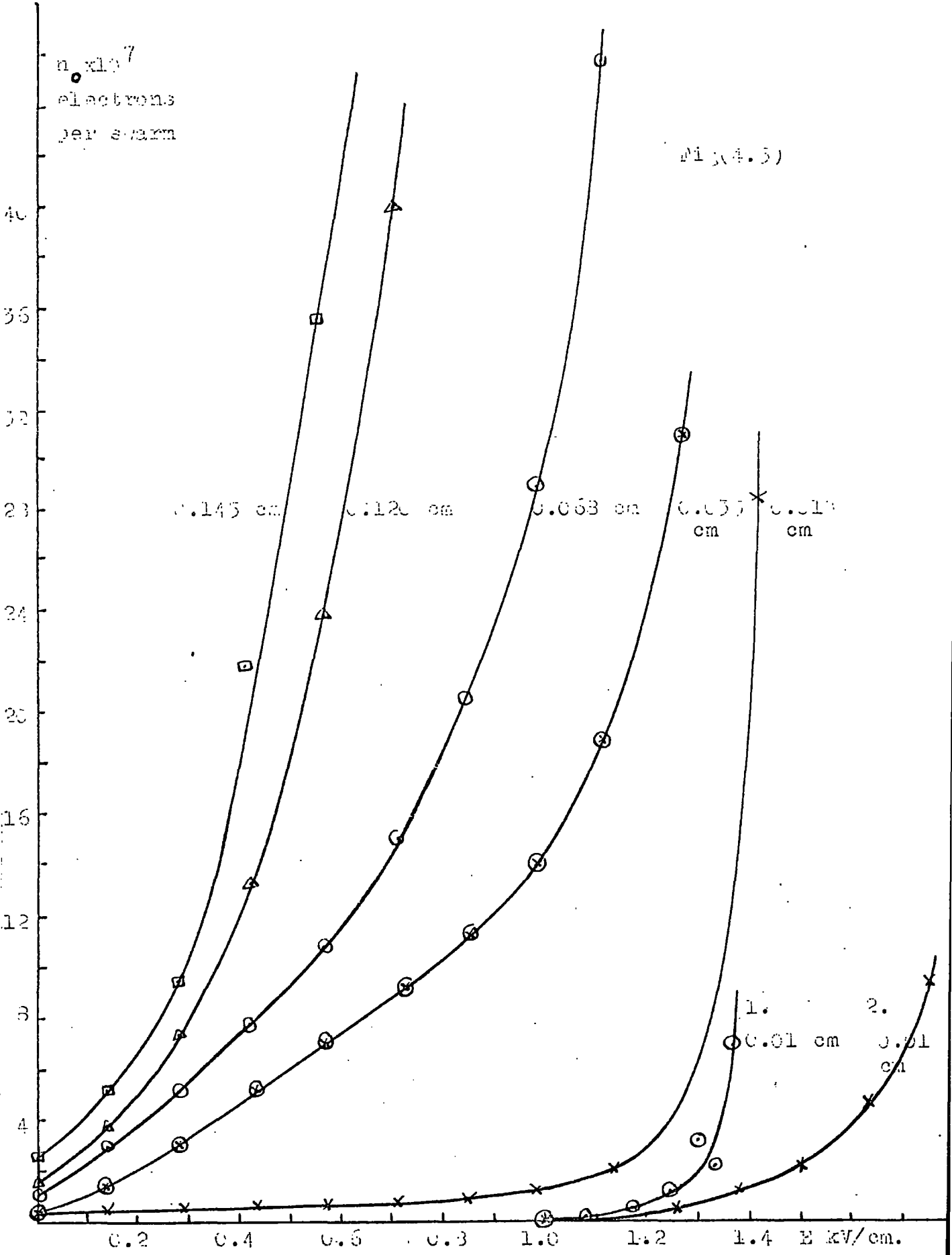
0.055 cm

0.018 cm

1. 0.01 cm

2. 0.01 cm

0.2 0.4 0.6 0.8 1.0 1.2 1.4 E kV/cm.



source emission to be studied over a considerable range of the parameter E/p without the occurrence of breakdown, (upto $E/p \sim 160 \text{ V cm}^{-1} \text{ mm}^{-1}$).

4.3.1 Effect of hole size

A number of cylindrical inserts were made which rested in the cathode of the test apparatus. Each cylinder had a different diameter hole drilled in the centre of the closed end, and Fig. (4.5) shows the number of electrons per swarm as a function of the applied field E in the plane-parallel gap for different hole diameters.

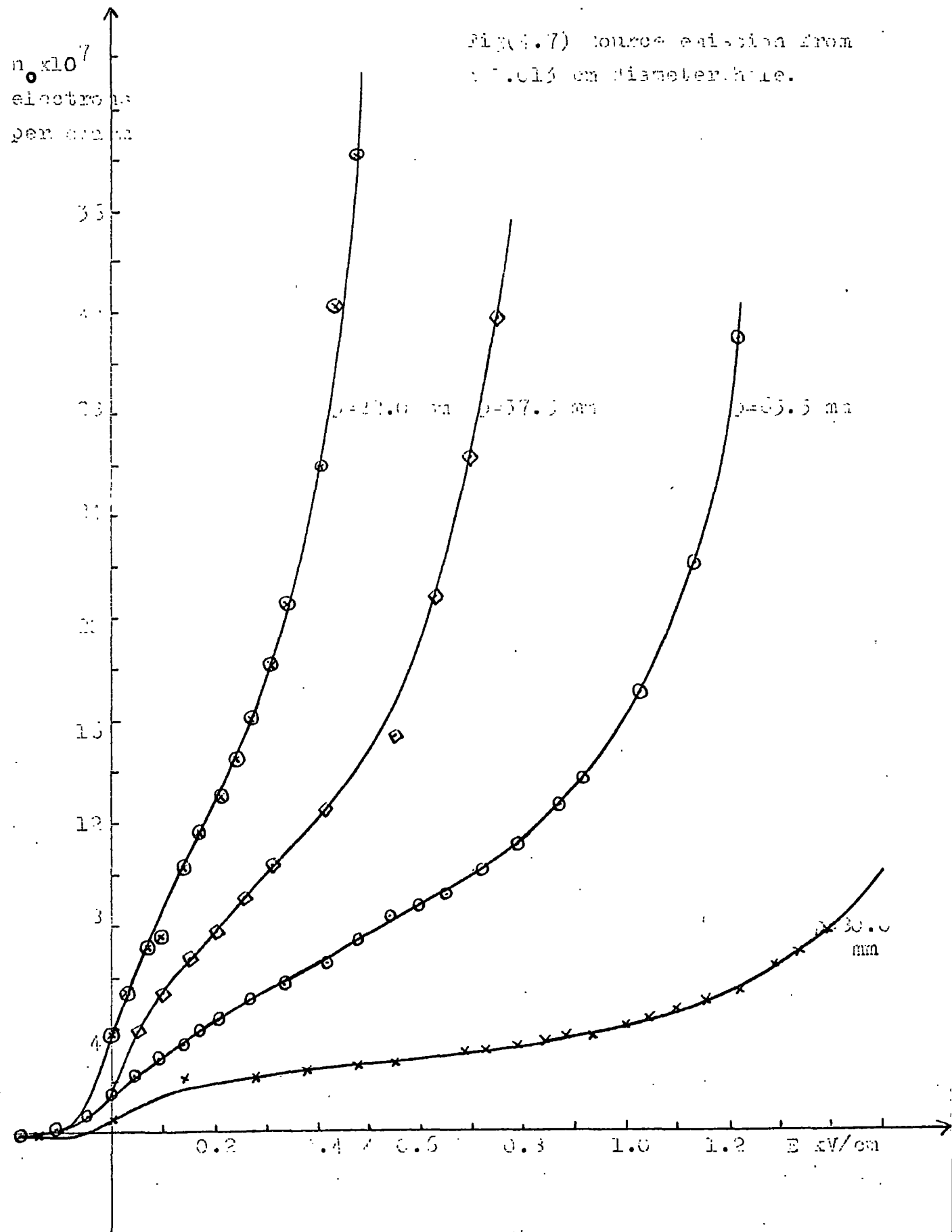
It is noted that there is a basic difference in form between the characteristics for the 0.01 cm hole and the other curves, in that the number of electrons per swarm does not show a marked dependence upon the applied field until the onset of ionization. In the case of the larger diameter holes it is probable that there is some penetration into the hole by the applied field, which results in more electrons drifting into the plane-parallel gap rather than into the cathode. Values for the applied field strength in this section of the graph are upto 1/5th of the field strength in the point-plane gap. However examination of the electron swarms with the photomultiplier and a 6 cm gap spacing showed that although the electron number per swarm for the larger diameter holes was increased, there was no significant increase in the important parameter, the number density. The increase in

electron number per swarm was found to be brought about by an increase in the time period over which the electrons emerged from the cathode; in general for the larger diameter holes, the swarms had a roughly spherical head which was followed by a long electron tail. Therefore because of the need for swarms with a high electron concentration and also because of the less-marked dependence of the emission on the applied field E , it was decided to use the 0.01 cm holes. Experiments were also performed with several holes in the cathode, but no significant change in the voltage-current characteristics resulted and the final hole configuration used was one of four 0.01 cm holes drilled close together in the centre of the cathode.

As it was necessary to disturb the point-plane arrangement in order to interchange the cylindrical inserts, it was not possible to reproduce the exact conditions for the point-plane discharge, and as a result no sensible relationship was observed between the number of electrons per swarm as a function of the area of the hole. The discharge conditions were not reproducible in this test arrangement for two reasons: firstly the point-plane separations involved are extremely small, a few thousandths of an inch; and second, observations of such discharges (Bandel⁽²⁸⁾) has shown that successive discharges, even when struck in the same gap do not necessarily occur from the same point on the tip of the wire.

Curves marked 1 and 2 in Fig. (4.5) were obtained from a point-plane source with a Wehnelt focussing cylinder, Fig. (4.6).

Fig. 4.7) source existing from
1.013 cm diameter hole.



The negative potential on the cylinder was adjusted until a maximum in the current flowing through the galvanometer was obtained; that is until the discharge was focussed to an area behind the hole in the electrode. However the introduction of the cylinder led to an increase in the path length which the electrons had to traverse to enter the main electrode gap, and the final emission was in fact less than in the unfocussed case.

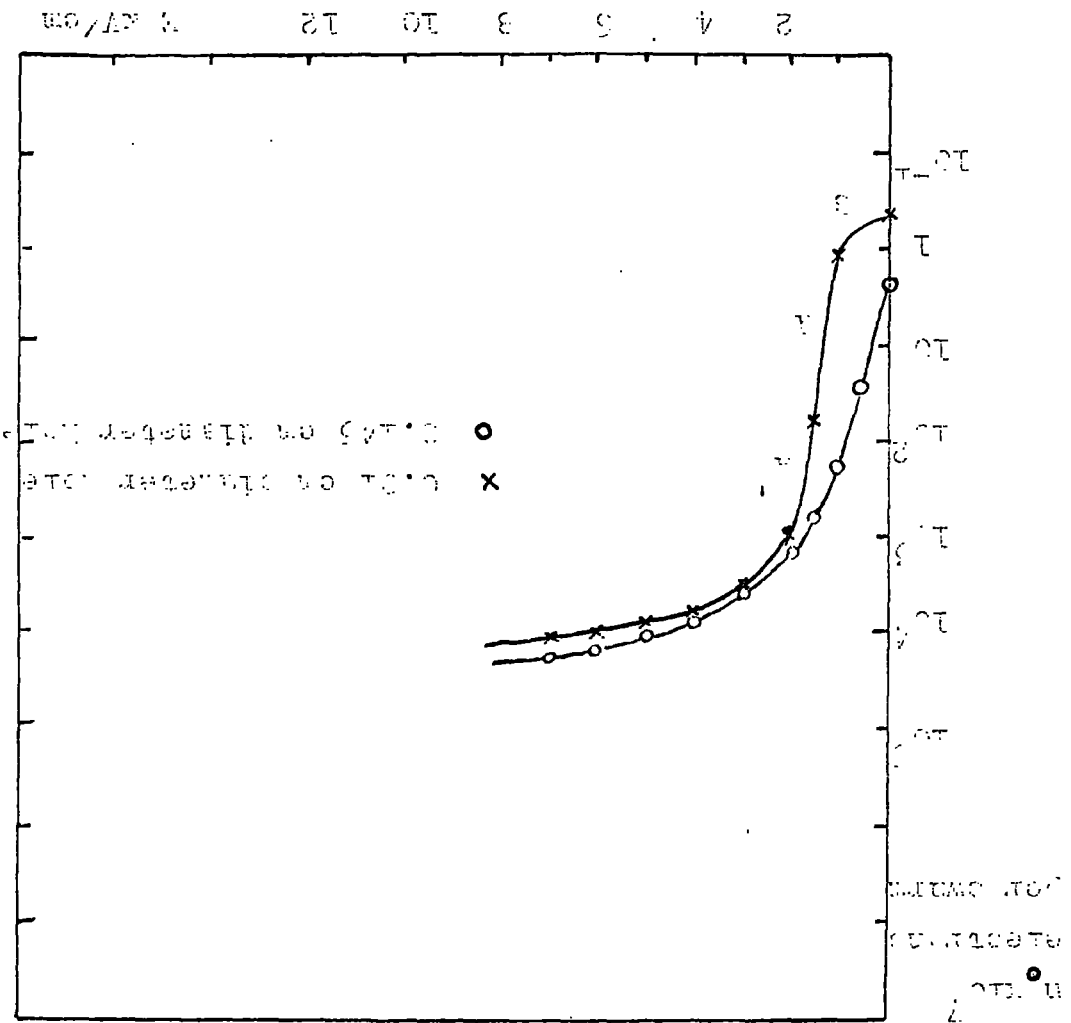
4.3.2 Effect of gas pressure

Fig. (4.7) shows the emission into the gap as a function of gas pressure and the applied voltage for a 0.013 cm hole. The decrease in emission into the drift section with increasing pressure is clearly seen. After consideration of the pressure dependence of the emission, it was decided that the working pressure should be about 60 mm Hg. This pressure ensured a reasonable emission, while reducing the spread by diffusion of the electrons in the swarm during its transit of the main electrode gap.

4.3.3 Effect of a wide range of applied field strengths

Fig. (4.8) shows the emission over a wider range of applied fields. It should however be pointed out here that these field strengths exceed those in the present experiment by upto a factor 7. It is however interesting to compare these curves with the current voltage characteristics of negative point-planes obtained by Bandel⁽²⁸⁾ and also by Weessler⁽²⁹⁾. In their experiments, the current collected by a plane from an irradiated negative point

of applied fields.
 (Fig. 1.3) Curves obtained over a wide range

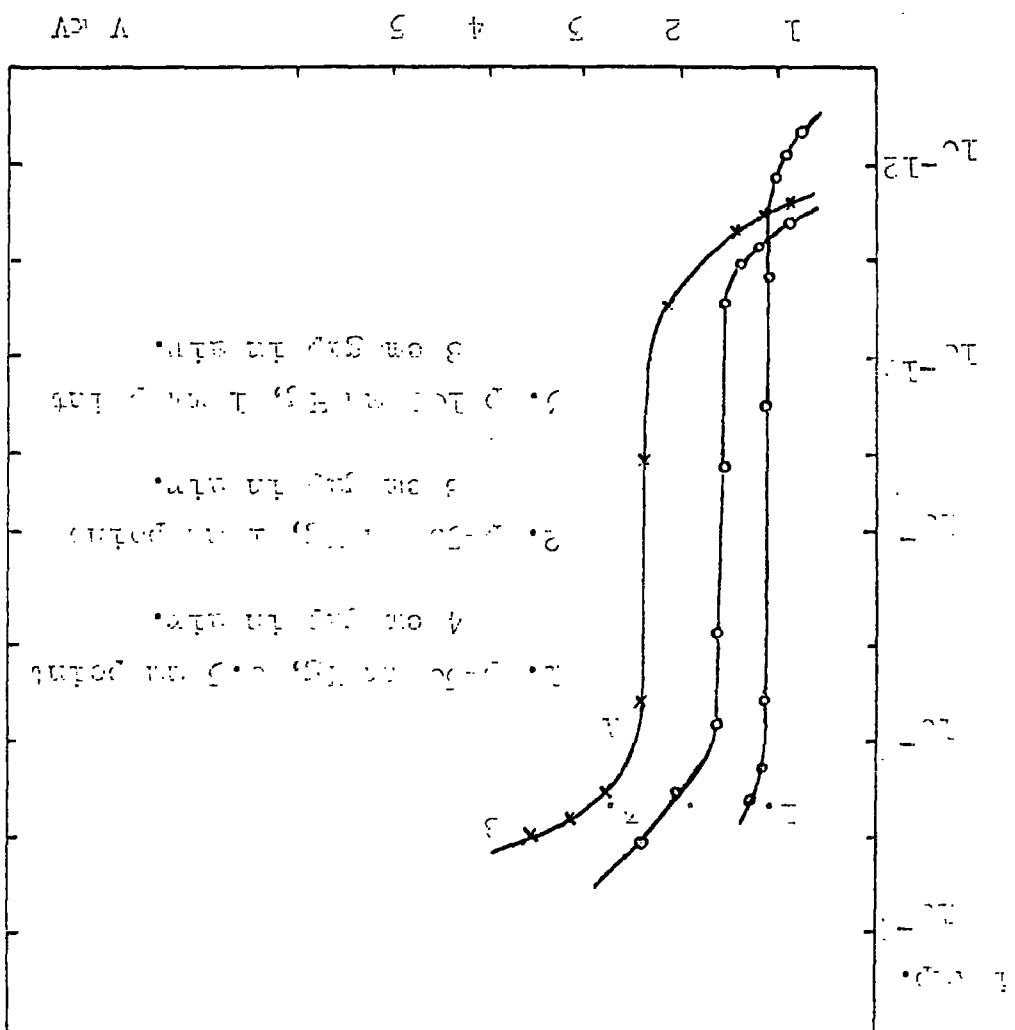


was measured, Fig. (4.9). The results show that as the applied voltage V is increased the current either remains constant or increases slightly over a considerable range of voltage. These currents were attributed to natural ionization in the gas. In the present experiment the initial slow rise in the current is caused by electrons collected from the discharge in the point-plane gap, after passing through the holes in the plane. The initial emission is dependent on the applied fields for the larger diameter holes, but is not as sensitive to the field in the 0.01 cm case.

In Bandel's characteristics, a steep rise in current of several orders of magnitude follows, which is caused by collision processes in the gas. This high rate of ionization is characteristic of point-plane electrode gaps. At still higher voltages a steady rise of current is recorded, and a corona discharge is observed. (Region A-B in Fig. (4.9)).

The characteristics obtained in this experiment (Fig. (4.8)) are seen to follow a very similar trend. It is suggested that in the section of the graph S-A Fig. (4.8), some penetration of the hole by the applied field is occurring, which is pulling electrons from the discharge behind the cathode, through the hole, to be collected by the anode. Evidence to support this view is that an increase in the source repetition rate occurs at the point A' on the characteristic. This indicates a considerable penetration

(5) Location curves for a positive plane electrode geometry (banded) of the applied voltage V for a negative plane,



of the hole by the applied field, for it is known that the source repetition rate is sensitive to the point-plane potential difference.

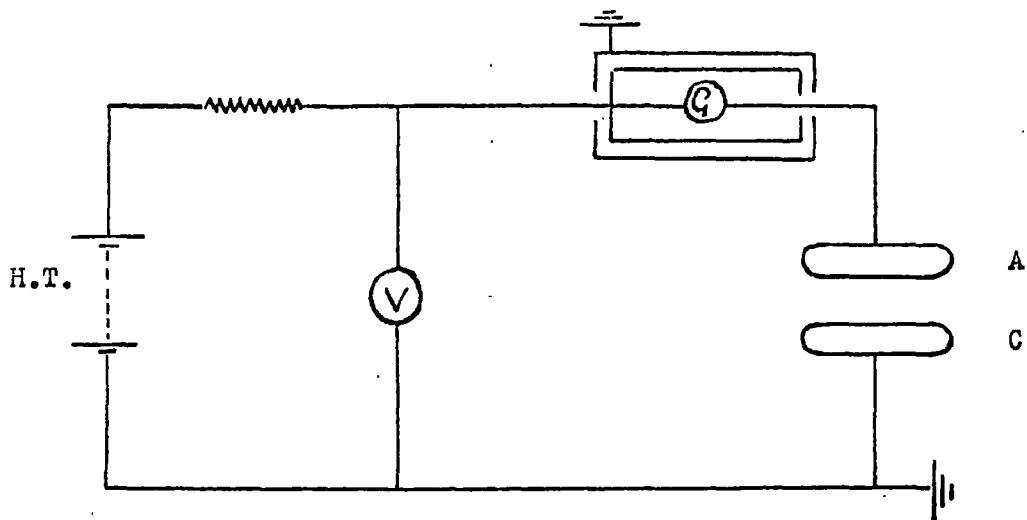
The source repetition rate is determined by:

- i) the time constant RC of the source circuit;
- ii) the -ve HT voltage;
- iii) the sparking potential of the point-plane gap;
- iv) the discharge maintainance potential V_m to which the potential of the wire falls.

If the field penetration of the holes is such that the electric field in point-plane gap is larger than that produced by a wire potential V_m , then the recovery time between discharges will be reduced.

At A' then, the source repetition rate is increased, and it is also noted that at this point on the characteristic the electric field strengths in both gaps are the same order of magnitude. A further increase in the applied voltage to the plane-parallel gap causes a corona discharge to be struck from the point to the upper electrode, through the hole in the cathode.

Consideration of the present experimental conditions, where 5-7 cm drift sections are employed, show that the source is being operated in the region of the up-turn of the characteristic. It is difficult therefore to obtain an accurate estimate of the number of electrons in a swarm entering the drift section because of the sensitivity of the emission to the applied voltage in this



Fig(4.10) Circuit for measurement of the source emission.

region. The following two sections describe two methods used during experimental runs to measure the number of electrons per swarm entering the main electrode gap.

4.4 Source emission at low values of E/p , ($E/p < 3 \text{ v cm}^{-1} \text{ mm}^{-1}$)

Measurements of the number of electrons per swarm entering the drift section were made using the circuit shown in Fig. (4.10), before and after a sequence of oscilloscope photographs. A moving coil galvanometer was connected into the anode supply lead and mounted inside the inner of two metal boxes. The inner box and the galvanometer case were maintained at the anode voltage, while the outer box was earthed. The current flowing in the anode circuit, produced by electron swarms moving across the gap was measured together with the source repetition rate (n_p), while a low value of anode voltage was employed to prevent the occurrence of collision ionization in the drift section. From this information, the number of electrons (n_o) per swarm could be calculated:

$$n_o = \frac{i_a}{n_p \cdot e} .$$

Here e is the electronic charge, and i_a the anode current. The value for n_o thus obtained is that given by the horizontal section of the graph in Fig. (4.5) before the up-turn.

4.5 Source emission at higher values of E/p , ($E/p \approx 25 \text{ v cm}^{-1} \text{ mm}^{-1}$)

Under the operating conditions of the present experiment it is difficult to use the method described in the preceding section because of the high voltages involved. An alternative method was

therefore employed. The motion of charged particles in the electrode gap produces a current $I(t)$ in the anode circuit, and thus a voltage pulse across the anode (limiting) resistor, which is a function of time. This voltage pulse was displayed on the oscilloscope, and using the following relations, values for the number of electrons per swarm entering the gap could be obtained.

If n_0 electrons drift in a plane parallel gap (of width d) under the influence of an electric field ($E_0 = V_0/d$) with a constant velocity v_- , then a current flows during the transit time ($T_- = d/v_-$) of the electrons:

$$I_-(t) = e n_0 / T_-$$

$$= \frac{e n_0 v_-}{d} \quad 0 \leq t \leq T_-.$$

If the number of electrons increases by ionizing collisions with the distance x from the cathode, then the electron component becomes a function of time, where $t = x/v_-$

$$I_-(t) = \frac{e n_-(t)}{T_-} \quad 0 \leq t \leq T_-,$$

and if

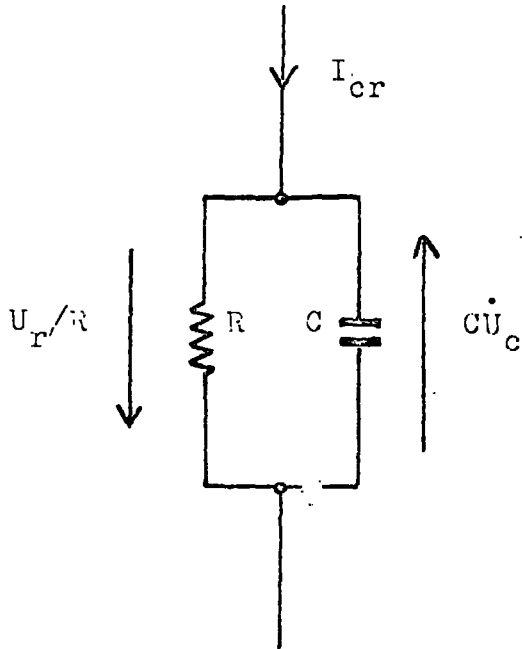
$$n_-(t) = n_0 \exp(\alpha v_- t),$$

then

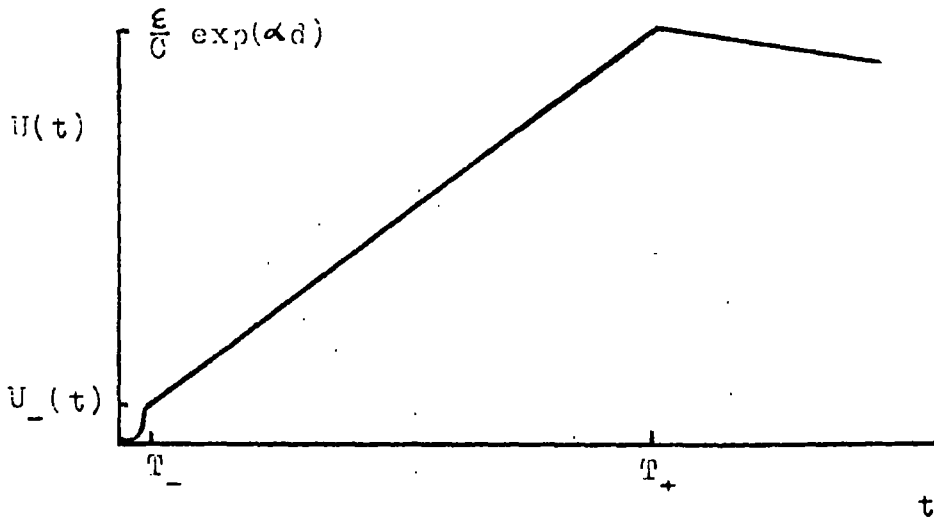
$$I_-(t) = \frac{e n_0}{T_-} \exp(\alpha v_- t) \quad 0 \leq t \leq T_-$$

$$I_-(t) = 0 \quad T_- < t$$

The time constant of this electron component is $1/\alpha v_-$. This current $I_-(t)$ flowing in the anode circuit will be supplemented by a current $I_+(t)$ caused by the drift of positive ions to the



Fig(4.11) Equivalent circuit.



Fig(4.12) Voltage pulse $U(t)$ of an avalanche with $RC \geq 1/\alpha v_+$.

cathode, and also by a displacement current arising from the gap and associated capacitances. The total current in the external circuit at a time t is:

$$\begin{aligned} I(t) &= I_-(t) + I_+(t) + C \frac{dU}{dt} \\ &= I_{cr} + C \frac{dU}{dt} \end{aligned} \quad (4.1)$$

where U is the amplitude of the displayed voltage pulse. The displacement current is important if the time constant RC of the anode circuit is long compared with the time constants of the carrier currents. In this case the high voltage supply feeds energy into the gap capacity too slowly, so that the electrostatic energy $\frac{C}{2} U^2$ is taken to produce and drive the carriers through the gap. The equation can be interpreted as a circuit of parallel branched R and C . Fig. (4.11). The time constant of the circuit in the experiment is 3.0×10^{-3} second, compared with $1/\alpha v_+ \sim 0.3 \times 10^{-4}$ second. An exact solution to equation (4.1) has the form:

$$U(t) = \frac{1}{C} \exp(-t/RC) \left[\int_0^t \exp(\nu/RC) I_{cr}(\nu) d\nu + CU(0) \right].$$

If $RC > 1/\alpha v_+$, as is the case in the present experiment, $U(t)$ is obtained as the integral of the current

$$U(t) = \frac{1}{C} \int_0^t I_{cr}(\nu) d\nu.$$

The amplitudes of the electron, ionic, and loading components are given by:

$$U(t) = \frac{1}{\alpha d} \frac{en_0}{C} (\exp(\alpha v_- t) - 1) \quad 0 \leq t \leq T_-$$

$$U(t) = \frac{en_0}{C} (\exp(\alpha d)) \frac{t}{T_+} \quad T_- < t < T_+$$

$$U(t) = U(T_+) \exp\left(-\frac{t-T_+}{RC}\right) \quad T_+ \leq t$$

The amplitude of the electron component reaches its maximum at $t = T_-$ and

$$U(t) = \frac{1}{\alpha d} \frac{en_0}{C} (\exp(\alpha d) - 1),$$

$U(t)$ amounting to $\sim 1/\alpha d$ of the total voltage $\frac{en_0}{C} \exp(\alpha d)$. A plot of $U(t)$ is shown in Fig. (4.12). After a time T_+ the capacity of the gap is reloaded with the time constant RC . From the above equation it is possible to obtain values for α and hence n_0 .

4.6 Comments

The oscilloscopic method of measurement of the number of starting electrons is only applicable to avalanches which finish when the last ions reach the cathode; it does not allow for the production of secondary electrons. Also it is difficult to see in the oscillograms the discontinuity which marks the arrival of the electron swarm at the anode, (at $t = T_-$). This is so because of the finite dimensions of the swarm, so that the time taken for the electrons to enter the anode is not small compared with the transit time.

Consequently the determination of the starting number of electrons n_0 by the oscilloscopic method is of limited accuracy, although values of n_0 determined at low values of E/p by both methods are in reasonable agreement. However the range of values of n_0 over which space charge effects may be observed is very restricted. This range is set by a lower limit below which space

charge effects are not observed, and by an upper limit above which the injected swarm causes breakdown to occur. In the experiments the initial number of electrons in the primary swarms is increased step-by-step through this range by fractional decreases of the wire-plate distance in the electron source. However the oscillographic method described is not sufficiently accurate to discriminate between adjacent values of n_0 in this narrow range and for this reason in the presentation of the experimental results, the number of starting electrons is given as determined using the galvanometer method at low voltages. These values are below the actual numbers of electrons emitted at the operating voltage, but they do on the other hand give an accurate picture of the relative electron starting numbers between sets of readings in an experimental run. A similar comparison could not be made as accurately using the oscillographic method.

--- ----- ---

CHAPTER 5

THE EXPERIMENTAL MEASUREMENTS

The measurements are presented in three sections, namely:

i) measurements of the ionization coefficient in primary and secondary swarms.

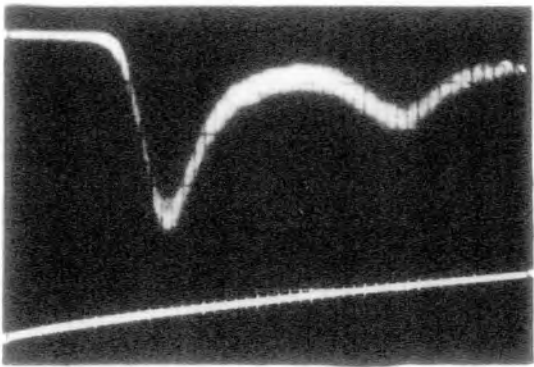
ii) measurements of the electron drift velocity.

iii) measurements of the electron diffusion coefficient, and of the electron distribution in the swarms during the transit of the electrode gap.

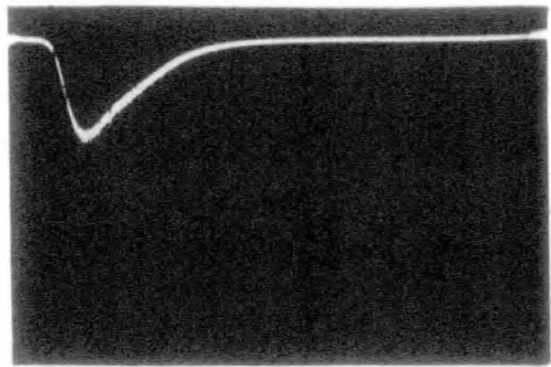
5.1 experimental procedure

The discharge vessel was evacuated to a pressure of less than 10^{-6} mm Hg before the working gas was admitted. Hydrogen was then let into the system through the heated palladium thimbles, taking about an hour to reach the working pressure of 60 mm Hg. A further half hour was allowed for the thimbles to cool, and for the gas pressure to become constant.

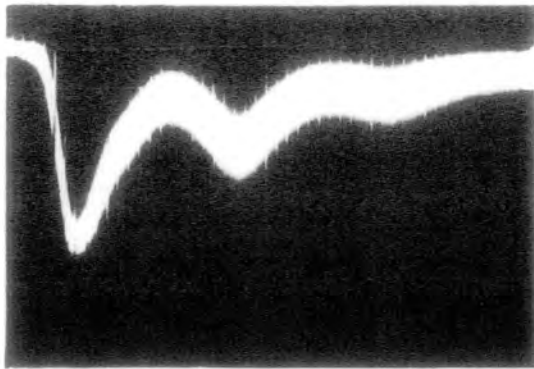
After the electron source had been switched on, the anode voltage was increased to a value just below the breakdown voltage, at which point secondary electron avalanches were usually observed with the photomultiplier looking at the anode region. (Fig. (5.1) shows typical oscilloscope traces in hydrogen and nitrogen at voltages below that required for the gap breakdown. The gas pressure in the system was about 60 mm Hg for the hydrogen oscillograms, and about 40 mm Hg for the nitrogen oscillograms.



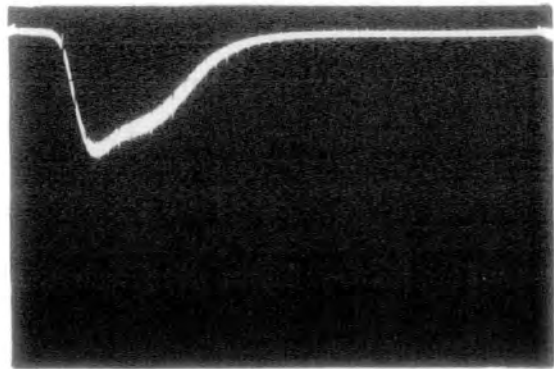
(a) H₂



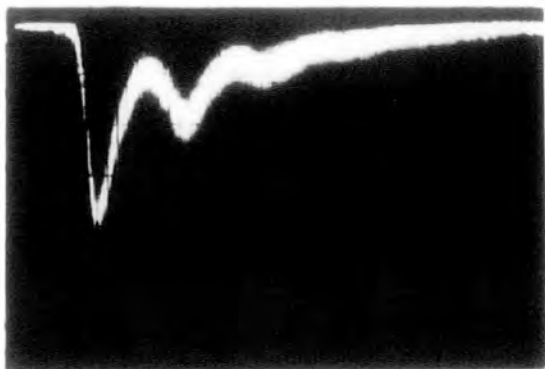
(d) N₂



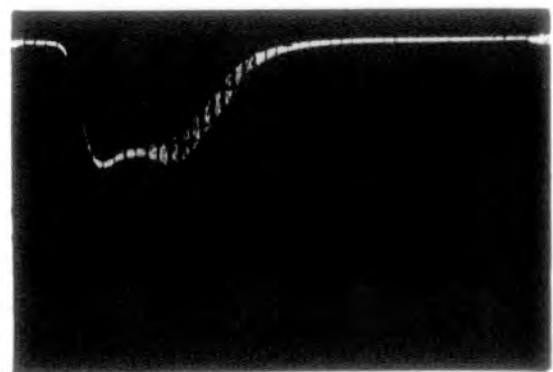
(b) H₂



(e) N₂



(c) H₂



(f) N₂

Fig (5.1)

The trace in Fig. (1a) was photographed at a sweep speed of 0.02 micro-seconds/cm, and is a typical example of the majority of photographs taken. The time interval between the primary and secondary avalanches is the order of the gap transit time for electrons, indicating that the secondary electrons are produced at the cathode by the photo-electric effect. Figs. (1b, 1c) are photographs taken at slower sweep speeds and show a third avalanche generation.

Figs. (1d, 1e, 1f) are photographs taken at various applied anode voltages. As the voltage is increased secondary avalanches become apparent. However the resolution of primary and secondary avalanches is not as high as in the other photographs and although these traces are from nitrogen, rather than hydrogen measurements, this lower resolution is attributed mainly to the lower gas pressure. Similar traces are obtained in hydrogen at 40 mm Hg, and the poor resolution is caused by a considerable diffusion of electrons between primary and secondary swarms.

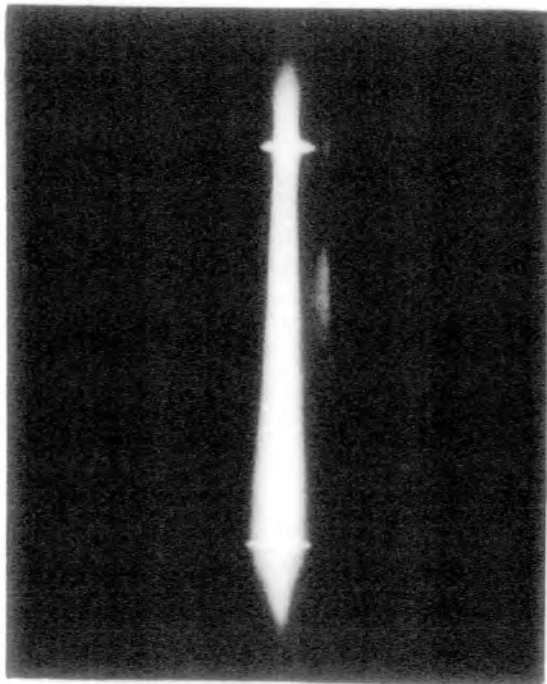
The amplitude of a trace at a particular time is a measure of the number of electrons drifting in the volume of gas observed by the photomultiplier. Since the light emitted from the swarms is isotropic, the trace shows the variation in the number of electrons in this volume with time, and thus the area under the pulse is a measure of the total number of electrons which have passed through this volume.

At a particular value of E/p , an experimental run comprised six sets of photographs of oscilloscope traces, each set corresponding to a different number of starting electrons n_0 . The photographs in a set were taken with the photomultiplier at 2.5 mm intervals across the electrode gap~~X~~; the gap being scanned once in either direction. Points on the graphs Figs. (5.3 etc.) marked \odot indicate a traverse cathode to anode, and points marked \times indicate a traverse from anode to cathode. The initial number of electrons per swarm was measured with the galvanometer circuit (see Ch.4) at low voltages, before and after a set of photographs were taken. This initial number was also measured at the operating voltage using the oscilloscope method, (see 4.6).

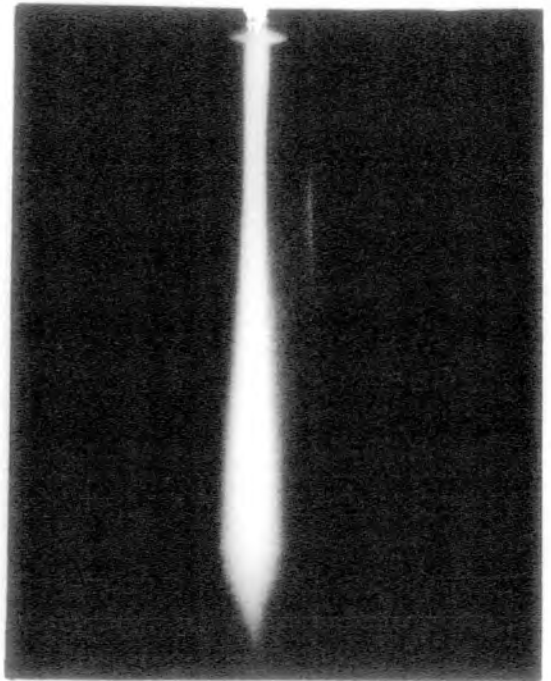
Six sets of photographs took about $2\frac{1}{2}$ hours to expose, bringing the total time for a run to about 4 hours. In all fifty-five films were exposed, comprising some 1,800 frames scanned and measured.

5.2 The path swept out by a primary electron swarm drifting across the electrode gap

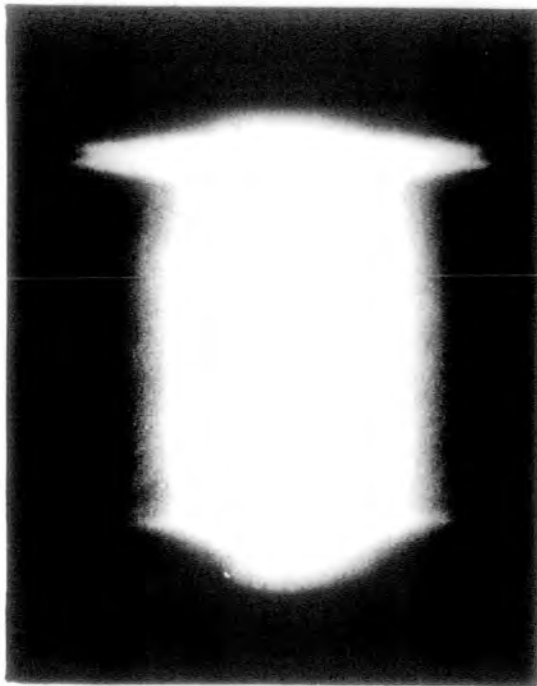
Although the diffusion coefficient for free electrons at a gas pressure of 60 mm Hg is comparatively small, the dimensions of an electron swarm will increase as the swarm drifts from cathode to anode. This can easily be verified by looking into the discharge gap in a darkened room, along the line of sight of the photo-



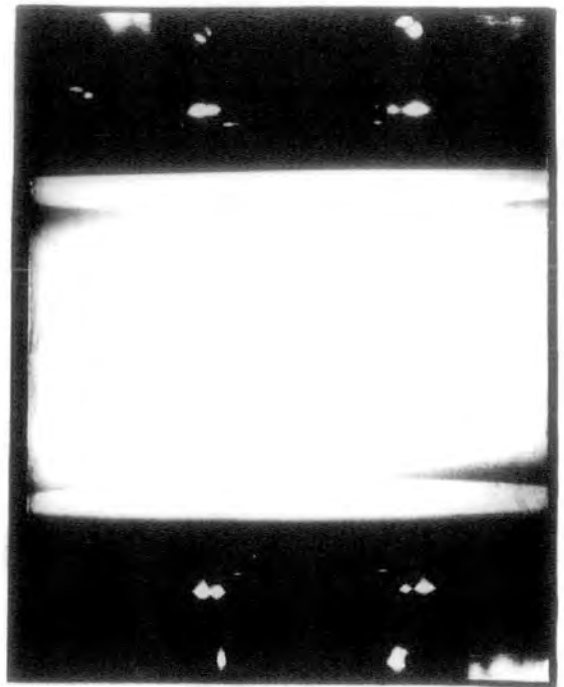
(a) H₂



(b) Air



(c) H₂



(d)

Fig (5.2)

multiplier. A very faint luminous column of gas is observed between the electrodes, which becomes broader moving from cathode to anode. This discharge is too faint for photographic purposes, however if the anode voltage is increased until breakdown occurs, a similar column of luminous gas is observed which is more intense. A photograph of this column is shown in Fig. (5.2a). It is noted that the diameter of this column does not increase linearly with distance from the cathode, but that the edge of the column is in fact a curve. It will be shown later in this chapter both by simple theory, and in some cases by experiment, that this diameter increases as the square root of the swarm drift time.

The electrode surfaces in Fig. (5.2a) are located along the two horizontal white lines in the discharge. These lines are reflections from the electrode surfaces, while the tails above and below these lines are reflections from the curved edges of the electrodes. The traces to the right of the columns in the photographs are also reflections, originating from the walls of the glass vessel. (Fig.(5.2d) is a photograph of the electrode gap illuminated from the side, cathode uppermost, without a discharge running. The other photographs were all taken in a darkened room. Fig. (5.2c) is a photograph of a discharge in the electrode gap without the electron source running. In the absence of the injected swarms breakdown has occurred by a discharge which covers most of the flat sections of the electrode surfaces, there being no preferential discharge channel.

Figs. (2a, 2b) may therefore be taken to indicate the path swept out by a primary swarm released from the cathode.

5.3 Measurements of the ionization coefficient

The expansion of a primary electron swarm during its transit of the electrode gap has in the last section been attributed to a diffusive motion of the electrons which is superimposed upon the drift motion. Consequently it is not possible to make accurate measurements of the ionization coefficient by taking the ratio of the trace amplitudes at two points in the electrode gap. If this were done, too small a value for the ionization coefficient would be obtained, because although electrons are not able to diffuse out of the field of view of the photomultiplier radially, they may do so by diffusing towards either electrode. It will be remembered from section 3.4, Fig. (3.5), that only radiation from a thin slice (6 mm) of the swarm path is collected at the photocathode. Thus in a trace obtained with the photomultiplier looking at a slice near the anode, the peak amplitude will be reduced because electrons have been lost from the thin slice by diffusion towards either electrode.

Measurements of the ionization coefficient were therefore made by comparing the total numbers of electrons in swarms at various positions across the gap. This has been done by plotting the area under an oscilloscope trace as a function of the photomultiplier position on semi-logarithmic paper. This area is proportional to the total number of photons emitted from the thin slice under observation, a quantity which in turn is proportional

to the total number of electrons which passed through the slice. The slope of these graphs gives the ionization coefficient α , provided the electric field in the gap remains uniform. From equation (2.1)

$$dp = \mathcal{E} n_e dx,$$

where dp is the total number of photons emitted as a result of n_e electrons drifting through a thin slice of the swarm path of width dx , located x cms from the cathode.

$$\begin{aligned} \bar{dp} &= \mathcal{E} n_0 \exp(\alpha x) dx \\ \log_e dp &= \alpha x + \log_e(n_0 \mathcal{E} dx) \end{aligned} \quad (5.1)$$

Actual values of the electron numbers involved may be calculated if several constants of proportionality are known, namely: the quantum efficiency and gain of the photomultiplier, and a gap geometry factor. However because the ionization coefficient may be determined from the slope of the graphs, these constants were not-evaluated. The units in which the electron number n_e is expressed in Figs. (5.3, etc.), is therefore cms^2 .

The plots represent a quantitative record of the experiments performed, but unfortunately because of the differing slopes are difficult to present on single axes. They may however be divided into three groups: the first in which the number of starting electrons was low, Figs. (5.3 - 5.8); the second group in which n_0 was sufficiently high for the resulting concentrations of charged particles in the primary swarms to distort the applied field,

Figs. (5.9-5.17); and in which the graphs are initially linear, but become concave to the distance axis. The third group, Figs. (5.18-5.23), consists of graphs showing the multiplication of secondary electrons released from the cathode by the photo-electric effect; these graphs are linear in form.

In the case of the hydrogen measurements the plots are labelled A, B, C, D etc. indicating that the measurements were made in different gas samples. Measurements were made with two gap spacings, ($d = 6.171$ cm or $d = 7.21$ cm), and the cathode and anode surfaces are at 1.30 cm and either 7.47 or 8.51 cms on the abscissa in Fig. (5.3 etc.) for the two gaps. In all these measurements it was necessary to ensure that the line of sight of the photomultiplier did not approach too closely either of the planes in which the electrode surfaces lay so as to avoid reflection and obstruction by the electrodes.

In the second group of graphs, Figs. (5.9-5.17) the slope of the linear sections may be taken to obtain values for the ionization coefficient in the first cm or so from the cathode. However the slopes of the curved sections, while indicating that a reduction in the value of α has occurred cannot be taken as a direct measure of α as the local electric fields in the gap can no longer be assumed to be constant. Because the excitation coefficient \mathcal{E} is field dependent, the area under an oscilloscope trace, (proportional to the number of photons emitted), is no longer directly proportional to the number of electrons moving past the probe. It is seen from equation (5.1) that a reduction

in the local field strength besides reducing the value of αdx will also decrease the value of $\log_e n_0 \epsilon dx$ the intercept on the vertical axis. The slope of the graph is therefore no longer equal to the ionization coefficient. At this stage it is concluded that primary electron swarms containing a high electron number density show a departure from an exponential growth rate brought about by space charge effects.

Figs. (5.18 - 5.23) show the amplification of secondary electron swarms across the gap. It will be shown later that these secondary electrons are generated over a large part of the cathode surface, and are not confined to the central channel through which the primary electrons passed. Thus it is to be expected that only a fraction of these secondary electrons will encounter field distortions produced by positive ions, which were left over as a result of the passage of the primary electron swarms. In fact no deviation from an exponential rate of growth was detected in the amplification plots for secondary electrons.

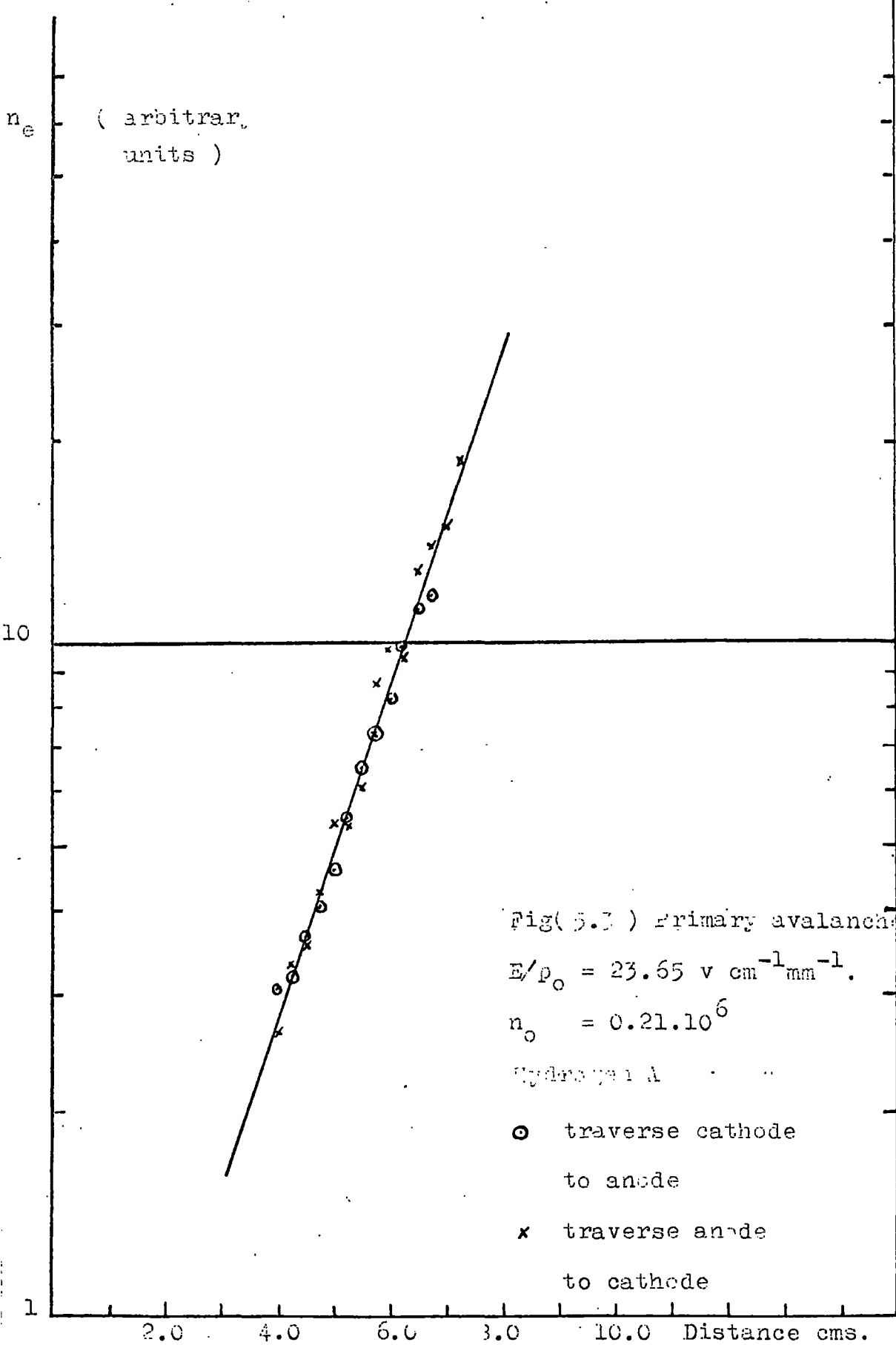
The maximum voltage available from the power supply was 11 kV, and in nitrogen at a pressure of 60 mm Hg, this voltage was not sufficient to produce breakdown. The nitrogen measurements were therefore carried out at gas pressures of about 40 mm. At this pressure the spreading of the primary swarms during their transit of the gap was quite considerable. Because of electron diffusion therefore, the electron densities were never sufficient

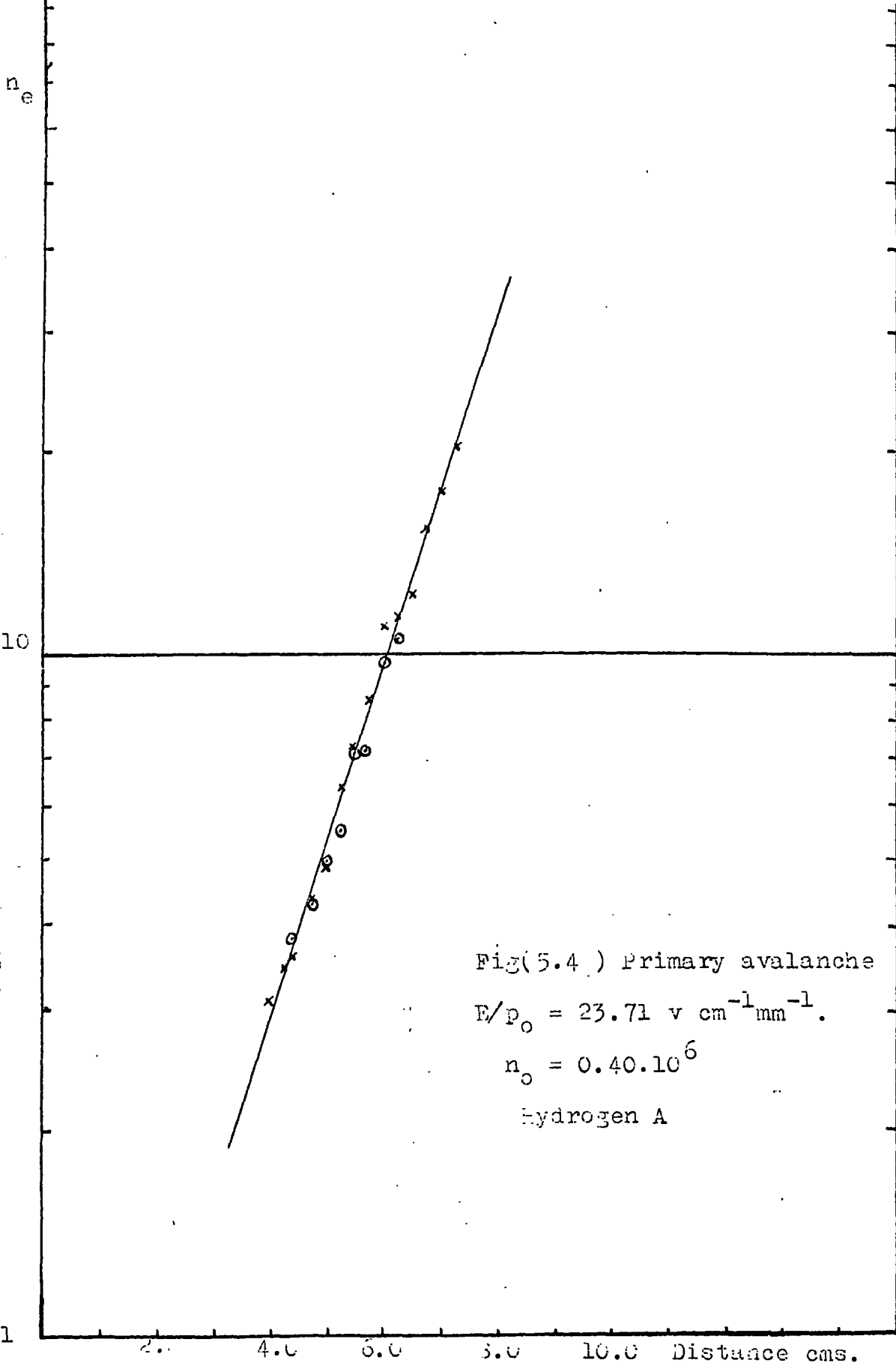
to produce detectable changes in the ionization rates.

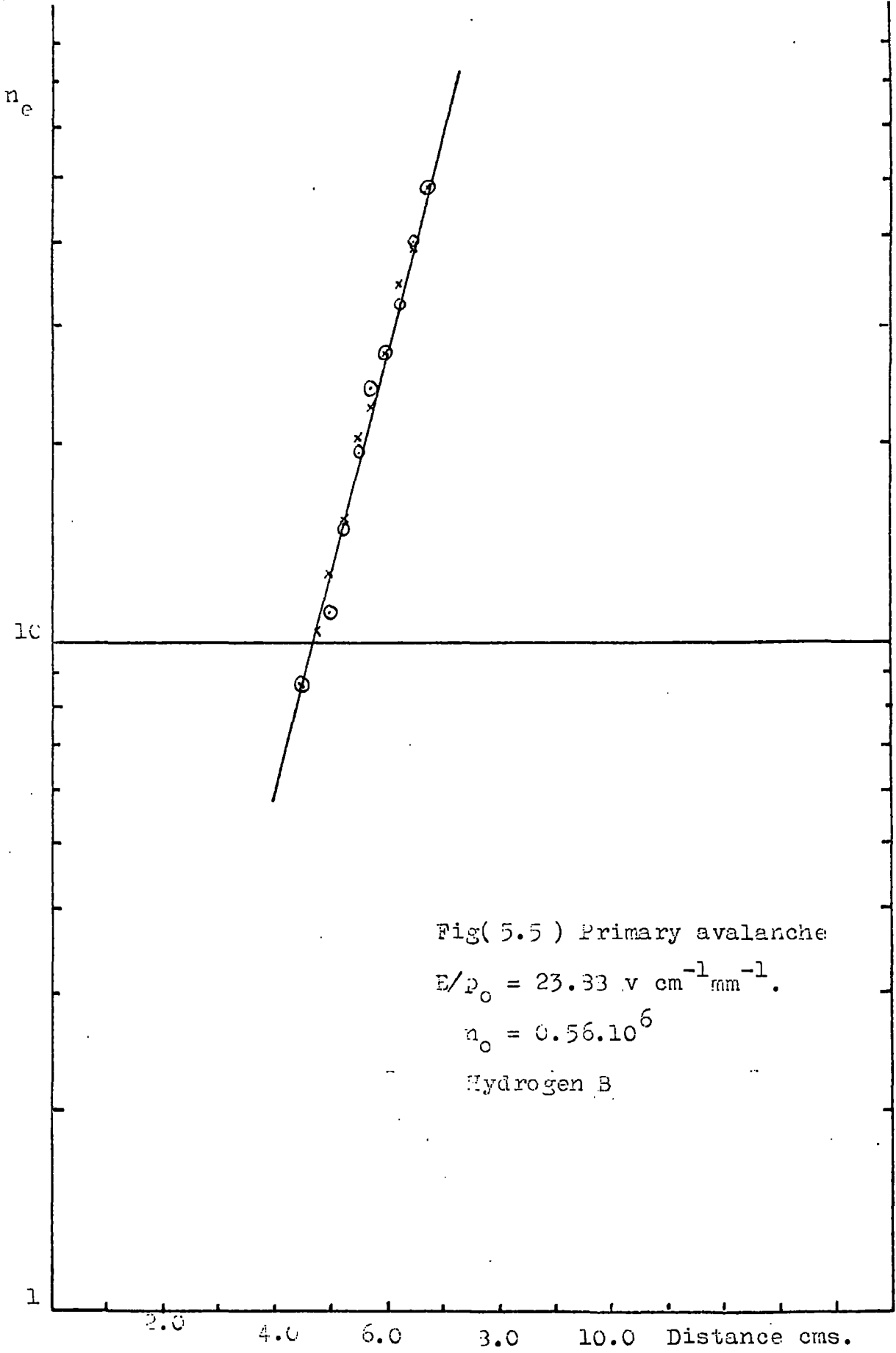
5.3.1 Comments

In the remainder of this chapter the measurements made of the electron drift velocities and of the electron distributions are presented. Although the departure from an exponential growth rate of some of the primary swarms has been attributed to space charge effects, the calculations made to determine the local field distortions in the gap are left to Chapter 6 of the thesis, and a comparison of the experimental and theoretical curves is presented in Chapter 7, together with a discussion of the experiment.

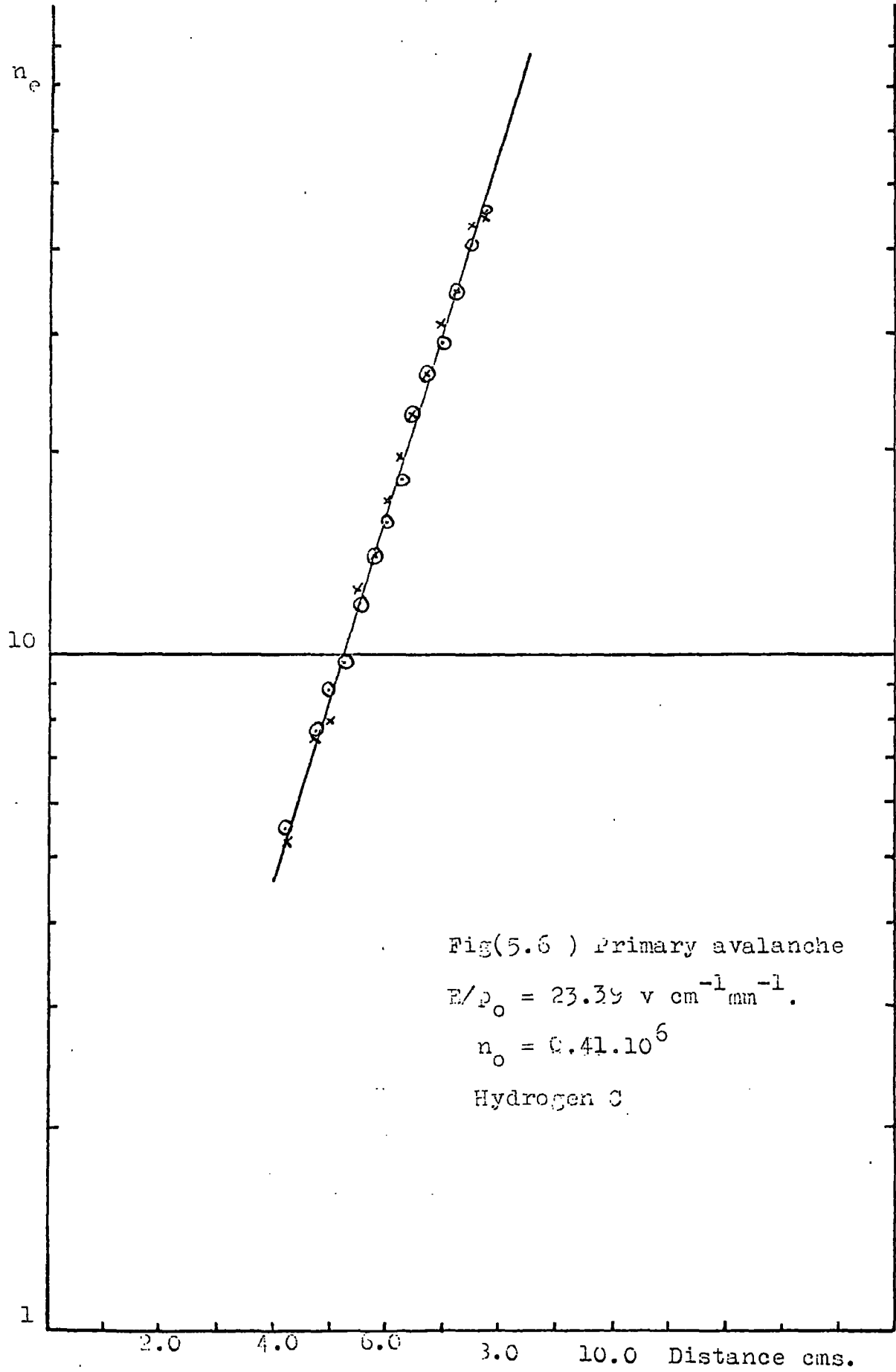
However the measured values of the ionization coefficient in hydrogen and nitrogen are tabulated in Table (2), (opposite p 65).

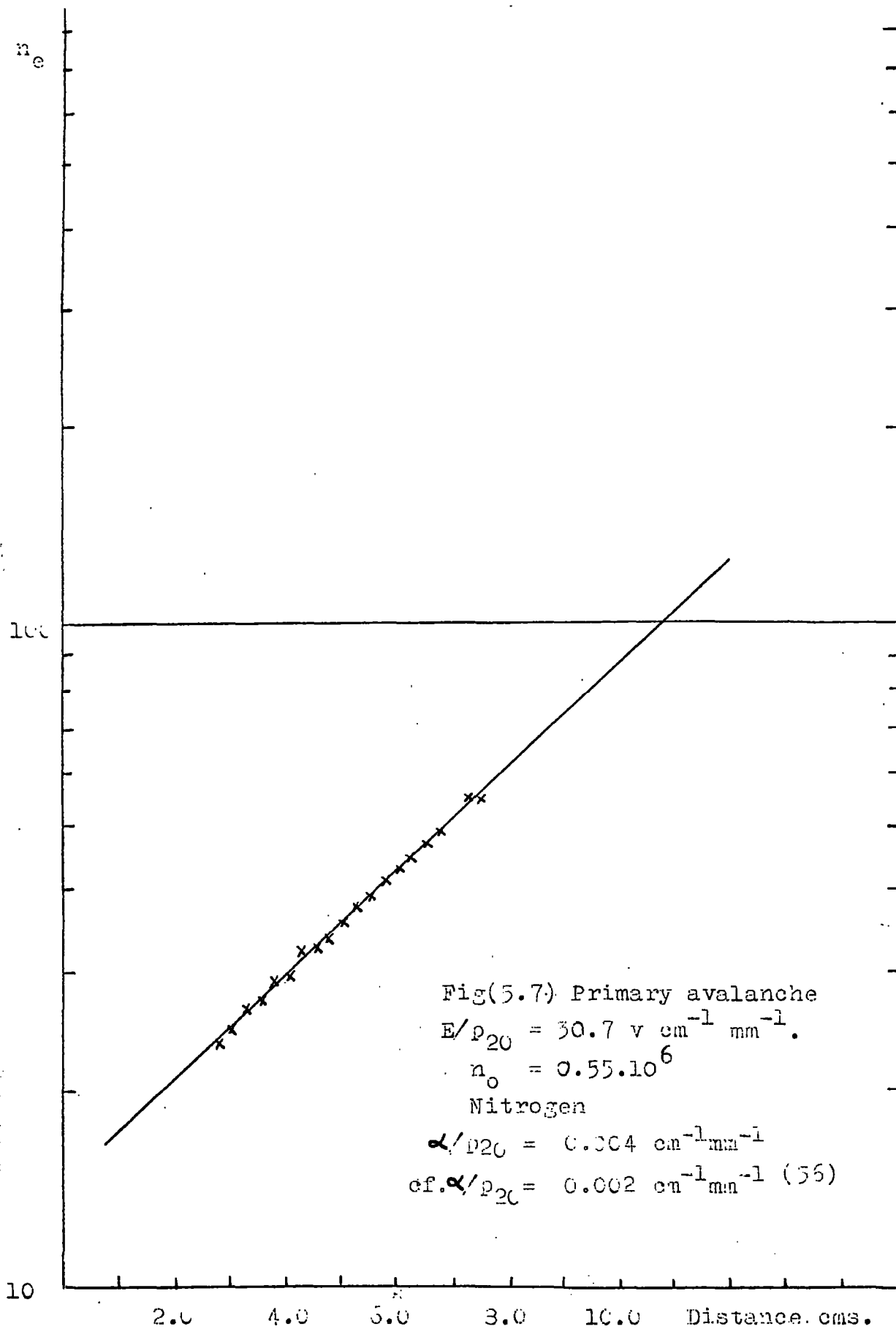


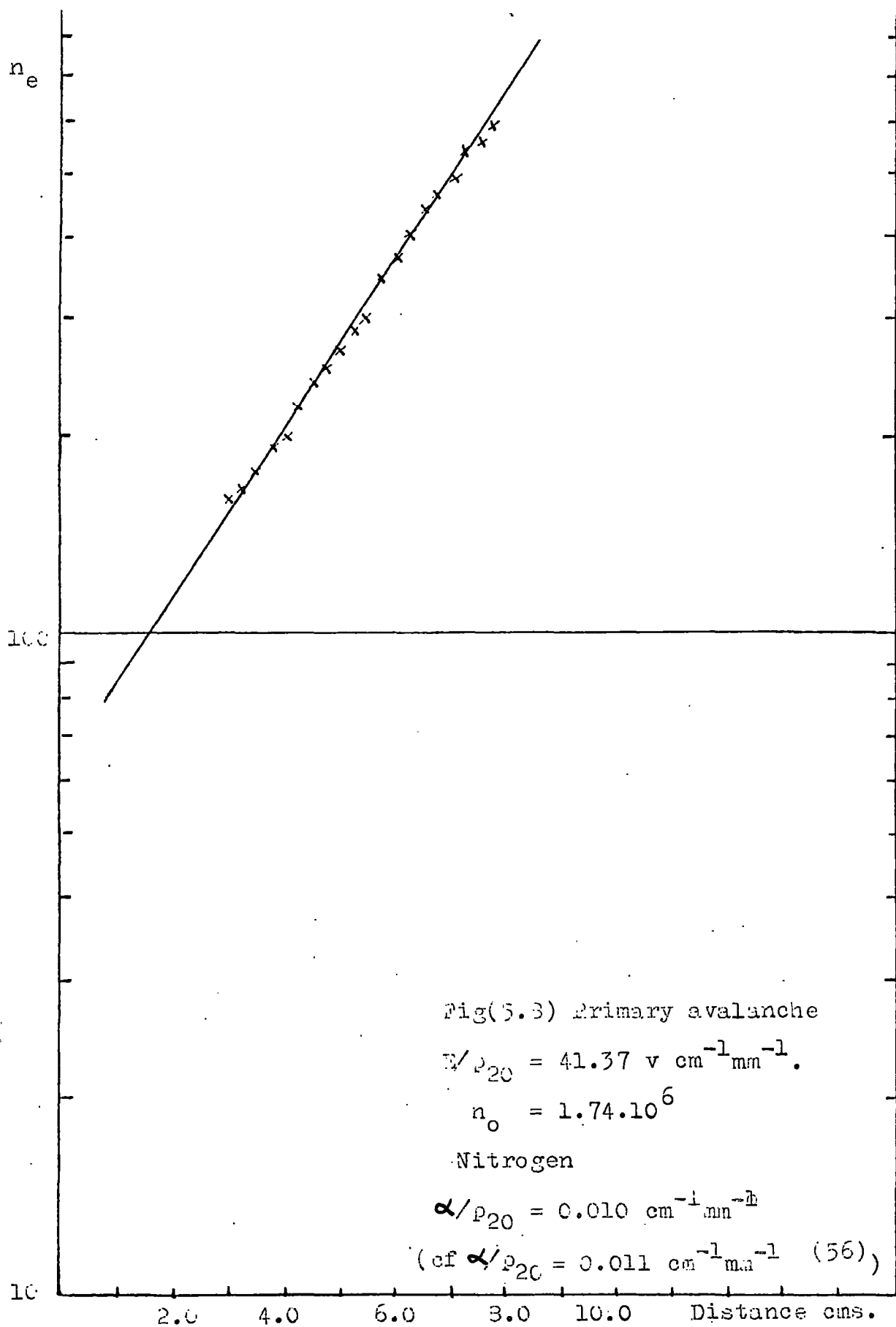




Fig(5.5) Primary avalanche
 $E/p_0 = 23.33 \text{ v cm}^{-1} \text{ mm}^{-1}$.
 $n_0 = 0.56 \cdot 10^6$
 Hydrogen B







Fig(5.3) Primary avalanche

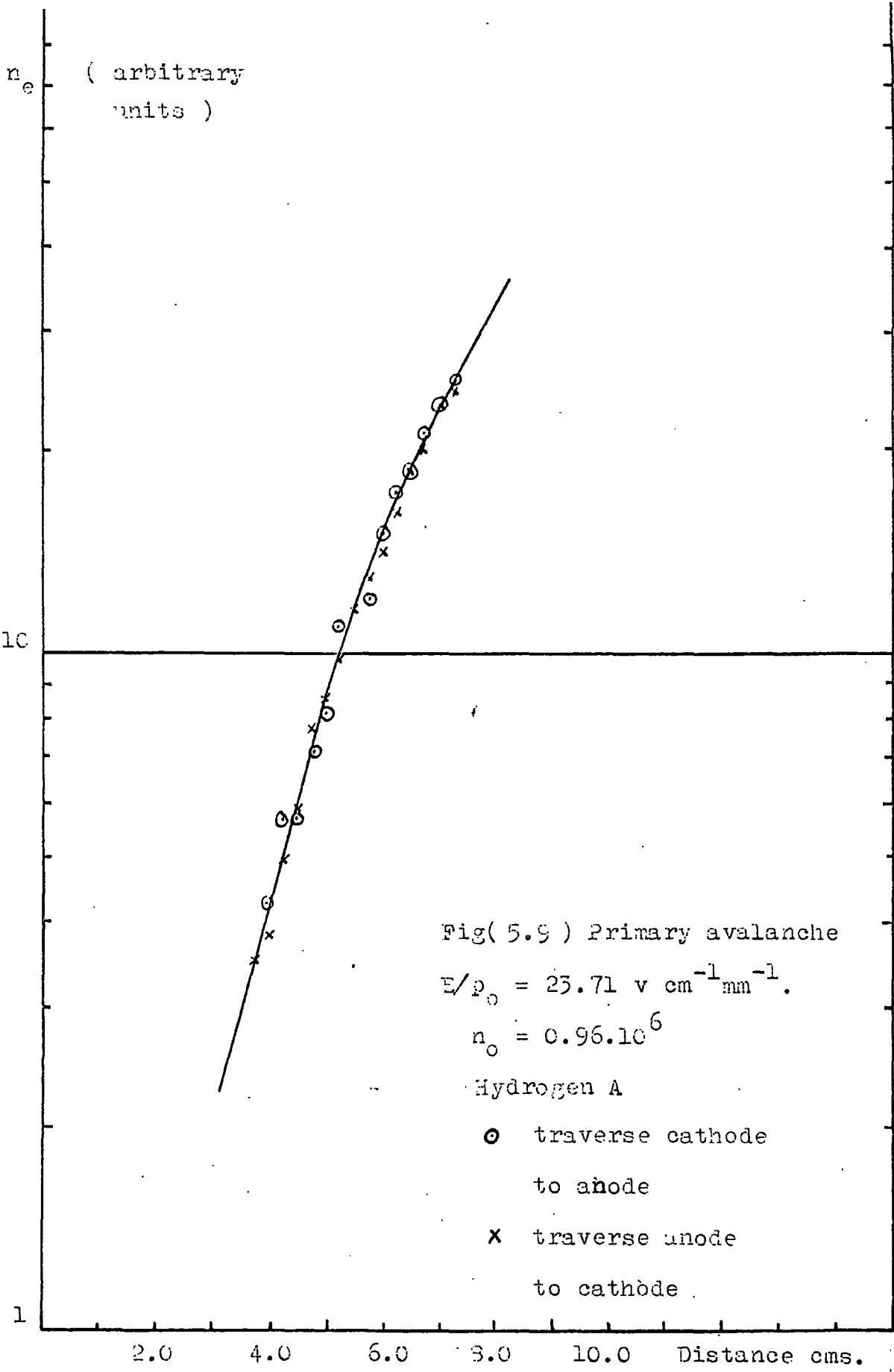
$E/p_{20} = 41.37 \text{ v cm}^{-1} \text{ mm}^{-1}.$

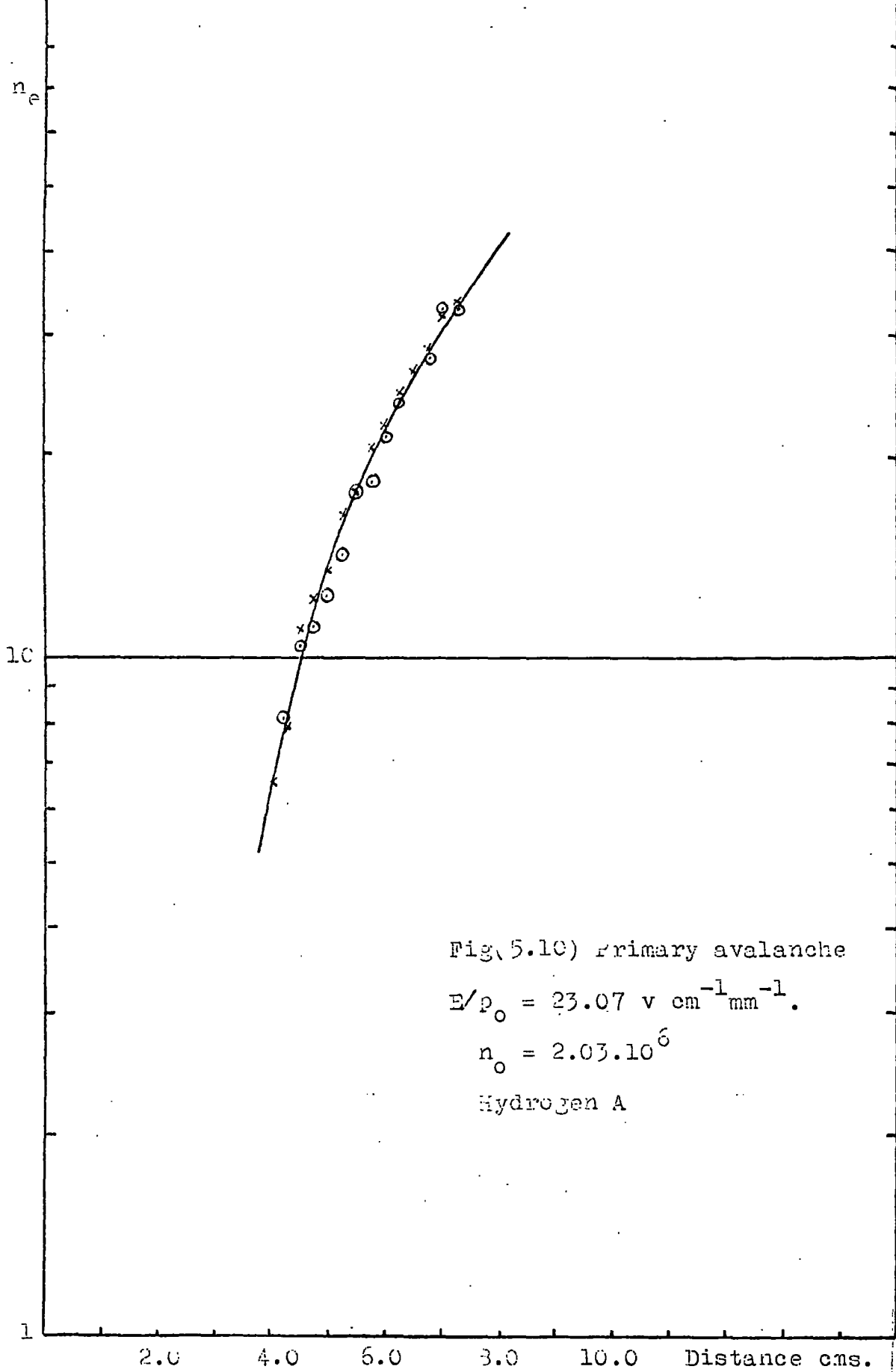
$n_0 = 1.74 \cdot 10^6$

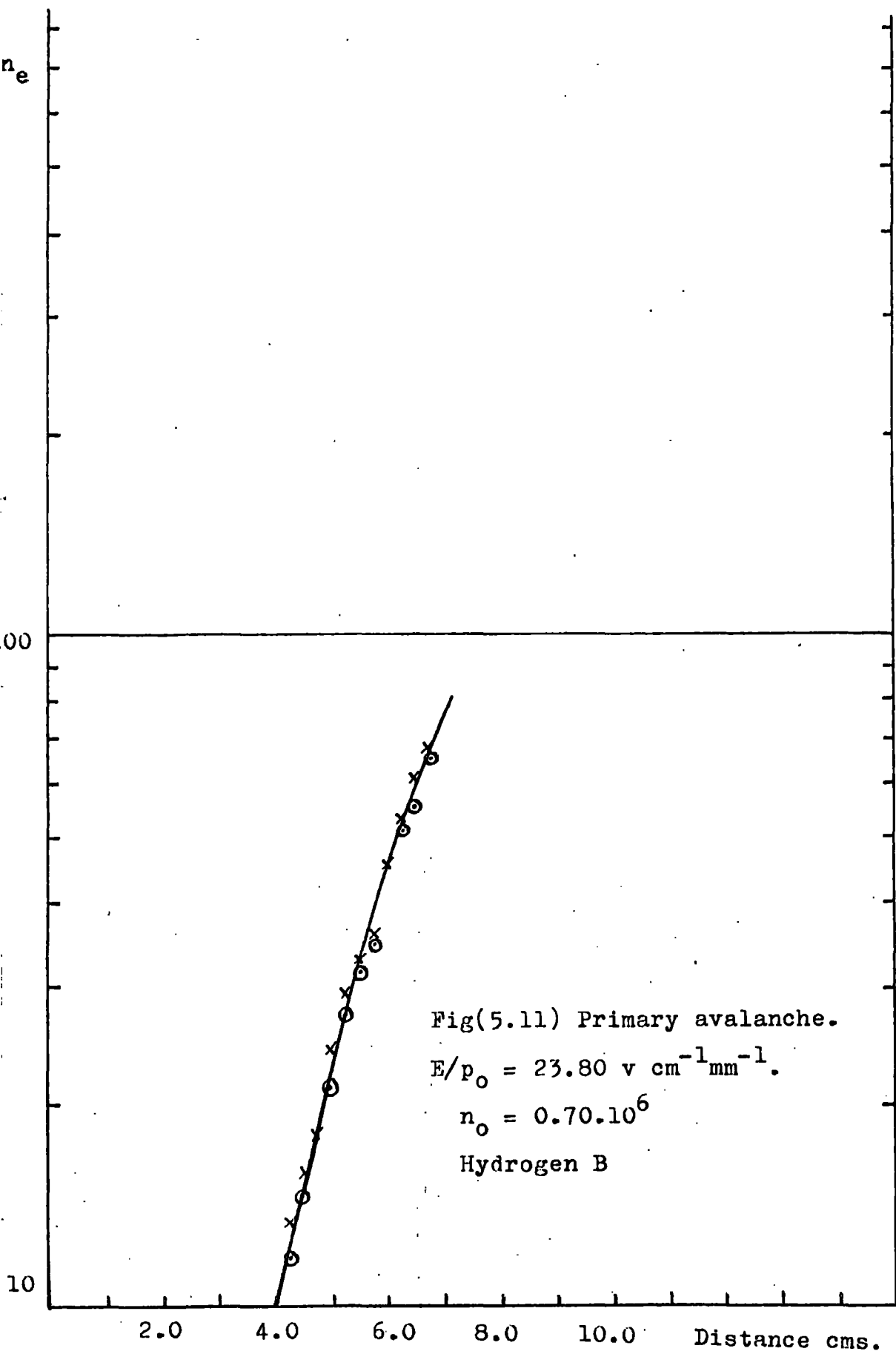
Nitrogen

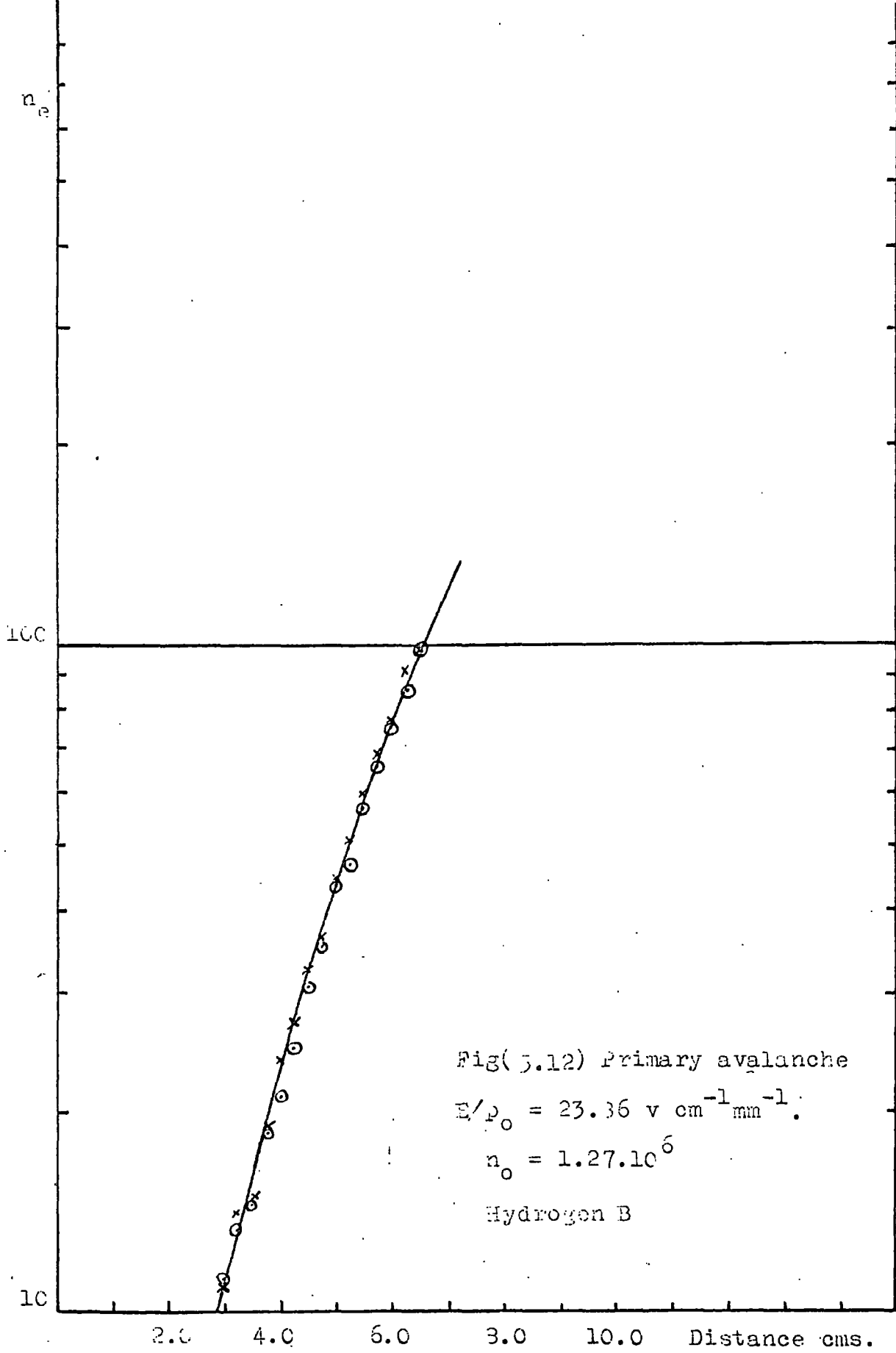
$\alpha/p_{20} = 0.010 \text{ cm}^{-1} \text{ mm}^{-1}$

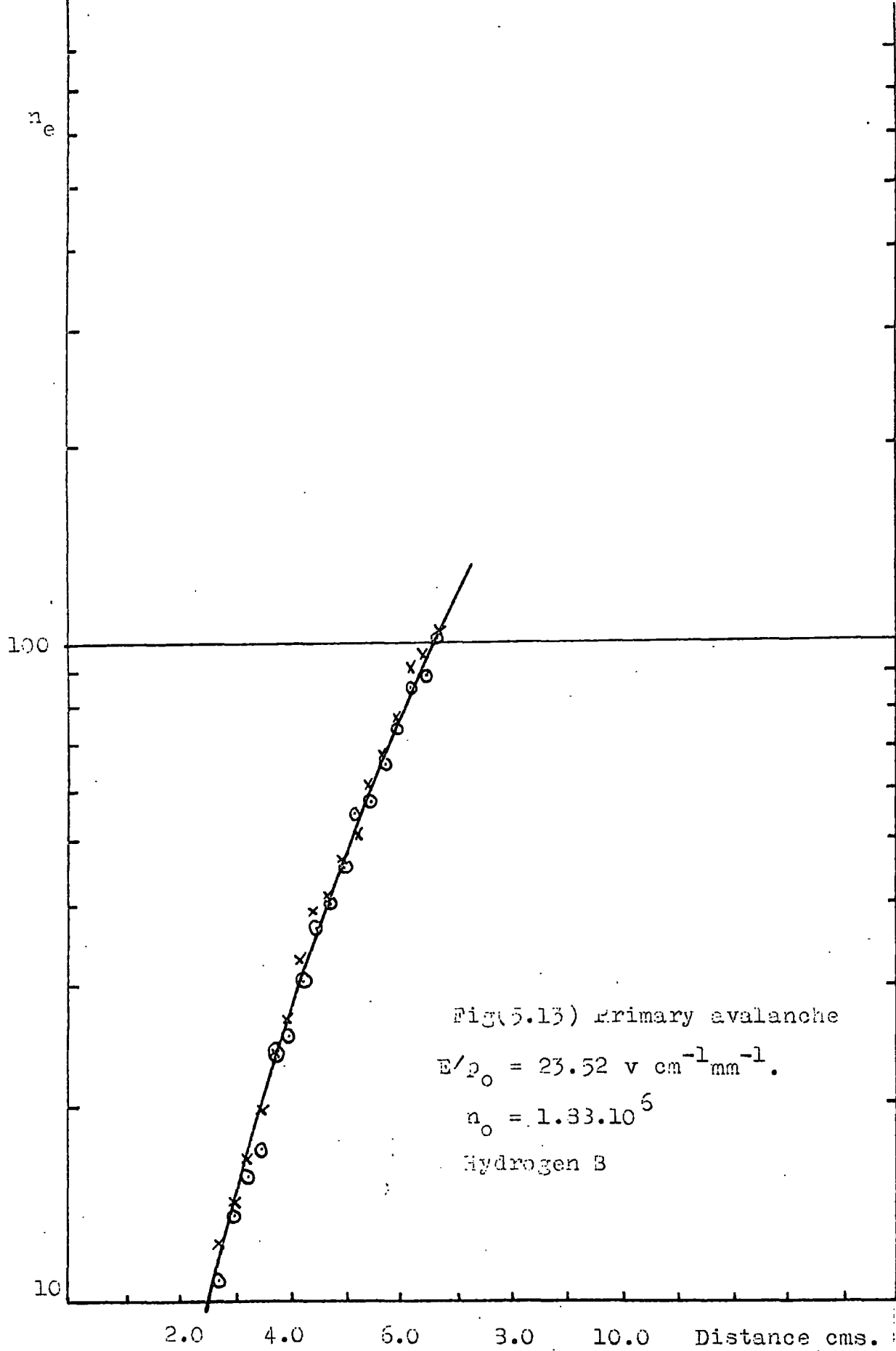
(cf $\alpha/p_{20} = 0.011 \text{ cm}^{-1} \text{ mm}^{-1}$ (56))

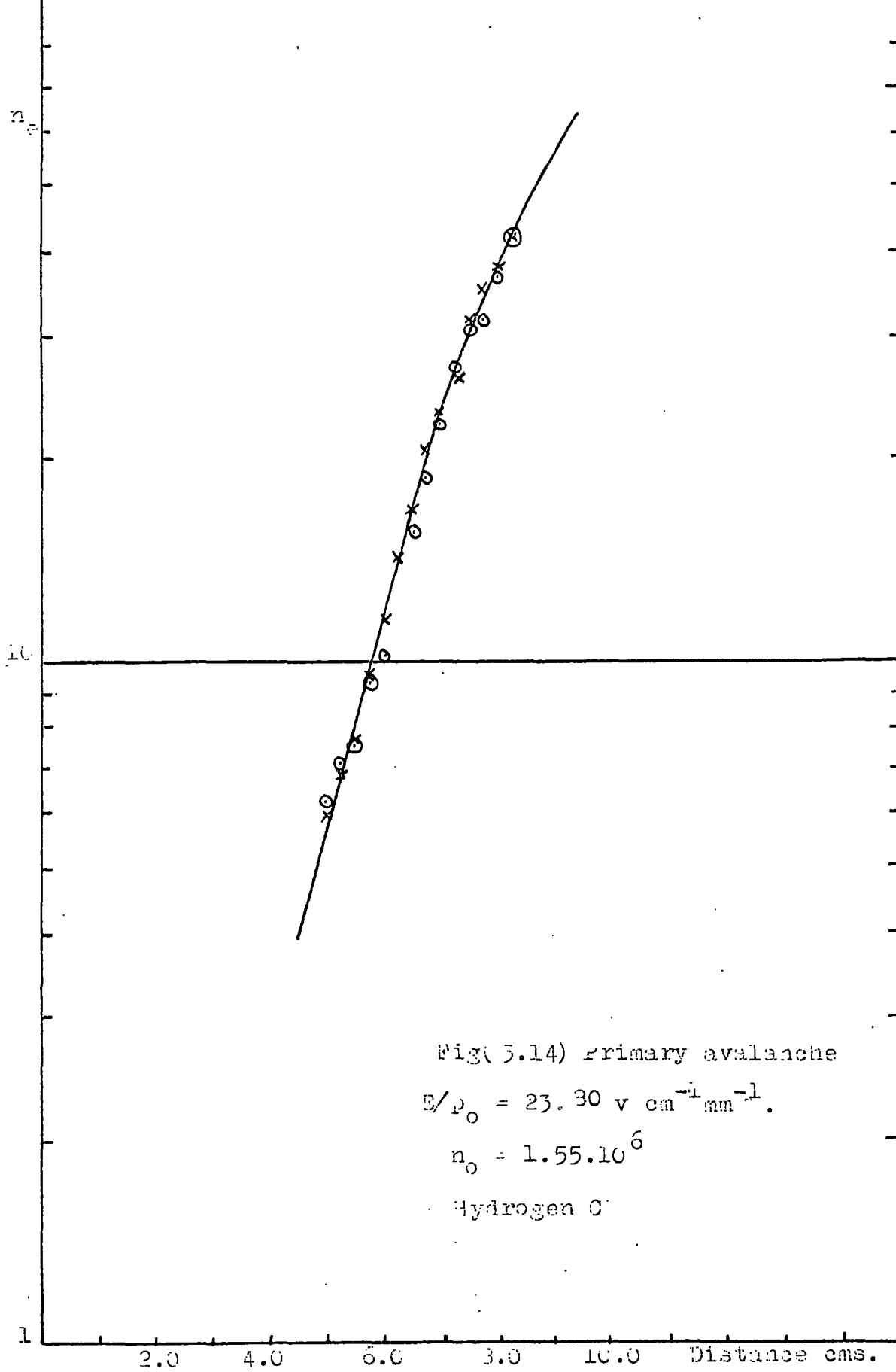


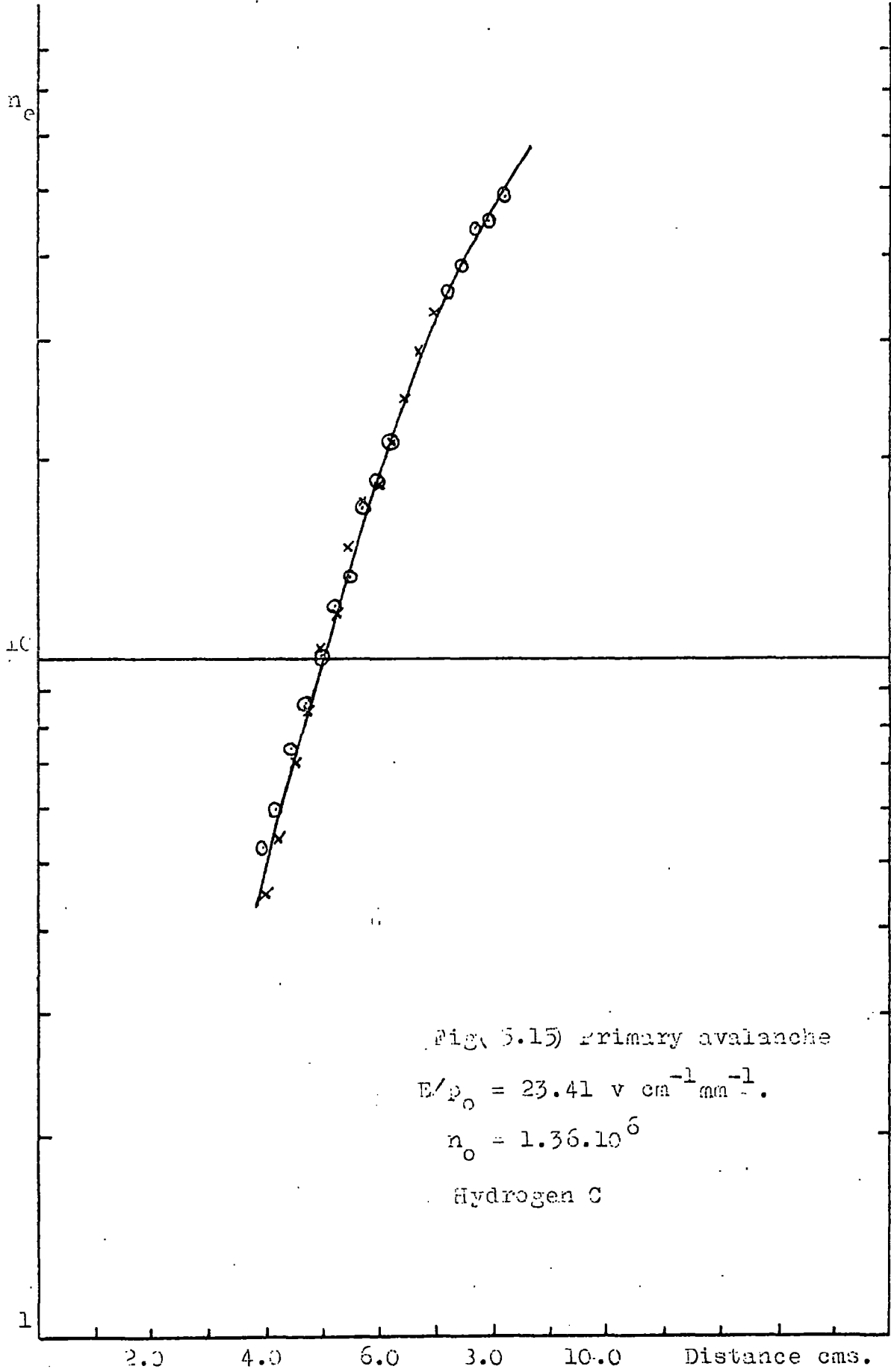


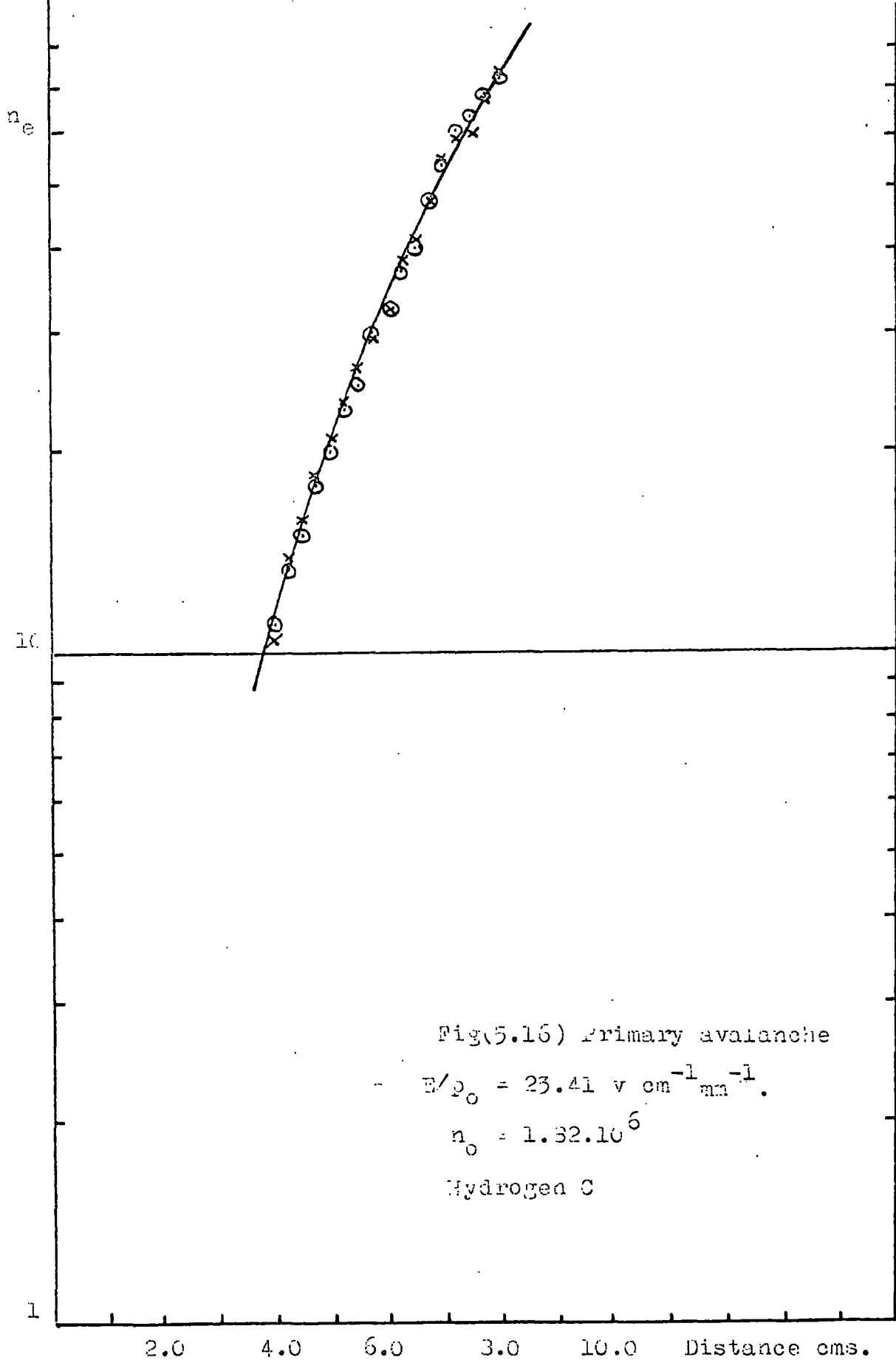


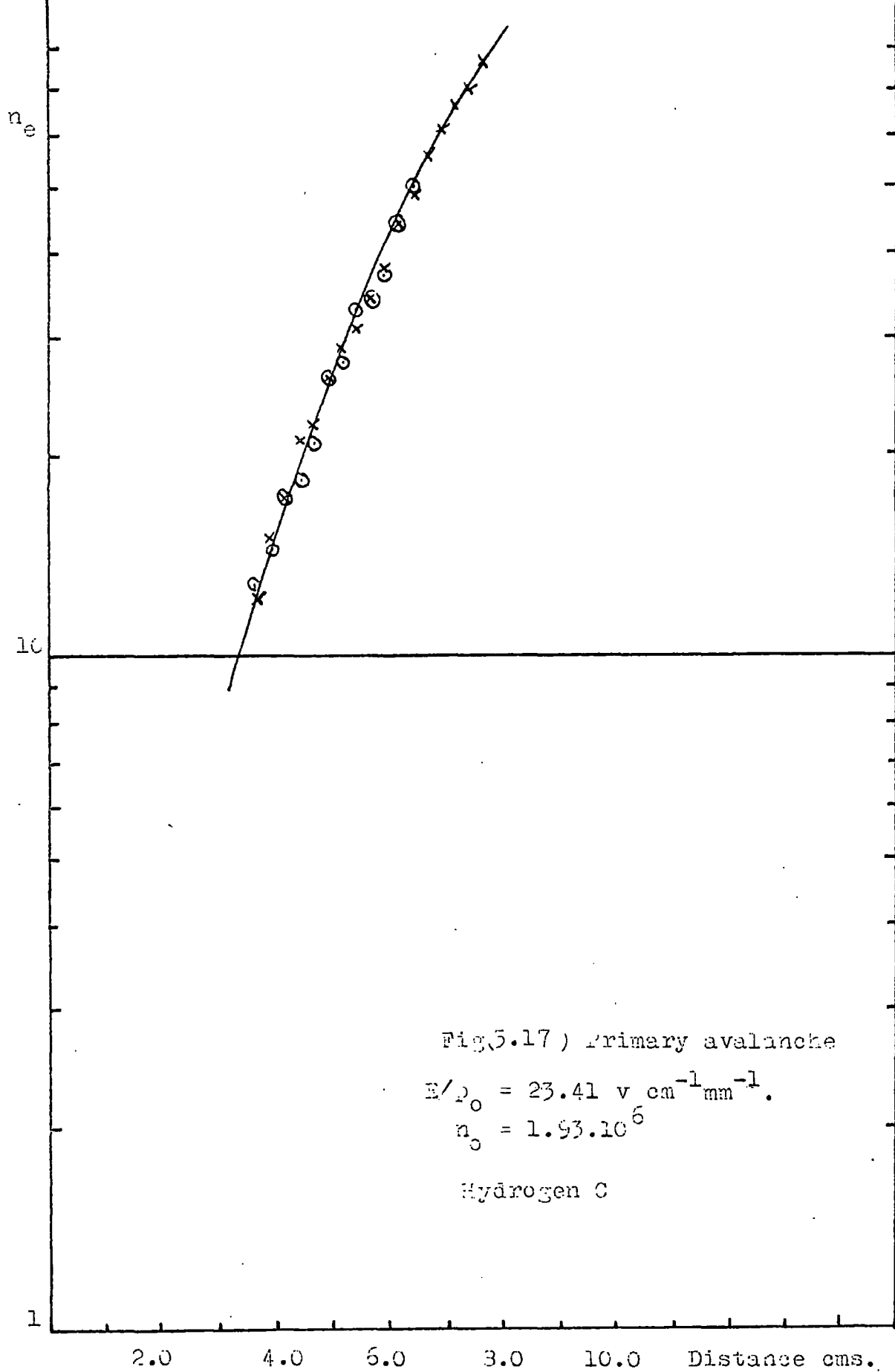


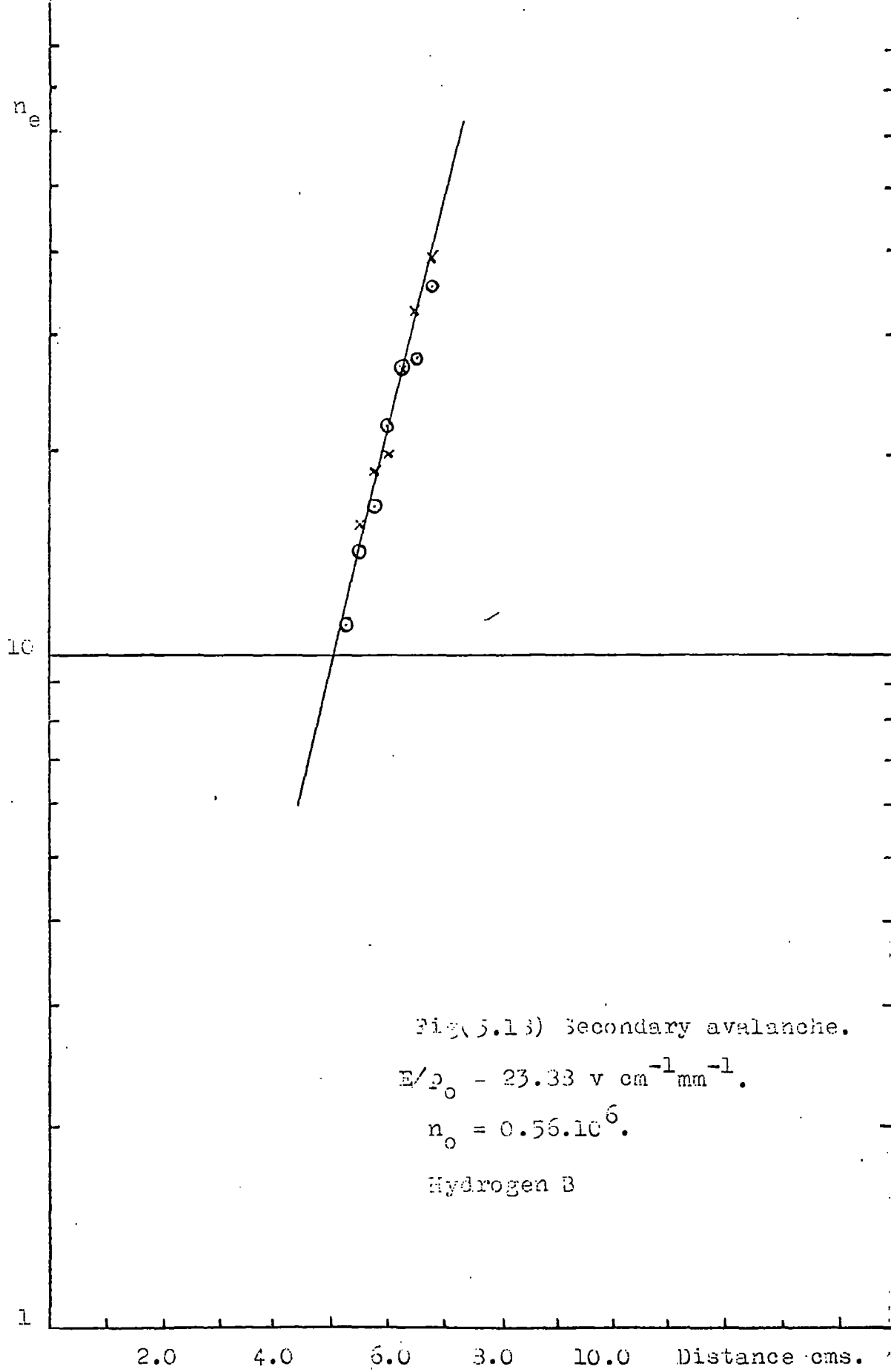


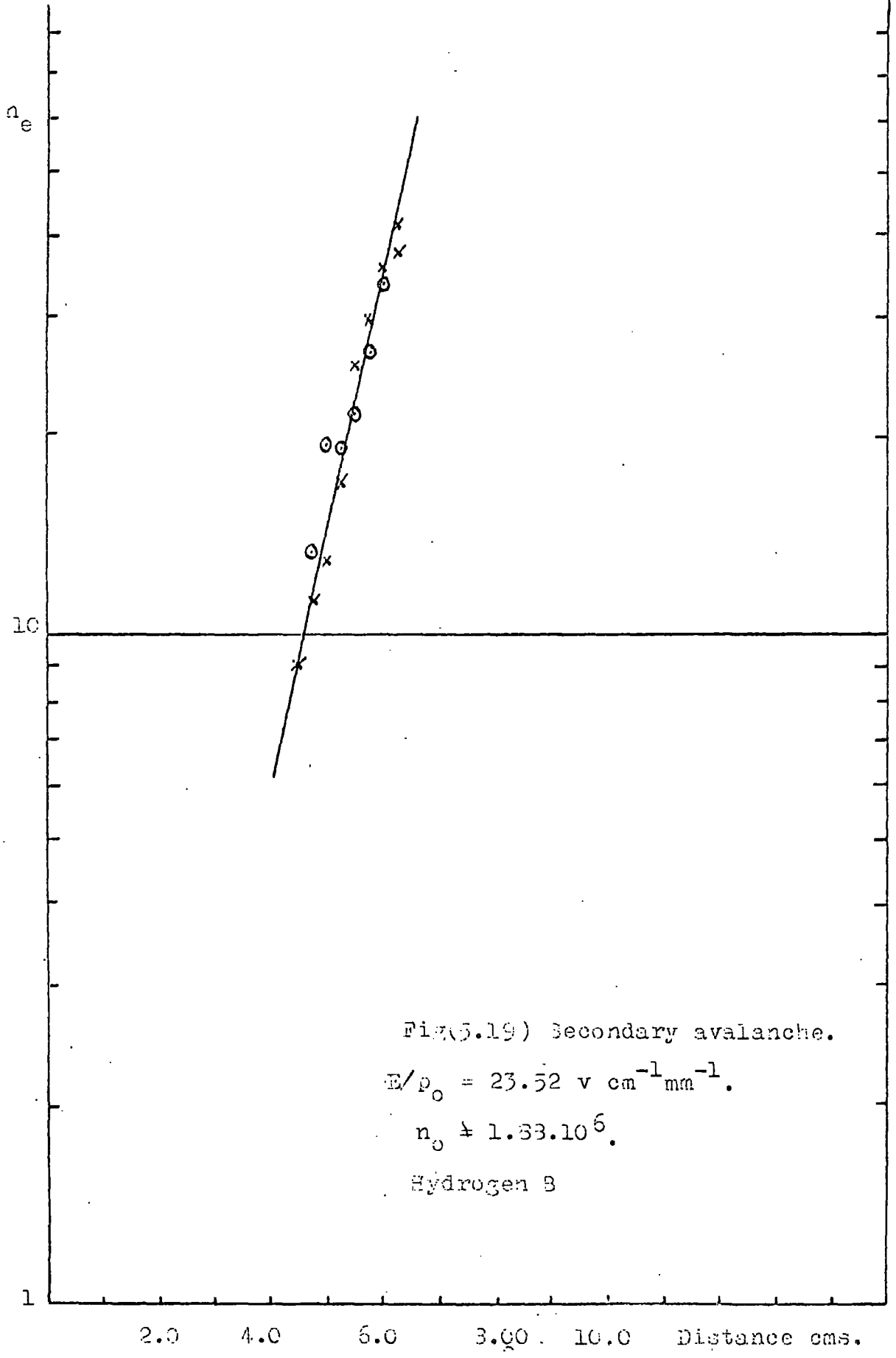










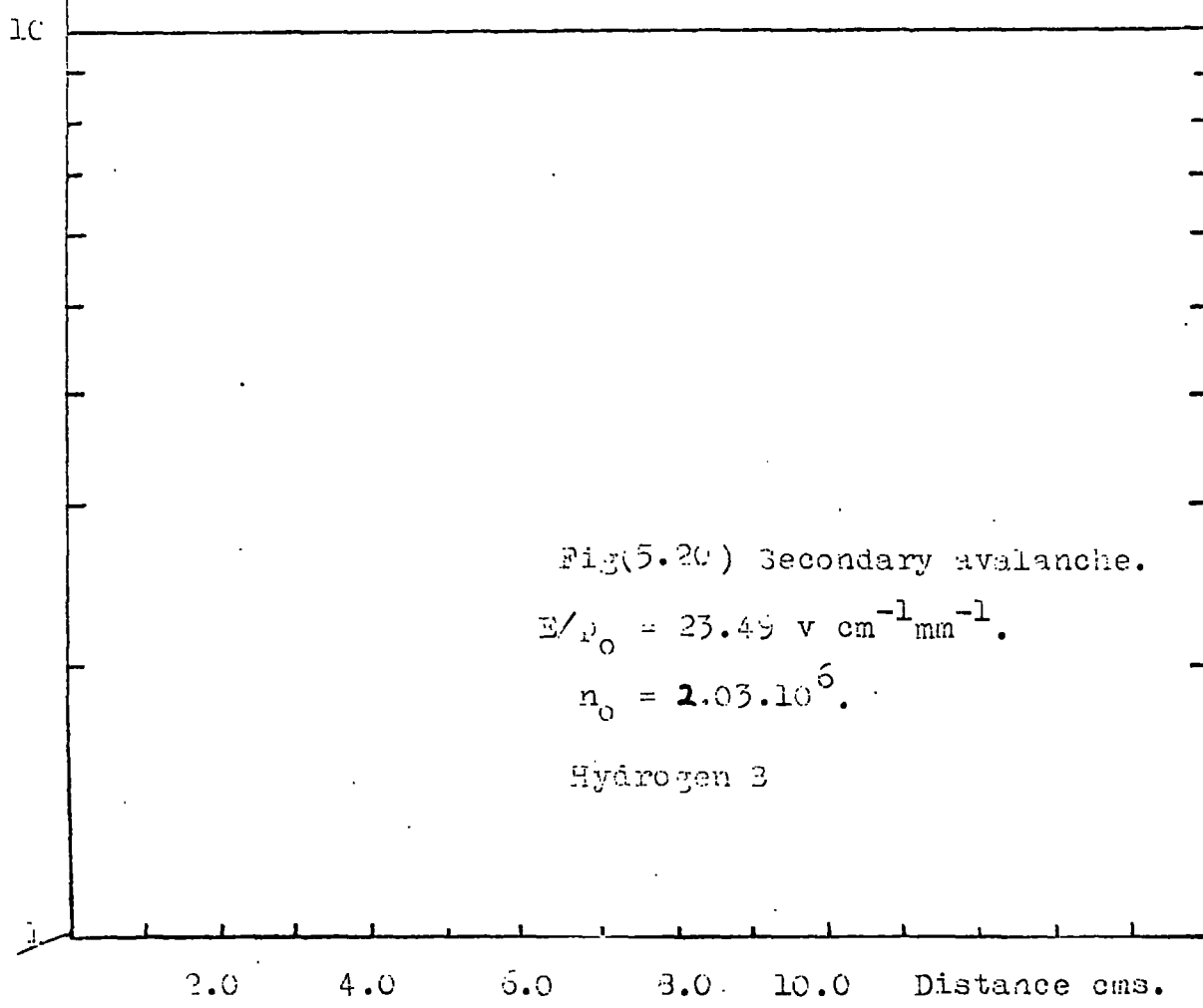
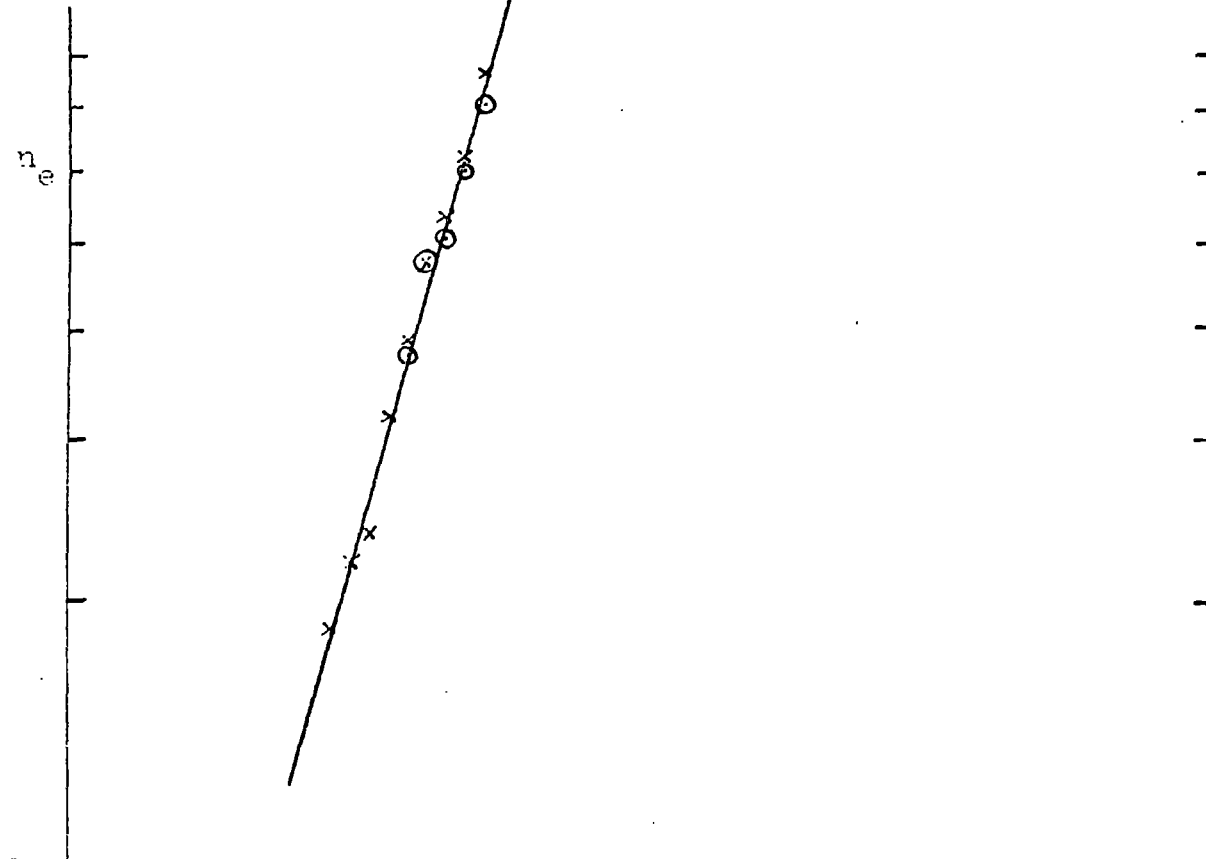


Fig(5.19) Secondary avalanche.

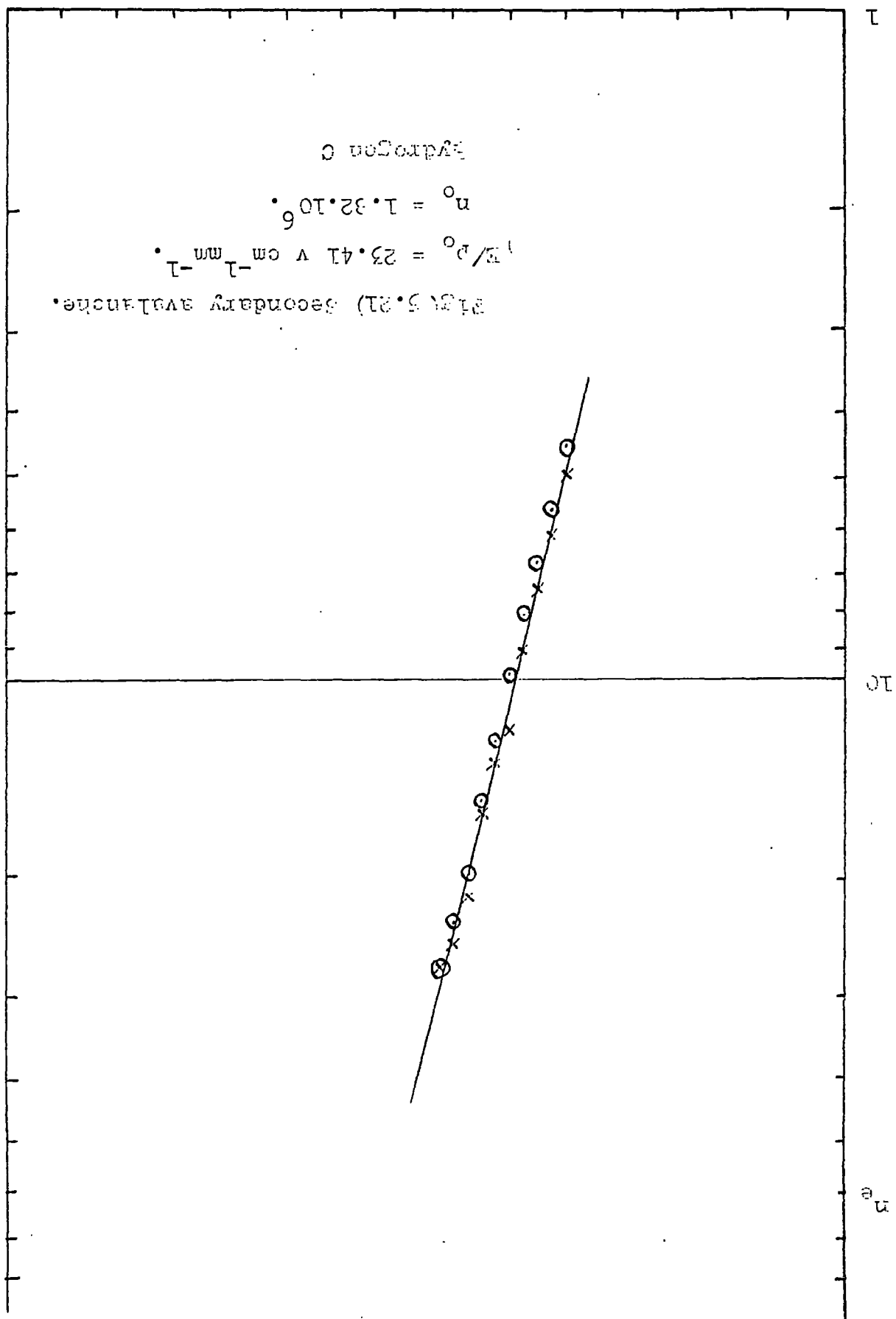
$E/p_0 = 23.52 \text{ v cm}^{-1} \text{ mm}^{-1}$.

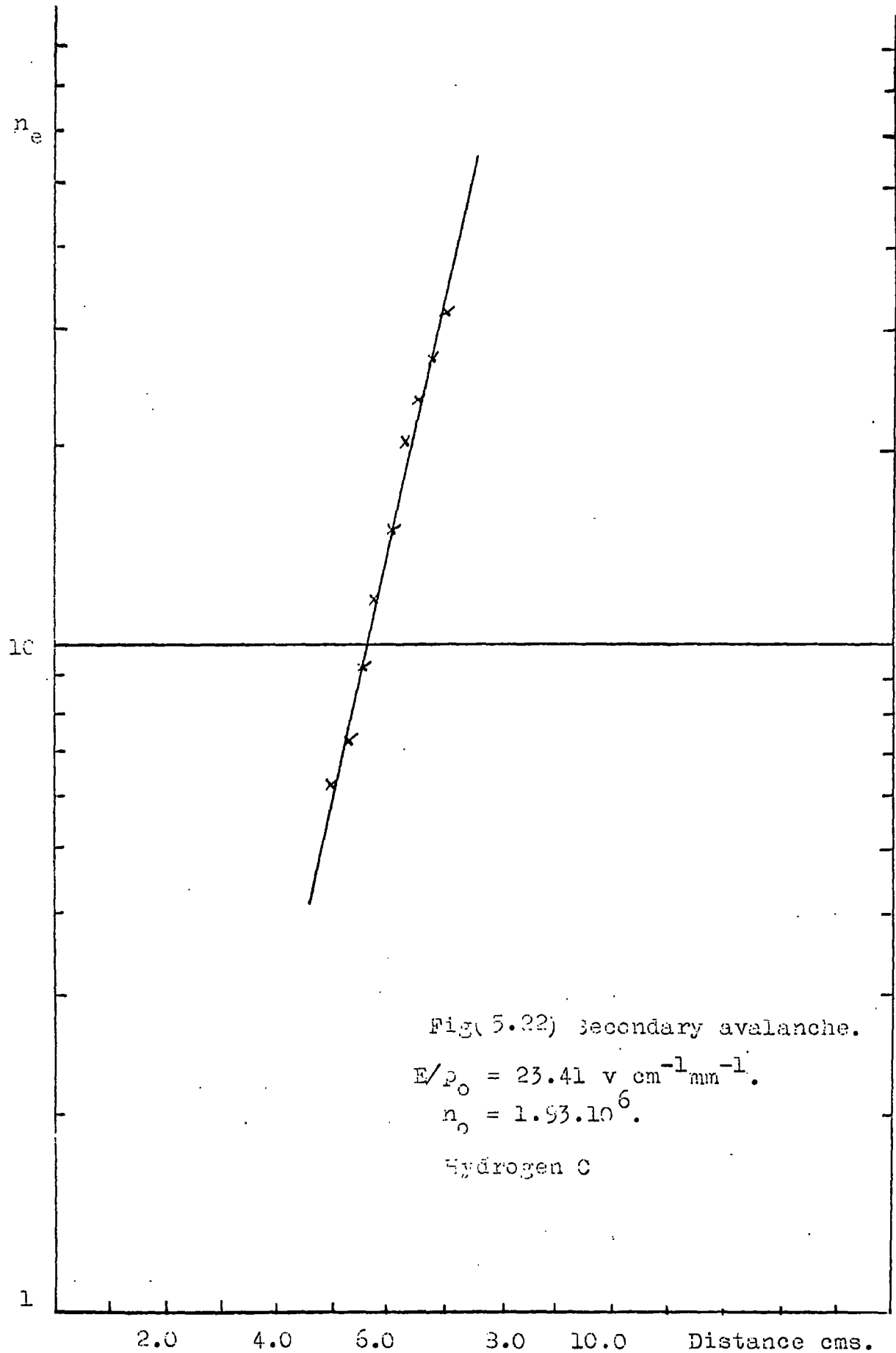
$n_0 \approx 1.33 \cdot 10^6$.

Hydrogen B



2.0 4.0 6.0 8.0 10.0 Distance cms.



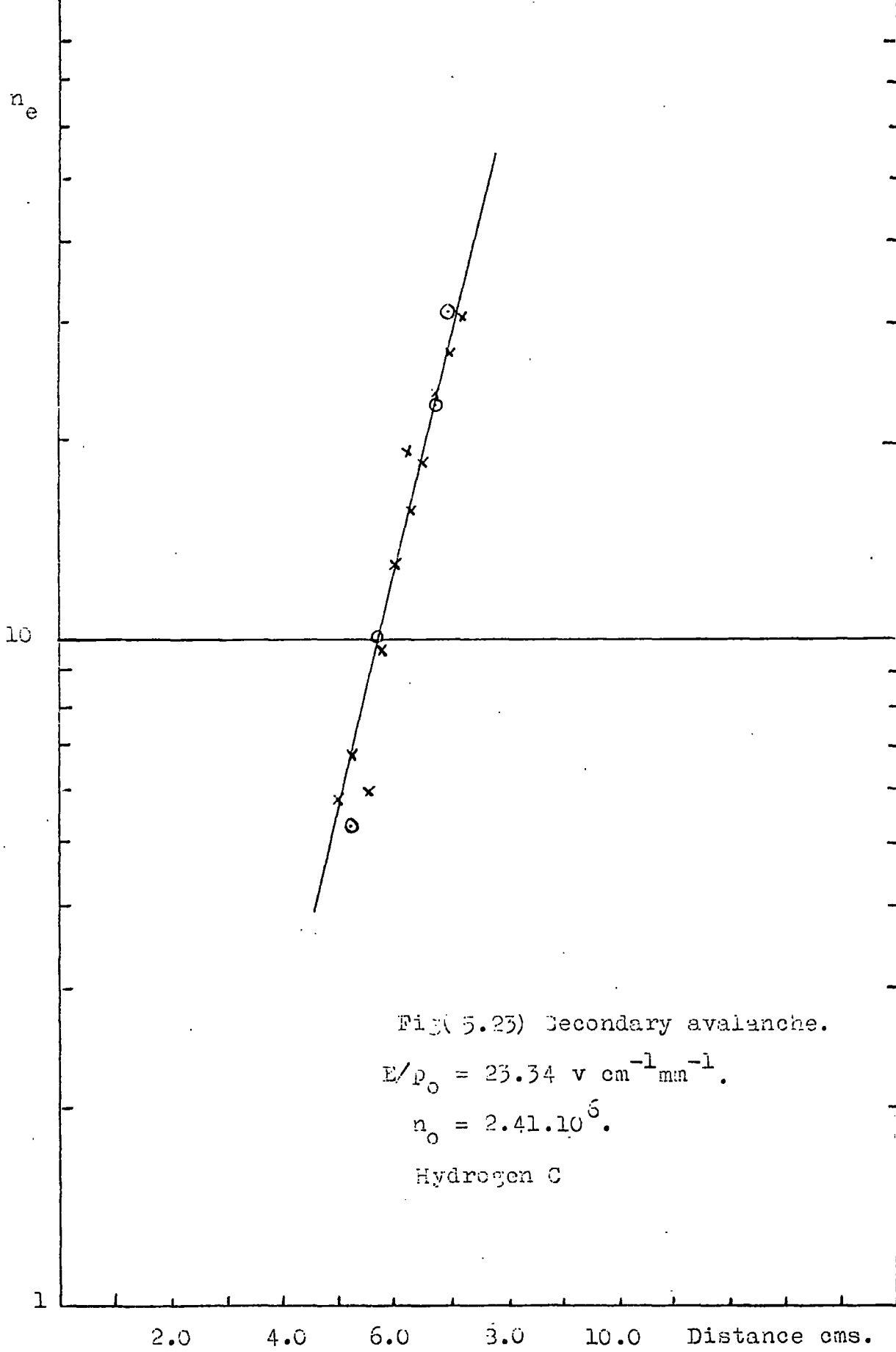


Fig(5.22) Secondary avalanche.

$E/p_0 = 23.41 \text{ v cm}^{-1} \text{ mm}^{-1}$.

$n_0 = 1.93 \cdot 10^6$.

Hydrogen C



Fig(5.23) Secondary avalanche.
 $E/p_0 = 23.34 \text{ v cm}^{-1} \text{ mm}^{-1}$.
 $n_0 = 2.41 \cdot 10^6$.
 Hydrogen C

Gas sample	Figure number	Initial no. of starting electrons $n_0 \times 10^6$		Primary swarms		Secondary swarms		α/p_0 (Rose)	E/p_0 $v \text{ cm}^{-1} \text{ mm}^{-1}$	p mm Hg	d cm
		Galv.	Oscill.	α	α/p_0	α	α/p_0				
A	5.3	0.21	10^6	0.58	0.009			0.014	23.65	67.75	6.171
A	—	0.21	10^6	0.56	0.009			0.014	23.71	67.75	6.171
A	5.4	0.40	10^6	0.61	0.010			0.014	23.71	67.75	6.171
A	5.9	0.96	5×10^6	0.72	0.012			0.014	23.71	67.75	6.171
A	—	1.45	—	0.79	0.013			0.014	23.56	67.75	6.171
A	5.10	2.03	—	0.71	0.011			0.012	23.07	67.75	6.171
B	5.11	0.70	3×10^6	0.75	0.012	0.78	0.013	0.015	23.80	64.00	6.171
B	5.5	0.56	10^6	0.74	0.012	0.81	0.013	0.015	23.88	64.00	6.171
B	5.12	1.27	6×10^6	0.66	0.011			0.015	23.86	64.00	6.171
B	5.13 & 19	1.88	9×10^6	0.63	0.010	0.89	0.014	0.014	23.52	64.00	6.171
B	5.20	2.00	9×10^6	0.63	0.010	0.89	0.014	0.014	23.49	64.00	6.171

Table (2) Ionization coefficients.

Gas sample	Figure number	Initial no. of starting electrons $n_0 \times 10^6$ Galv. Oscill.		Primary swarms		Secondary swarms		α/p_0 (Rose)	E/p_0 $v \text{ cm}^{-1} \text{ mm}^{-1}$	p mm Hg	d cm
				α	α/p_0	α	α/p_0				
C	5.6	0.41	$< 10^6$	0.64	0.012	0.88	0.016	0.013	23.39	60.45	7.210
C	5.14	1.55	6×10^6	0.72	0.013	0.65	0.012	0.015	23.80	60.45	7.210
C	5.16*21	1.82	6×10^6	0.63	0.010	0.79	0.014	0.013	23.41	60.45	7.210
C	5.17*22	1.93	6×10^6	0.50	0.009	0.86	0.015	0.013	23.41	60.45	7.210
C	5.23	2.41	—	0.58	0.010	0.80	0.014	0.013	23.34	60.45	7.210
D	—	0.58	$< 10^6$	0.82	0.015	0.80	0.015	0.012	23.14	60.95	7.210
D	—	0.96	5×10^6	0.53	0.010	0.87	0.016	0.012	23.14	60.95	7.210

Primary swarms:

Value of α/p_0 , if the values of E/p_0 are normalized to $23.50 \text{ v cm}^{-1} \text{ mm}^{-1}$.

$$\alpha/p_0 = 0.011 \text{ cm}^{-1} \text{ mm}^{-1}$$

$$\sigma = 0.002 \text{ cm}^{-1} \text{ mm}^{-1}$$

Secondary swarms:

Value of α/p_0 , if the values of E/p_0 are normalized to $23.50 \text{ v cm}^{-1} \text{ mm}^{-1}$.

$$\alpha/p_0 = 0.014 \text{ cm}^{-1} \text{ mm}^{-1}$$

$$\sigma = 0.003 \text{ cm}^{-1} \text{ mm}^{-1}$$

Table(2) cont.

5.4 Measurements of the electron drift velocities

Drift velocities of the primary and secondary electron swarms have been calculated in the following manner. The oscilloscope traces represent the variation in the number of electrons within a swarm with time, at given points across the gap. The position of the photomultiplier has been plotted against the time at which the amplitude of the oscilloscope trace reaches a maximum. This has been done for both primary and secondary swarms, and the times are measured from a time-zero set by the discharge of the source condenser. The slope of these graphs gives the drift velocity of the point of maximum electron density in the swarm.

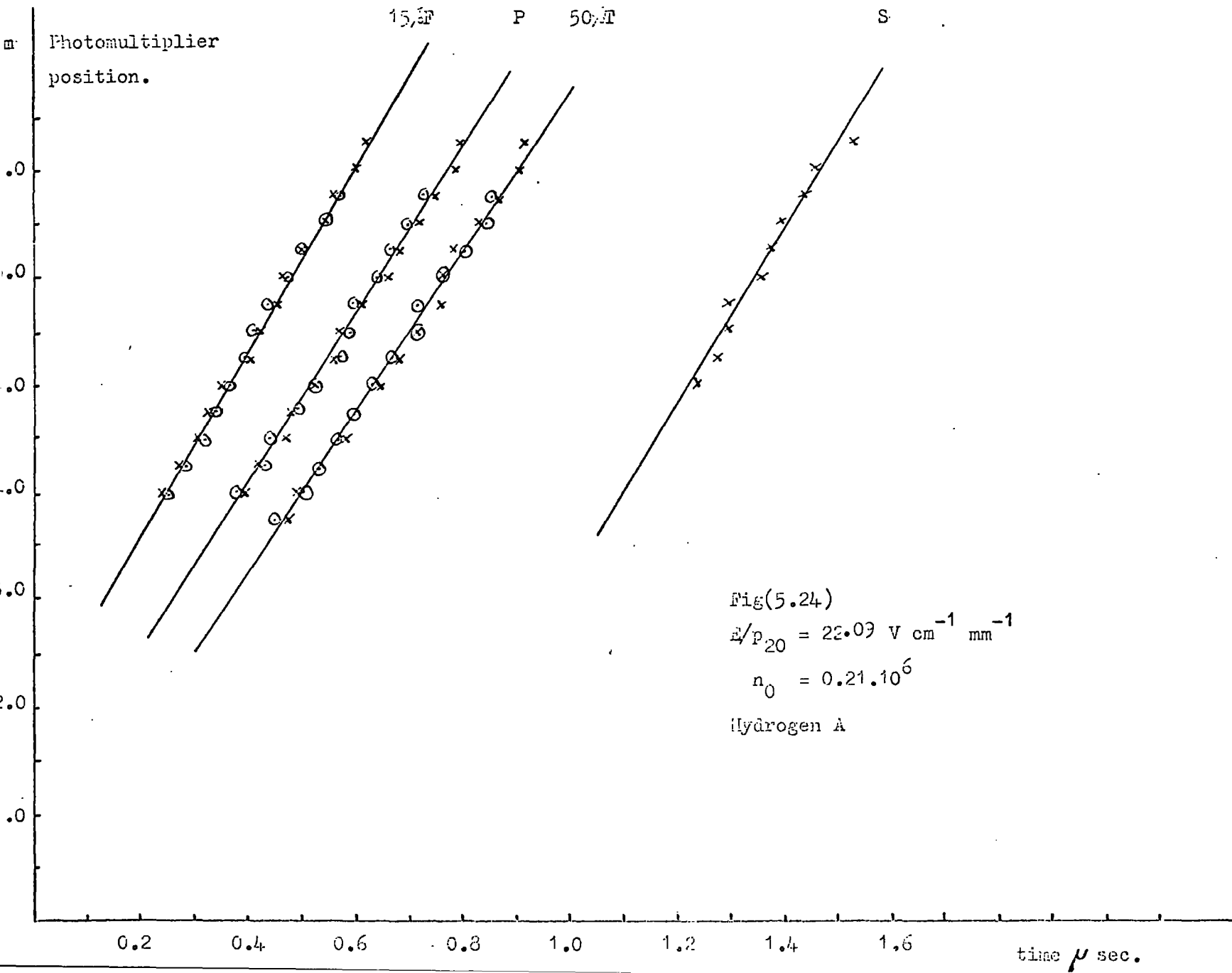
Figs. (5.24 - 5.31) are typical examples; the graphs marked P refer to **p**rimary swarms, and the graphs marked S refer to secondary swarms. Drift velocities of various sections of the primary electron swarms have also been measured. Graphs marked $x\%F$ or $x\%T$ in Figs. (5.23-5.31) refer to the motion of sections of the swarm where the electron number is $x\%$ of the peak value. F and T refer to sections in the front and tail of a swarm respectively.

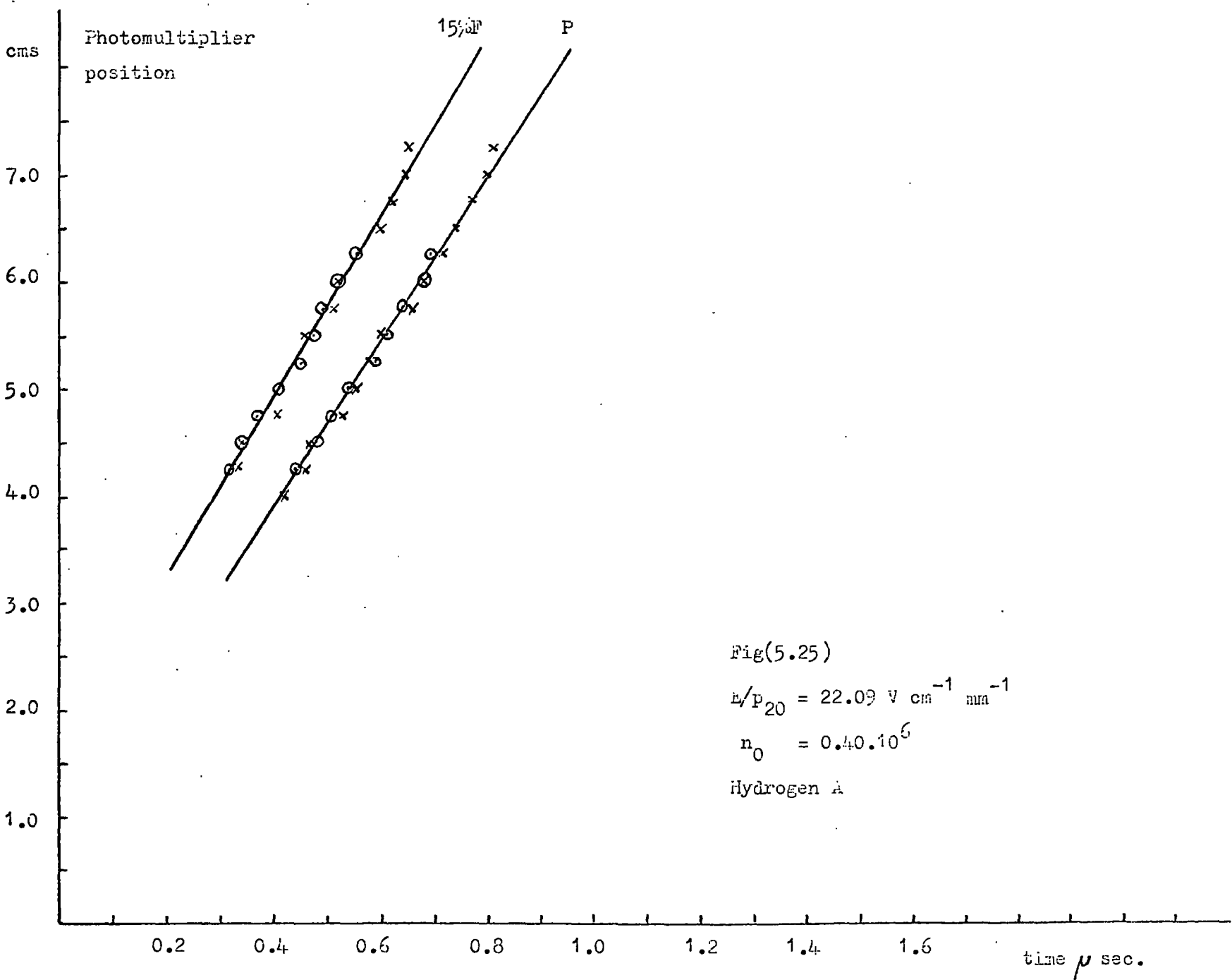
The values for the drift velocities so obtained are shown in Table (3), and are compared with values obtained by Bradbury and Nielson⁽³⁰⁾ and others^{(31), (32), (33)} at similar values of E/p . The values obtained in the present experiment are seen to be above

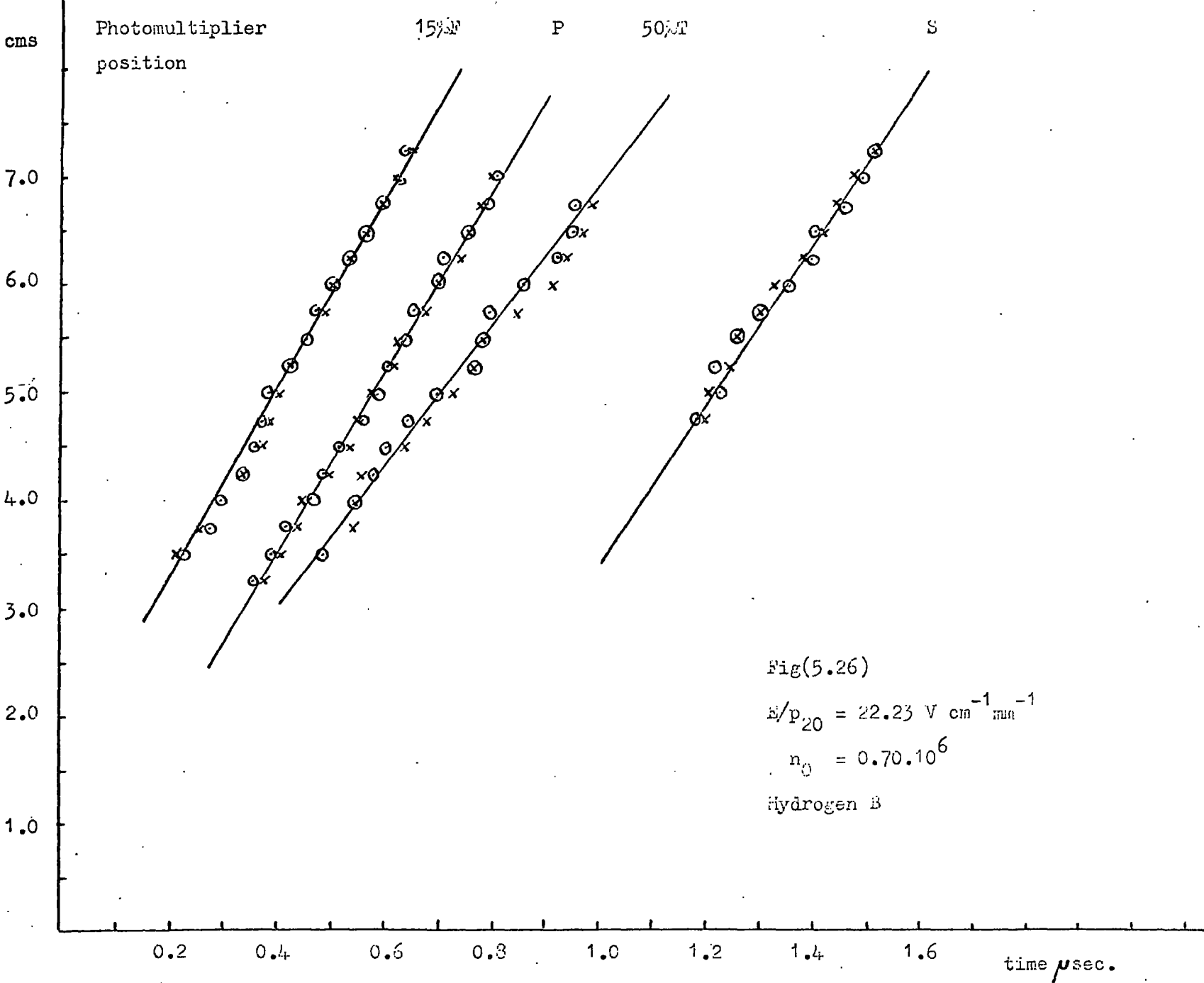
these published values; values of upto 18% higher are recorded.

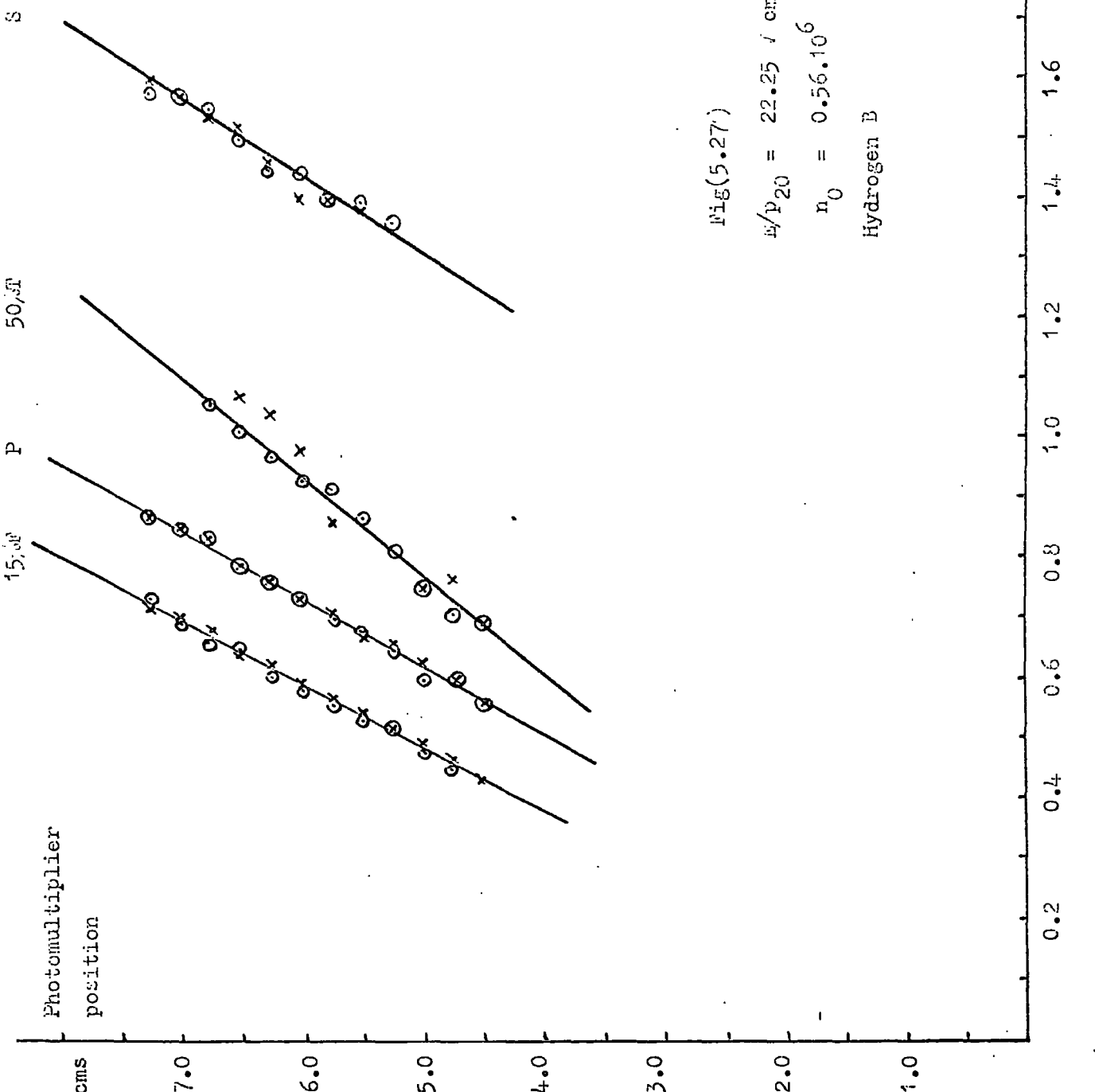
It is also apparent from the graphs, that viewed from an inspection window at the side of the electrode gap, the velocities of electrons contained in the front of the swarm (anode-side), are above the velocities of electrons in the swarm centre. The converse is true of electrons in the tail (cathode-side) of the swarm.

In the following sections these effects are treated by considering the motion of the primary swarms by drift and diffusion.







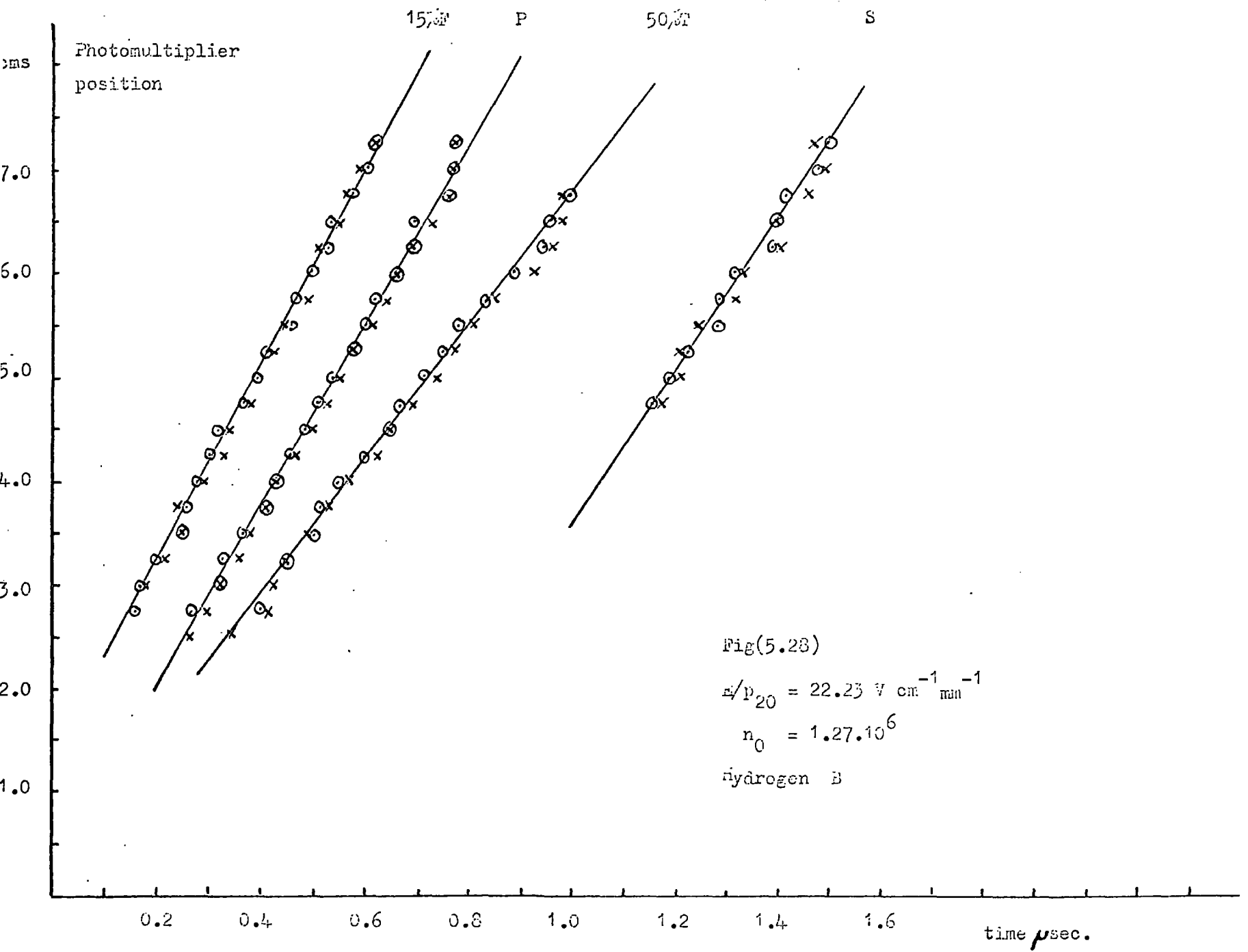


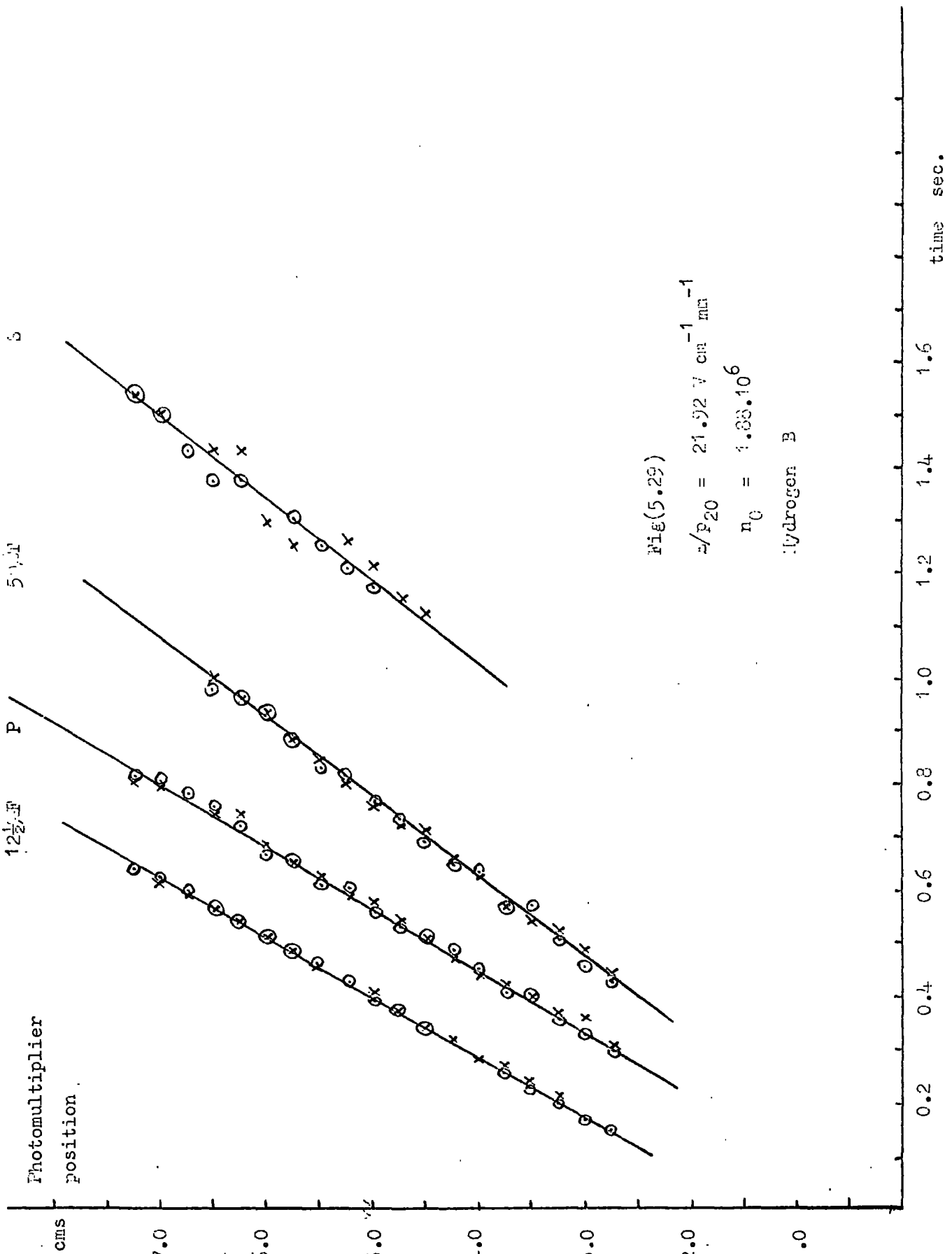
Fig(5.27)

$$\omega/p_{20} = 22.25 \text{ } \nu \text{ cm}^{-1} \text{ min}^{-1}$$

$$n_0 = 0.56 \cdot 10^6$$

Hydrogen B





S

P

Pulse front

Photomultiplier position

ms

3.0

7.0

5.0

5.0

4.0

3.0

2.0

1.0

0.2

0.4

0.6

0.8

1.0

1.2

1.4

1.6

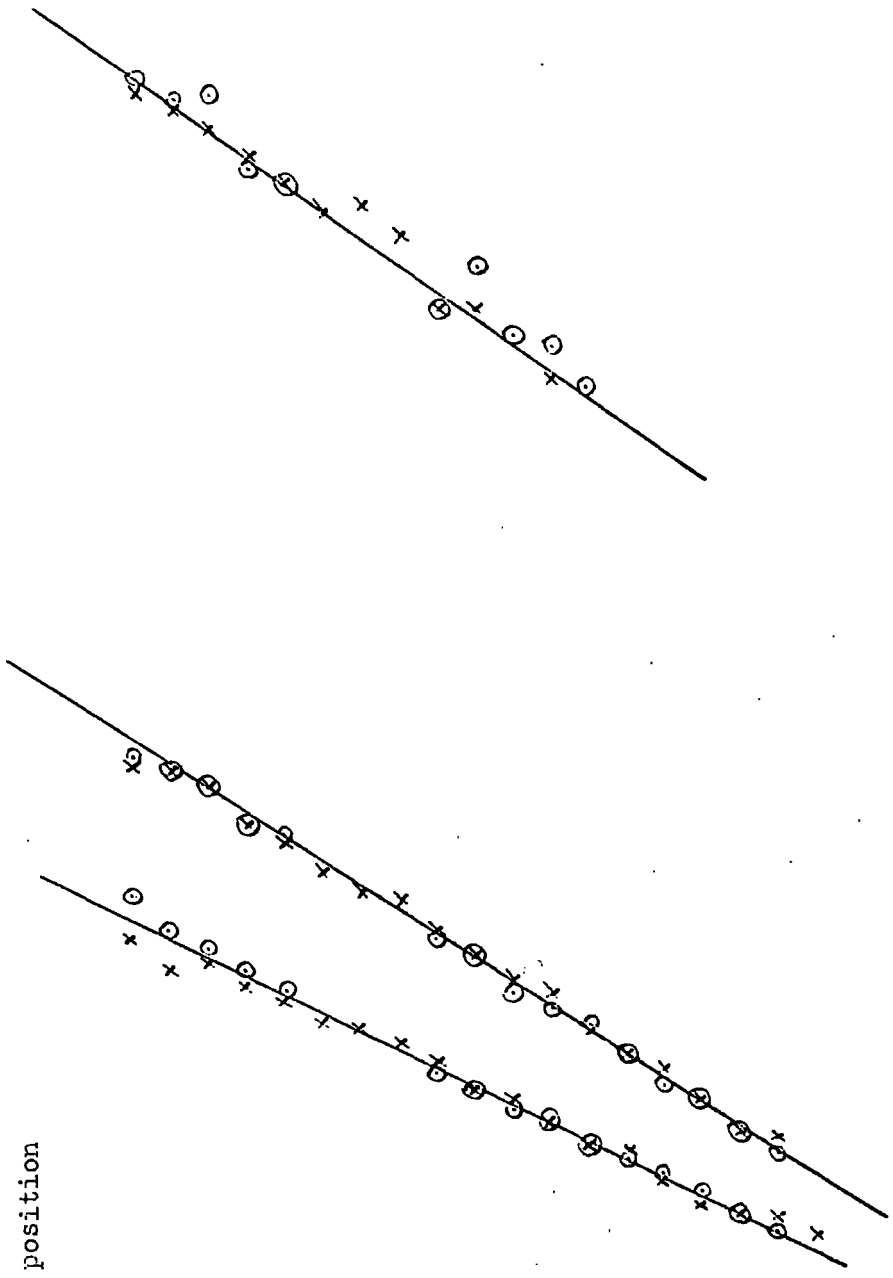
1.8

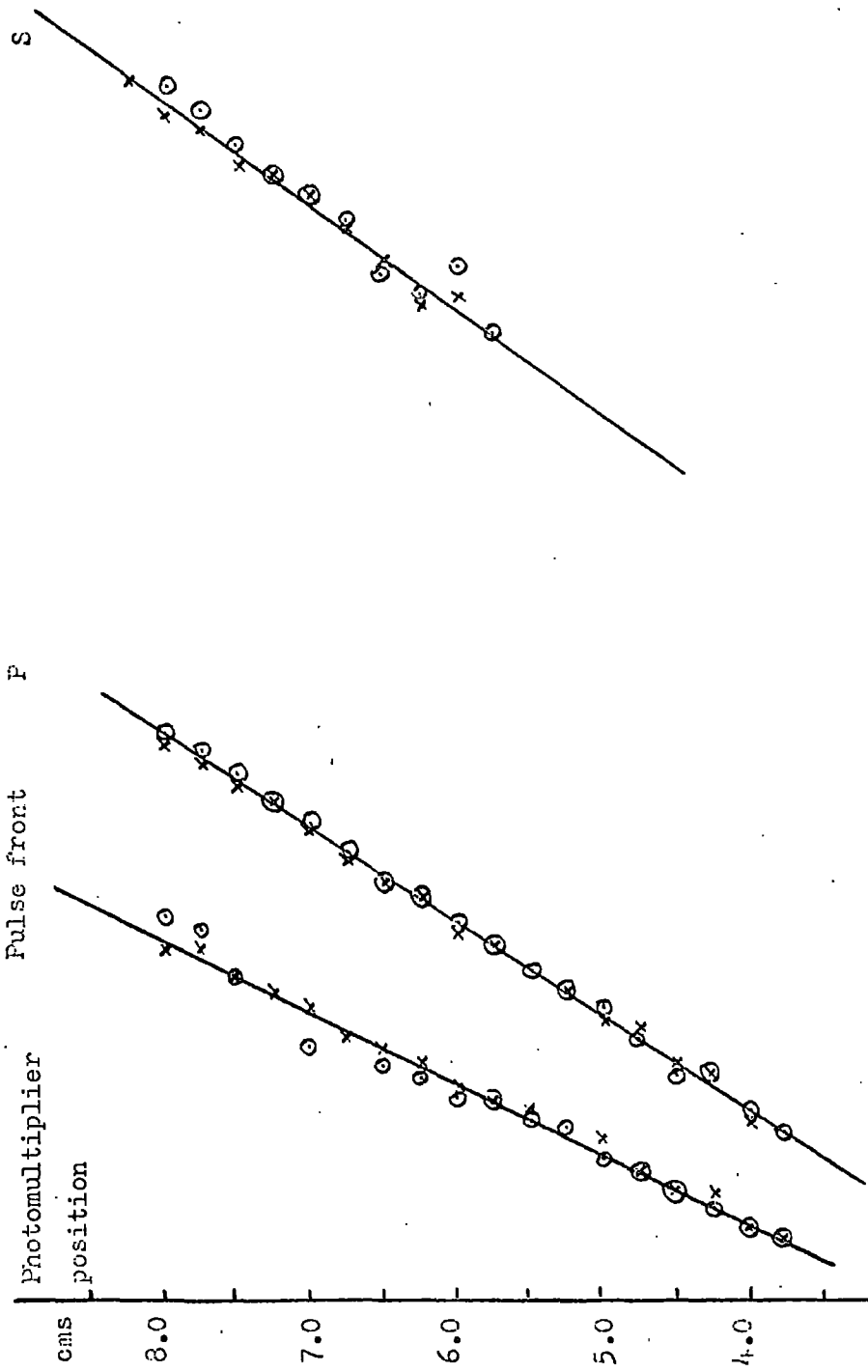
Fig (5.50)

$E/P_{20} = 21.81 \text{ V cm}^{-1} \text{ mm}^{-1}$

$n_0 = 1.56 \cdot 10^6$

Hydrogen C



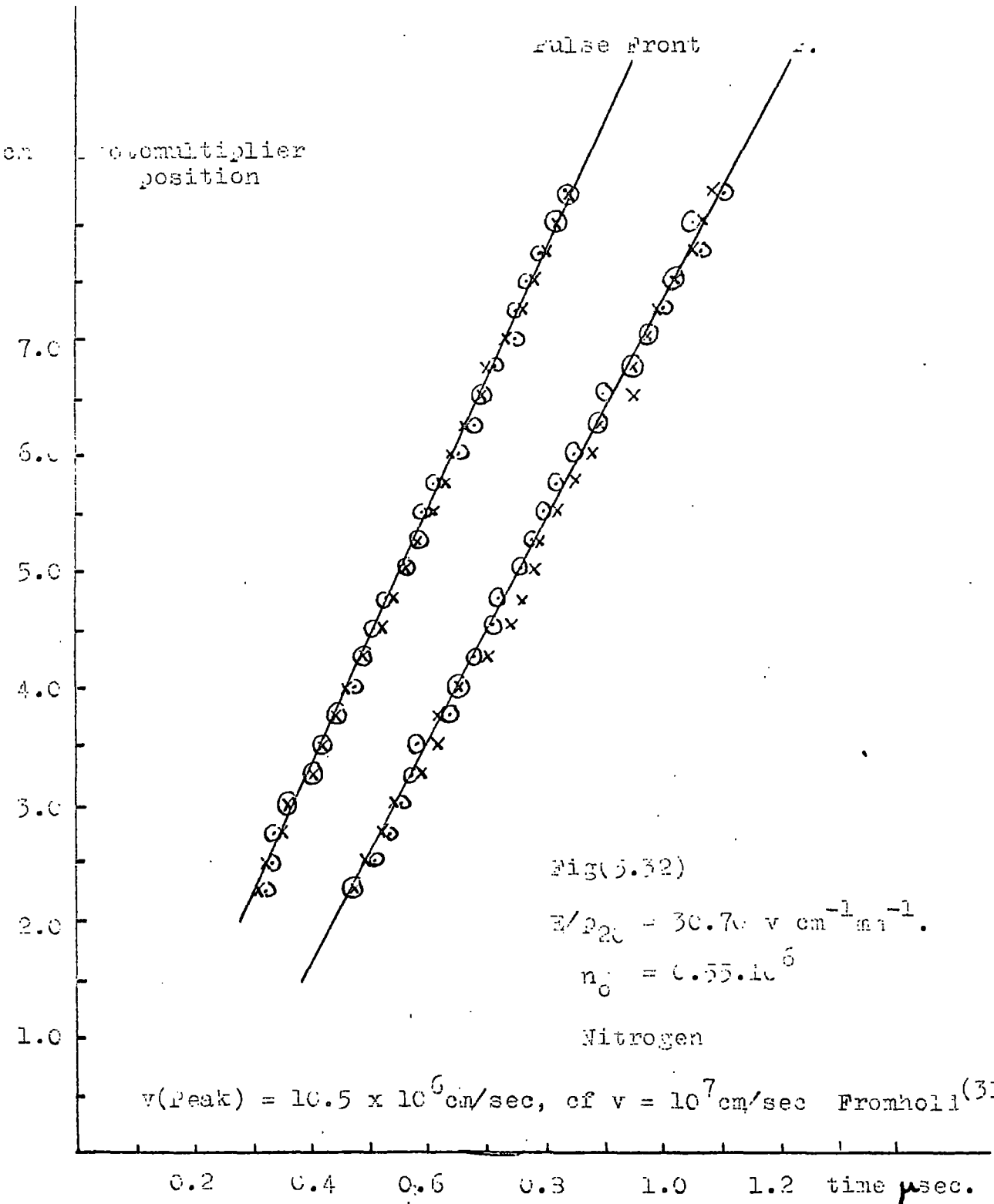


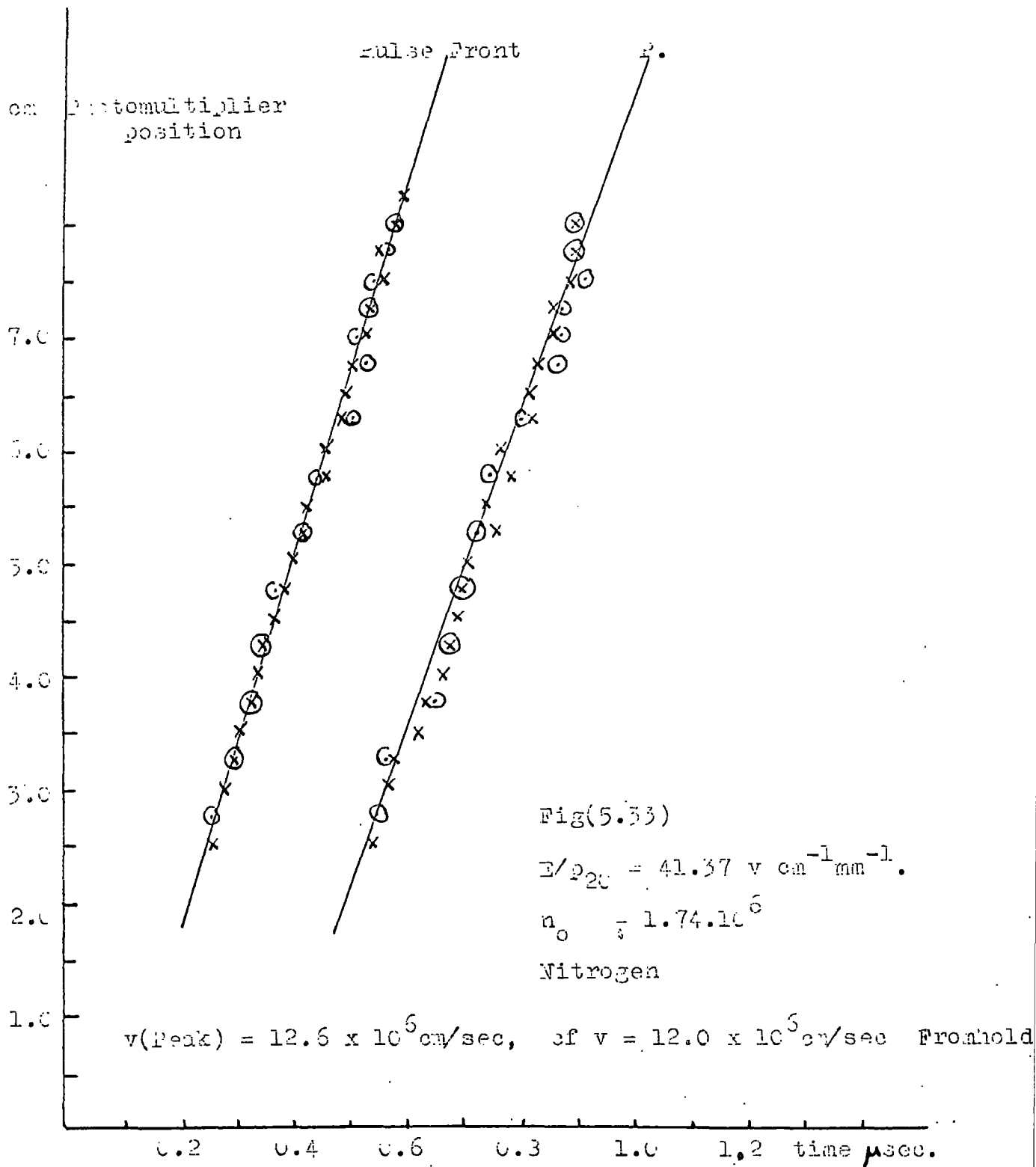
FIG(5.31)

$\omega/P_{20} = 21.56 \text{ V cm}^{-1} \text{ min}^{-1}$

$n_0 = 1.03 \cdot 10^6$

Hydrogen D





Gas sample	Figure number	Initial no of electrons per swarm $n_0 \times 10^6$	Primary $v_d \times 10^6$ cm/sec	Secondary $v_d \times 10^6$ cm/sec	Bradbury Nielson $v_d \times 10^6$ cm/sec	E/p_{20} $V \text{ cm}^{-1} \text{ mm}^{-1}$
A	5.24	0.21	7.77		7.60	22.09
A	5.25	0.40	7.71		7.60	22.09
A	5.31	0.96	8.32	7.83	7.60	22.09
A		2.03	8.35		7.40	21.49
B	5.27	0.56	8.88	7.66	7.66	22.25
B	5.26	0.70	8.32	7.45	7.66	22.23
B	5.28	1.27	8.67	7.39	7.66	22.23
B	5.29	1.88	8.47	6.39	7.57	21.92
C		0.41	7.60		7.50	21.80
C	5.30	1.36	7.85	7.13	7.50	21.81
C		1.55	8.44	7.93	7.65	22.18
C		1.93	8.22	7.37	7.50	21.81
C		2.41	8.21		7.50	21.75
D	5.31	0.96	7.72	7.06	7.42	21.56

Table (3) Electron drift velocities
in hydrogen.

5.5 Drift and Diffusion

5.5.1 Basic diffusion relations and particle distribution under diffusion

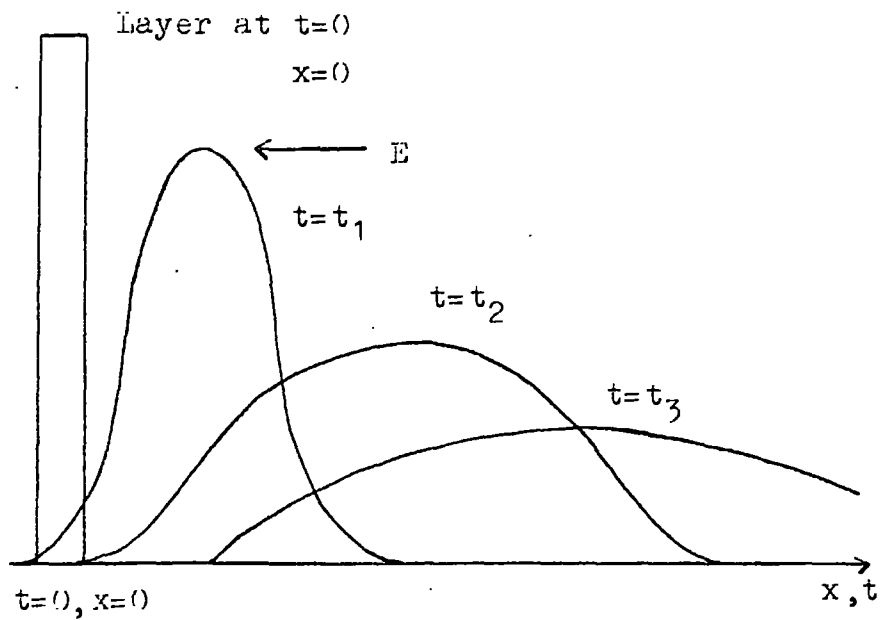
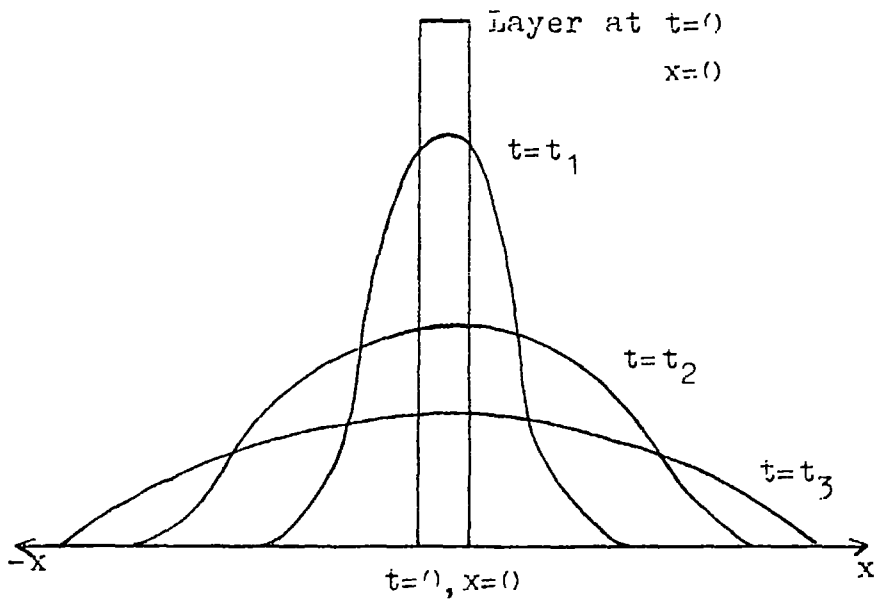
Diffusion of particles is said to have occurred if there is a net transfer of particles from a region of high concentration to one of low concentration. The origin of the motion is thermal, and the particles, which are in constant collision with each other, follow random paths. Eventually this diffusive motion will bring about a uniform density of particles within the gas, and although diffusion of particles from one region to another still occurs, a steady state condition is reached.

Fick's law describes a system of particles to which no external forces are applied. In a gas, consider a plane along which the electron density is constant and equal to n . The concentration gradient at the plane is then $\partial n / \partial x$, and Fick's law states—that:

$$\begin{array}{l} \text{the particle flow crossing unit} \\ \text{area of plane per second} \end{array} = - D \partial n / \partial x.$$

The negative sign indicates that the flow of particles is in the direction of decreasing concentration. In the case of electrons, D is the diffusion coefficient for free electrons, and is given approximately by⁽³⁴⁾

$$D = \lambda \bar{c} / 3$$



Figs(5.34 & 5.35) Diffusion of an electron layer in field free space (34) and in an electric field.

where λ is the mean free path of an electron between collisions with gas molecules, and \bar{c} is the average random velocity of the electrons, assuming a Maxwellian distribution.

Einstein⁽³⁵⁾ considered the spatial and temporal distribution of particles moving independently of each other with chaotic heat motions. Consider an origin at $x=0$, at which there are N_0 particles at time $t=0$. Then the number of these particles which are located between x and $x+dx$ at a time t is

$$N_x = \frac{N_0}{\sqrt{(4\pi Dt)}} e^{-x^2/4Dt} dx$$

This expression has the form of the Gaussian error curve, and as t increases, the scale factor $4Dt$ increases, causing the curve to decrease in height, (N_x/N_0 decreases), Fig. (5.34). It has been shown that the average displacement of any electron, considering the motion in one, two, or three dimensions is $(\frac{4Dt}{\pi})^{\frac{1}{2}}$, $(\frac{8Dt}{\pi})^{\frac{1}{2}}$, or $(\frac{12Dt}{\pi})^{\frac{1}{2}}$ respectively. These relations are useful in estimating the average dispersion of particles in time, or the average distance a particle diffuses in a time t .

If now the electron layer is considered to be drifting under the influence of a small electric field, the electron distributions are shown with respect to the same axes in Fig. (5.35). Although the field strengths employed in the present experiment are comparatively high, this diagram gives a good indication of the expansion of a primary electron swarm in the absence of ionization. It also indicates how the observed range of velocities for different

sections of the swarms occurs, and a comparison is made in section 5.6 between this simple theoretical model and the swarm distributions measured in the experiment.

5.5.2 The velocity of the primary electron swarms

The drift velocity of the primary swarm centres is higher than that recorded by other workers at this value of E/p . This is in agreement with the experimental work of Breare⁽²⁰⁾ in which electron drift velocities in hydrogen were measured over a range of gas pressures. ($p = 2, 20, 40, 80$ and 90 mm Hg). The drift velocities of the electrons in his experiments were measured in two ways. At $p = 2$ mm, the drift velocity was calculated from the time taken for the centre of an electron swarm to drift between two points in an electrode gap some cms apart. At the higher pressures the drift velocity of the front of the electron swarms was measured. The results obtained at 2 mm showed that the drift velocity of the swarm centres was higher than would be expected at the reduced field applied to the gap. The drift velocities of the front of the electron swarms were also higher than expected at 20, 40, and 80 mm Hg. However at $p = 90$ mm Hg, the values of the drift velocity agreed well with the generally accepted values published by Bradbury and Nielson⁽³⁰⁾.

Breare concluded that the variation in velocity with pressure was caused by diffusion; and that there was a component of velocity in the field direction superimposed on the drift motion

resulting from diffusion of electrons in the swarm. This conclusion indicates that there was a net transfer of electrons in the field direction, or that there was an anisotropy in the number density distribution. As the gas pressure was increased, diffusion became less pronounced, and the velocity of the front of the swarm slowly decreased. The velocity measured at $p = 90$ mm, corresponded to the true drift velocity.

The measurements of swarm drift velocities in the present experiment at a gas pressure of 60 mm Hg support this argument of a forward velocity component produced by electron diffusion. The factors causing this increased swarm velocity become more apparent by considering the one dimensional continuity equation governing the increase of the electron component of the discharge current:

$$\frac{\partial \rho_e}{\partial t} = \alpha(x,t) J_e(x,t) - \frac{\partial J_e}{\partial x} \quad (5.2)$$

Here ρ_e is the electron charge density,

$$\rho_e = n_e e$$

x is a distance measured from the cathode of a gap, which increases to $x=d$ at the anode. J_e is the current density, and is defined as

$$J_e = \rho_e \mu_e E - D \frac{\partial \rho_e}{\partial x} \quad (5.3)$$

μ_e is the electron mobility; D is the diffusion coefficient for free electrons, and E is the electric field strength in the electrode gap. J_e is considered positive for electrons moving

from cathode to anode.

Substituting for J_e in equation (5.2)

$$\frac{\partial n_e}{\partial t} = \alpha n_e \mu_e E - \alpha D \frac{\partial n_e}{\partial x} - \mu_e E \frac{\partial n_e}{\partial x} + D \frac{\partial^2 n_e}{\partial x^2} \quad (5.4)$$

If E is assumed to be constant, i.e. there is no significant space charge distortion of the applied field, α and D will also be constants. If now the second term on the right of equation (5.4) is considered, at the leading edge of the electron swarm $\frac{\partial n_e}{\partial x}$ is negative, and hence $\frac{\partial n_e}{\partial t}$ at this point exceeds that which would be the case if $\frac{\partial n_e}{\partial x}$ were zero. The converse is true at the trailing edge of the swarm, so that in each case the edge of the swarm experiences an increase in velocity. The combined effect is to increase the velocity of the electrons in the centre of the swarm above that determined by the electric field.

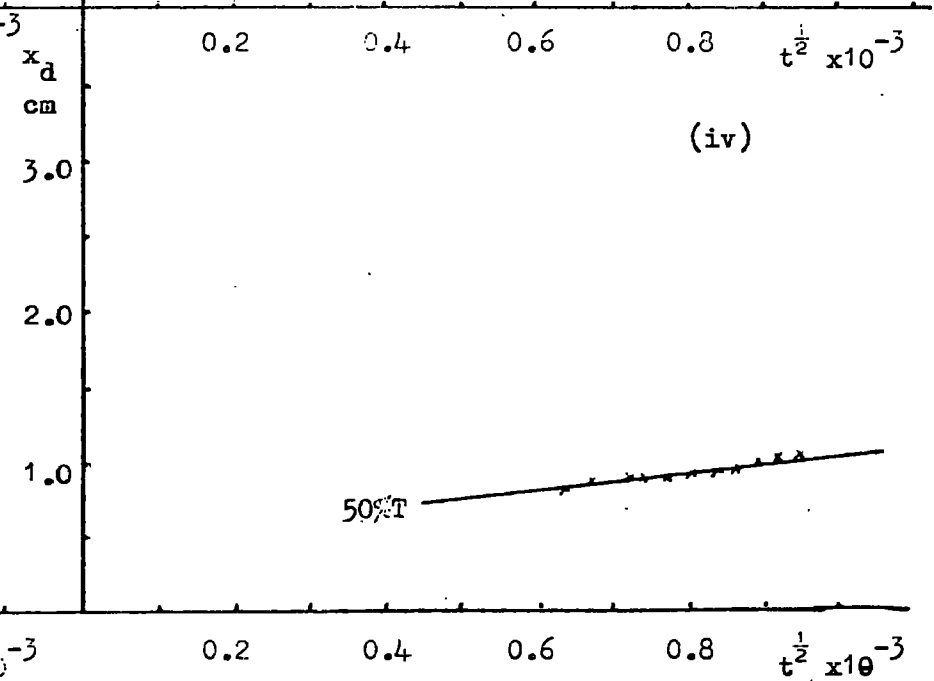
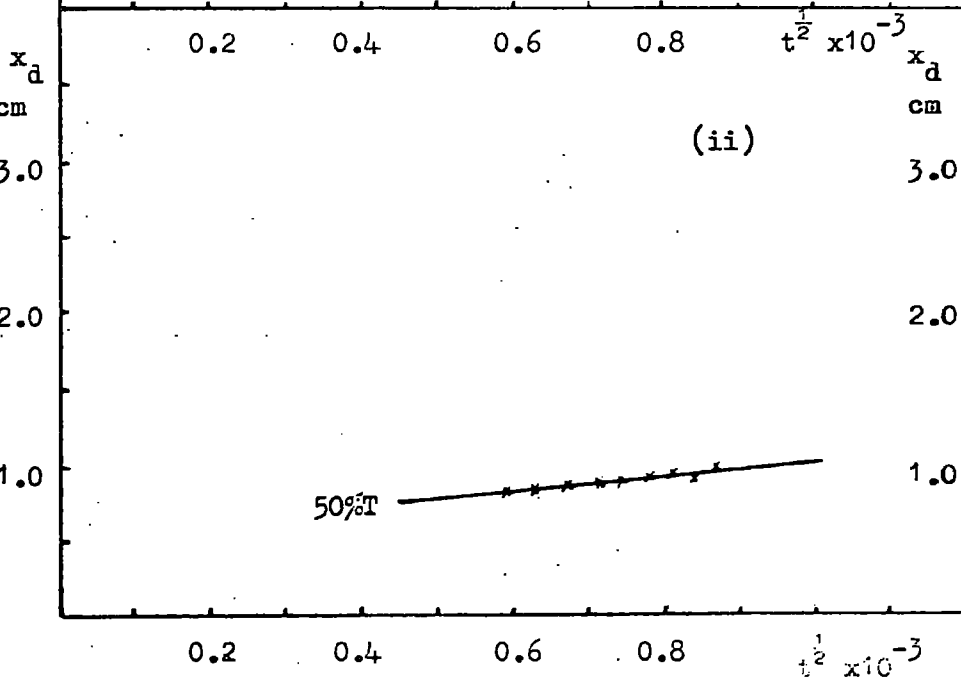
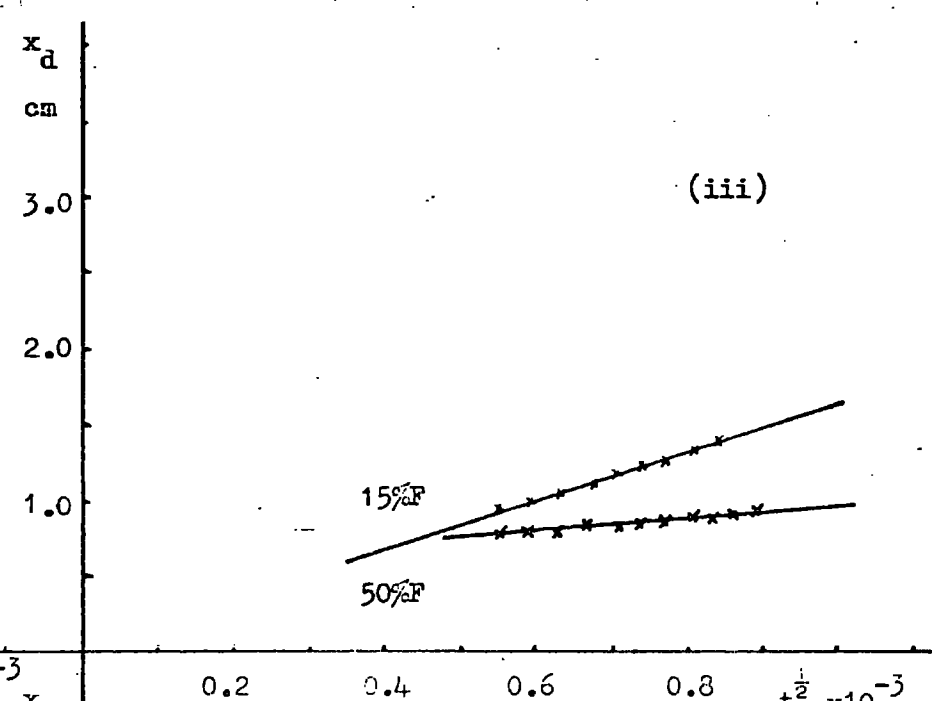
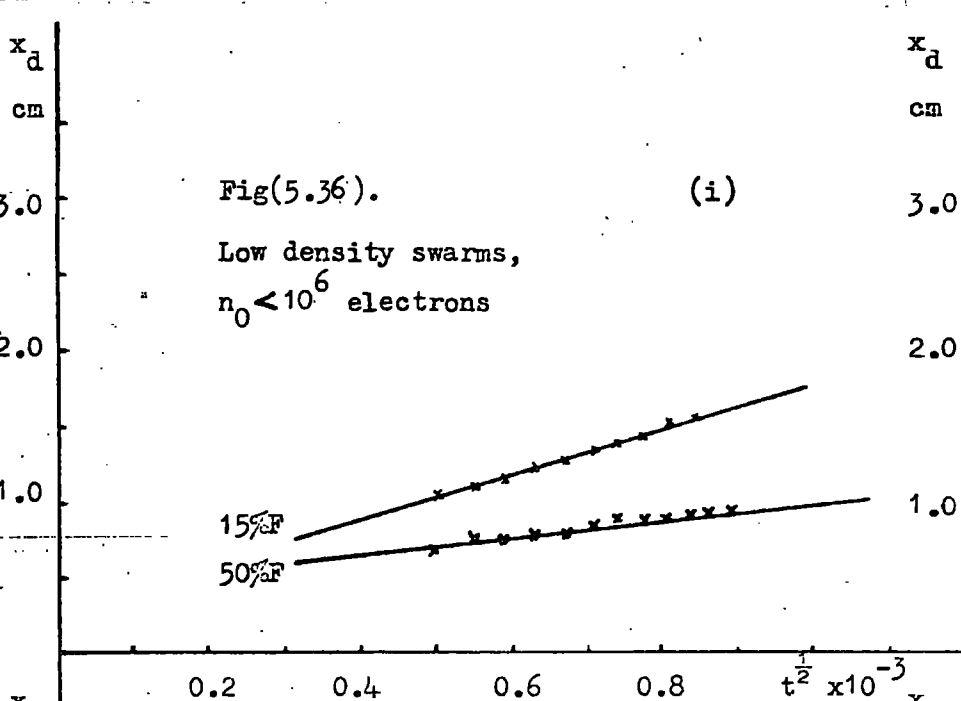
Unfortunately, at high values of the applied field it is not a valid approximation to consider the drift velocity of the swarm as the sum of two components; one caused by the action of the electric field, and the other resulting from a particle concentration gradient. The average drift velocity may not be calculated in this way because the electrons have a mean energy or temperature which is much higher than that of the gas molecules, and also in the present experiment, the drift velocity of the electrons is an appreciable fraction of the random electron velocity.

A quantitative analysis of the drift and diffusive motion of a high density electron swarm would be extremely complex and is beyond the scope of this thesis. However some of the aspects of the problems involved have been treated by Huxley⁽³⁶⁾, and by Crompton and Smith⁽³⁷⁾, who have discussed the diffusion of low energy electrons. Another treatment of the combined effects of drift and diffusion upon the motion of electron swarms has recently been published by Vincent⁽³⁷⁾. Here higher energy electrons are considered which were excited with a uhf electric field.

Summarising briefly, the experimental values obtained for the drift velocities of low density electron swarms at $p \sim 60$ mm Hg, in which the particle concentration gradients are not abrupt, agree with the experimental values published by Breare, and are somewhat above those recorded by other workers. In general, it is found that for swarms of high particle density, the drift velocity is further increased. This effect is attributed to the free diffusion of electrons within the swarm, which besides causing an enlargement of the swarm as it drifts across the electrode gap, also changes the electron distribution within the swarm with time, making measurement of the motion of the centre of the swarm, as opposed to the point of maximum electron density difficult to carry out.

The measurements of the drift velocities of the secondary electrons were of limited accuracy because of the lower intensity of the emitted radiation. However the velocities of these electrons is seen from Table (3) to be appreciably lower than the velocities

of the parent, primary swarms. It should be mentioned here that in none of the examples listed were the local field distortions sufficient to influence the drift velocity measurements.



5.6 Measurements of the electron diffusion coefficient

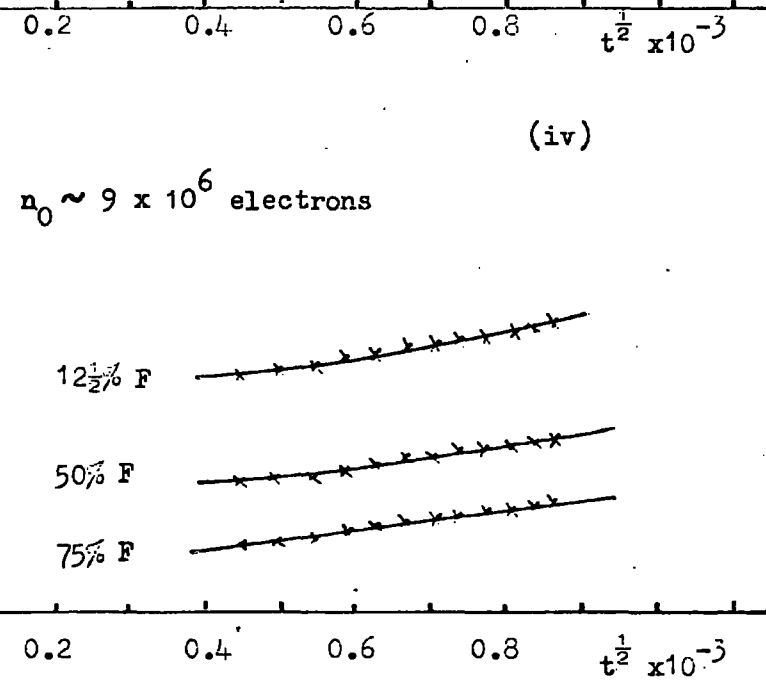
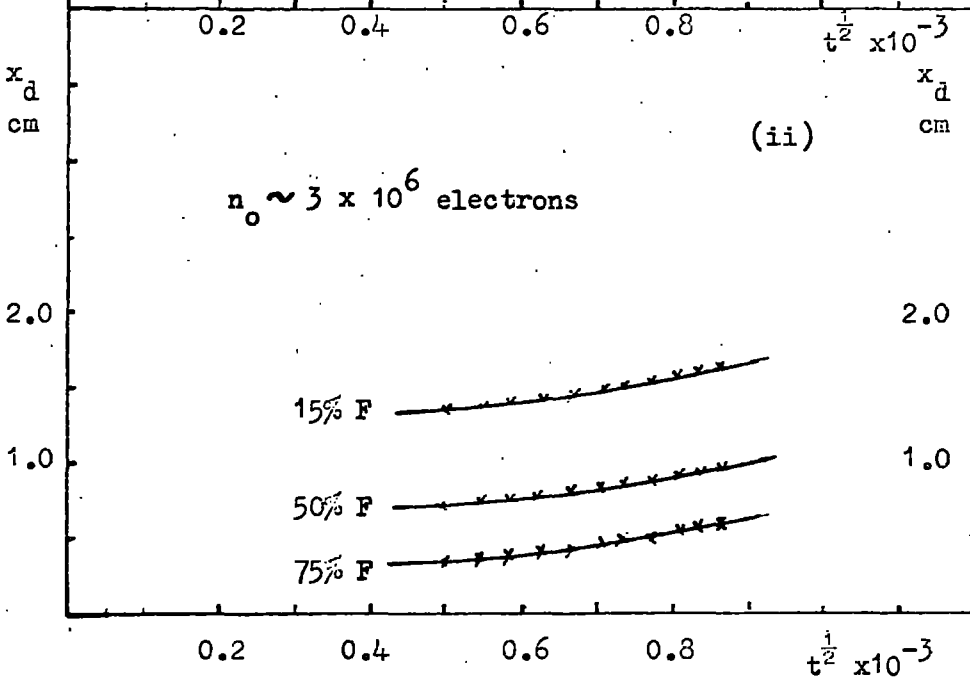
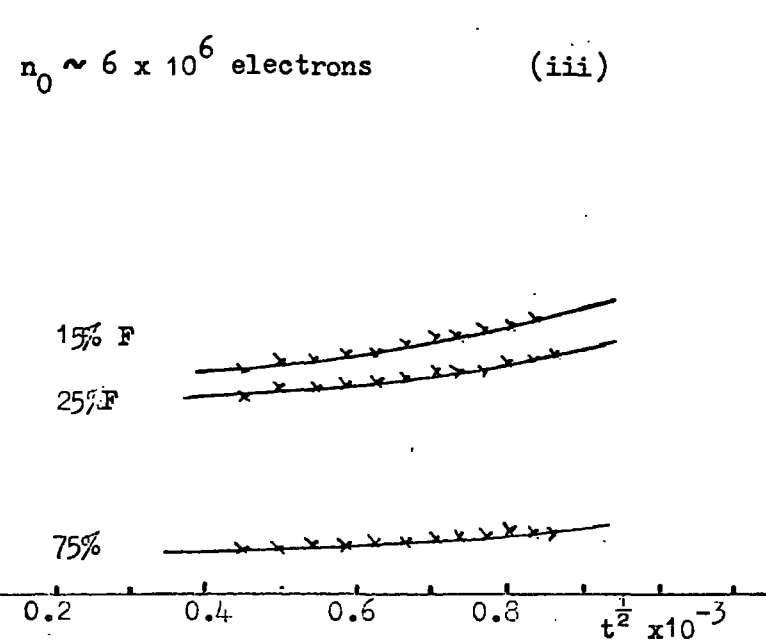
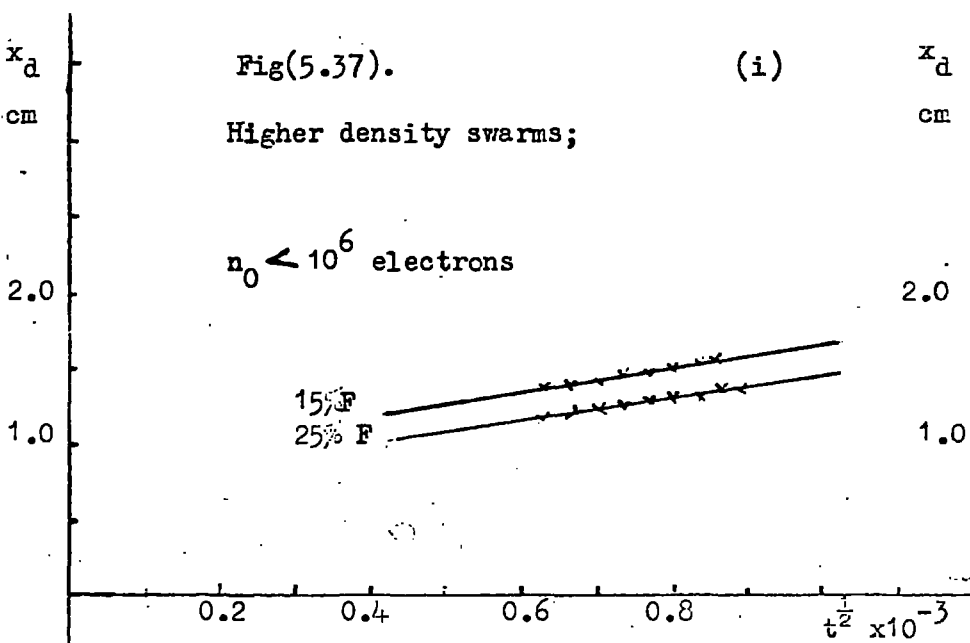
5.6.1 Axial diffusion of the electron swarms.

The method used to calculate the electron drift velocities has been described in a previous section of this chapter. The distance-time plots used, also yield information as to the motion of the electrons within the swarm, and in particular Figs. (5.30-5.33) besides showing the motion of the peak of a primary electron swarm, also describe the motion of the front of the swarm. The plots marked 50%T refer to points in the tail of the swarm at which the electron number is 50% of the peak value.

To investigate how the dimensions of the swarm increase with time, graphs have been plotted of the motion of various sections of the swarms, (Figs. (5.23-5.31)). From these plots a distance x_d has been measured, where x_d is the distance between the peak of the swarm and the % position under consideration. (At a particular time t , x_d is the difference in ordinates of the $x\%$ - graph and the P graph). This distance x_d has been plotted as a function of $t^{\frac{1}{2}}$, where t is the swarm drift time. Several examples may be seen in Fig. (5.36). For these low number density electron swarms the plots are linear, and an approximate value for the electron diffusion coefficient may be obtained by considering the slope of the graphs.

$$x_d = \sqrt{\frac{12Dt}{\pi}}$$

$$D = (\text{slope})^2 \frac{\pi}{12}$$



Other examples of this type of plot are shown in Fig. (5.37) and Fig. (5.57a), and values for the electron diffusion coefficient obtained are shown in Table (4). In the cases where the plots are curved, the slope was measured at the bottom of the graphs.

The values obtained for the diffusion coefficient from the 50%F and 50%d' graphs in Fig. (5.36) are similar. This agreement indicates that the rates of diffusion of electrons in either direction along the central electrode axis are also similar. However it would appear that at the front edge of the swarm (15%F position), the rate of diffusion is appreciably higher. This increased rate of diffusion is partly responsible for the curved plots shown in Fig. (5.37), which refer to the motion of electrons in various sections of the front of higher number density swarms. It is noted here that the curvature of the graphs becomes less marked as sections of the swarm located nearer to the swarm centre are considered.

A theoretical estimate of the diffusion coefficient may be obtained from the relation:

$$D = \frac{\lambda_e \bar{c}}{3}$$

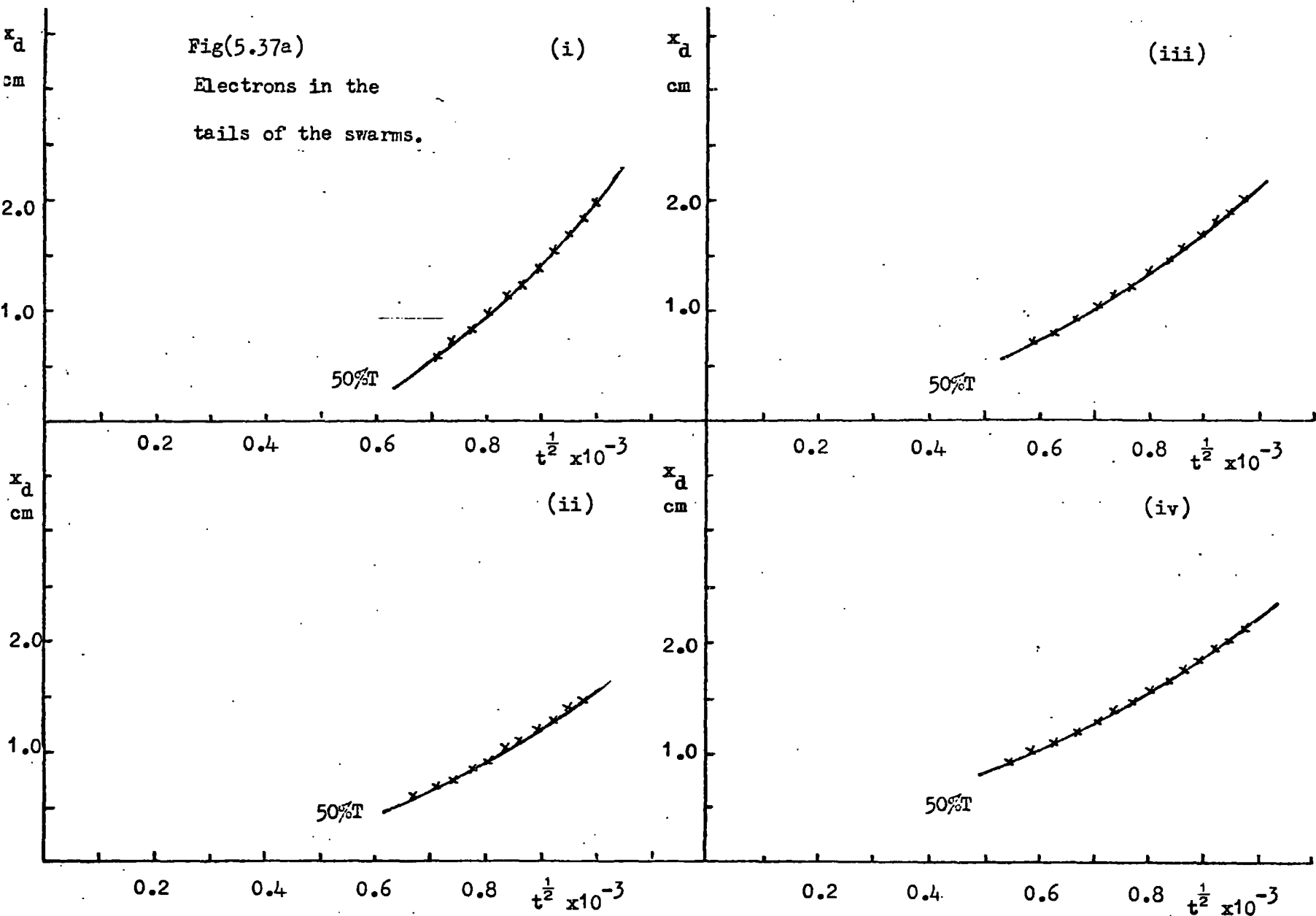
$$\sim 2.10^5 \lambda_e \sqrt{T_e}$$

$$\sim 2.10^7 \lambda_e \sqrt{V}$$

Here λ_e is the electron mean free path between collisions with gas molecules; \bar{c} is the average random velocity of the electrons, assuming a Maxwellian distribution; and T_e and V are the electron

Fig(5.37a)

Electrons in the
tails of the swarms.



Fig(5.37)	Measured from Fig()	D x10 ⁵ cm ² /sec.		
		15%F	25%F	75%F
(i)	5.27	1.2	1.2	
(ii)	5.26	1.3	1.5	1.4
(iii)	5.28	1.1	1.1	1.6
(iv)	5.29	1.4*	1.1	1.2

* 12.5%F

Fig(5.36)	Measured from Fig()	D x10 ⁵ cm ² /sec.		
		15%F	50%F	50%T
(i)	5.24	4.8	0.85	
(ii)		5.8	0.56	
(iii)	5.24			0.71
(iv)				0.65

Table (4) Electron diffusion coefficients.

temperatures in $^{\circ}\text{K}$ and eV respectively⁽³⁴⁾. Taking $T_e = 3.25$ eV at $E/p = 23.5$ V cm^{-1} mm^{-1} , and $\lambda_e = 0.5 \times 10^{-3}$ cm at $p = 60$ mm⁽³⁹⁾

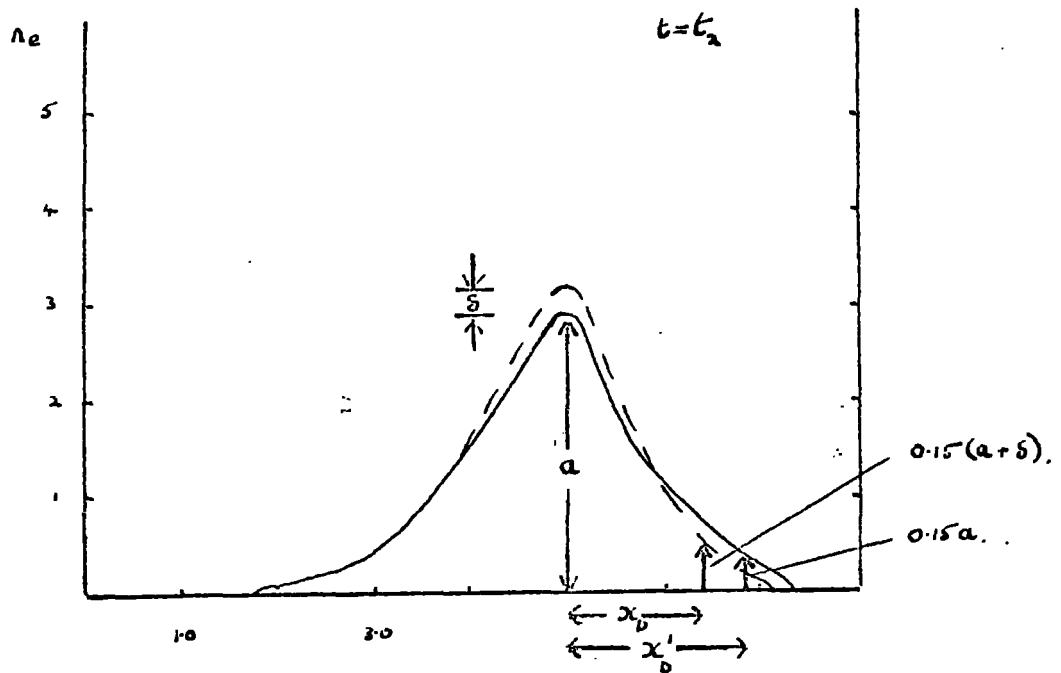
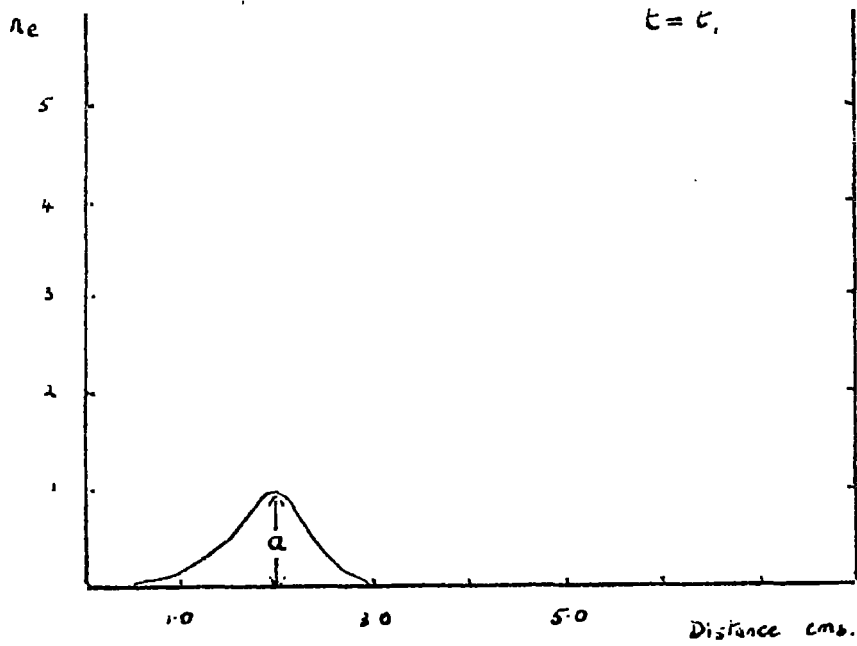
$$D = 1.8 \times 10^4 \text{ cm}^2/\text{sec.}$$

(of the value for D obtained by Varnerin and Brown⁽⁴⁰⁾ at $E/p = 25$ V cm^{-1} mm^{-1}

$$D = 1.6 \times 10^4 \text{ cm}^2/\text{sec.})$$

The values obtained for the diffusion coefficient in the present experiment therefore, are upto an order of magnitude greater than that predicted by the simple expression.

There are various reasons for this discrepancy; firstly, the present measurements were carried out under strong electric field conditions, whereas the relation is based upon an assumption of weak field conditions. Secondly, the light signals originate from collisions involving fast electrons, whose energy is well above the average. Such electrons, having lost most of their energy in inelastic collisions, will move off again in the field direction, whereas elastically scattered electrons will leave the point of collision in random directions. Hence electrons which have suffered exciting or ionizing collisions will have a higher velocity in the field direction. Further, as these electrons gain energy they will be presented with a steadily decreasing collision cross-section, or an increasing mean free path (i.e. they will be associated with a larger diffusion coefficient). Furthermore, as their energies increase, forward scattering of electrons emerging

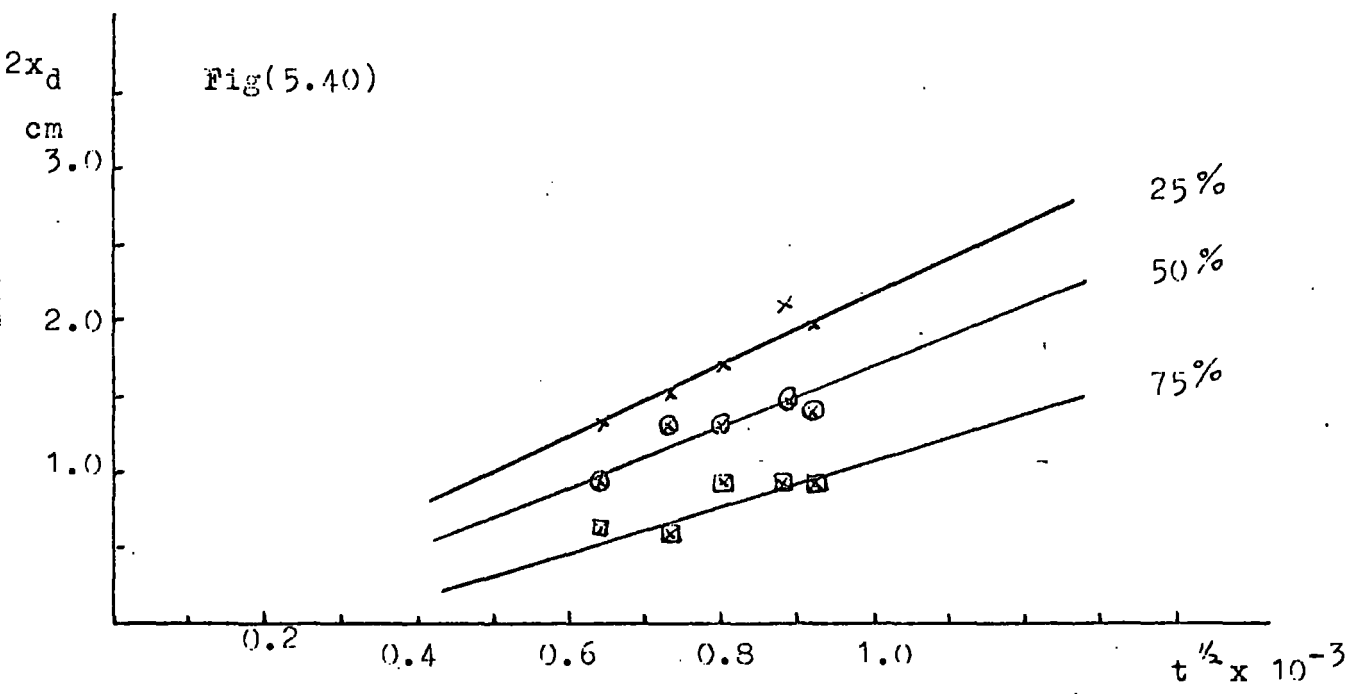
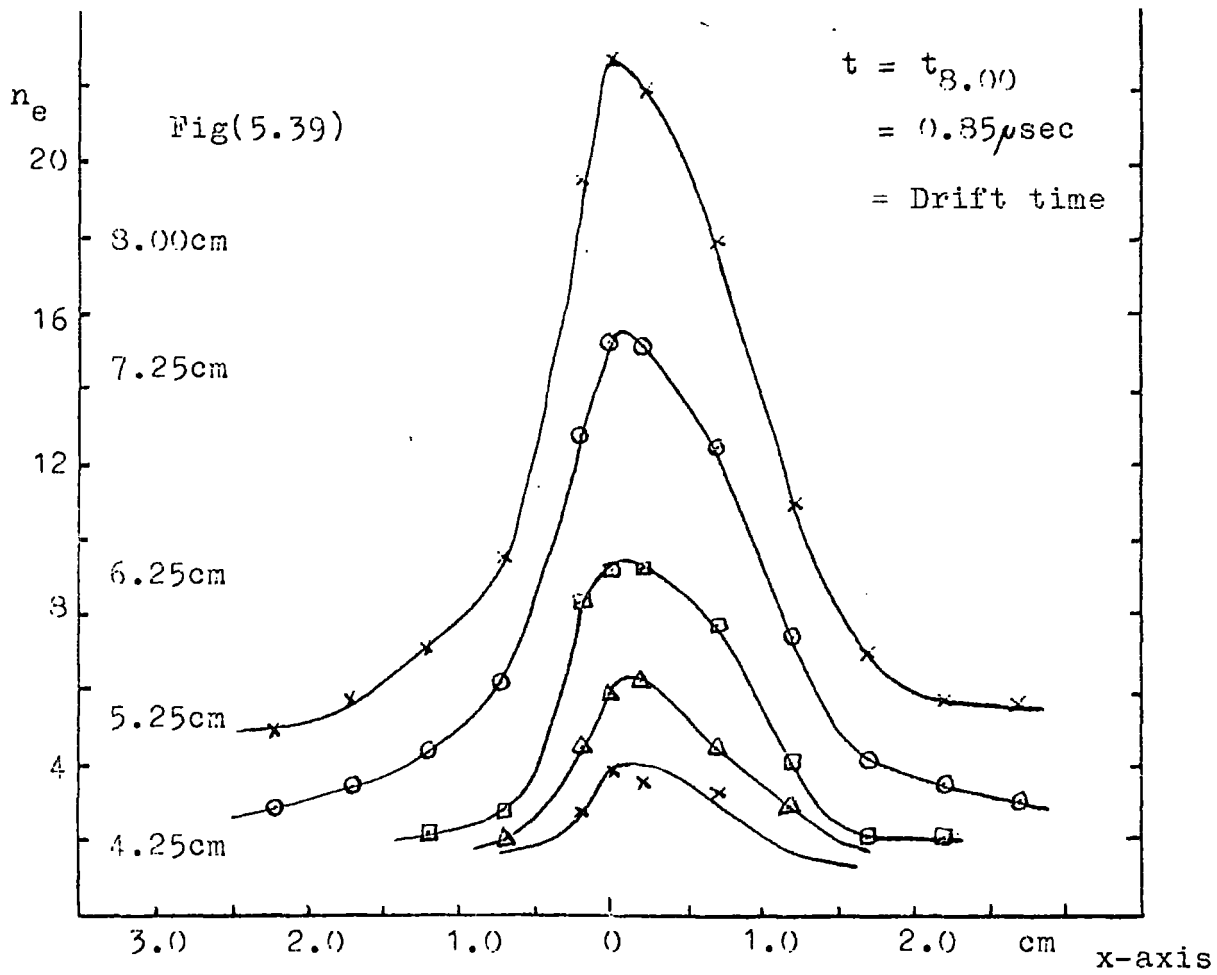


Fig(5.38) $x'_d > x_d$

from elastic collisions will become predominant, thus improving their chances of acquiring yet more energy. Electrons which attain large energies in this manner are known as "run away electrons"⁽⁴¹⁾.

The upcurving of the $x_d - t^{\frac{1}{2}}$ plots for the electrons in the leading edge of a swarm is attributed partly to these so-called 'runaway' electrons, however this effect is caused to some extent by the method of measurement. The up-curving is only noticed in plots where the electron number density is high, and in these cases the electron multiplication has been modified. Fig.(5.38) shows profiles of the electron number as a function of distance at two times during the transit of the electrode gap. The full line represents the probable profile at these times, while the dotted line indicates the profile if the ionization coefficient had remained constant during the transit time. It is known that the amplitude of this profile is certainly reduced, and this by itself is sufficient to increase the measured values of x_d . However, it is also probable, as will be shown in a later chapter, that electrons in the front edge of the electron swarm will drift in an enhanced electric field, and will multiply at an over-exponential rate. Thus the measured values of x_d will be further increased.

Fig. (5.37a) shows four $x_d - t^{\frac{1}{2}}$ plots referring to 50% positions in the tails of electron swarms. The slopes of these graphs are high when compared to the previous ones and this is again attributed to the method of measurement of the 50%T position. In the case of the low number density swarms, the amplification is

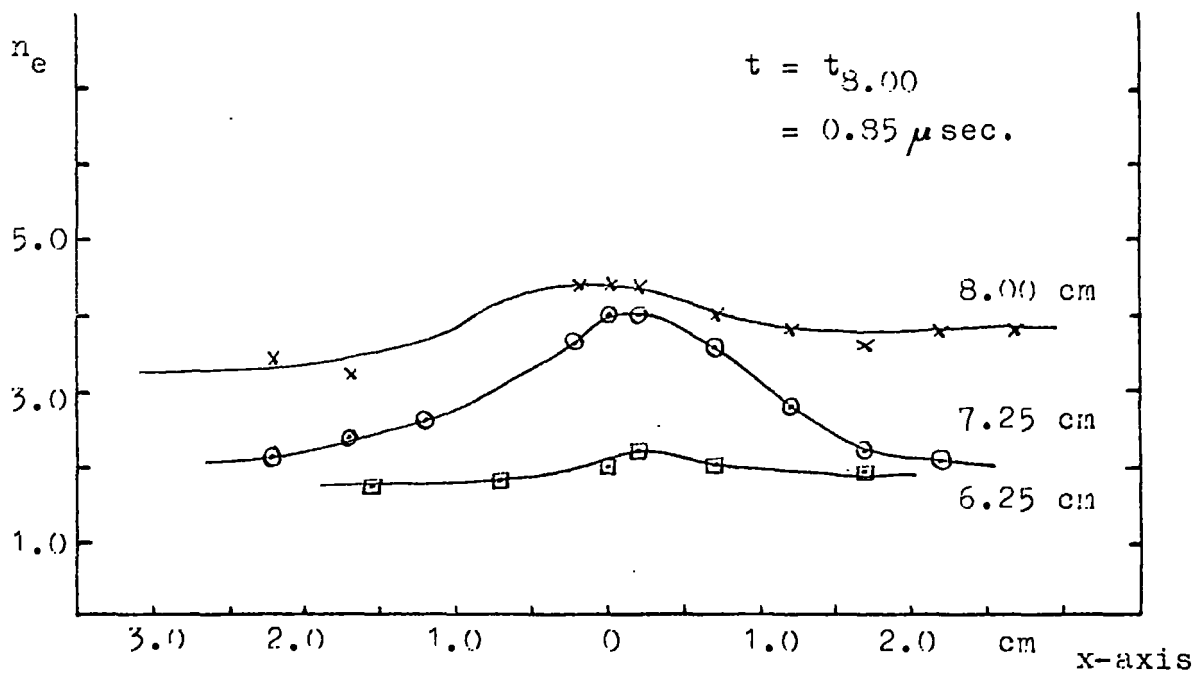


such that only a few secondary electrons are released from the cathode. It is therefore relatively easy to locate the 50% position in the tail of the profile. This has been done in several cases, two of which are shown in Fig. (5.36). The values of the diffusion coefficient obtained for electrons in the 50%F and 50%T sections of the swarm were similar. However the measurements shown in Fig. (5.37a) were made from high number density electron swarms, which produced large numbers of secondary electrons. Some of these are contained in the tail sections of the electron profiles, and as it was not possible to distinguish between primary and secondary electrons, a considerable error arose in determining the position of the 50%T point. Therefore no definite conclusions as to the diffusion of electrons in the tail of these swarms may be drawn.

5.6.2 Radial diffusion

To study the radial distribution of electrons in the electrode gap, the length of the slit at the cathode of the photomultiplier was reduced from 2.5 cm to 2 mm. In effect this reduced the field of view along the x-axis (that is perpendicular to the line of sight and to the central electrode axis) from 7 cms to 6 mm. This was necessary to obtain better spatial resolution of the electrons in the gap. Further reduction of the slit width reduced the collected light intensity below a detectable level.

Fig. (5.39) shows the radial distribution of electrons within a primary avalanche at various positions across the electrode



Fig(5.41) Radial distribution of secondary electrons, after $0.85 \mu \text{sec}$ at various distances from the cathode.

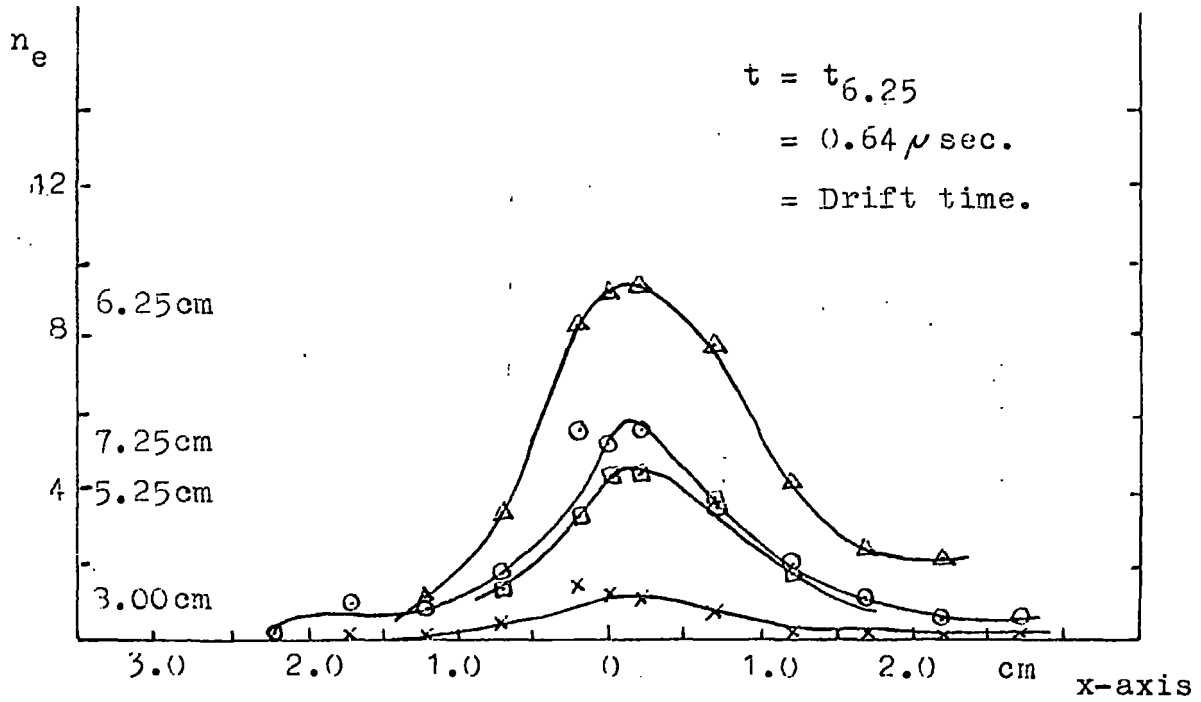
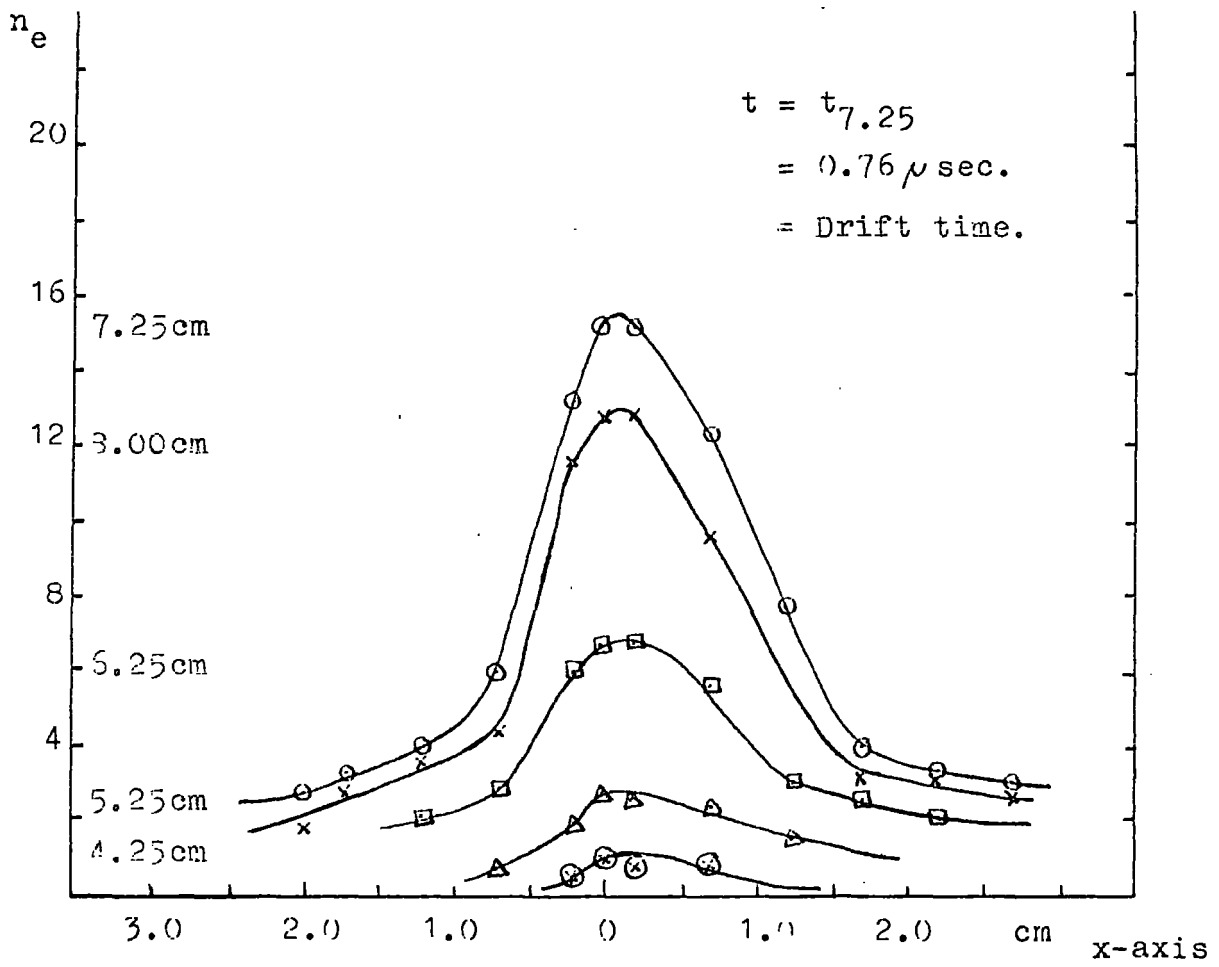
gap. The distribution was obtained by scanning with the photomultiplier along the x-axis, (i.e. towards the electrode edges), at intervals across the gap.

An estimate of the diffusion coefficient was made from Fig. (5.40) in which the width of the distribution $2x_d$, at ordinates which were 25, 50, 75% of the maximum value, was plotted against $t^{\frac{1}{2}}$.

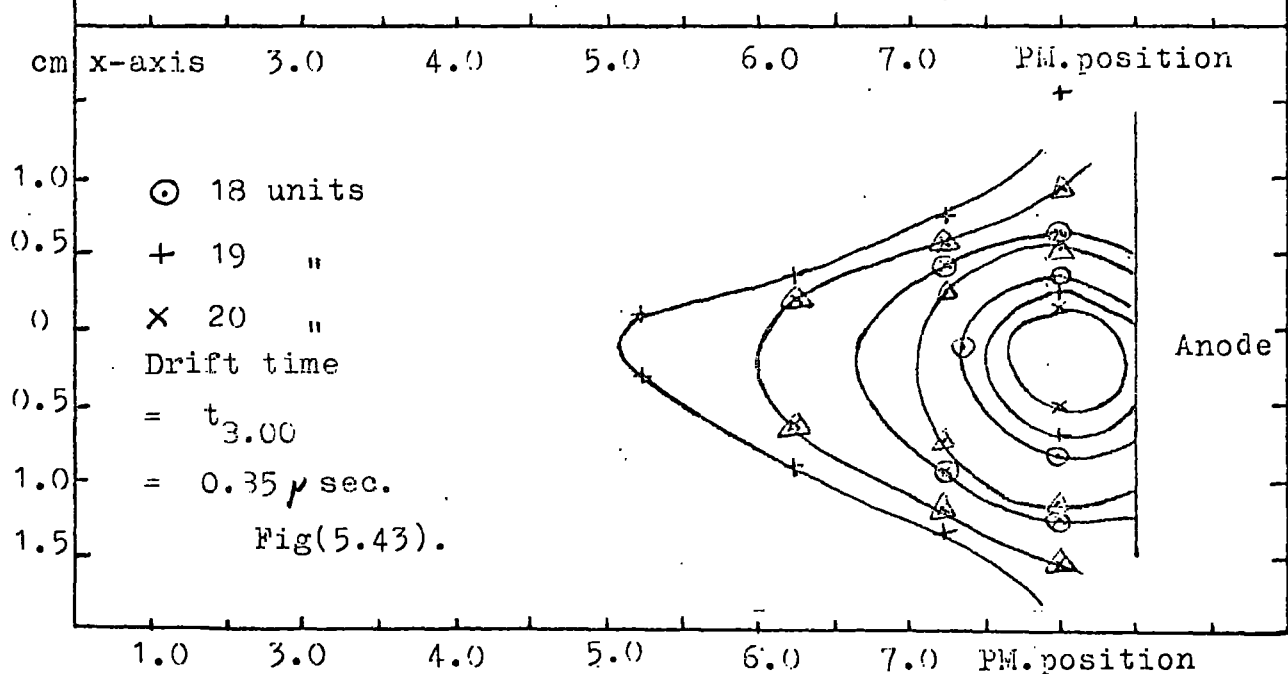
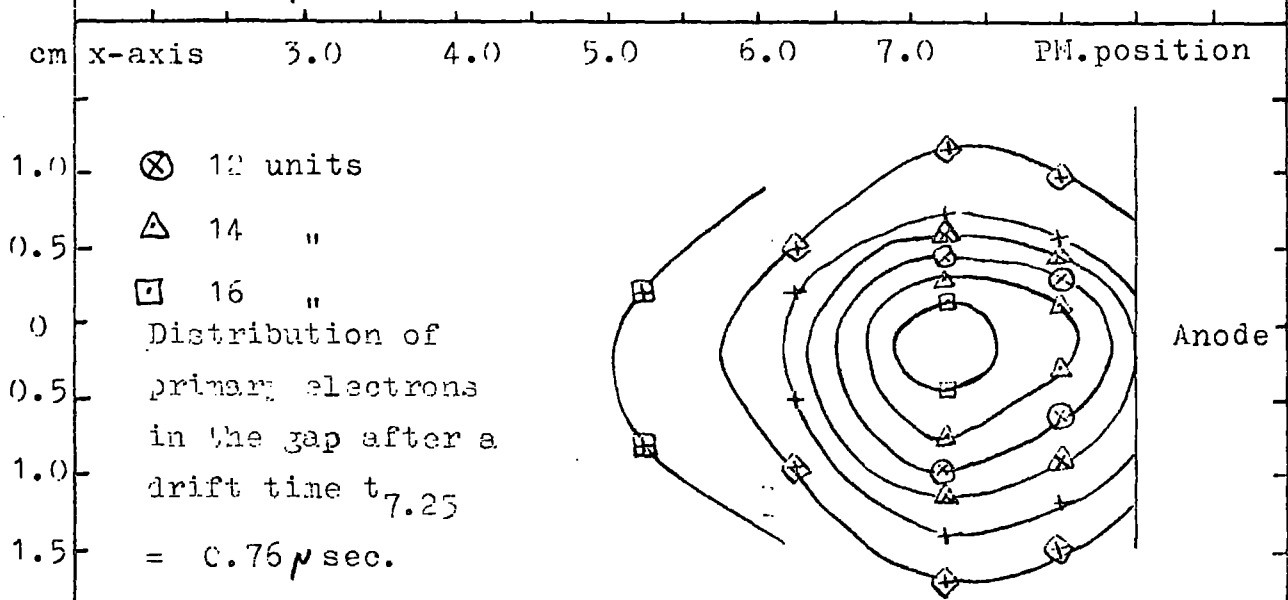
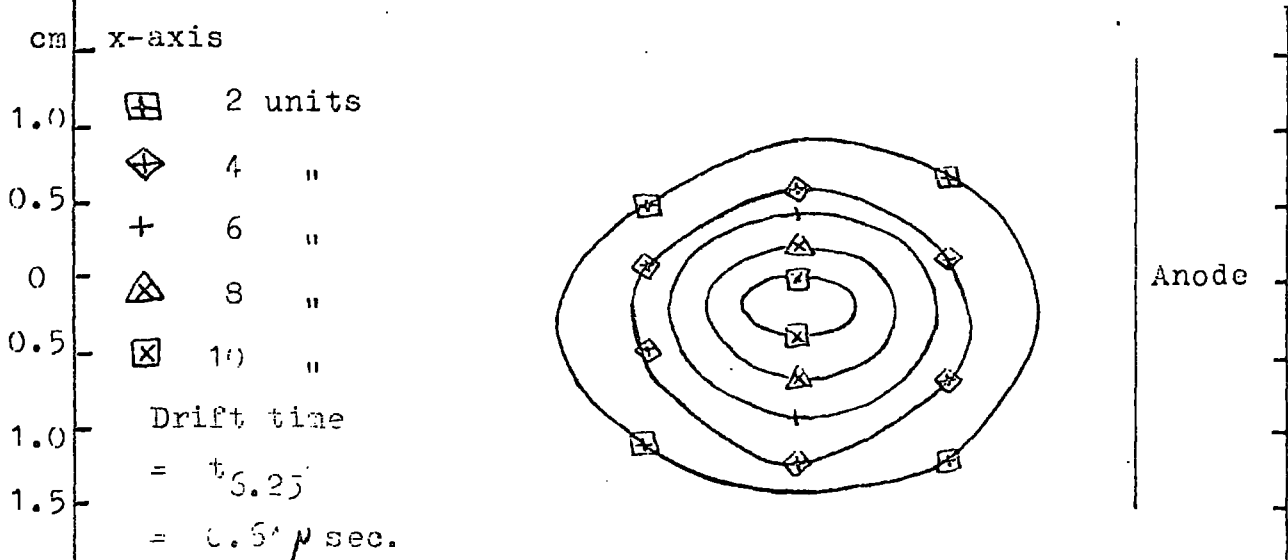
	25%	50%	75%
$D \times 10^5$ cm ² /sec.	3.5	2.6	1.5

These results indicate that within the experimental error, the rates of diffusion of electrons, outwards from the point of maximum electron density in the swarm, are similar both radially and along the central electrode axis.

The radial distribution of electrons within a secondary avalanche is shown in Fig. (5.41). It is noted that while the electrons in the primary avalanches were contained within a primary channel around the central electrode axis, the secondary electrons are distributed over most of the flat portion of the electrodes. Some falling off in the secondary electron density is to be expected as the photon path length increases towards the electrode edges, and hence the number of photons incident on the cathode decreases.



Fig(5.42).



5.7 Electron distribution within a primary swarm

The oscillograms represent the variation in electron number with time at a particular point in the electrode gap. As has been shown in the preceding section, it is possible to obtain from these oscillograms the radial distribution of electrons in the electrode gap. Fig. (5.39) shows a radial distribution at a certain time $t_{8.0}$ after the source has fired, at various distances from the cathode. The subscript 8.0 refers to the position of the photomultiplier, and the time $t_{8.0}$ is that at which the number of electrons at this position reaches a maximum. Similar distributions may be plotted at times $t_{7.25}$, $t_{6.25}$, $t_{5.25}$, etc., (Fig. (5.42). Taking one example, say $t_{7.25}$, points in the gap are found at which the electron number is 2, 4, 5, 8, etc., (arbitrary units). A reconstruction of the spatial distribution of electrons in the gap may then be made at a particular time, as opposed to a plot of the variation in number with time, at a given point. Fig. (5.43) shows the spatial distribution of a primary swarm at times $t_{8.0}$, $t_{7.25}$, and $t_{6.25}$.

5.8 Comments

From the measurements of the oscillograms it has been found that the effective value~~s~~ of the diffusion coefficient in the swarms is above that predicted from classical theory. In particular it has been found that in the front of the swarms where the electron number is about 15% of the peak value, a spatial anisotropy

in the electron distributions occurs. After several cms of drift motion these electrons move in the field direction at a velocity which is above that predicted by simple drift and diffusion theory, and they have been associated with so-called 'runaway' electrons.

CHAPTER 6

A THEORETICAL STUDY OF THE DEVELOPMENT OF THE PRIMARY ELECTRON SWARMS

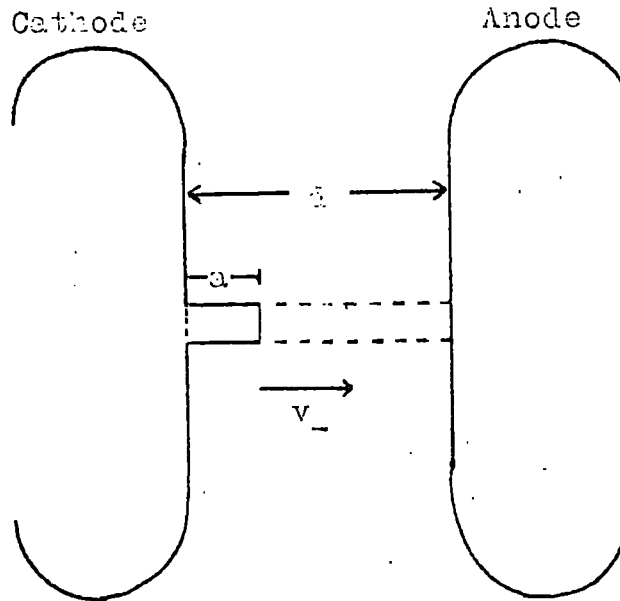
The experimental measurements of the primary ionization coefficient show that for the low number density electron swarms, the ionization coefficient has a constant value across the electrode gap. This is not the case when the number of starting electrons in a primary swarm is increased. Then an under-exponential growth rate is observed.

This chapter sets out to investigate theoretically the local field conditions which exist in the gap during the transit of a primary swarm, and to determine the subsequent effect on the ionization coefficient and light emission from the gap.

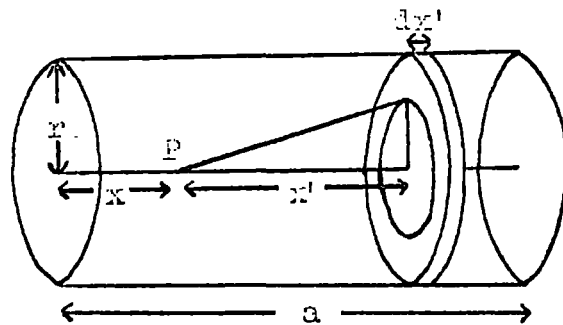
The development of the avalanche is simulated using an electronic computer; initially an Elliott 803 computer, but later an English Electric KDF9 computer was used. The program, coded in Algol language, is reproduced in full in Appendix I.

6.1 General description of the program

For the purpose of these calculations, the effects of electron diffusion are neglected so that the overall dimensions of a primary swarm may be assumed to be constant during its transit of the electrode gap. As a first approximation therefore, the electrons in a swarm are assumed to drift from cathode to anode within a tube-shaped path, and the shape of the swarm itself



Fig(6.1) Cylindrical path swept out by the motion of a primary electron swarm.



Fig(6.2) Illustration of the method of calculating the field distortion caused by a cylinder of charge.

is assumed to be cylindrical. Fig. (6.1) shows such a swarm in the gap with the last of the electrons just leaving the cathode surface. Positive ions formed in ionizing collisions are also assumed to be contained within this tube-shaped path, and as the mobility of these ions is two orders of magnitude less than that of the electrons, such ions are considered to be stationary during the swarm transit time.

At the stage of development shown in Fig. (6.1), the numbers of charged particles in the electrode gap are not sufficient to significantly alter the ionization rates within the swarm. Therefore the initial distribution of electrons and positive ions in the gap at this time, may be calculated using a value of the ionization coefficient determined by the applied field and the gas pressure. However, further motion of the electrons towards the anode must take into account the local field distortions produced by the concentrations of ions and electrons and the subsequent effect upon the ionization rates within the swarm. During the swarm transit time the electrons are assumed to drift in the field direction with a constant velocity v_+ , so that in a time interval Δt , the swarm will move a distance dx towards the anode, where

$$dx = v_+ \Delta t.$$

The current growth in the gap subject to modified ionization rates has been treated by considering the swarm to be made up of a number of thin discs also of width dx . The electron number density

in one such disc located x cm from the cathode is then

$$n_-(x) = n_0 e^{\int_0^x \alpha(x) dx}$$

where n_0 is the initial electron density at the cathode, and $\alpha(x)$ is the value of the ionization coefficient determined in the drift path by the applied field plus any field distortion produced by the concentrations of ions and electrons. In the program the drift motion of such a disc of electrons is therefore by steps of length dx towards the anode, and local field distortions are calculated to determine values of the ionization coefficient applicable during each step movement. The situation becomes more complicated when a swarm of finite axial length is considered, then the local values of the ionization coefficient within the swarm have to be calculated from a summation of the field distortions produced by the other swarm elements. The method used to do this is described in detail in the following sections, and is given in terms of the parameters used in the program.

In the experiment the growth of the electron component of the current has been measured by monitoring the light emission from slices of the swarm path. So in order to make a direct comparison between theory and experiment, the photon emissions from these slices of the path are also calculated by the computer.

6.2 Local field distortions

Many attempts have been made to estimate the effect of fields produced by space charges on ionization rates. In these calculations two main methods of approach have been used. One method relates the field distortion E to the electron and ion densities $n_-(x,t)$ and $n_+(x,t)$, by means of the one-dimensional Poisson equation

$$\frac{\partial E(x,t)}{\partial x} = -4\pi e (n_+(x,t) - n_-(x,t)).$$

Here the electric field strength is considered positive when directed from anode ($x=d$) to cathode, ($x=0$) (e.g. Ward and Jones⁽⁴²⁾, Ward^(17,43), Lucas⁽⁴⁴⁾, Borsch-Supan and Oser⁽⁴⁵⁾). However the use of this method is only valid when the radius of the discharge is small compared with the electrode gap separation; at higher gas pressures ($p \sim 60$ mm Hg), this is not generally the case. In the present experiment for example, the radius of an avalanche is of the order $\frac{1}{2}$ cm, compared with an electrode separation of 7 cms.

An alternative method used by Davies, Evans and Llewellyn Jones⁽⁴⁶⁾ in calculations of formative breakdown times, is more suitable when the discharge approximates to a long thin cylinder. It has therefore been assumed in the present case that electrons in a primary swarm drift from cathode to anode within a cylinder of length d and radius r , Fig. (6.1). Fig. (6.2) shows the primary swarm from the last diagram with one of the disc-shaped elements previously described. If the charge density in this disc is defined as

$$\rho(x) = e (n_+(x,t) - n_-(x,t)),$$

then the field at P produced by an annular element of such a disc at a distance x' from P is

$$\frac{2\pi r' dr' dx' \rho(x+x')}{(r'^2 + x'^2)}$$

where r' is the radius of the ring, and dr' is the width of the ring. The field at P, acting along the axis of the cylinder is

$$\begin{aligned} & \frac{2\pi r' dr' dx' \rho(x+x')}{(r'^2 + x'^2)} \cos \theta \\ = & \frac{2\pi r' dr' dx' \rho(x+x') x'}{(r'^2 + x'^2)^{3/2}} \end{aligned}$$

and the field produced by all these elements in the disc is

$$\begin{aligned} & \pi x' \rho(x+x') dx' \int_0^r \frac{2r' dr'}{(r'^2 + x'^2)^{3/2}} \\ = & \pi x' \rho(x+x') dx' \left(-\frac{2}{(r'^2 + x'^2)^{1/2}} \right)_0^r \\ = & 2\pi x' \rho(x+x') dx' \left(\frac{1}{x'} - \frac{1}{(r^2 + x'^2)^{1/2}} \right) \\ = & 2\pi \rho(x+x') dx' \left(1 - x'(r^2 + x'^2)^{-1/2} \right) \end{aligned}$$

If $x' < 0$, the expression for the field becomes

$$- 2\pi \rho(x+x') dx' \left(-1 - x'(r^2 + x'^2)^{-1/2} \right).$$

The axial field at P produced by all the charges in the cylinder is thus

$$2\pi \left(\int_{-x}^0 \rho(x+x') (-1 - x'(x'^2 + r^2)^{-1/2}) dx' + \int_0^{a-x} \rho(x+x') (1 - x'(x'^2 + r^2)^{-1/2}) dx' \right)$$

If the charge distribution $\rho(x)$ is known then a direct integration of the above expression may be possible. However the contribution of all the discs to the field may be summed without going to the

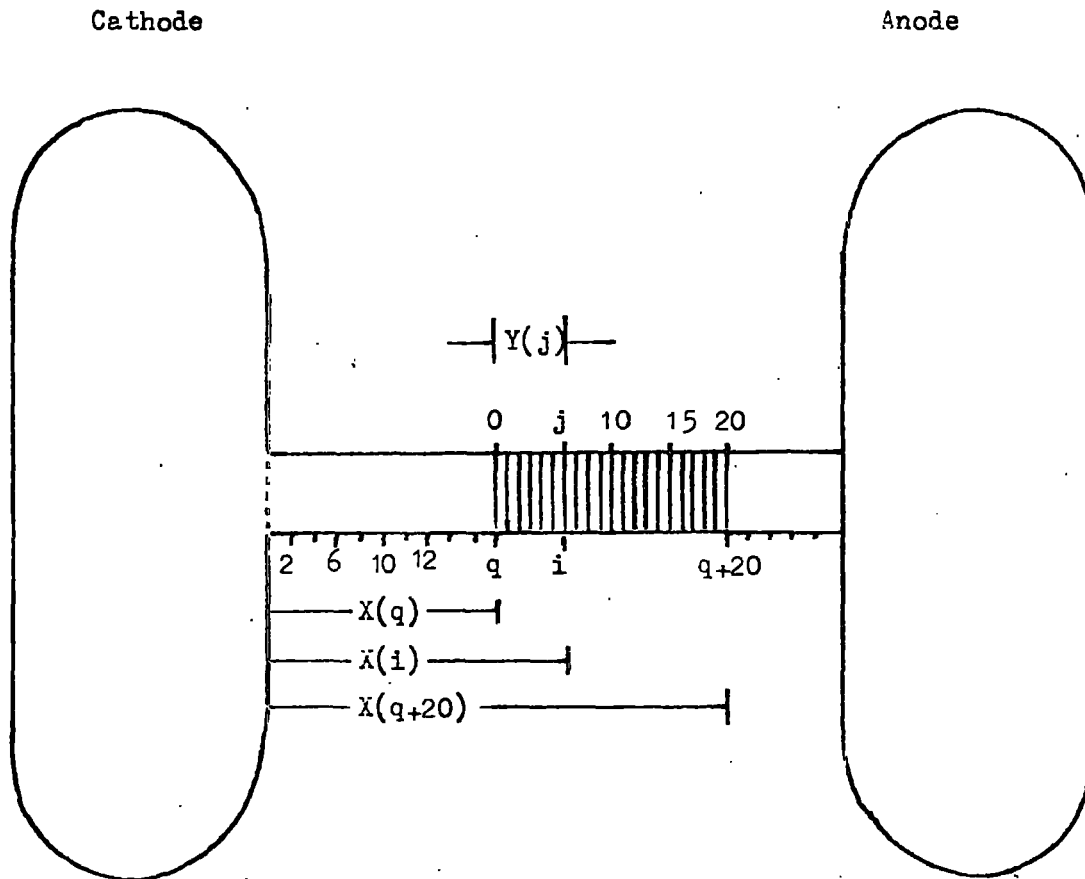
limit $dx' \rightarrow 0$, if numerical values of the charge density are known at a number of points along the x-axis. The cylinder of charge shown in fig. (6.1) has therefore been divided into elements of width h , and the charge density is calculated in these elements, (see section 6.4). It is then convenient to evaluate quantities $a_0, a_1, a_2, \dots, a_{-1}, a_{-2}$, which are coefficients of $\rho(x), \rho(x+h), \rho(x+2h), \dots, \rho(x-h), \rho(x-2h)$, in the above integral. The field distortions at given points within the cylinder may then be calculated by applying a formula for numerical integration (e.g. Simpson's rule), to the list of numbers

$$\dots, a_{-2} \rho(x-2h), a_{-1} \rho(x-h), a_0 \rho(x), \\ a_1 \rho(x+h), a_2 \rho(x+2h), \dots, \dots,$$

the summation extending from the cathode to the front of the swarm. These field distortions are then used to determine the local values of the ionization coefficient within the swarm, and at this stage the step-by-step movement of the swarm towards the anode commences.

6.3 Parameters used in the program

The width of a disc element h used in the program was determined empirically by performing a set of calculations, and then repeating them with the disc width halved. It was found that for $h < 2$ mm, halving the disc width produced only a slight change in the calculated field distortions. The overall axial



Fig(6.3) Diagram showing an electron swarm in mid-gap and the division of the swarm path into disc elements.

lengths of the swarms used in the calculations were taken from observed values, for convenience however, values of h were chosen so that when in mid-gap the swarm was made up of twenty discs of width h , Fig. (6.3). A typical value of h was then 1.4 mm.

Fig. (6.3) shows a swarm in mid-gap at a time t after the discharge of the source condenser. In this diagram various parameters are shown with which particular disc elements are identified. The cylindrical swarm path is itself divided into disc elements which are labelled 1, 2, 3, ..., i , ..., counting from the cathode, and the distance of a particular disc from the cathode is $X(i)$ cms, where

$$X(i) = i \times h.$$

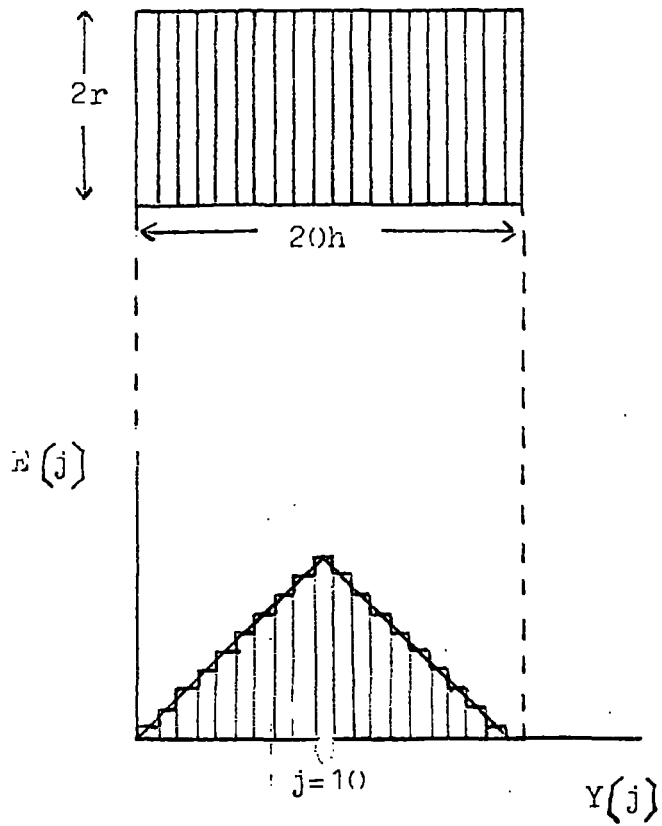
The position of the swarm in the gap is determined by a distance $X(q)$, which is the distance of the last electrons in the tail of the swarm from the cathode. The discs within the swarm which contain both electrons and positive ions are numbered 1, 2, 3, ..., j , ..., 20, counting from the tail of the swarm. Thus a particular disc element within a swarm is located $Y(j)$ cms from the tail of the swarm, where

$$Y(j) = j \times h,$$

and the distance of this element from the cathode is

$$X(i) = X(q) + Y(j).$$

As has been mentioned, the computation begins with the tail of the swarm touching the cathode, so initially both q and $X(q)$ are zero.



Fig(6.4) Initial electron distribution.

6.4 The initial charge distribution

The charge distribution in any cross-section of the cylindrical path has been taken to be constant and is defined by

$$N(i) = P(i) - E(i)$$

where $P(i)$ and $E(i)$ are the ion and electron densities in a particular disc element of the swarm path.

6.4.1 The initial axial distribution of electrons

In the absence of collision ionization the axial electron distribution within a swarm produced by the electron source is assumed to be triangular. During the swarm transit time, the swarm motion is considered as that of twenty disc elements, so that before the swarm enters the gap, it is convenient to express the distribution in the form of a histogram, Fig. (6.4). The electron density in a disc j , counting from the tail of the swarm is

$$E(j) = \frac{j}{100} B \frac{1}{Ch} \dots \quad 0 \leq j \leq 10$$

or

$$E(j) = \left(\frac{20-j}{100}\right) B \frac{1}{Ch} \quad 11 \leq j \leq 20$$

where $C = \pi r^2$, the cross-sectional area of the cylinder, and B is the total number of starting electrons in the swarm.

Alternatively,

$$E(j) = AY(j) \quad 0 \leq j \leq 10$$

or

$$E(j) = 2AY(j) - AY(j) \quad 11 \leq j \leq 20$$

where

$$A = \frac{B}{(100 C h^2)}$$

and

$$Y(j) = j \times h.$$

Therefore the first disc-shaped element in the swarm contains 1/100th of the total number of electrons, the second 2/100ths, the third 3/100ths, etc. The eleventh disc contains 9/100ths, the twelfth 8/100ths, and there are no electrons in the twentieth disc, i.e. the front of the swarm rises more steeply than the tail.

The computation begins with a swarm located in the gap and the tail of the swarm touching the cathode surface, thus the first nineteen disc elements of the swarm path will contain electrons, and positive ions formed in ionizing collisions. However because of the comparatively low density of charged particles during this part of the transit time, the ionization coefficient may be considered to be constant across the gap. Therefore the electron densities in the first nineteen disc elements of the swarm path, numbered 1, 2, 3, ..., i, ..., 19, are given by

$$E(i) = AY(j) \exp(\alpha X(i)) \quad 0 \leq j \leq 10$$

or

$$E(i) = (2AY(10) - AY(j)) \exp(\alpha X(i)) \quad 11 \leq j \leq 20$$

6.4.2 The production of positive ions

When the tail of the swarm is just leaving the cathode, q and $X(q)$ are equal to zero, Fig. (6.1). With the swarm in this position the ion density in the first disc of the swarm path

($i=1$), produced by the drift of a disc j in the swarm will be

$$\begin{aligned} p(1,j) &= AY(j) (\exp(\alpha X(1))-1) & 0 \leq j \leq 10 \\ &= E(1) - E(0). \end{aligned}$$

The total ion density in this first disc, caused by the drift of all the electrons in the swarm will be

$$P(1) = \sum_{j=1}^{j=20} p(1,j).$$

Similarly in the second disc ($i=2$); the ion density produced by the drift of a disc j in the swarm is

$$\begin{aligned} p(2,j) &= AY(j)(\exp(\alpha X(2))-1) - AY(j)(\exp(\alpha X(1))-1) \\ & & 0 \leq j \leq 10 \\ &= E(2) - E(1). \end{aligned}$$

The total ion density in the second disc at this time will be

$$P(2) = \sum_{j=2}^{j=20} p(2,j)$$

The total ion density in a disc i of the swarm path at this time is therefore

$$P(i) = \sum_{j=i}^{j=20} p(i,j) \quad (j \geq i).$$

where

$$\begin{aligned} p(i,j) &= AY(j)(\exp(\alpha X(i))-1) - AY(j)(\exp(\alpha X(i-1))-1) \\ & & 0 \leq j \leq 10 \\ &= E(i) - E(i-1). \end{aligned}$$

At some later stage in the step-by-step motion towards the anode when $q \neq 0$, the total positive ion density in a disc i of the swarm path will be

$$P(i) = \sum_{j=i}^{j=q+20} p(i,j) \quad (j+q) \geq i,$$

where

$$p(i,j) = E(i) - E(i-1).$$

6.5 Development of the avalanche

Basically the program may be split into two sections. In the first section preliminary calculations of the field distortions within the swarm are made when $q = 0, 10, 20$, etc., i.e. when the tail of the swarm is located at the cathode surface, and $X(10), X(20)$ cms from the cathode. In these calculations α is determined by the applied field and the gas pressure. This process is continued until the space charge distortion of the applied field exceeds 5 volts/cm, or about $\frac{1}{2}\%$ of the applied field. Further development of the avalanche must then take into account local field distortions and their effect upon the ionization rates within the swarm.

If the field distortion exceeds 5 volts/cm when $q = 10$ say, then the second section of the program operates. Values of $F(i)$ are calculated at $i = 10, 11, 12, \dots, 31$, together with the new values of the ionization coefficient at these points. The swarm is then advanced h cms towards the anode ($X(q)$ becomes $X(q+1)$), and the new electron and ion distributions are calculated using the local values of the ionization coefficient. This second section of the program is then repeated until the whole of the swarm has passed into the anode.

In order to correlate the measurements obtained experimentally with the computed growth of the electron avalanche, the second section also computes the total number of photons emitted from each disc element in the path, by exciting collisions during the transit of the swarm. The number of photons emitted from a disc is proportional to the number of electrons drifting in that disc. So that the number of photons emitted from a disc i is

$$L(i) = E(i-1) \times C \times h \times \epsilon(i-1) \times h$$

where C is the cross-sectional area of the swarm, and ϵ is the excitation coefficient. The computer counts the number of photons emitted from each disc of the path as the swarm moves step-by-step into the anode, and the total number of photons emitted per disc is output when $X(q) > d$ cm, (the electrode separation).

6.6 Field dependence of the ionization excitation coefficients

The field dependence of the Townsend primary ionization coefficient may be expressed empirically as

$$\alpha/p = A e^{-(Bp/E)}$$

over a certain range of the parameter E/p . Generally accepted values for these coefficients in hydrogen are to be found in a paper by D.J. Rose⁽⁴⁷⁾. For $17 \leq E/p_0 \leq 1,000$

$$\alpha/p_0 = 5.1 \exp(-138.8)p_0/E$$

where p_0 is the pressure of hydrogen at 0°C . Rose's expression becomes

$$\alpha/p_{20} = 4.7 \exp(-127.8)p_{20}/E$$

if p_{20} is the gas pressure at 20°C .

In the present calculations a slight adjustment was made to the constant A, to fit values for α from the above expression to values obtained in the experiment. An example of the relation used in the computation is

$$\alpha/p_{20} = 4.4 \exp(-127.8)p_{20}/E$$

Measurements of \mathcal{E}/p (the excitation coefficient) as a function of E/p ($E/p \sim 20$), have been made by Legler⁽²²⁾. The dependence of \mathcal{E}/p upon E/p was found to be similar to that between α/p and E/p , although in general \mathcal{E}/p was an order of magnitude greater. (At $E/p_{20} = 25 \text{ V cm}^{-1} \text{ mm}^{-1}$, $\mathcal{E}/p_{20} = 0.28$ quanta/cm mm electron, $\alpha/p_{20} = 0.018 \text{ cm}^{-1} \text{ mm}^{-1}$). The following expression for \mathcal{E}/p was used in the calculations

$$\mathcal{E}/p_{20} = D \exp(-127.8)p_{20}/E$$

$$\text{where } D = 4.4 \left(\frac{\mathcal{E}_a}{\alpha_a} \right).$$

\mathcal{E}_a and α_a are taken from the published values at the appropriate value of E/p_{20} .

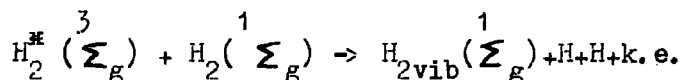
It is noted that these values for the excitation coefficient take into account so-called "quenching effects". At hydrogen pressures greater than 5 mm Hg, it has been shown^{(21), (22)} that the value of \mathcal{E}/p depends not only upon the reduced field, but also upon the gas pressure p ; \mathcal{E}/p decreasing with increasing gas pressure. Two possible causes of this quenching are:

- 1) the absorption of quanta in the gas itself, followed by re-emission at some other point;

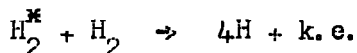
ii) the quenching of excited states by collisions with gas molecules.

Fortunately the imprisonment of radiation is unlikely in molecular hydrogen, and at no time was radiation observed from regions in front of the electron swarms in the gap. Corrigan and Von Engel⁽²⁾ have shown that imprisonment of radiation was absent at low gas pressures, and also the close agreement of Breare's drift velocity measurements at $p=90$ mm with those of Bradbury and Nielson, indicates that photon-absorption may be neglected at these gas pressures.

However as the gas pressure increases, the number of collisions made by an excited molecule H_2^* during a mean lifetime, increases, and so correspondingly does the probability that the excited state will lose its potential energy by some other process than by quantum emission. Possible deactivation processes⁽²¹⁾ concerning the \sum_g^3 state which gives rise to the hydrogen continuum are



and

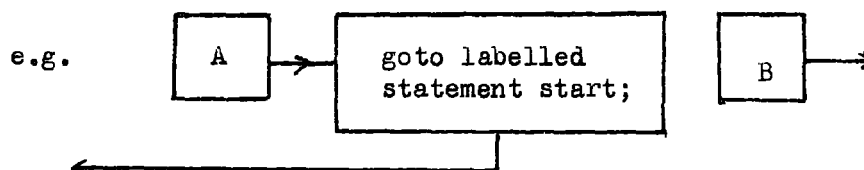


This effect however, will not effect the measured values of the ionization rate from a particular experimental run, as the measurements were all made at the same gas pressure; further the values of α were obtained from relative measurements of the areas under the pulse oscillograms.

6.7 Order of Computation

The sequence of operations performed by the computer is

shown in the flow chart at the end of this section. Various basic Algol structure statements are used in this chart, the significance of which will be explained here. (The symbol := used in the chart is pronounced "becomes"). In general the sequence of operations followed by the computer is indicated by the arrows in the flow chart, however sections of the program are identified by labels such as start, run, here, etc, and control may be transferred from one section to another (either backwards or forwards), by the use of a goto statement:



Single conditional statements used take the form:

if statement A is true then perform instruction B.

In this conditional statement, if statement A is false, then instruction B will not be carried out and control will pass to the next instruction in the program.

Alternatively, a double conditional statement may be used:

e.g. if statement A is true then perform instruction B

else perform instruction C.

Instructions B and C may themselves be compound statements containing goto statements which transfer control to other sections of the program.

A sequence of operations which is repeated many times is referred to as a cycle. These cycles are generally terminated in one of the following ways:

i) Count-terminated cycle;

for the given initial value I of a counter V, and subsequent values changed by a given step S until the given limiting value L is passed, do the given action A.

i.e. for V:= I step S until L do A;

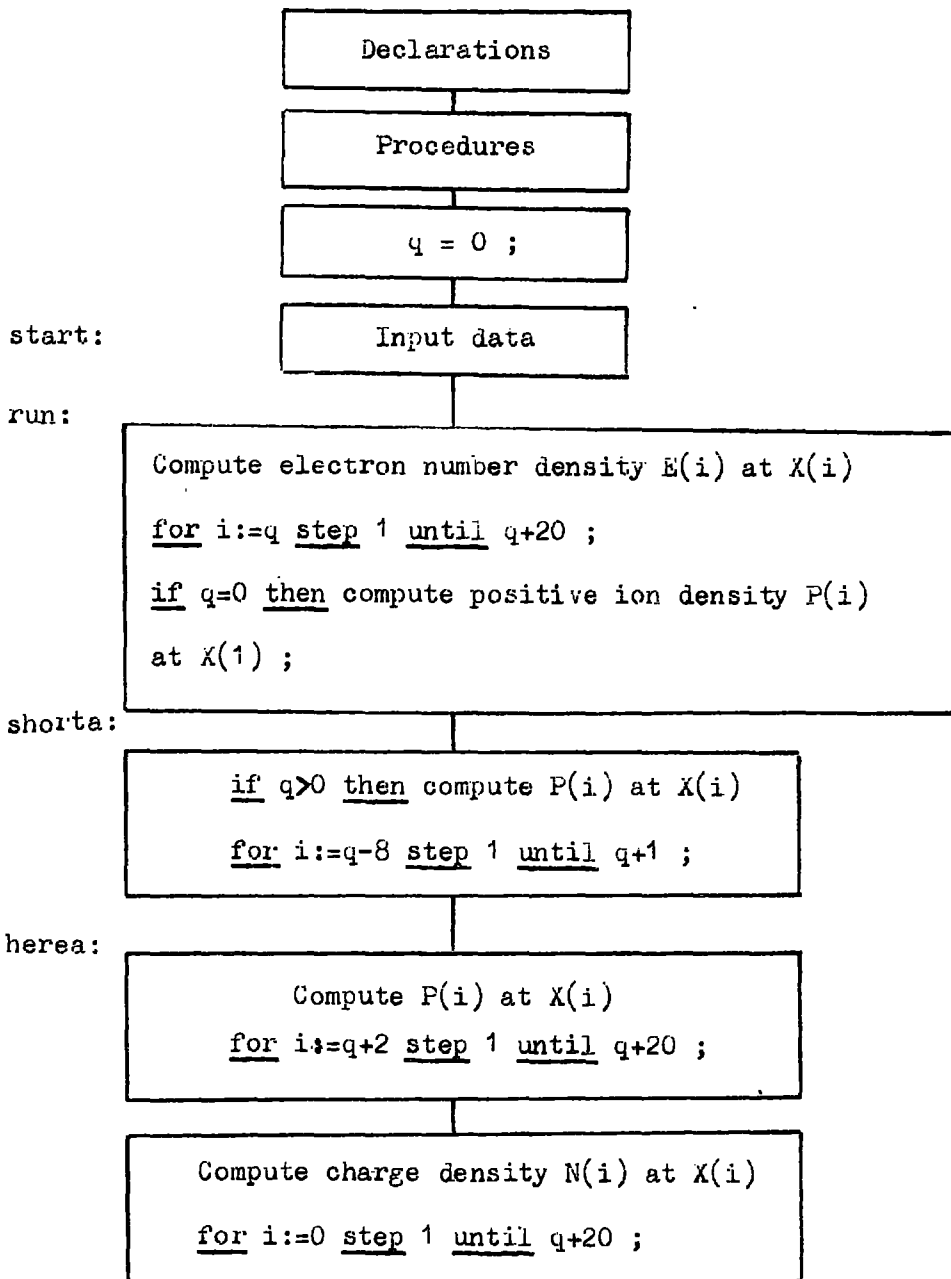
ii) Condition-terminated cycle;

for the given initial value of counter V, and subsequent values changed according to the given rule R while the given condition C is true, do the given action A.

i.e. for V:= I,R while C do A;

Cycles which are required many times during the running of the program may be taken from the main body of the program and written out once under the declaration section. Such cycles are then referred to as procedures, and each procedure has a name known as the procedure identifier. The use of the name in the body of the program is the procedure call, and causes the instructions in the cycle to be carried out for particular parameters.

Two such procedures are used in the present program: one is a formula for the numerical integration of a list of numbers (Simpson's rule); the other is to decide whether or not there is an even or odd number of elements in the list. (An odd number of elements is required for summation using Simpson's rule. If there happens to be an even number of elements, an additional term, equal to zero, is added to the list).



sum:

```
Compute field distortion F(i) at X(i)
for i:=q step 4 until q+20 ;
Output F(i), P(i), E(i),
for i:=q step 4 until q+20 ;
if F(i) > 1/2% of the applied field e
goto sum (1) ;
```

```
q:= q+10 ;
goto run ;
```

sum(1):

```
Compute F(i) at X(i)
for i:=q-1,q,q+1, --- q+21
while X(i) < d ;
```

sum(2):

```
Compute F(i) at X(i)
for i:=0,1,2,3, --- q+21
while X(i) < d ;
```

```
Compute ionization coefficient t(i) at X(i)
for i:=q-1,q,q+1 --- q+21
while X(i) < d;
```

exit:

```
if q is a multiple of 4
then output F(i), P(i), E(i), at X(i)
for i:=0,2,4,6 ---- q+20
while X(i) < d;
```

(Used during the
first run only)

```
Compute L(i) at X(i)  
for i:=0, 1, 2, 3, --- q ;
```

```
Compute E(i), P(i), L(i) at X(i)  
for i:=q-1, q, q+1 --- q+21  
while X(i) < d ;
```

```
if X(q) > d then output t(i) and the  
photon emission without distortion at X(i)  
for q:=0, 4, 8, --- q+20 ;  
q:=0 ;  
goto start ;
```

```
if q is a multiple of 4  
then goto sum (2)  
else goto sum (1) ;
```

CHAPTER 7

A DISCUSSION OF THE MEASUREMENTS OF THE

IONIZATION COEFFICIENT

The experimental measurements have shown that under certain conditions, the growth of primary electron swarms occurs at an under-exponential rate. The previous chapter has outlined calculations performed to account for this effect, based on the assumption that the decreased rate of ionization is caused by the build up of a space-charge electric field in the gap, produced by concentrations of charged particles. Before the results of these calculations are discussed, other processes will be considered which might lead to similar experimental results, but which are discounted.

7.1 Electron attachment

A well known gas process which leads to reduced values of the ionization coefficient is that of electron attachment. When electrons attach to gas molecules to form negative ions, the large mass and low drift velocity of the ions are such they cannot ionize other gas molecules by collision. The net result is that ionization currents in electro-negative gases tend to rise at a rate which is under-exponential. Only a small number of gases are effective in attaching electrons, e.g. oxygen, atomic hydrogen, freon, halides, and various other organic molecules; molecular hydrogen hardly forms negative ions.



In the present experiment it has been stated that the gas pressure in the discharge vessel rises over a period of four hours, from less than 10^{-6} mm to 10^{-4} mm Hg with the pumps closed off. Therefore the ratio of the number of impurity molecules (e.g. O_2 , N_2 , oil vapour) to hydrogen molecules, per cc, will be of the order $1:10^6$; the ratio being that of the residual gas pressure to the pressure of the working gas. Even assuming that the atomic cross-sections for attachment and ionization are similar, any reduction in α caused by electron attachment to impurity molecules will be negligible because of the low concentration of these molecules in the working gas.

If the electrons in a swarm drifting across the electrode gap are assumed to be inequilibrium with the electric field, i.e. if the energy gained by an electron drifting through one cm of the gap is lost in collision processes, then at $E/p = 20 \text{ v cm}^{-1} \text{ mm}^{-1}$ and a hydrogen pressure of 60 mm

the energy supplied
 (per cm of path) = 20×60
 to an electron = 1,200 eV.

So that if 75% of the energy losses are assumed to be dissociation losses⁽²⁾

the energy lost by
 dissociation in one = 900 eV per electron.
 cm of drift path

If the number of electrons per swarm is 10^8 , then

$$\begin{aligned} \text{the energy lost} & & & = 9 \times 10^{10} \text{ eV.} \\ \text{per swarm} & & & \end{aligned}$$

Dissociation losses follow from the cross-section for excitation to the \sum_u^3 state, and according to the Frank-Condon principle, transition to this state is likely to be associated with an energy loss of about 12 eV. Thus the maximum number of hydrogen atoms likely to be produced in 1 cm of the electrode gap

$$\begin{aligned} & = 2 \times \frac{9 \times 10^{10}}{12} \\ & = 1.5 \times 10^{10} \text{ atoms.} \end{aligned}$$

If the only loss process considered for these atoms is diffusion from the gap, then the time taken for hydrogen atoms produced on the central electrode axis to diffuse radially out of the drift section is approximately

$$\begin{aligned} t & = \frac{\pi r^2}{12 D_H} \\ & \sim 3.3 \text{ seconds.} \end{aligned}$$

Where D_H is the diffusion coefficient for atomic hydrogen, ⁽³⁴⁾ taken to be $\sim 2 \text{ cm}^2/\text{sec}$ at $p=60 \text{ mm Hg}$, and $r \sim 5 \text{ cms}$. After this time period, a state of equilibrium will be set up in which the rate of production of atoms will equal the loss from the electrode gap by diffusion. If the swarm repetition rate is maintained below 1,000 swarms per second, (a figure chosen so that ions produced by the passage of one swarm are lost to

the electrodes by drift motion before the appearance of the next), then the number of hydrogen atoms per cc, in the gap after 3.3 seconds will be

$$\begin{aligned} &\sim \frac{1.5 \times 10^{10} \times d \times n_p}{\text{Volume of the drift section}} \\ &= \frac{1.5 \times 10^{10} \times 6 \times 3,300}{\pi \times 5^2 \times 6} \\ &\sim 6 \times 10^{11} \text{ atoms/cc.} \end{aligned}$$

However if this figure is compared with the number of hydrogen molecules per cc, ($\sim 2 \times 10^{18}$), it is again apparent that the probability of electron attachment is extremely small when compared with that for collision ionization.

It is, however, interesting to consider what effect electron attachment would have upon the shape of the multiplication graphs. A quantity a/p has been defined as the number of attachments of electrons to molecules, per cm of path in the field direction, per mm Hg. The increase in the number of electrons in an electron swarm produced in a distance dx in the field direction, is therefore

$$dn_e = (\alpha - a) n_e dx.$$

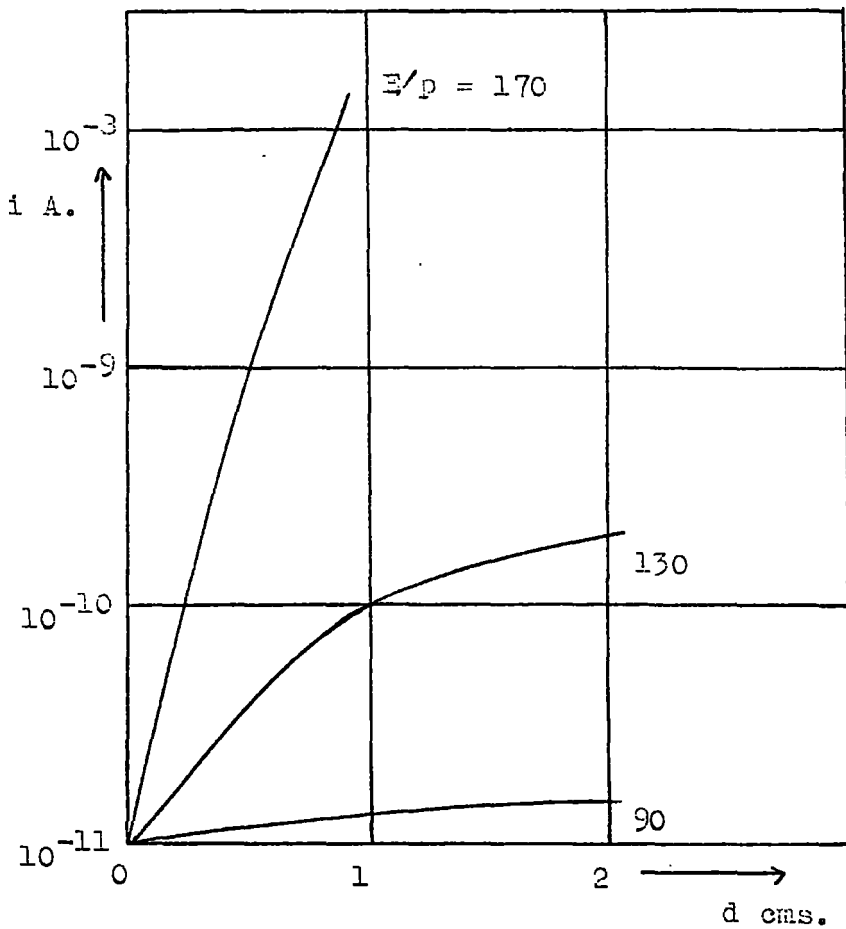
If the number of electrons in the swarm n_e is equal to n_0 at $x=0$, then integrating between 0 and d ,

$$n_e/n_0 = e^{(\alpha-a)d}. \quad (7.1)$$

The increase in the number of negative ions produced in dx is

$$dn_- = a n_e dx,$$

which integrated between 0 and d , and substituting for n_e gives



Fig(7.1) Total currents i measured in Freon as a function of electrode separation by Harrison and Gabelle, (43).

$$n_-/n_0 = \frac{a}{\alpha - a} (e^{(\alpha - a)d} - 1). \quad (7.2)$$

The multiplication rate

$$i/i_0 = \frac{n_e + n_-}{n_0} \quad (7.1 + 7.2)$$

$$= \frac{1}{\alpha - a} (\alpha e^{(\alpha - a)d} - a). \quad (7.3)$$

A semi-logarithmic plot of this relation when $a < \alpha$ is a curve which is concave to the d-axis, rather than a straight line graph:

$$\log i/i_0 = \log\left(\frac{1}{\alpha - a}\right) + \log(\alpha e^{(\alpha - a)d} - a) \quad (7.4)$$

of equation 7.1, for the multiplication of the electron component of the current

$$\log \frac{n_e}{n_0} = (\alpha - a)d.$$

This predicted departure from linearity is in agreement with experimental work done by Harrison and Gabelle⁽⁴⁸⁾ in freon, Fig. (7.1). It should be noted however, that the departure from linearity is obtained by measurement of the current caused by the drift of electrons and negative ions. Using the optical method, only the motion of the electron component of the current is observed, and plots of the current as a function of electrode separation in electro-negative gases will be straight lines whose slopes are $(\alpha - a)$.

Attachment processes therefore, are not responsible for the curvature of the current growth graphs in the present experiment.

7.1.2 Experimental factors

It is also necessary at this stage to consider whether the curvature exhibited in the current growth plots may be attributed to the method of observation.

Although the photomultipliers used in the experiments were all operated at the recommended voltages, it is possible that the output signals were not linear functions of the incident light intensities over the range measured. It is also possible that the electron current in a tube was approaching a saturation level for the higher light intensities.

The current from a photomultiplier may be calibrated directly using a suitable light source placed at various distances from the photo-cathode. However, an 'inverse-square law' calibration of this kind was not thought to be necessary for the following reasons. In the course of the experiments three different photomultipliers were used to record the multiplication of low density electron swarms in the gap. The overall voltage applied to the dynodes of these tubes was varied from 1-2 kV, and in each case the $\log n_e$ -d plots were linear. This linearity of the plots indicates that the photomultiplier output is a true representation of the current growth in the electrode gap.

The non-linear growth curves were obtained only with high-number density electron swarms, and these were reproducible despite the considerable variation in the overall dynode voltage. In many cases it was found that the amplitudes of the output

pulses were greater in the cases of the low density swarms (V_{dynode} - high), than when signals from high density swarms were detected (V_{dynode} - low). Such results indicate that over the test range of dynode voltages, the incident light intensity was not sufficient to produce excessive electron currents in the tubes.

It was concluded therefore that the curvature resulted from gas processes, and was not characteristic of the method of measurement, or of the geometry of the experimental system.

7.2 Initial conditions

An account of the method of calculating the effects of space charges on the ionization rates in a primary swarm has already been given. Briefly the electrons in a swarm of finite dimensions are considered drifting in an electrode gap in which a uniform electric field E is maintained. The electron swarm leaves behind positive ions which are considered to be stationary and these ions produce an electric field in the gap which tends to retard the motion of the electrons towards the anode. In particular, this field tends to reduce the rate of ionization in the gas.

The calculations do not take into account the diffusion of the electrons within the swarm, but the values for the radii of the swarm paths are taken from experimental measurements of this radius when the swarm is in the vicinity of the anode. The

overall lengths of the swarms in the three cases considered, range from 2.9 - 3.5 cms; the actual dimensions are shown on the particle distribution diagrams.

Secondary action at the cathode is not considered on the grounds that the space charge fields produced by secondary electrons will not significantly alter the ionization rates in the primary swarm. However the field conditions which secondary electrons will encounter during their transit of the gap are calculated.

As indicated in Chapter 4, the number of electrons entering the drift section from the cathode has been measured in two ways. The electron number shown in the multiplication plots is the initial number n_0 , measured using the galvanometer circuit at low values of E/p . However measurements of the source emission made during the experimental runs at the operating voltage, ($E/p \sim 23$), have shown that the former values for n_0 were too low. It has been concluded therefore that the galvanometer measurements refer to the horizontal section of the emission characteristic in Fig. (4.5), whereas at the operating voltage the source emission lay on the upturn of the characteristic and was field dependent. The values of n_0 shown in the plots in Chapter 5 therefore, may only be taken to indicate the relative numbers of electrons per swarm emerging from the cathode. The graphs have been labelled in this manner because of the inability

of the oscilloscopic method to resolve accurately values of n_0 within the narrow range over which space charge effects could be observed. The estimated deviation on the values of n_0 shown in Table (2) using the oscilloscopic method was about 25%.

It is realized that this field-dependence of the source emission is a serious failing in the use of a thermionic source in an experiment of this kind. However of the various source configurations tested, the present arrangement was the only one capable of producing the required electron densities. More accurate measurements of the electron starting number would be possible with higher density swarms, but it seems doubtful at this gas pressure, whether such an emission is possible with this type of source.

A possible solution to this problem might be found by using a pulsed laser beam to generate electrons from the cathode photo-electrically. A more accurate determination of the initial electron density would then be possible.

7.3 A comparison of the measured and computed growth curves

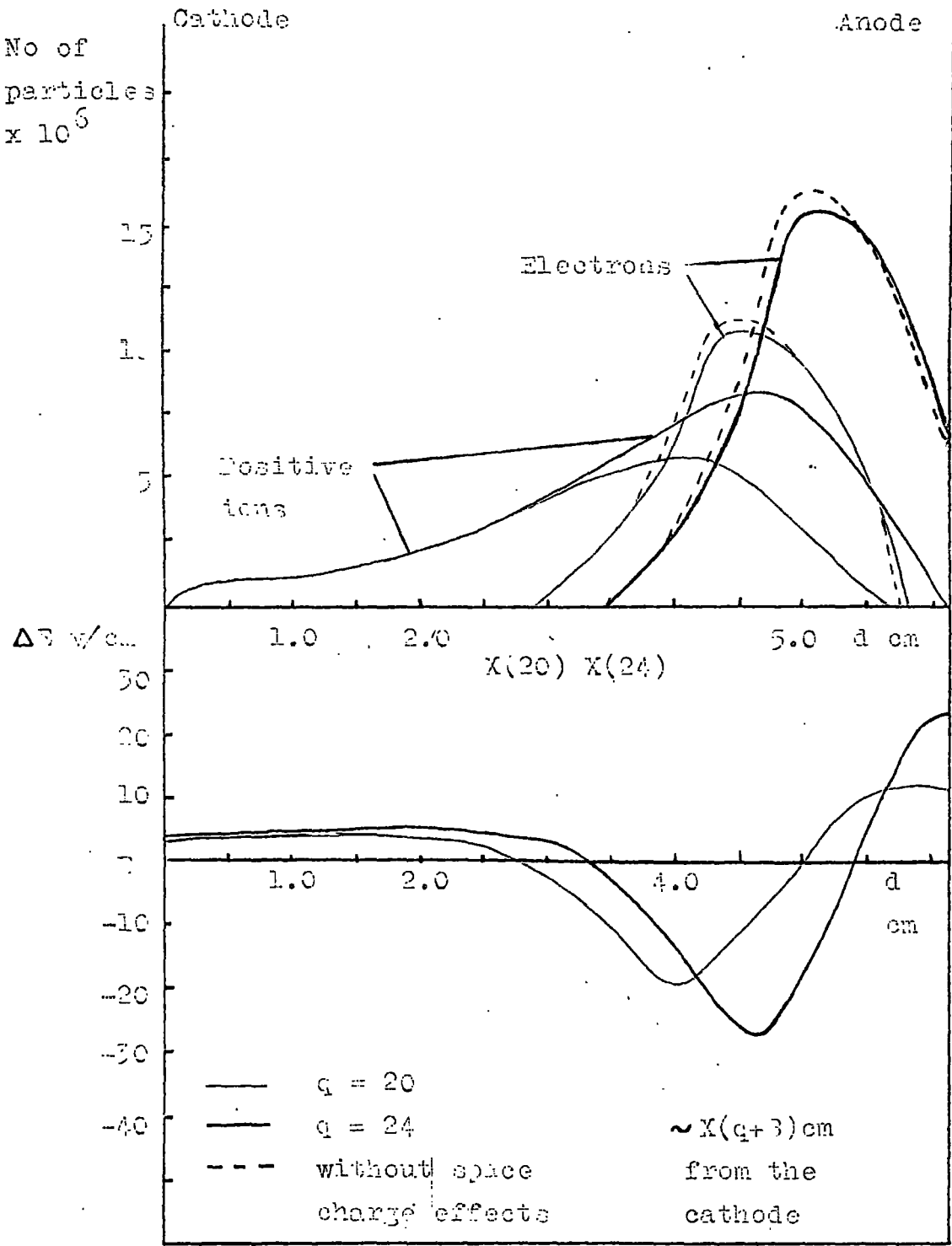
The computer results for three sets of experimental data are shown in Figs. (7.2-7.12), the initial data consisting of the experimental conditions for Figs. (5.12, 5.13, and 5.9). Figs. (7.2-7.6) show the electron and positive ion distributions in the electrode gap at various times, when the trailing edge of the swarm was X(12), X(20), X(24), etc., cms from the cathode. That is, when the electrons in the last disc shaped element in

the swarm were 12h, 20h, 24h cms from the cathode. The dashed lines in these distributions indicate the numbers of electrons calculated without the effects of space charge fields. Underneath each distribution is shown the distortion ΔE of the applied field E , at these times.

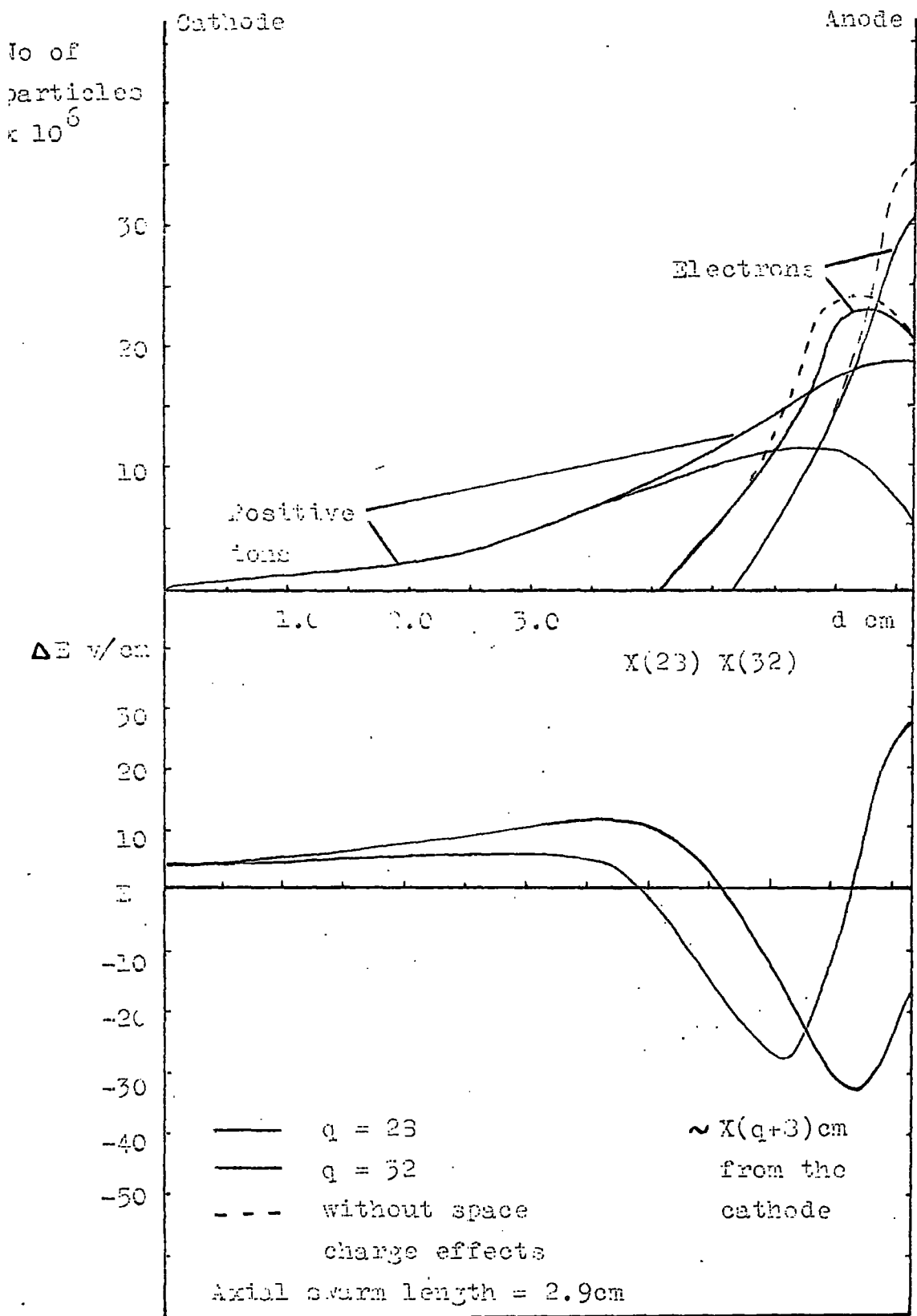
Fig. (7.7) shows the calculated value of α , as seen by electrons in a disc in the swarm. The electrons in this disc are located 8 cms from the cathode and are subject to the maximum-negative field distortions. The subsequent multiplication rate of electrons in this eighth disc in the swarm is shown in Fig. (7.8) for one of three cases considered.

In Fig. (7.9) a comparison is made between the slopes α^* , of the experimental and calculated photon-emission graphs. It will be remembered that when appreciable field distortions occur, the slope of these graphs may not be identified with the ionization coefficient α , because of the field dependence of the excitation coefficient ϵ .

Finally the calculated photon emissions from 6 mm sections of the swarm paths are shown in Figs. (7.10, 7.11, 7.12), together with the experimental growth curves. The dashed lines here indicate an exponential growth rate.



Fig(7.2) Particle distributions; $n_0 = 6 \times 10^6$,
 $E = 1.410$ kV/cm, $h = 1.45$ cm, radius = 5mm,
 axial swam length = 2.5cm.

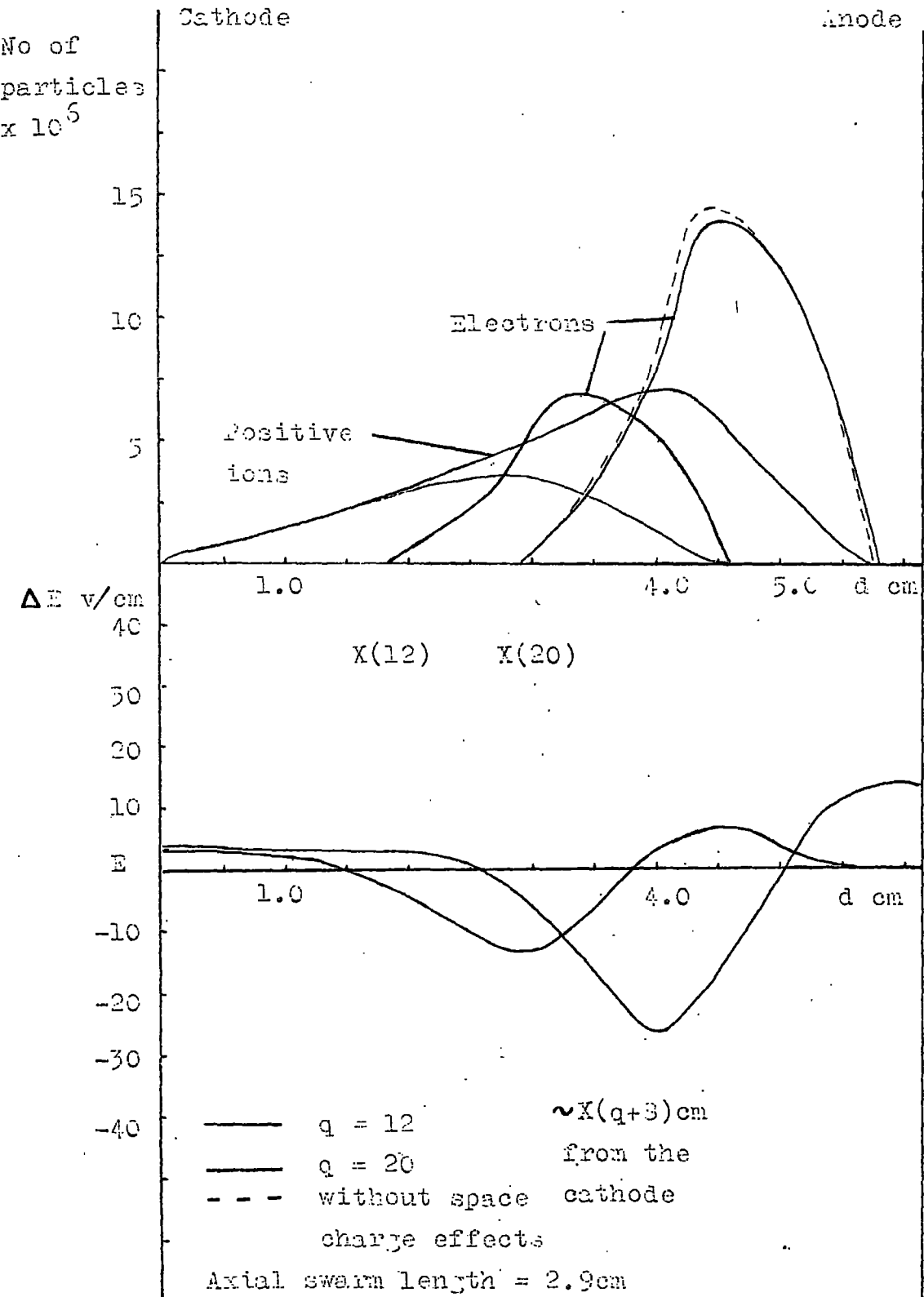


Fig(7.3) Particle distributions; $n_0 = 6 \times 10^5$,
 $E = 1.41 \text{GkV/cm}$, $h = 1.45 \text{mm}$, radius = 5mm.

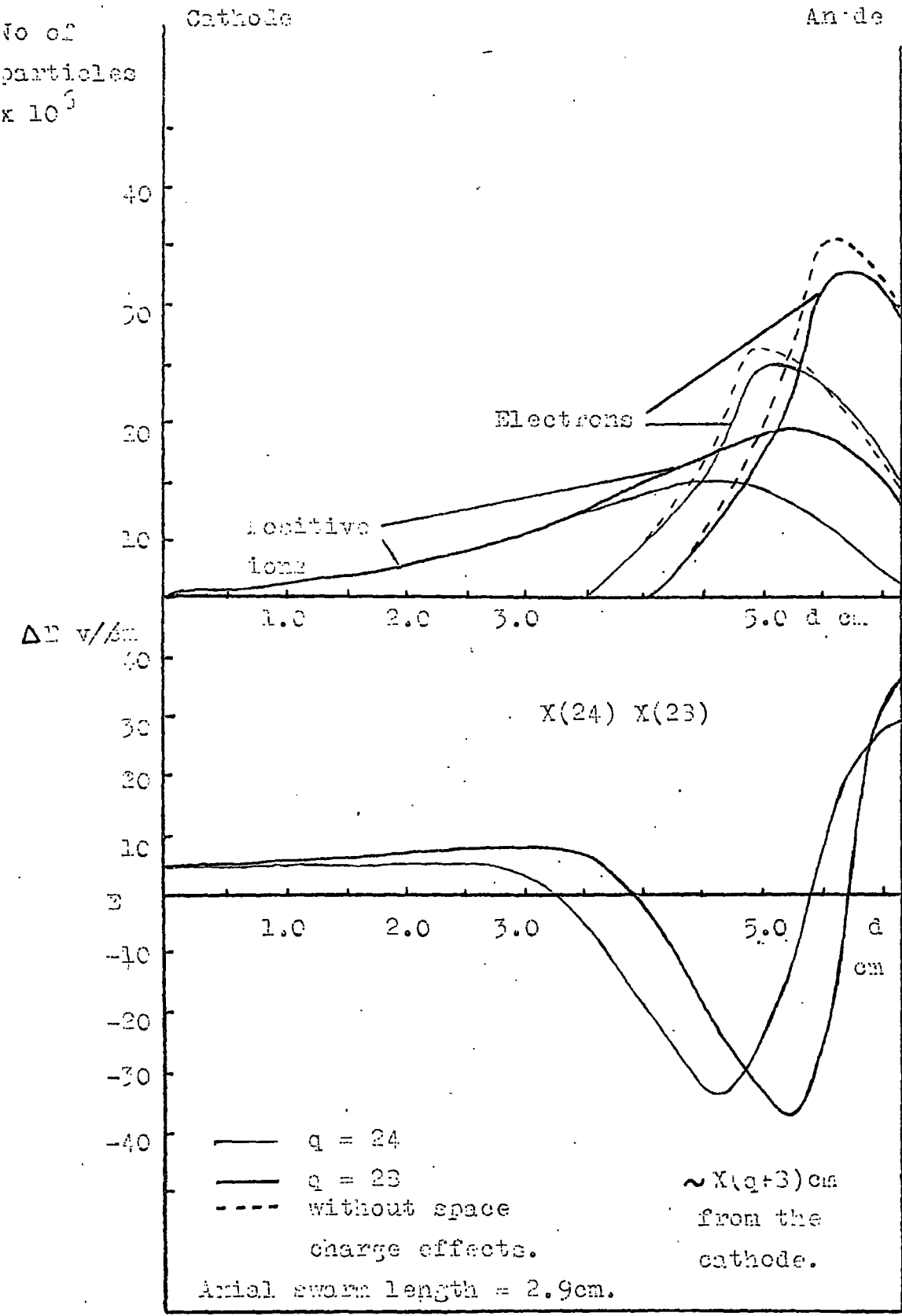
Disc No.	Distance from the cathode in cm.	$n'_e \cdot 10^6$ without space charge	$n_e \cdot 10^6$ with space charge	Disc No.	Distance from the cathode in cm.	$n'_e \cdot 10^6$ without space charge	$n_e \cdot 10^6$ with space charge
q = 12							
2	2.03	0.5	0.5	10	4.06	<u>11.2</u> *	<u>10.3</u> *
4	2.32	1.2	1.2	12	4.35	10.3	10.6
6	2.51	2.1	2.1	14	4.64	9.9	9.3
3	2.90	3.4	3.4	15	4.93	3.0	3.1
10	3.19	<u>5.2</u> *	<u>5.2</u> *	q = 24			
12	3.43	5.1	5.0	2	3.43	1.5	1.5
14	3.77	4.6	4.6	4	3.77	3.7	3.5
15	4.06	3.7	3.7	6	4.06	6.7	6.3
13	4.35	2.2	2.3	3	4.35	10.9	10.0
q = 16				10	4.64	<u>16.4</u> *	15.3
2	2.61	0.7	0.7	12	4.93	15.9	<u>15.4</u> *
4	2.90	1.7	1.7	14	5.22	14.5	14.4
6	3.19	3.1	3.1	16	5.51	11.3	12.0
3	3.43	5.1	4.9	q = 23			
10	3.77	<u>7.6</u> *	<u>7.5</u> *	2	4.35	2.2	2.1
12	4.06	7.4	7.3	4	4.64	5.4	5.0
14	4.35	6.7	6.7	6	4.93	9.9	3.9
16	4.64	5.5	5.7	3	5.22	15.9	14.1
13	4.93	3.2	3.3	10	5.51	<u>24.1</u> *	21.3
q = 20				12	5.80	23.4	<u>22.4</u> *
2	2.90	1.0	1.0				
4	3.19	2.5	2.5				
6	3.43	4.6	4.4				
3	3.77	7.4	7.1				

* - indicates peak position

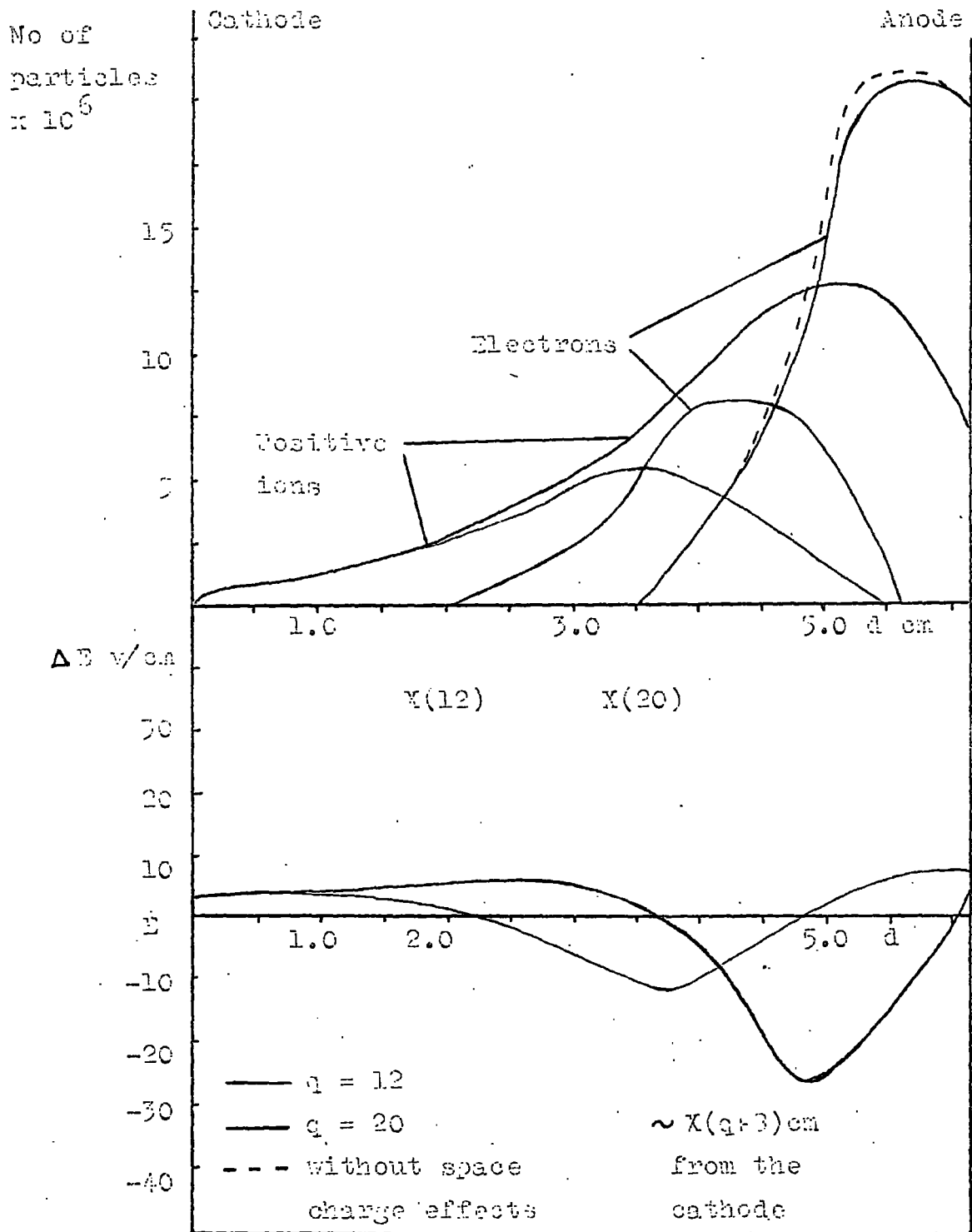
Table(5) Calculated electron distribution within a swarm at various positions in the gap to illustrate the forward shift of the electron peak within the swarm,



Fig(7.4) Particle distributions; $n_0 = 9 \times 10^6$
 $E = 1.390$ kv/cm, $h = 1.45$ mm, radius = 5mm.



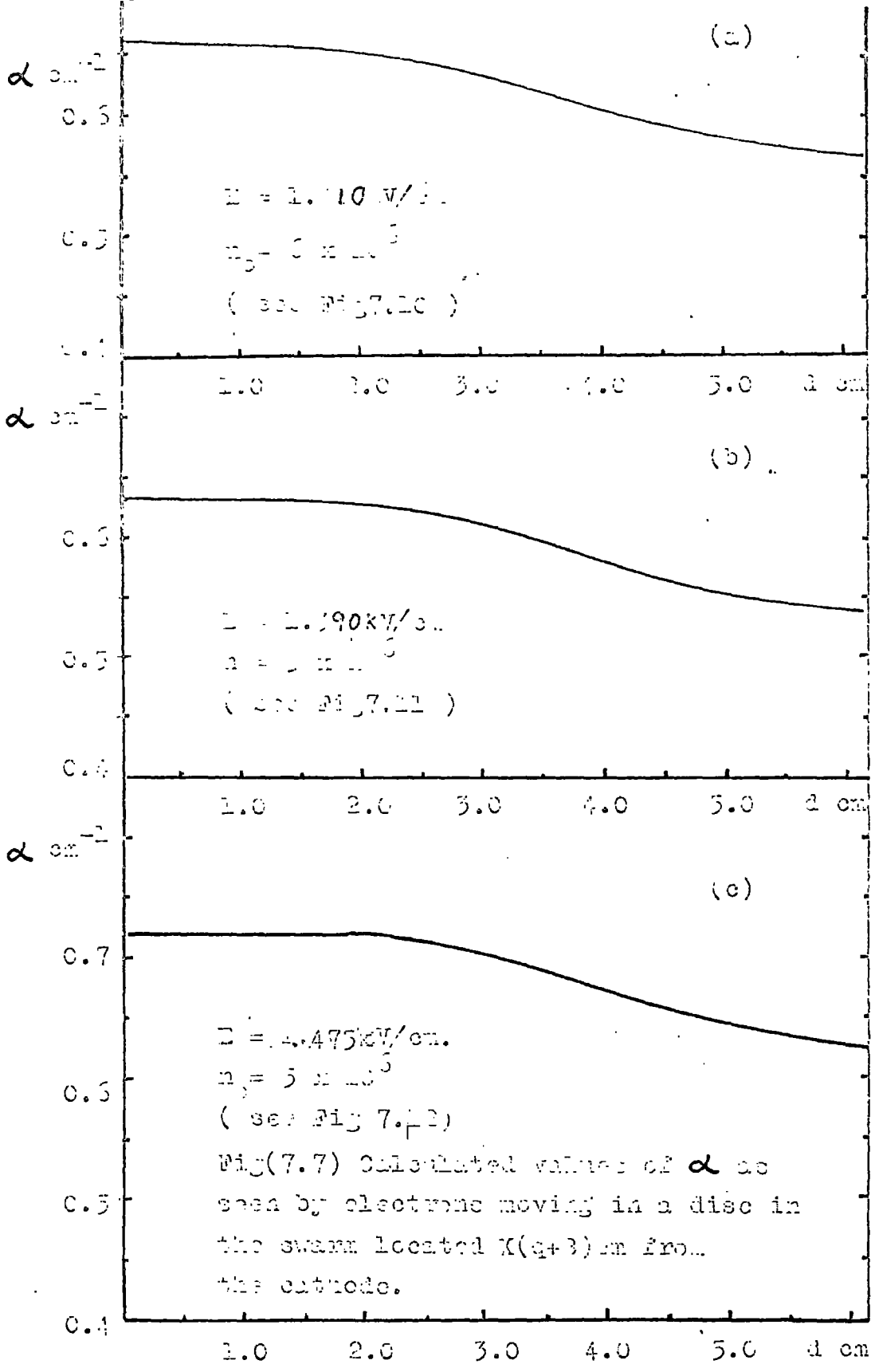
Fig(7.5) Particle distributions; $n_0 = 9 \times 10^5$,
 $E = 1.350$ kV/cm, radius = 5mm, $h = 1.45$ mm.

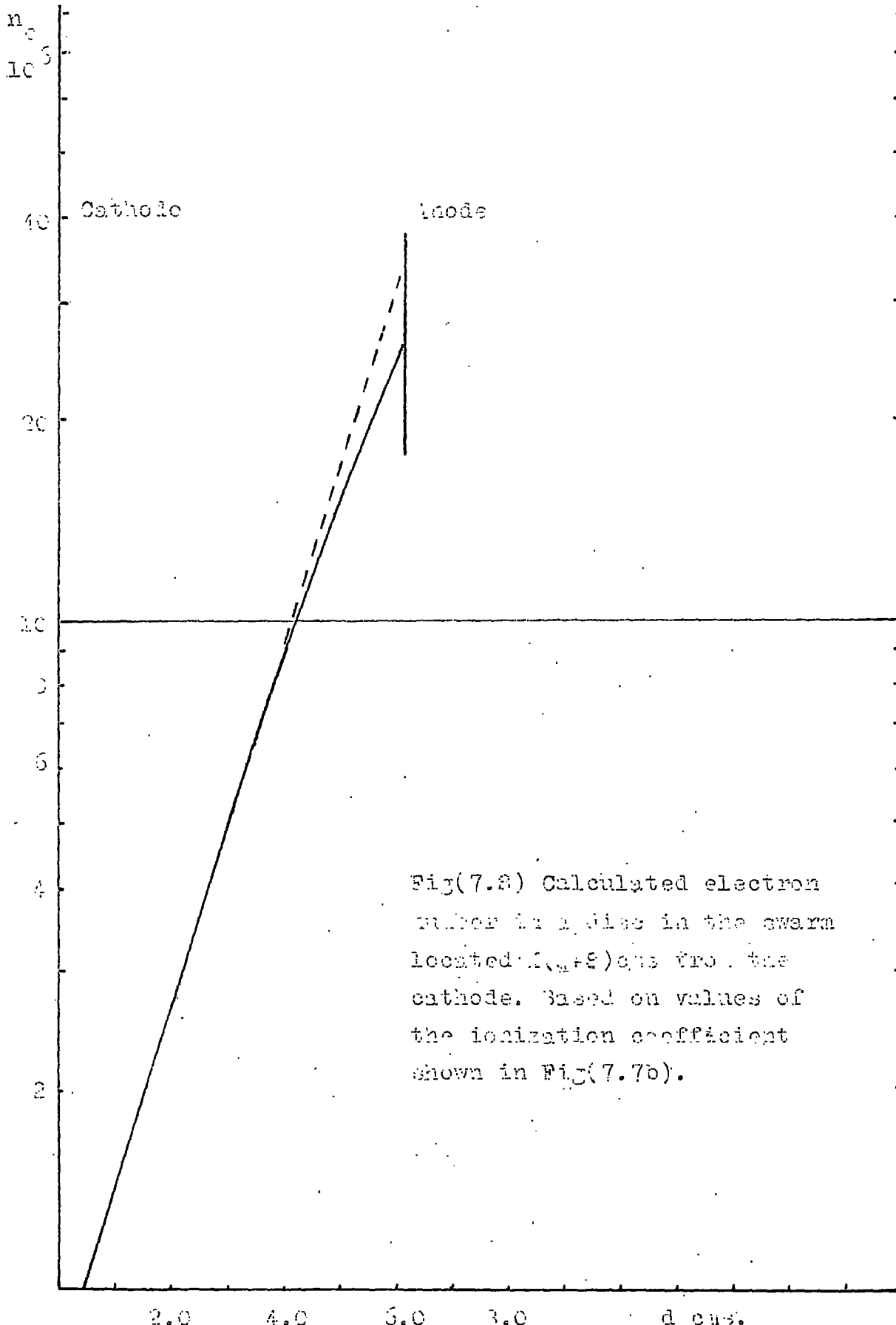


Fig(7.6) Particle distributions; $n_0 = 5 \times 10^6$,
 $E = 1.475$ kV/cm, $h = 1.75$ mm, axial swarm length
 $= 3.5$ cm, radius = 5 mm.

cathode

anode

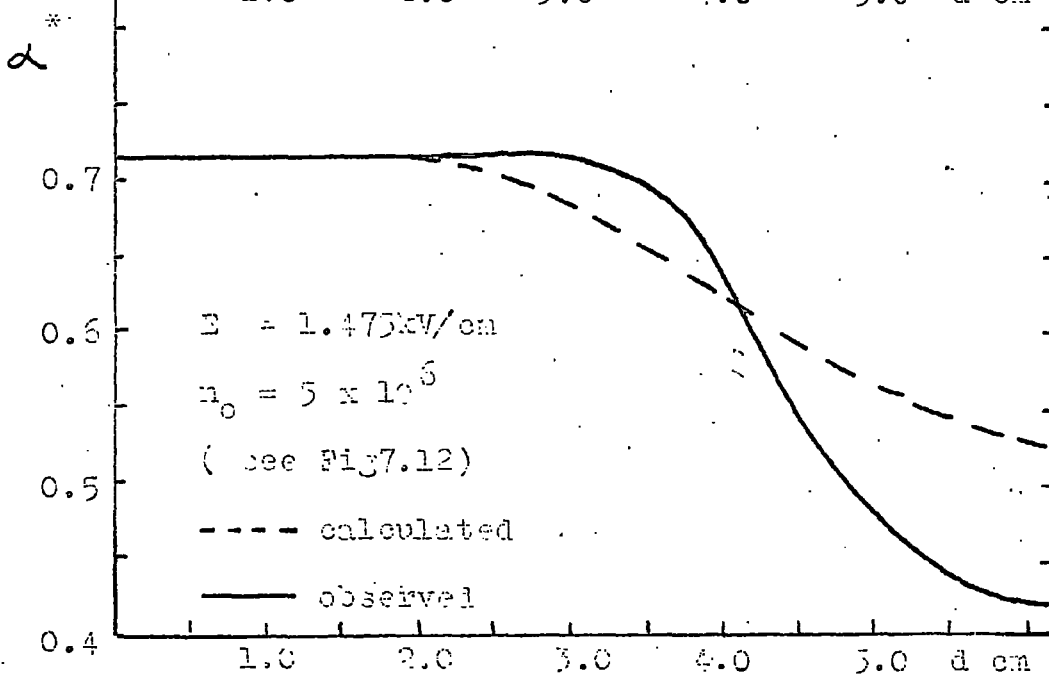
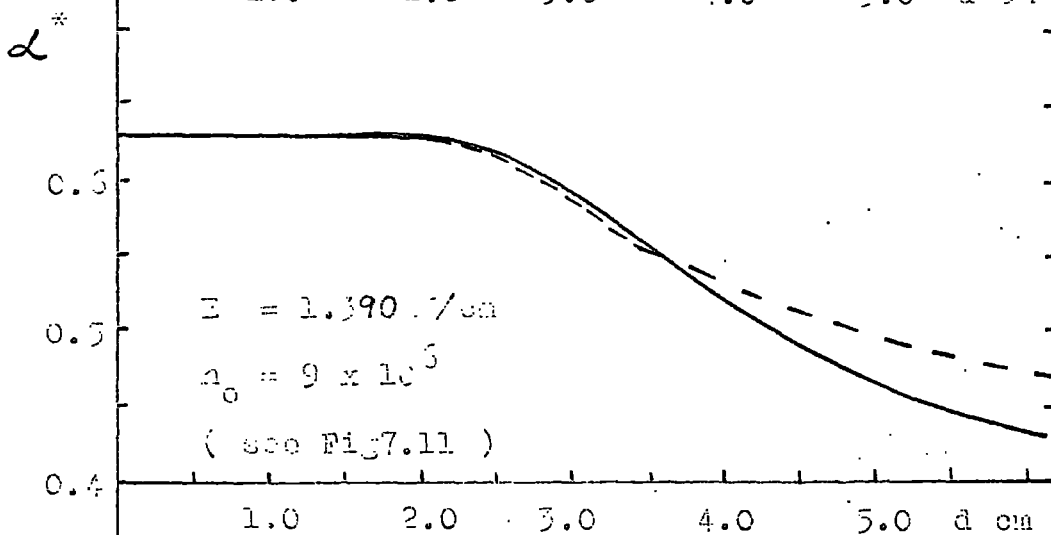
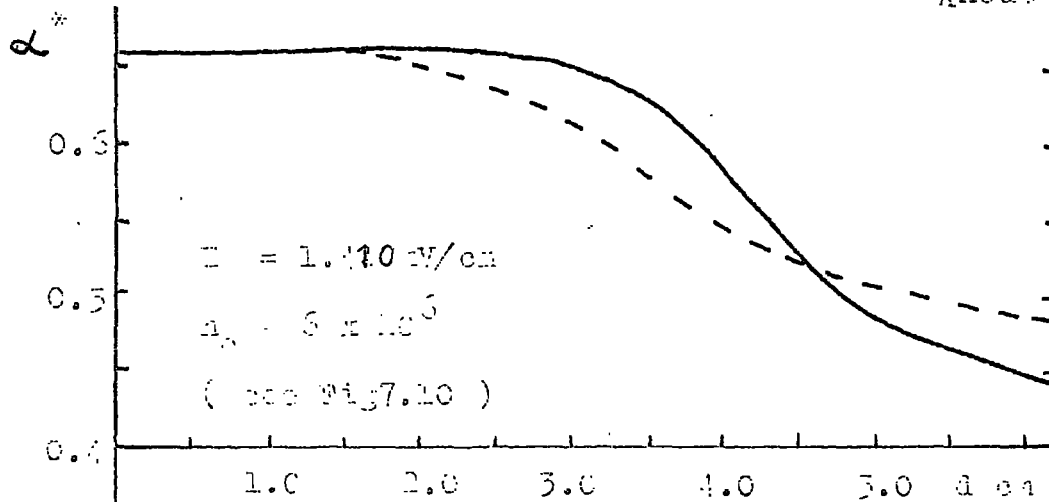




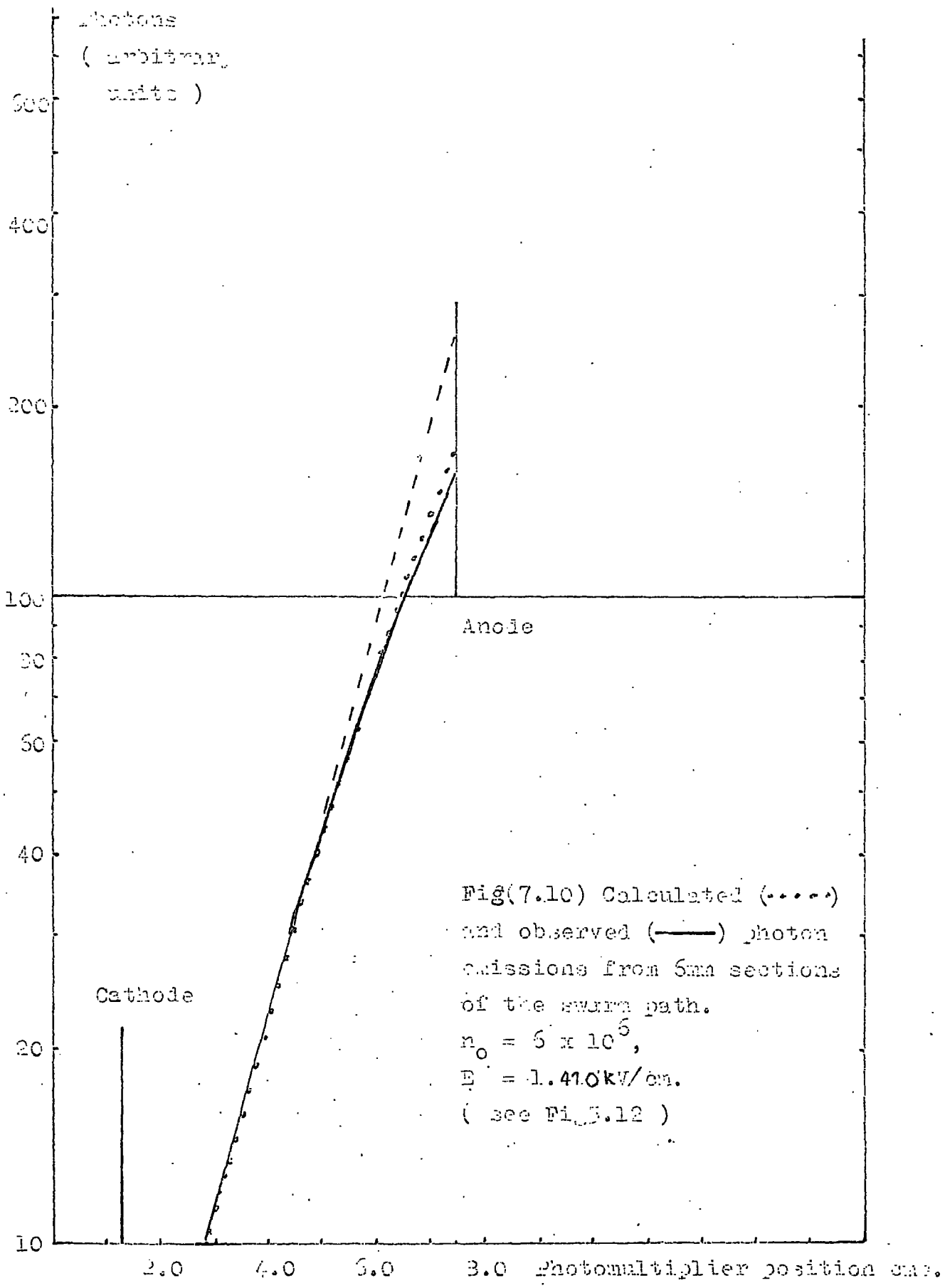
Fig(7.8) Calculated electron number in a plane in the swarm located $(x_0 + \delta)$ cm from the cathode. Based on values of the ionization coefficient shown in Fig(7.7b).

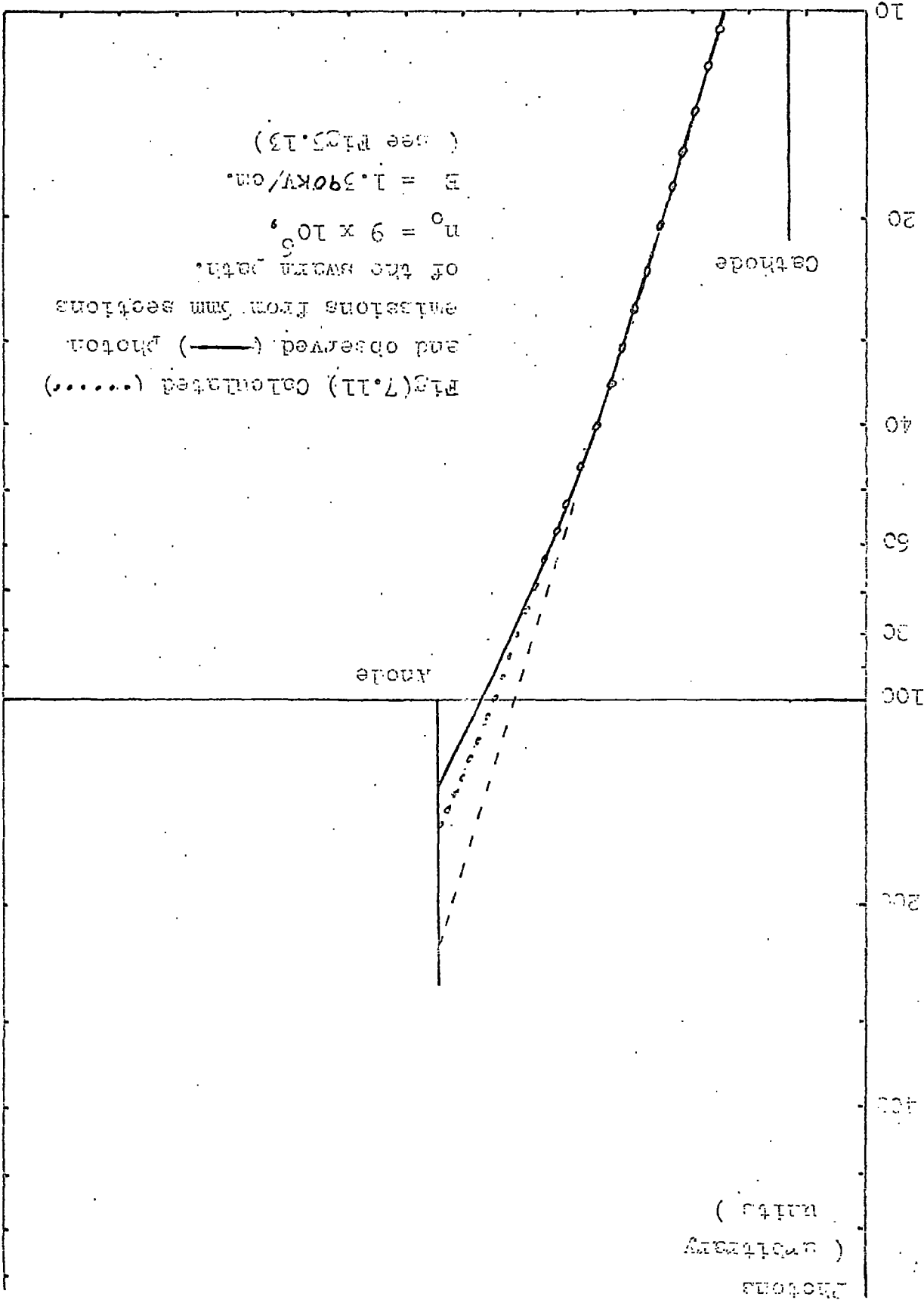
Cathode

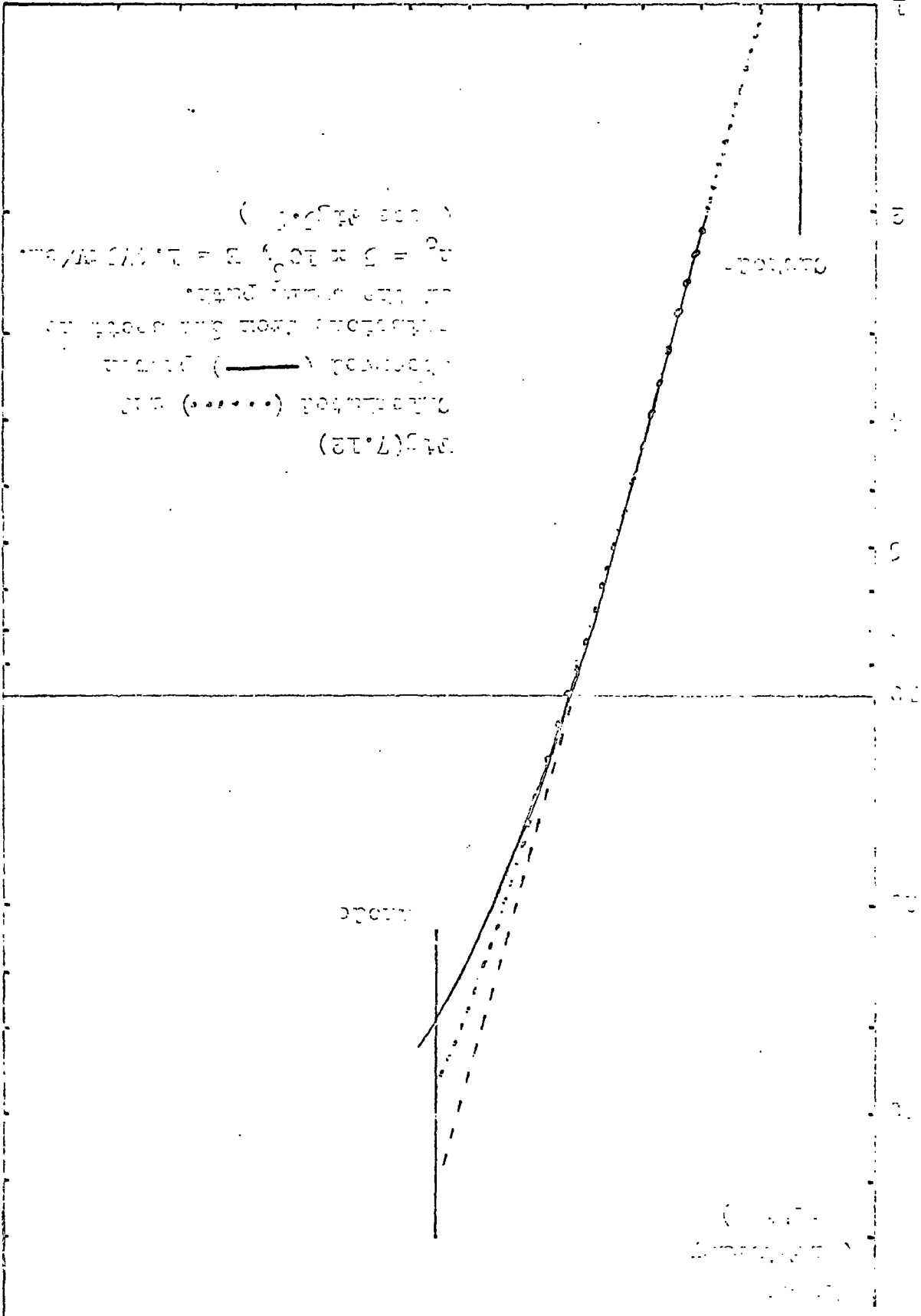
Anode



Fig(7.9) Comparison of the slopes α^* of the calculated and observed photon emission graphs.







$\frac{dP}{dt} = k_p \sqrt{\frac{I_0}{k_d}}$
 $\frac{dP}{dt} = 0.01 \sqrt{I_0}$
 $I_0 = 100 \text{ photons/cm}^2 \cdot \text{sec}$
 $\frac{dP}{dt} = 0.01 \sqrt{100} = 0.01 \cdot 10 = 0.1$

(7.12)
 Critical Photon Flux
 0.75

If the particle distributions in the electrode gap are considered first, it may be seen that the initial distribution of particles within a swarm changes as the swarm moves across the electrode gap, even though diffusive motion is not considered in the program. This change in the electron distribution occurs with and without the influence of space charges, although the effect is accentuated by space charge fields. The initial distribution of electrons as a swarm enters the drift section is such that the maximum number of electrons per disc occurs in the tenth disc, Fig. (6.4). However because of the exponential rate of multiplication, and because the swarm emerges from the cathode over a finite time interval, electrons in the front of the swarm will have travelled further in the gap than those in the centre of the swarm. Thus the position of maximum electron density will be shifted successively from the tenth disc to the eleventh, twelfth, etc. This effect becomes more marked when the influence of space charges is considered, because the multiplication rate of electrons in the swarm centre is reduced. This forward motion is noticeable in Figs. (7.2 and 7.3), and the calculated values for the electron distributions with and without space charge effects are shown in Table (5).

Although this shift in the position of the peak shows in plots of the electron distribution in the electrode gap, the effect will not invalidate the measurements made of the electron drift velocity of low density swarms, ($n_0 < 10^6$). This is so

because the positions of the electron maxima were measured from oscillograms which showed the variation of electron density at a fixed point in the gap, as a function of time. Thus at this point, the electrons had all drifted through the same distance in the gap, and consequently had all suffered the same degree of amplification. In the case of the high density swarms, the forward shift of the peak results in a broadening of the oscillogram pulse, making the location of the peak position more difficult to detect.

The position of the disc containing the maximum number of positive ions occurs some distance behind the electron maxima, while the maximum negative field distortion at a particular time, occurs between these two positions. In general this is approximately $X(q+8)$ cm from the cathode, i.e. in the eighth disc element in the swarm, counting from the tail of the swarm, Figs. (7.2-7.6). It is noted that the field in the gap is increased behind the swarm, between the swarm and the cathode. This enhanced field is caused by the accumulation of positive ions, which effectively screen the region from the primary electrons in the gap. Similarly ahead of the swarm, the field is also considerably enhanced and the electrons in the leading edge of the swarm move in this enhanced field. It is seen that while the number of electrons produced by collision ionization in the centre of the swarm is reduced, there is a slight over-

exponential growth in the leading edge of the swarm.

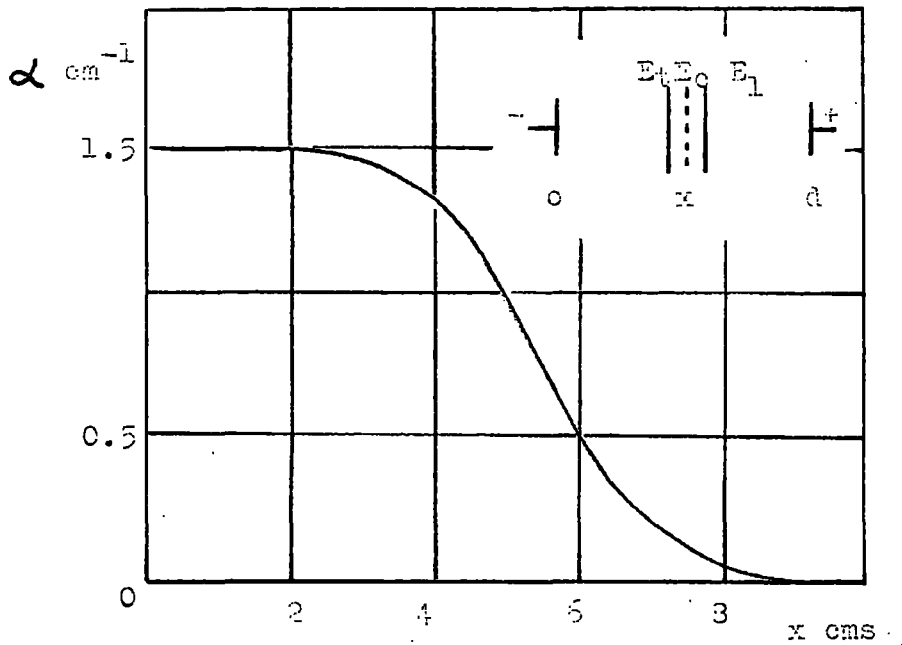
Fig. (7.7) shows the calculated variation of the ionization coefficient α as seen by electrons moving in the eighth disc in a swarm. A steady decrease in α occurs until the front of the electron swarm arrives at the anode. The subsequent loss of primary electrons from the front of the swarm into the anode, causes the ionization coefficient in this eighth disc to decrease less rapidly. It appears therefore that the space charge fields produced by the electrons in the swarms form a significant fraction of the total-negative field distortion within the swarms. The calculated multiplication rate of electrons in the eighth disc-element of a swarm and subject to these negative field distortions, is shown in Fig. (7.8).

It is interesting at this stage to compare the results of the present calculations in which a swarm of finite dimensions is considered with a theoretical example considered by Francis⁽⁴⁹⁾. In this paper the motion of a thin-ion-free layer is treated. The field at the centre of this layer was labelled E_c , and E_t and E_1 at the tailing and leading edges respectively, Fig. (7.13). The number of electrons at x is

$$n_x = n_0 e^{\int_0^x \alpha dx}$$

and by Gauss' theorem,

$$E_c = E_1 - 2\pi n_0 e^{\int_0^x \alpha dx}$$



Fig(7.13) Variation of the ionization coefficient α with position x in a 10cm wide gap, for a single electron avalanche in H_2 at 30 mm Hg, (Francis).

A simple relationship between α and E was assumed:

$$\alpha = c_1 E_c,$$

and the above relation was solved with a constant applied field $E_1 = E_c$ at the electrodes. An expression for α was obtained:

$$\alpha = \frac{A}{1 + Be^{Ax}}$$

where $A = \alpha_0 + 2\pi n_0 ec_1$ and $B = \frac{2n_0 ec_1}{\alpha_0}$

The variation of the ionization coefficient α with position in the gap is shown in Fig. (7.13), and it is seen that for a 10 cm gap $\alpha \rightarrow 0$, with the electrons moving through a steadily decreasing local field. In the present experiment the swarm motion has been studied over a limited drift section, necessary to avoid breakdown of the gap. The particle densities reached in Francis' theoretical example were not therefore attainable with the present apparatus. This limitation on the development of the swarm, together with the finite swarm dimensions, prevents further reduction of the ionization coefficient, Fig. (7.7), and as would be expected, the use of a large electron swarm rather than a thin electron layer, results in a more gradual change in the ionization coefficient. Francis' example is therefore an idealized case which may not be realized experimentally. A further drawback is that the field distortions are calculated using Gauss' theorem and thus the method is limited to cases where the plane radius is comparable with the electrode radius.

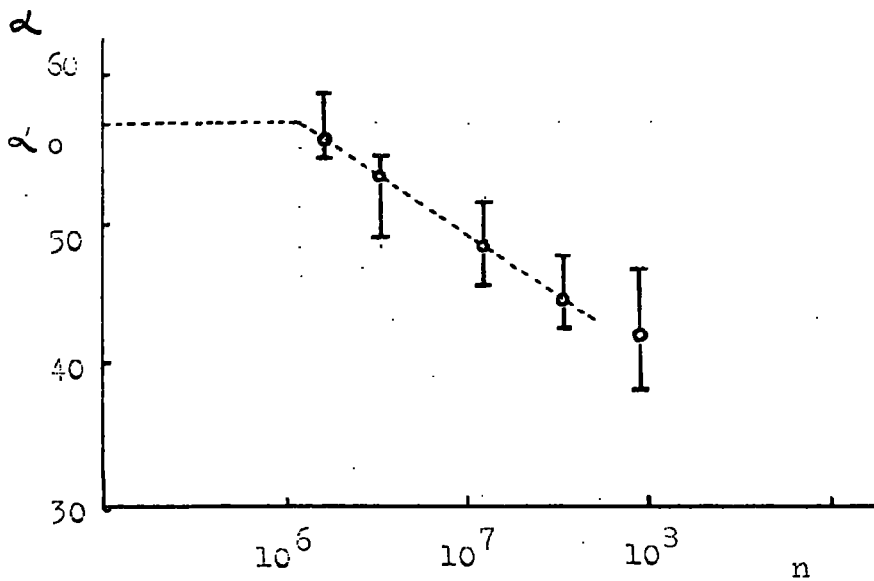
When the swarm path approximates to a thin cylinder, too large values are obtained for the field distortions using this method.

In the present experiment the drift section may be split into three sections: the first, in which space charge fields have a negligible effect upon α , and in which the electron multiplication occurs at an exponential rate; the second, in which field distortions are produced by electrons and positive ions causing a rapid decrease in the ionization coefficient within the swarm; and the third section, in which the increases in the field distortions in the centre of the swarms are determined by the positive ions in the gap rather than by the electrons, and in which the decrease in α is less rapid. These three sections are apparent in the calculated values of α , Fig. (7.7), and also in the calculated and observed slopes α^{*} of the photon emission graphs, Fig. (7.9). The variation of this quantity α^{*} enables a direct comparison to be made between the calculated and observed ionization rates across the gap. In both cases the ionization coefficient is constant over the first one or two cms of the drift section, but then a discontinuity occurs at which both α and α^{*} are reduced. This is followed by a final section in which the multiplication rate is also reduced, but in which the rate of change of α and α^{*} is less rapid.

Figs. (7.10-7.12) show the observed and calculated photon emissions from 6mm sections of the swarm paths. The dashed

lines in these plots indicate an exponential growth rate. The experimental graphs are copies of those shown in Chapter 5, and the photon emission is shown as a function of the photomultiplier position. The cathode and anode surfaces are located at 1.30 and 7.47 cms respectively, for the 6.17 cm gap. The calculated photon emission curves are plotted between the planes containing the electrode surfaces, and the initial linear sections of the observed and calculated curves are superimposed. This alleviates the necessity of evaluating the quantum efficiency and gain of the photomultiplier, and also the gap geometry factor. These quantities are all constants of proportionality which relate the number of electrons drifting in a slice of the swarm path to the photon emission.

The calculated curves show an under-exponential growth rate caused by distortions of the applied field, but this is less marked than that observed experimentally. As may be seen from Fig. (7.9), the calculated change in slope is not as abrupt as in the observed plots, however the three divisions of the drift section are apparent in both cases. In the simplified model used to simulate the development of a primary swarm, it will be remembered that the initial axial electron distribution was taken to be approximately triangular, and also that the electron density in a cross-section of the cylindrical swarm path was made uniform. The rate of change of the ionization coefficient is strongly dependent upon the choice of these



Fig(7.14) Dependence of α on the electron number in ether, $d = 0.3\text{cm}$, $pd = 110\text{ mm cm}$, $E/p = 77$, ().

initial distributions, and a closer fit between the calculated and observed curves can be obtained by trying more complicated initial distributions. If for example, the program were adjusted to take into account the radial distribution of electrons within a swarm, then more particles would be concentrated around the central electrode axis, and the discrepancy between the observed and calculated curves would be reduced.

Direct comparison of the present experimental findings with those of other workers is not possible. However some experiments have been performed to study the effects of space charges on single avalanches which developed in highly-stressed electrode gaps⁽⁵⁰⁾. However to prevent sparking in these gaps it is necessary to work in either organic gases, or gas mixtures in which the secondary emission coefficients are very low. The experiments are necessarily of a statistical nature, but they do show that a reduction of the ionizing efficiency is to be expected when avalanches containing more than 5×10^6 electrons are considered. Fig. (7.14) shows this dependence of the ionization coefficient upon the electron number in ether.

Most of the theoretical treatments in the literature consider idealized cases in which the motion of thin planes of charge is studied. However of particular interest is a series of papers by Ward^(43,51,17), in which mid-gap breakdown is considered on the basis of a one-dimensional Townsend model. The calculations were made using a computer to solve numerically the one-dimensional

continuity equations governing the growth of ionization currents in an electrode gap. The papers are mainly concerned with the gap breakdown and possible avalanche-streamer transitions, but it is noted that during the first stages of the avalanche growth, this model also predicts a reduction of the ionizing efficiency within the avalanche. However as has been mentioned earlier, field distortions calculated using Poisson's equation will be too large when the avalanche radius is small compared with the electrode radius. Another serious criticism of Ward's work is that the electron energies required in his calculations to obtain agreement with experiment, are one-two orders of magnitude above that which one would expect in most electron avalanches.

7.4 Comments

Summarising briefly, in an experiment in which a primary electron swarm was initiated at the cathode of a plane - parallel gap, the calculated rates of growth of electrons within the swarm, and of the photon emission from sections of the swarm path, are seen to be of the same form as the observed growth curves. That is, the field distortions produced within a primary electron swarm by the electrons and positive ions, act in such a way as to reduce the multiplication of the electrons by collision ionization.

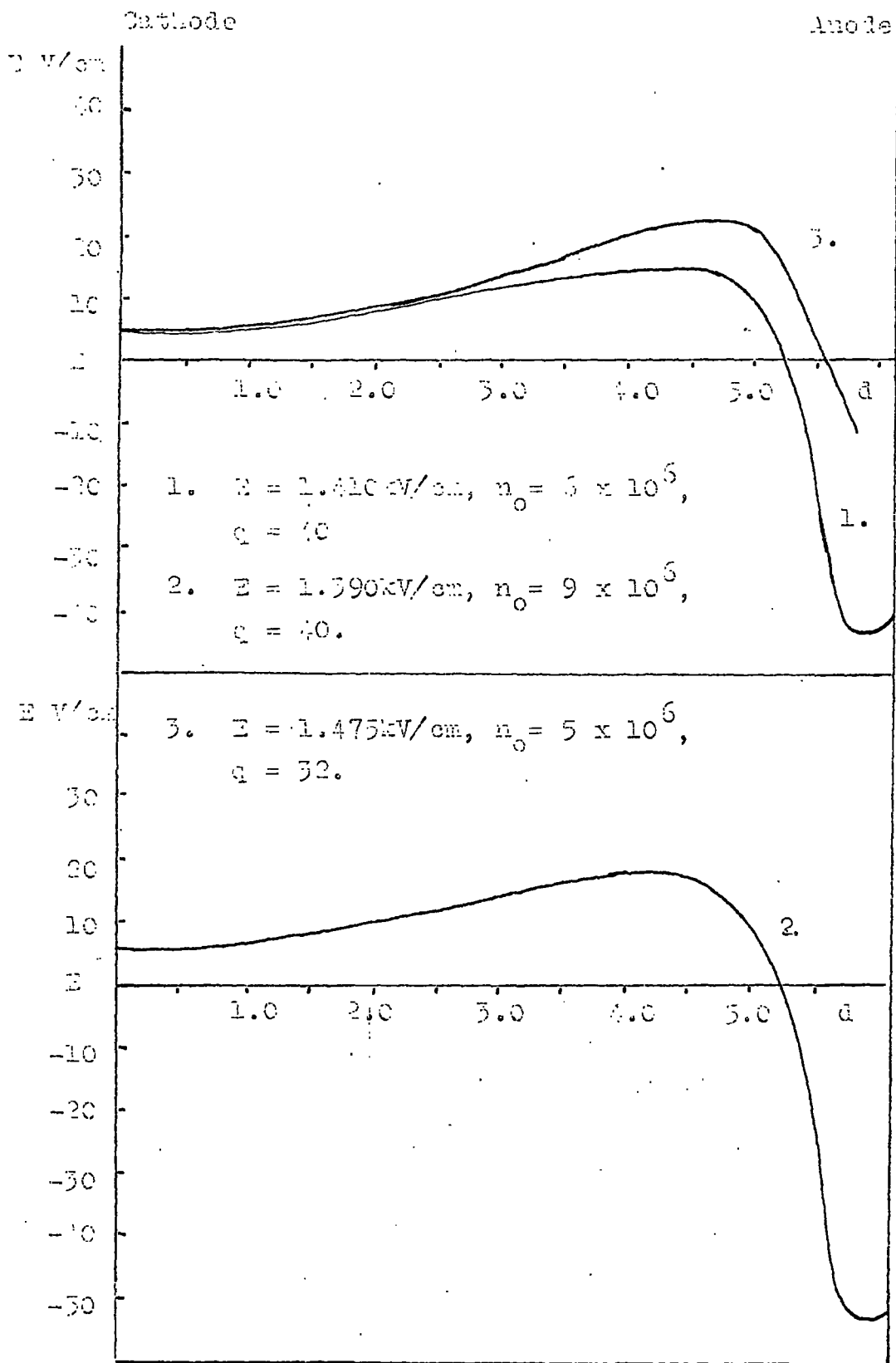
The calculated current growth curves show this under-exponential growth, caused by field distortions of 3-4% of the applied field within the swarm. In general the calculated departure from an exponential growth rate is less marked than has

been observed experimentally. However this is attributed to the simple particle distribution used in the computer program, and also to experimental inaccuracies in determining the initial number of electrons in a swarm. It is noted that these findings refer to non-steady state conditions in which the discharge current is produced by the motion of a single electron avalanche. Thus even though α/p is below the point of inflexion on the $\alpha/p - E/p$ curve, a reduction of the total ionization occurs during this first avalanche transit time. This result is not a contradiction of the findings of other workers at these values of α/p . Over a period of many transit times, an increase in the total ionization currents is to be expected, (see p.11).

When the initial number of electrons per swarm leaving the cathode was kept below a figure of 10^6 electrons and the applied voltage to the gap was several percent below the gap breakdown voltage, the observed rate of multiplication of the electrons in the swarms was always exponential; the number of electrons at a point x cms from the cathode being accurately determined by the equation

$$n_x = n_0 e^{\alpha x}$$

The mean experimental value for α/p_0 in hydrogen, corrected to $E/p_0 = 23.50 \text{ V cm}^{-1} \text{ mm}^{-1}$ for electrons in primary swarms was found to be $0.011 \text{ cm}^{-1} \text{ mm}^{-1}$. The values taken for α in cases where $n_0 > 10^6$, were from the linear sections of the plots. This mean value lies somewhat below that found by Rose⁽⁴⁷⁾ at this value of



Fig(7.15) Field distortions in the gap as the electron swarms move into the anode.

E/p_0 , ($\alpha/p_0 = 0.014 \text{ cm}^{-1} \text{ mm}^{-1}$). However the mean value of α/p_0 obtained from the motion of secondary electrons in the experiment was found to be $0.014 \text{ cm}^{-1} \text{ mm}^{-1}$. It is well known that at these values of the reduced field, the value of the ionization coefficient is strongly dependent upon the gas purity in the system, and the close agreement of the present experimental values for α to those given by Rose is a good indication of the cleanliness of the present system, and of the suitability of the optical method for measurements of the ionization coefficient.

Although the growth curves for secondary electron swarms produced in the electrode gap were found to be linear, the time and spatial resolution in the gap of these secondary swarms was not as good as in the case of the primary swarms. This was so chiefly because of the lower photon emission, and more reliance must be placed on the value obtained for primary electrons.

The field distortions in the electrode gap at times when the last of the primary electrons are entering the anode are shown in Fig. (7.15). It is apparent that secondary electrons moving down the central electrode axis, will move in an enhanced electric field, and suggests that an over-exponential rate of growth should have been observed for these electrons. However, the calculated field distortions shown, refer only to points located on the central electrode axis, and the distortions will decrease towards the edges of the electrode gap. While the assumption that these distortions do not vary appreciably over

the cross-section of the cylindrical path followed by the primary swarm is acceptable, ($r_{\text{cylinder}} \sim 5 \text{ mm}$) this cannot be assumed to hold over the whole electrode surface ($r_{\text{drift section}} \sim 3 \text{ cms}$). Thus only secondary electrons moving along the central electrode axis will experience appreciably distorted fields. It has been shown previously that secondary emission occurs over most of the cathode surface, and hence a considerable distortion of the applied field would be required before a detectable change in the ionization rate for secondary swarms could be observed.

CHAPTER 8

SUGGESTIONS FOR FUTURE WORK

In the experiments to determine the effects of space charge fields upon the development of an electron avalanche, one of the main difficulties has been the introduction of sufficiently high density swarms into the gap. If more profitable experiments are to be carried out in hydrogen, with conventional cathodes, then the electron density within the diffusion radius of an avalanche must be increased by upto an order of magnitude. However, as has been indicated, it seems doubtful whether such an emission is possible with the present electron source.

An alternative method by which electrons may be liberated from the cathode is that of photo-electric emission from the cathode surface. Until recently the number of starting electrons produced by this method has been limited by the low intensity of the available light sources. (It is noted that the wavelength of the incident radiation must be short enough ($<3,500\text{\AA}$), for the associated quantum energies to be greater than the work function of the cathode material). However recent research work has extended the range for coherent radiation emission for gas lasers in the spectral band $2,300\text{-}4,000\text{\AA}$,^o (52,53) and it is anticipated that such light sources will be capable of generating the required numbers of starting electrons. This method of production has two further advantages: first the emission will

not be pressure dependent, and thus experiments may be carried out at pressures >90 mm Hg when the spreading of the avalanche head by diffusion is negligible; secondly, the energy of the swarm electrons may be determined from the work function of the cathode material and the wavelength of the incident radiation.

The use of the optical method has so far been confined to molecular gases in which the mean life-time of the relevant excited states is about 10^{-8} second. It would be interesting to experiment with atomic gases in which the higher ionization coefficient would accelerate the onset of space charge conditions; of particular interest then would be to see whether the already increased ionization rates in the front of a swarm are still further enhanced by the space charge fields. However it is noted here that the existence of long-lived excited states in atomic gases would reduce the spatial electron resolution of the method of observation. In helium for instance, by re-absorption of resonance light, the mean lifetime of excited states is prolonged to 10^{-7} second. During this time period the original exciting electrons would have moved about a cm from the point of the exciting collision. It is also noted that while an increase in the electron multiplication rate in the drift section would be obtained, a close approach to the breakdown voltage would be more difficult in these gases, because of the increased secondary emission coefficients.

In order to avoid breakdown in the gap it was necessary in the experiments to limit the length of the drift section and hence the amplification of the swarms. However the computer simulation of an avalanche development is not subject to this practical limitation, and it would be of considerable interest to allow the avalanche motion to continue until the field distortions became comparable with the applied field. To do this, the present program would need some revision to make more economical use of computer time, or alternatively, access to a faster computer system would be required.

It has been shown that when the ionization rates in the gap are low, the method of observation can be used to study directly the effects of drift and diffusion on the motion of electron swarms. Additional measurements are required here to determine more completely the radial and axial rates of diffusion within the swarms, and of particular interest would be a study of these effects over a wide range of gas pressures, ($1 < p < 100$ mm Hg).

Appendix I
The Computer Program

Parameter changes

$n_0 := B$	$0.005E := \text{field}$
$\alpha := T$	$A := \text{constA}$
$\alpha(i) := t(i)$	$B := \text{constB}$
$E := e$	$\frac{\epsilon}{\alpha_a} := \text{excite}$

ESTABLISH D0737DMOORPU; Avalanche Distortion; O/PL

```
begin library AO,A6;
integer i,j,c,m,n,z,u,v,w,x,b;
real A,T,r,e,B,C,d,pres,constA,constB,excite,
field;
real array X(1:100),Y(0:20),E(1:100),p(1:100,1:20),
P(0:100),N(0:100),Z(0:100),a(0:100),F(0:100),
t(0:100),L(0:100);

Boolean procedure even(m); value m; integer m;
begin even:= if m-(m+2)*2=0 then true else false;
end;

real procedure simps(m,n); integer m,n;
begin real O,Q,R;
O:=N(m)*a(m)+N(n)*a(n);
Q:=0;
if n=3 then go to hered;
for i:=m+2 step 2 until n-2 do
Q:=Q+2*N(i)*a(i);
hered: R:=0;
if n=3 then
begin R:=4*N(2)*a(2);
goto heref;
end;
for i:=m+1 step 2 until n-1 do
R:=R+4*N(i)*a(i);
heref: simps:=(O+Q+R)*h/3;
end;
open(20): open(30);
start: q:=0;
input h,B,T,r,e,d,pres,constA,constB,x,excite,field;

for i:=0 step 1 until 100 do
X(i):=i*h;
for j:=0 step 1 until 20 do;
Y(j):=j*h;
C:=3,14,16*r2;
A:=0;
A:=B/(100*C*h2);
b:=0;
for i:=q step 1 until 100 do
begin L(i):=0;
E(i):=0;
end;
end;
```

```

run:      for i:=q step 1 until q+10 do
begin     j:=i-q;
          if X(i)<d then
          E(i):=(A*Y(j))*(exp(T*X(i)));

end;

begin    for i:=q+11 step 1 until q+20 do
          j:=i-q;
          if X(i)<d then
          E(i):=(2*A*Y(10)-A*Y(j))*(exp(T*X(i)));

end;

          if q>0 then goto shorta;
          i:=1;
          for j:=1 step 1 until 10 do
          p(i,j):=(A*Y(j))*(exp(T*X(i))-1);
          for j:=11 step 1 until 20 do
          p(i,j):=(2*A*Y(10)-A*Y(j))*(exp(T*X(i))-1);
shorta:   if q=0 then goto herea;
          for i:=q-8 step 1 until q+1 do
begin     for j:=1 step 1 until 10 do
          begin if j>=i then p(i,j):=0 else
          p(i,j):=(A*Y(j))*(exp(T*X(i))-1)-(A*Y(j))*
              (exp(T*X(i-1))-1);

end;
end;
herea:   for i:= q+2 step 1 until q+10 do
begin     for j:=1 step 1 until 10 do
          begin if j<i-q then p(i,j):=0 else
          if X(i)>d then p(i,j):=0 else
          p(i,j):=(A*Y(j))*(exp(T*X(i))-1)-
              (A*Y(j))*(exp(T*X(i-1))-1);

end;
end;

          if q=0 then goto heree;
          for i:=q+2 step 1 until q+10 do
begin     for j:=11 step 1 until 20 do
          begin if j>=i then p(i,j):=0 else
          if X(i)>d then p(i,j):=0 else
          p(i,j):=(2*A*Y(10)-A*Y(j))*(exp(T*X(i))-1)-
              (2*A*Y(10)-A*Y(j))*(exp(T*X(i-1))-1);

end;
end;

          for i:=q+11 step 1 until q+20 do
begin     for j:=11 step 1 until 20 do
          begin if j<i-q then p(i,j):=0 else
          if X(i)>d then p(i,j):=0 else
          p(i,j):=(2*A*Y(10)-A*Y(j))*(exp(T*X(i))-1)-
              (2*A*Y(10)-A*Y(j))*(exp(T*X(i-1))-1);

end;
end;
heree:   goto hereg;
          for i:=q+2 step 1 until q+20 do

```

```

begin          for j:=1 step 1 until 20 do
begin          if j<i-q then p(i,j):=0 else
                if X(i)>d then p(i,j):=0 else
                p(i,j):=(2*A*Y(10)-A*Y(j))*(exp(T*X(i))-1)-
                    (2*A*Y(10)-A*Y(j))*(exp(T*X(i+1))-1);

end;
end;
hereg:         for i:=q+11 step 1 until q+20 do
begin         for j:=1 step 1 until 10 do
                p(i,j):=0;
                P(0):=0;
                if q>0 then goto shortb;
                for i:=q step 1 until 100 do
                P(i):=0;
shortb:       if q≥20 then z:=q-8 else z:=1;
                for i:=z step 1 until q+20 do
begin         for j:=1 step 1 until 20 do
begin         P(i):=P(i) + p(i,j);
                p(i,j):=0;
end;
end;

                for i:=0 step 1 until 100 do
                N(i):=(P(i)-E(i));
                u:=0;
                v:=20;
                w:=h;
sum:          for c:=u step w until v do
begin         if w=4 then m:=q+c else
begin         m:=c;
                if q-(q+x)*x≠0 then
                if m<q then goto distor;
                if m>q +20 then goto distor;
end;
end;

                if w=4 then n:=q+20 else n:=v;
                F(m):=0;
                for i:=m step 1 until n do
begin         Z(i):=X(i)-X(m);
                a(i):=1.6*10-12/17.7*(1-Z(i)/sqrt(Z(i)2+r2));
end;

                if w=4 then
begin         if c=20 then goto hereb;
end;
                if w=1 then
begin         if X(c)>d then goto exit;
                if even(m) then n:=n-1;
end;         F(m):=simps(m,n);
hereb:       F(m):=F(m)-2*N(m)*a(m)*h/3;

```

```

        if m<=3 then goto herec;
        for i:=1 step 1 until m-1 do
begin
    Z(i):=X(m)-X(i);
    a(i):=1.6*102/17.7*(1-Z(i)/sqrt(Z(i)2+r2));
end;

    n:=m-1;
    if even (n) then F(m):=F(m)-simps(0,n) else
    F(m):=F(m)-simps(1,n);

herec:
begin
end;

begin
begin
    if w=1 then
    if m<=q +20 then
    if m>=q then
    t(m):=constA*pres*exp(-constB*pres/(103*(e+F(m))));
    goto distor;

    if abs(F(m))>field then
    v:=50;
    u:=0;
    w:=1;
    goto sum

end;
end;

begin
distor:
end;

    if w=1 then goto exit;
    if q>=20 then z:=q-8 else z:=0;
    for i:=z step 2 until q+20 do
    write X(i),C*h*P(i),C*h*E(i);

begin
    q:=q+10;
    for i:=0 step 1 until q-1 do
    E(i):=0;
    if d<X(q+1) then
    q:=0;
    goto start;

end;

    goto run;
    if q-(q+x)*x=0 then
begin
begin
    for i:=0,i+4 while X(i)<d do
    write X(i),F(i);

begin
    for i:=q, i+2 while i<q+20 do
    write X(i),C*h*P(i),C*h*E(i);

end;
end;

    q:=q+1;
    b:=b+1;
    if b=1 then

```

```

begin      for i:=q+1 step 1 until q+10 do
begin      z:=0;
            for j:=0 step 1 until i-q do
            z:=z+j;
            L(i):=B*(1-z/100)*exp(T*X(i-1))*T*excite*h;
end;
            for i:=q+11 step 1 until q+19 do
begin      z:=55;
            for j:=9 step -1 until 20-i+q do
            z:=z+j;
            L(i):=B*(1-z/100)*exp(T*X(i-1))*T*excite*h;
end;
            for i:=q+20 step -1 until q+1 do
end;      if X(i)>d then
begin      E(i):=0;
            L(i):=0;
begin
            end;
            else
            L(i):=L(i)+E(i-1)*C*h*t(i-1)*excite*h;
            E(i):=E(i-1)*exp(t(i-1)*h);
            end;
            j:=i-q;
            if X(i)>d then p(i,j):=0 else
            p(i,j):=E(i)-E(i-1);
            P(i):=P(i)+p(i,j);
            end;
            E(q):=0;
            E(q-1):=0;
            for i:=q-1 step 1 until q+20 do
            N(i):=P(i) - E(i);
            if d<X(q) then
            for i:=2, i+2 while X(i) d do
            begin      write X(i),L(i)B*exp(T*X(i-1))*T*excite*h;
            begin
            end;
            q:=0;
            goto start
            end;
            u:=0;
            write q;
            goto sum
            close (20); close (30);
            end

```

Appendix II

Gas Breakdown in U.H.F. Fields

During the period Oct. 1963-Dec. 1964, the author and Mr. R. Kirkwood continued experiments which were begun in the University by Messrs. Rowbotham and Monk. These experiments were initially designed to measure the formative and statistical time lags associated with gas breakdown at 187 Mc/sec. Later work by Boyer and Earl increased the sensitivity of the apparatus and formative delays ranging from 0.2-400 μ sec were measured as a function of gap overvoltage in both molecular and atomic gases.

The apparatus used to measure these time lags is described fully elsewhere, (Prowse, Rowbotham, and Monk⁽⁵⁴⁾; Boyer⁽⁵⁵⁾), briefly however, the method is based on the use of an oscillator giving a long pulse, (400 ns.), at 187 Mc/s. This voltage pulse is applied across a plane-parallel gap by means of an open-ended, coaxial transmission line, which is approximately two wavelengths long, (~165 cms). A time-zero is then set by the firing of an auxiliary spark gap which provides photo-electrons between the electrodes. The envelope of the uhf voltage pulse is displayed on an oscilloscope by means of a piston attenuator and rectifying circuit, and the delays may be measured from oscillograms of the collapse of the gap voltage.

This collapse of the gap voltage indicates three stages in the formation of a discharge:

- i) pre-breakdown current growth;
- ii) the transition stage between a non-conducting and highly conducting states;
- iii) post-breakdown or maintenance conditions. The more recent measurements by Boyer have indicated that during the pre-breakdown current growth the controlling process in the discharge is electron diffusion. Whereas in all the gases considered, it was found that the maintenance fields were consistent with electron losses by ambi-polar diffusion.

During the period indicated, the author with Mr. R. Kirkwood continued the investigation in the transition stage, and attempted to measure directly the electron population in the gap from the occurrence of the initial ionization, until a maintained discharge was established. The method of approach to the problem was to employ a bridge circuit in the existing apparatus in order to separate the conduction current in the gap from the associated capacitative currents. However considerable difficulties were encountered using such circuits to measure these high-frequency transient currents, and in particular it was found that cross-coupling occurred between the transmission line and the detector used in the bridge circuit. In addition it was found that asymmetrical leakage impedances were associated with the circuit, and these proved to be of sufficient magnitude to swamp the effects of the variable bridge elements and also to introduce phase displacements between the voltages to be balanced.

Although some preliminary results were obtained, it was concluded that the bridge circuits developed were more suited for measurements of steady currents in a maintained discharge. The transient current experiments were therefore discontinued at this juncture although a successful investigation into the variance of maintenance potentials with conduction currents has since been carried out by Mr. Kirkwood. In his experiments particular attention has been paid to the determination of the phase angle between the displacement and conduction currents.

REFERENCES

1. Raether, H., 'Electron avalanches and breakdown in gases'; Butterworths, 1964.
2. Corrigan, S. and Von Engel, A., Proc. Roy. Soc. A245, 335, 1958.
3. Dutton, J., Llewellyn Jones, F. and Palmer, R.W., Proc. Phys. Soc. 78, 569, 1961.
4. Crowe, R.W., Bragg, J.K. and Thomas, V.G., Phys. Rev. 96, 10, 1954.
5. Kluckow, R., Z. Phys., 161, 353, 1961.
6. Bandel, H.W., Phys. Rev., 95, 1177, 1955.
7. Menes, M., Phys. Rev., 116, 481, 1959.
8. Schlumbohm, H., Unpublished, see ref. 1, p121.
9. Von Engel, A. and Steenbeck, M., 'Elektrische Gasentladungen', Springer, Berlin, 1934. See also ref. 34, p202.
10. Clarke, J.D. and Hutton, P.J., VIth International Conference on Ionization Phenomena in Gases, Paris, 1963.
11. White, H.J., Phys. Rev., 48, 113, 1935.
12. Rogowski, W. and Walraff, Z. Phys., 97, 666, 1935.
13. Loeb, L., 'Handbuck der Physik'; XXII, pp445-550, 1956.
14. Raether, H., Z. Phys. 112, 464, 1939.
15. Franke, W., Z. Phys. 158, 96, 1960.
16. Wagner, K.H., Proc. VIIth International Conference on Ionization Phenomena in Gases, Belgrade, 1966.
17. Ward, A.L., J. Appl. Phys., 36, 2540, 1965.
18. Tholl, H., Z. Naturforsch, 18a, 587, 1963.
- 18'. Dibbern, U., Proc. Vth International Conference on Ionization Phenomena in Gases, Munich, 1961.

19. Ramien, Z. Phys., 70, 353, 1931.
20. Breare, J.M., 'A study of ion avalanches in electric fields'; D. Phil. Thesis, Oxford University, 1963.
21. Breare, J.M. and Von Engel, A., Proc. Roy. Soc. A282, 390, 1964.
22. Legler, W., Z. Phys. 173, 169, 1963.
23. Massey, H.S. and Burhop, E.H.S., 'Electronic and ionic impact phenomena'; Clarendon press, Oxford, 1952.
24. Jones, H. and Whiddington, R., Phil. Mag., 6, 889, 1928.
25. Coolidge, A.S., and James, H.M., Phys. Rev., 55, 184, 1939.
26. Nygaard, J., Proc. VIth International Conference on Ionization Phenomena in Gases, Paris, 1963.
27. Bruce, F.M., J. of Inst. Elec. Eng. 94, Pt II, 138, 1947.
28. Bandel, H., Phys. Rev. 84, 92, 1951.
29. Weissler, G.L., Phys. Rev. 63, 96, 1942.
30. Bradbury, N.E. and Nielson, R.A., Phys. Rev. 49, 388, 1936.
31. Fromhold, L., Z. Phys. 160, 551, 1960.
32. Townsend, J.S. and Bailey, V.T. Phil. Mag. 42, 881, 1921.
33. Gill, E.W.B., and Von Engel, A., Proc. Roy. Soc. A197, 107, 1948.
34. Von Engel, A., 'Ionized Gases'; Clarendon press, Oxford, 1965.
35. Einstein, A., Ann. d. Physik, 17, 549, 1905.
36. Huxley, L.G.H., Phil. Mag. 30, 396, 1940.
37. Crompton, R.W. and Sutton, D.J., Proc. Roy. Soc. A215, 467, 1952.
38. Vincent, J.H., 'The behaviour of an electron swarm in mixed oscillatory and unidirectional electric fields'; Ph.D. thesis, Durham University, 1966.

39. Deas, H.D. and Emeleus, K.G., Phil. Mag. 40, 460, 1949.
40. Varnerin, L.J. and Brown, S.C., Phys. Rev. 79, 946, 1950.
41. Philips Res. Rep., 13, 335, 401, 1958.
42. Ward, A.L. and Jones, E., Phys. Rev. 122, 376, 1961.
43. Ward, A.L., 'Proc. of Vth International Conference on Ionization Phenomena in Gases'; Munich, 1961.
44. Lucas, J., as above, p693.
45. Borsch-Supan, W. and Oser, H., J. Res. Nat. Bur. Stand., Washington, 67B, 41, 1963.
46. Davies, A.J., Evans, C.J., and Llewellyn Jones, F., Proc. Roy. Soc. A281, 164, 1964.
47. Rose, D.J., Phys. Rev., 104, 273, 1956.
48. Harrison, M.A. and Gabelle, R., Phys. Rev. 91, 1, 1953.
49. Francis, G., Proc. Phys. Soc. Lond. B 68, 369, 1955.
50. Richter, K., 1959. see ref.1, p82.
51. Ward, A.L., J. Appl. Phys. 36, 1291, 1965.
52. Cheo, P.K. and Cooper, H.G., Amer. J. Appl. Phys. 36, 1862, 1965.
53. Parts, L., Scientific Research, 2, 2, 46, 1967.
54. Prowse, W.A., Rowbotham, J.R., Monk, P.G., Proc. Phys. Soc. 79, 158, 1962.
55. Boyer, M., Ph.D. thesis, Durham University, 1965.
56. Dutton, J., Haydon, S.C., Llewellyn Jones, F., Proc. Roy. Soc. A213, 203, 1953.